DYNAMICS OF TRANSMISSION AND CONTROL OF MEASLES

A THESIS SUBMITTED TO THE

CENTRAL DEPARTMENT OF MATHEMATICS
INSTITUTE OF SCIENCE AND TECHNOLOGY
TRIBHUVAN UNIVERSITY
NEPAL

FOR THE AWARD OF
DOCTOR OF PHILOSOPHY
IN MATHEMATICS

BY
ANJANA POKHAREL

August, 2024

DYNAMICS OF TRANSMISSION AND CONTROL OF MEASLES

A THESIS SUBMITTED TO THE

CENTRAL DEPARTMENT OF MATHEMATICS
INSTITUTE OF SCIENCE AND TECHNOLOGY
TRIBHUVAN UNIVERSITY
NEPAL

FOR THE AWARD OF
DOCTOR OF PHILOSOPHY
IN MATHEMATICS

BY

ANJANA POKHAREL

August, 2024

TRIBHUVAN UNIVERSITY

Institute of Science and Technology

DEAN'S OFFICE

Kirtipur, Kathmandu, Nepal

Reference No.:

Institute of Science & Technology
Dean's Office
Kirtipur 2045

EXAMINERS

The Title of Ph.D. Thesis: "Dynamics of Transmission and Control of Measles "

Name of Candidate: Anjana Pokharel

Internal Examiner:

Prof. Dr. Jivandhar Jnawali
Ratna Rajya Laxmi Campus
Tribhuvan University, NEPAL

External Examiners:

(1) Prof. Dr. Dil Bahadur Gurung
Kathmandu University
Dhulikhel, NEPAL

(2) Prof. Dr. Kapil Sharma
South Asian University
Delhi, INDIA

(3) Dr. Elissa J. Schwartz
Washington State University
USA

August 25, 2024

(Dr. Surendra Kumar Gautam)
Asst. Dean

DECLARATION

Thesis entitled **"Dynamics of Transmission and Control of Measles"** which is being submitted to the Central Department of Mathematics, Institute of Science and Technology(IOST), Tribhuvan University, Nepal for the award of the degree of Doctor of Philosophy (Ph.D.), is a research work carried out by me under the supervision of Prof. Dr. Kedar Nath Uprety, Central Department of Mathematics, Tribhuvan University, Nepal and co-supervised by Prof. Dr. Naveen K. Vaidya, Department of Mathematics, San-Diego State University, San Diego, CA USA.

This research is original and has not been submitted earlier in part or full in this or any other form to any university or institute, here or elsewhere, for the award of any degree.

.....

Anjana Pokharel

RECOMMENDATION

This is to recommend that **Anjana Pokharel** has carried out research entitled **"Dynamics of Transmission and Control of Measles"** for the award of Doctor of Philosophy (Ph.D.) in **Mathematics** under our supervision. To our knowledge, this work has not been submitted for any other degree.

She has fulfilled all the requirements laid down by the Institute of Science and Technology (IOST), Tribhuvan University, Kirtipur for the submission of the thesis for the award of Ph.D. degree.

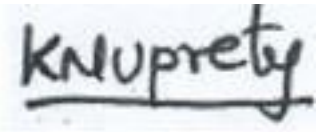

.....
Kedar Nath Uprety, Ph.D.
Supervisor
(Professor)
Central Department of Mathematics
Tribhuvan University
Kirtipur, Kathmandu, Nepal

.....
Naveen K Vaidya, Ph.D.
Co-Supervisor
(Professor)
Department of Mathematics
San Diego State University
CA, USA

August, 2024

Phone No. :00977- 14331977

TRIBHUVAN UNIVERSITY

CENTRAL DEPARTMENT OF MATHEMATICS

Institute of Science and Technology

KIRTIPUR, KATHMANDU
NEPAL

Ref No.

Date: July 25, 2024

Letter of Approval

On the recommendation of Prof. **Dr. Kedar Nath Uprety** and **Prof. Dr. Naveen K. Vaidya**, this Ph.D. thesis submitted by **Mrs. Anjana Pokharel**, entitled " **Dynamics of Transmission and Control of Measles"** is forwarded by Central Department Research Committee (CDRC) to the Dean, IOST, T.U..

Chet Raj Bhatta, PhD
Professor & Head,
Central Department of Mathematics
Tribhuvan University,
Kirtipur,Kathmandu

ACKNOWLEDGEMENTS

I am deeply grateful to Prof. Dr. Kedar Nath Uprety and Prof. Dr. Naveen K. Vaidya for their unwavering guidance and support throughout my Ph.D. research. Prof. Uprety's motivation and confidence in my abilities have been a constant source of inspiration, and I am equally thankful to Prof. Vaidya for enriching my research with diverse perspectives and international exposure, enhancing the quality of my work including opportunities and financial support for publication in prestigious journals. Despite battling breast cancer during my PhD journey, the understanding and supports from Prof. Uprety and Prof. Vaidya were crucial in helping me persevere and complete this thesis.

I thank Prof. Dr. Chet Raj Bhatta, Head of the Central Department of Mathematics, for his support. I am also grateful to the professors, faculty, and colleagues at the Central Department of Mathematics, Padma Kanya Multiple Campus, and Dean's office, IOST, TU for their encouragement and support.

A special thanks to my colleagues Mr. Ramesh Gautam and Dr. Khagendra Adhikari, for their continuous motivation, support, and collaborative research making this journey enjoyable and enriching despite my difficult battle with breast cancer.

I appreciate the Nepal Mathematical Society for the NMS-Fellowship award, IMU for GRAID, the National Science Foundation (NSF) for grants DMS-1951793, and San Diego State University for the UGP award.

Lastly, heartfelt thanks to my family, especially my husband Nilmani Pokharel, and my children Manisha, Amrit, Manish, and Manjari, for their unwavering love and support. Their faith and patience have been my anchor. I am also grateful to Sarita Ghimire and her family for their love and care during my PhD journey. I extend my thanks to all my friends and well-wishers for their support.

Anjana Pokharel
August, 2024

शोध सार

सङ्क्रामक रोगहरू रोगजनक सूक्ष्मजीवहरू जस्तै ब्याक्टेरिया, भाइरस, परजीवी वा ढुसीहरूबाट उत्पन्न हुन्छन् । यी रोगहरू संसारभरि फैलिरहेका छन् र मानव जातिलाई खतरा बनाइरहेका छन् । यी रोगहरू बाहिरी स्रोतबाट सर्न सक्छन् र उस्तै प्रकारले फैलिन सक्छन् । यस्ता रोगहरू मृत्युको प्रमुख कारण बनेका छन्। यस्ता सङ्क्रामक रोगहरूको उदय र पुनःउदय संसारभरि एक विश्वव्यापी समस्या बनेको छ ।

दादुरा अत्यधिक सङ्क्रामक मानव भाइरल रोगहरू मध्ये एक हो । खोप उपलब्ध हुँदाहुँदै पनि, खोपको अनुपालनको अभावका कारण नेपाल सहित धेरै ठाउँहरूमा दादुराको प्रकोप बारम्बार देखा परेको छ । राष्ट्रिय खोप कार्यक्रमको कार्यान्वयन हुँदाहुँदै पनि, नेपालमा बारम्बार देखा परेको दादुरा बालबालिकाको रोग र मृत्युदरको प्रमुख कारण बनेको छ। सङ्क्रामक रोगहरूको लागि गणितीय मोडेलले यस्ता रोगहरूको गतिको पूर्वानुमान गर्न र बुझ्न मद्दत गर्दछ जसले प्रभावकारी सार्वजनिक स्वास्थ्य हस्तक्षेपहरूको परिनियोजन र स्रोतहरूको वितरणलाई सहज बनाउँछ ।

यस अध्ययनमा, हामीले नियमित खोप कार्यक्रम छुटाएका व्यक्तिहरूको लागि अनुगमन गरिएको खोप कार्यक्रमहरूको प्रभाव मूल्याङ्कन गर्न गैर रेखीय साधारण भिन्नात्मक समीकरणहरूको विशेषता भएको एक नयाँ प्रसारण गतिको मोडेल विकास गर्छौं, जसले दादुरालाई सही रूपमा नियन्त्रण र उन्मूलन गर्ने लक्ष्य राख्छ । हामी हाम्रो मोडेललाई, नेपालमा देखिएको २००० देखि २०१९ सम्मको वार्षिक घटनाका केसहरूद्वारा प्रमाणीकरण गर्दछौं । नेक्स्ट जेनेरेशन म्याट्रिक्स (Next Generation Matrix) विधि प्रयोग गरेर हामी खोप प्राप्त प्रजनन सङ्ख्या, (Vaccinated Reproduction Number) Rv साथै नेपालमा दादुराको प्रभावकारी प्रजनन सङ्ख्या (Effective Vaccinated Reproduction Number) गणना गर्दछौं। हामीले Rv<1 को लागि रोग-रहित सन्तुलन बिन्दुको वैश्विक विषम स्थिरता र Rv>1 को लागि रोगको एकरूप निरन्तरता स्थापनाका लागि मोडेल विश्लेषणहरू प्रदर्शन गर्दछौं । यसबाहेक, हामी नेपालमा दादुरा नियन्त्रण गर्न सफल हुने अनुगमन गरिएको खोप - रणनीतिहरू पहिचान गर्न मोडेल सिमुलेसनहरू प्रदर्शन गर्दछौं। थप रूपमा, हाम्रो मोडेल प्रयोग गरेर हामी महामारीको दीर्घकालीन गतिको विश्लेषण गर्दछौं। साथै, हाम्रो मोडेलले पूर्वानुमान गर्छ कि, अनुगमन गरिएको खोप कार्यक्रमहरूले रोगको सम्भावित पुनरावृत्ति नियन्त्रण गर्न मद्दत गर्न सक्छ ।

कोभिड-१९ महामारीको समयमा नेपाल सरकारद्वारा २०२० मार्च २४ मा देशव्यापी लकडाउन लागू गऱ्यो। लागू गरिएको देशव्यापी लकडाउनका कारण निर्धारित खोप कार्यक्रम अवरुद्ध भयो। त्यसको परिणामस्वरूप, जारी लकडाउनका बीच, नेपालका धेरै जिल्लाहरूमा दादुराका प्रकोपहरू, जसमा केही घातक घटनाहरू पनि रिपोर्ट भएका छन्। साथै, वयस्क समूहहरूमा भएका दादुराका केसहरूले, यद्यपि थोरै संख्यामा भए पनि, पहिले उपेक्षित भएको वयस्क समूहलाई दादुराको खोपको दायरामा ल्याउनुपर्ने

आवश्यकता देखाउँछ, जसले गर्दा विश्व स्वास्थ्य सङ्गठन (WHO) को विश्वभर दादुरा उन्मूलन गर्ने लक्ष्य हासिल गर्न सकियोस्। वयस्क समूहमा संक्रमित दादुराको भूमिकालाई जाँच गर्न र उन्मूलनका लागि वयस्क- शिशु संयुक्त खोप कार्यक्रमको मूल्याङ्कन गर्न, हामीले वयस्क र शिश बालबालिकामा भएका दादुराका केसहरूलाई वर्णन गर्ने एक विस्तारित संक्रमण गतिको मोडल विकास गरेका छौं।

हामीले २४ नोभेम्बर २०२२ देखि १० मार्च २०२३ सम्म नेपालमा दादुराका प्रकोपहरूद्वारा हाम्रो मोडेल प्रमाणीकरण गर्छौं । मोडेलको विश्लेषणले खोप सङ्ख्या, दादुरा उन्मूलन लागि आवस्यक सर्तहरू, र सम्पर्क सञ्जालको भूमिका प्रदान गर्दछ। साथै, हाम्रा परिणामहरूले बालबालिका तथा शिशु लक्षित खोपहरूद्वारा प्रभावकारी रुपमा नियन्त्रण गर्न सकिन्छ, सानो सङ्ख्यामा भएपनि वयस्कहरूमा संक्रमण भएको दादुराको प्रकोपले भण्डारको रूपमा कार्य गर्न सक्छ, जसले रोग उन्मूलनमा अवरोध उत्पन्न गर्दछ। यसबाहेक, हाम्रो मोडलले, बालबालिकामा केन्द्रित प्रभावकारी खोपहरूद्वारा, दादुरा नियन्त्रण गर्न सकिन्छ भने, वयस्क-बालबालिका दुबैलाई समेट्ने खोप कार्यक्रमले रोगको उन्मूलन सुनिश्चित गर्न मद्दत गर्न सक्छ भन्ने कुराको भविष्यवाणी गर्दछ।

मुख्य शब्दहरू: *स्थिरता र दृढता - दादुराको भण्डार - वयस्क-शिशु खोप - वयस्क र बालबालिका समूहहरू -अग्र द्विखण्डन - संवेदनशीलता विश्लेषण ।*

ABSTRACT

The emergence and re-emergence of infectious diseases have become a global problem. Measles is a highly contagious human viral disease whose outbreaks frequently occur in many countries, including Nepal, despite the availability of vaccines partly due to the lack of compliance with vaccination. While the National Immunization Program is in place in Nepal, the frequent occurrence of measles in Nepal remains a major cause of child morbidity and mortality. Mathematical modeling for infectious diseases aids in forecasting and comprehending the dynamics of such diseases, facilitating the deployment of effective public health interventions and the allocation of resources.

In this work, we developed a novel transmission dynamics model in the form of system of nonlinear ordinary differential equations to evaluate the effects of monitored vaccination programs on individuals who have skipped the regular vaccination program, aiming to control and eliminate measles properly. Our model was validated by Nepal's yearly incidence case data from 2000 to 2019. We calculated the vaccinated reproduction number, R_v, using the Next Generation Matrix method. We also computed the effective reproduction number of measles in Nepal. We performed model analyses to establish the global asymptotic stability of the disease-free equilibrium point for $R_v < 1$ and the uniform persistence of the disease for $R_v > 1$. Moreover, we performed model simulations to identify monitored vaccination strategies for successfully controlling measles in Nepal. Additionally, using the model, we analyzed the long-term dynamics of the epidemic. Our model demonstrates that the monitored vaccination programs can help control the potential resurgence of the disease.

Due to the nationwide lockdown enforced by the government of Nepal during the COVID-19 pandemic, the scheduled immunization program was disrupted. As a result, amid the ongoing lockdown, measles outbreaks, including fatal cases, have been reported in several districts of Nepal. Moreover, measles cases in adult groups, albeit small in number, indicate that the previously neglected adult group may need to be brought into vaccine coverage to achieve the WHO's goal of measles eradication around the world. To examine the role of measles-infected adult groups and to evaluate combined adult-child vaccination programs for eradication, we develop a further extended transmission dynamics model describing measles cases in adults and children. We validated the new model using measles outbreak cases in Nepal from

November 24, 2022, to March 10, 2023. Detailed analyses of our model provide the vaccination reproduction number, conditions for measles eradication or persistence, and the role of contact network size. Furthermore, our results highlight that while children are the primary targets for measles outbreaks, a small infection in adults may act as a reservoir for measles, posing obstacles to eradication. Moreover, our model predicts that while impactful controls can be achieved by children-focused vaccines, a combined adult-child vaccination program may help ensure the eradication of the disease.

Keywords: *Stability and persistence - Measles reservoir - Adult-child vaccination - Adults and Children Groups- Forward Bifurcation - Sensitivity Analysis.*

LIST OF ACRYNOMS AND ABBREVIATIONS

CBR	: Crude Birth Rate
CDC	: Centers of Disease Control and Prevention
CFR	: Case Fartlity Rate
CI	: Class Interval
COVID-19	: Coronavirus Disease of 2019
DNA	: Deoxyribonucleic Acid
DFE	: Disease Free Equilibrium
EE	: Endemic Equilibrium
GoN	: Government of Nepal
IMR	: Infant Mortality Rate
LHS	: Latin Hypercube Sampling
MR	: Measles and Rubela
MoHP	: Ministry of Health and Population
ODE	: Ordinary Differential Equation
PRCC	: Partial Rank Coefficient Correlation
RNA	: Ribonucleic Acid
SARS-CoV-2	: Severe Acute Respiratory Syndrome Coronavirus-2
SA	: Sensitivity Analysis
SIA	: Supplimentary Immunization Activities
WHO	: World Health Organization

LIST OF SYMBOLS

S	: Susceptible Population
E	: Exposed Population
I	: Infected Population
U_V	: Un- monitored Vaccinated Population
M_V	: Monitored Vaccination Population
I_M	: Immunized Population
R_V	: Vaccinated Reproduction Number
R_t	: Effective Reproduction Number
U_C^V	: Un-monitored Vaccinated Population
M_C^V	: Monitored Vaccinated Population
I_{mC}	: Immuneized Child Population
S_A	: Adult Susceptible Population
V_A	: Vaccinated Adult Population
E_A	: Infected Adult Population
I_A	: Infectious Adult Population
I_{mA}	: Immunized Adult Population
Λ	: Recruitment Rate to Children Group

LIST OF TABLES

Page No.

LIST OF FIGURES

Page No.

TABLE OF CONTENTS

Page No.

CHAPTER 1

1. INTRODUCTION

1.1 Background

Measles is an acute and highly contagious viral disease, documented as early as the 7th century William et al. (2015). Caused by the morbillivirus, it remains a major global health concern. Despite the availability of effective vaccines, measles outbreaks occur frequently, especially among children, causing severe complications in those infected. The disease spreads either through direct contact with infectious droplets or by airborne transmission Education (2024); Edward et al. (2015).

Children under five years old are particularly vulnerable, and globally, measles continues to be a leading cause of death among young children. Before vaccines were developed, measles epidemics occurred every 2 to 5 years, resulting in 20 to 30 million infections and at least 1 million deaths annually worldwide Unicef for Every Child (2019); WHO (2019b). In response to these catastrophic infection rates, the World Health Organization (WHO) South-East Asia Region (SEAR) set a goal in 2013 to eliminate measles by 2020, but this target was not met and was extended to 2023 Joshi (2009).

Initial symptoms of the illness usually appears 8-12 days after infection with a high fever runny nose, bloodshot eyes, and small white spots inside the mouth. After about four days of fever, rashes emerge on the face, and upper neck and then gradually spread downward (Figure 1). Such symptoms can lead to severe complications, such as pneumonia, diarrhea, and encephalitis. Consequently, many children who get infected may later experience blindness, deafness, or vision problems, and sometimes death. An infected individual is infectious for about 8 days: 4 days before and after the appearance of rashes, and then typically recover within 2 to 3 weeks.

Measles can be successfully prevented with two doses of vaccines received at the recommended ages of 9 months (first dose) and 15 months (second dose) MoHP (a). However, due to various reasons, such as poor health systems, lack of access to vaccination, and fear or skepticism about vaccines, the proper implementation of vaccination programs has been a huge issue. Improper and insufficient vaccines have presumably contributed to frequent measles outbreaks in developed and developing countries, including Nepal.

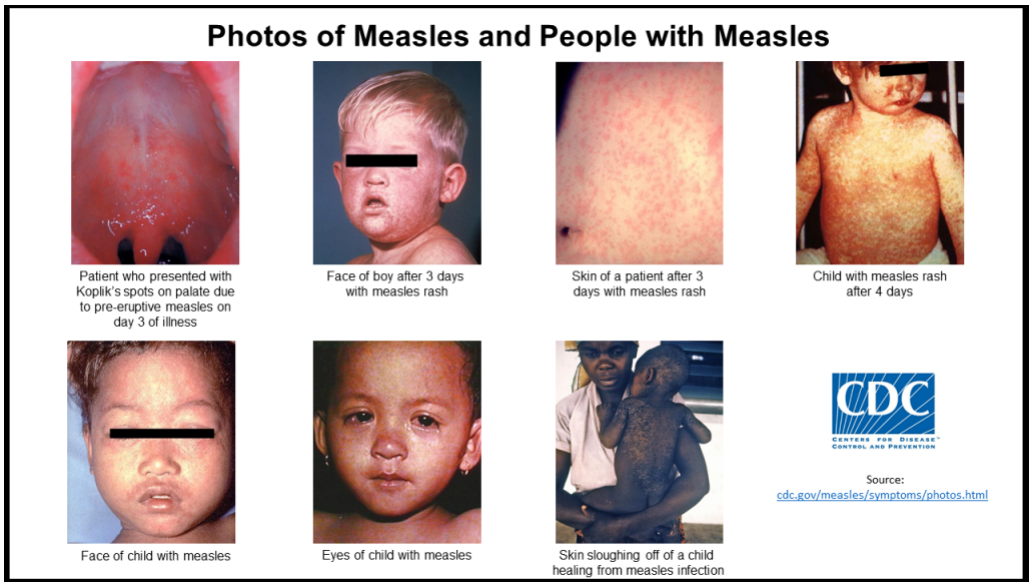

Figure 1: Pathognomonic for measles Source: District (2023)

Due to Supplementary Immunization Activities (SIAs) by WHO, measles incidence and related deaths decreased globally during 2000 - 2016 Patel et al. (2020); UN, News (2020). However, measles cases have begun to increase again after 2017. In 2017, the global vaccine coverage of the initial dose was about 85%, significantly lower than the 95% recommended by the WHO to achieve herd immunity Unicef for Every Child (2019). Even among developed countries such as the United States, France, United Kingdom, Argentina, Italy, Japan, Canada, Germany, Australia, and Chile, the vaccine coverage has not met the WHO-recommended a threshold for herd immunity Unicef for Every Child (2019). According to WHO, measles vaccination averted around 56 million deaths globally between 2000 and 2021 WHO (2023a). However, in 2021, there were still 128,000 recorded deaths due to measles, primarily among unvaccinated or partially vaccinated children. These deaths underscore the urgent need for more focused prevention efforts to reduce global measles cases WHO (2023a).

Efforts by anti-vaccine activists worldwide B.Zadrozny and Edwards (2019); Sun and Guarino (2019) may have partially contributed to inadequate vaccine coverage, and eventually to occasional outbreaks, such as the one observed in New York during 2018–2019 Guarino and H. (2019); NYC (2019). Moreover, the number of cases in 2019, reached the highest in the past 23 years. Deaths due to measles also increased by 22% in 2017 and climbed up to 50% in 2019 Patel et al. (2020); UN, News (2020). Particularly, 187 Member States reported 413,308 confirmed cases as of November 5, 2019 to the World Health Organization (WHO) through official monthly reporting

in 2019 (Figure2) World Health Organization (2019). Despite the implementation of routine immunization, measles remains a global concern due to insufficient vaccination coverage and gaps in population immunity.

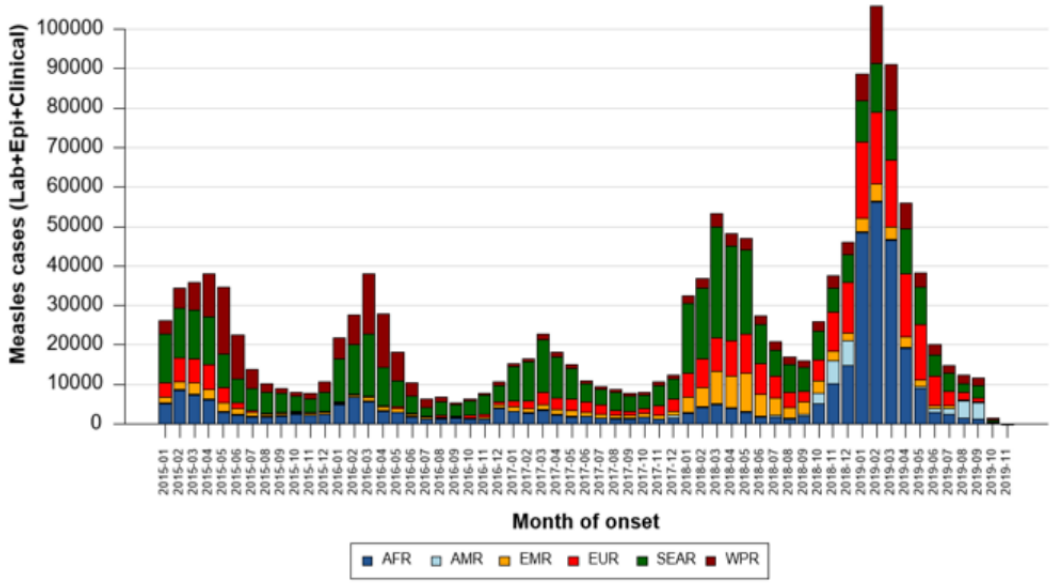

Figure 2: Measles case distribution by month and WHO Region (2015-2019), Data as of 8 November 2019. Source: World Health Organization (2019)

.

1.1.1 Measles in Nepal

Measles has been occurred endemically in Nepal. Based on a prediction from routine surveillance reports Joshi (2009) from 1994 to 2002, an average of 90,000 cases occurred per year. A Demographic and Health Survey, conducted in 2001, estimated that coverage with one dose of measles vaccine among children aged 12–23 months was approximately 71% overall, with regional variability from 65% to 79% Joshi (2009). Measles was one of the major causes of childhood death before 2007, presumably because of the low coverage of MCV1. When the coverage of MCV1 increased from 81% to 88% during 2007-2014, along with Supplementary Immunization Activities (SIAs), the suspected measles incidence declined by 13% MoHP (b); Child Health Division, DoHS,MoHP (2011); Khanal et al. (2016); Poudel (2019b, 2020); Suvedi (2005). However, the measles cases began to increase in Nepal in 2017 (99, 247, 430, and 388 measles cases in 2017, 2018, 2019, and 2020 respectively) New Spotlight online (2019); Poudel (2019a). Figure 3 also represents the increasing trend of measles

outbreaks in Nepal. Particularly in 2019, measles outbreaks occurred in many districts like Morang, Dang, Kapilvastu, Kathmandu, and Lalitpur districts of Nepal New Spotlight online (2019); Poudel (2019a, 2021); Uprety (May 2020). Notably, a frequent measles outbreak has been reported in districts with low vaccine coverage where 95% of children were not vaccinated in 2016 Karki et al. (2016); Poudel (2016); Sitaula et al. (2010). Even in vaccinated people, the protection level may be reduced because of improper timing and incomplete doses. As a member of SEAR, WHO, Nepal had committed to eliminate measles by 2023, which seems difficult to achieve due to the outbreaks in many districts.

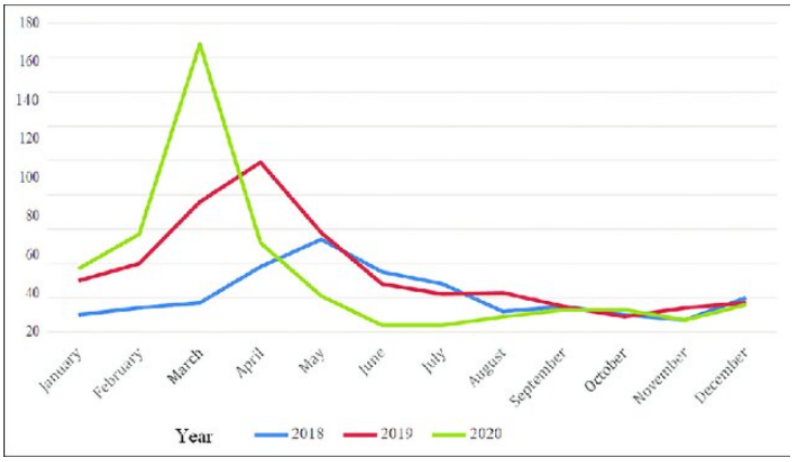

Figure 3: Measles cases were reported to WHO by Nepal for the years 2018, 2019, and 2020. Source: Sunuwar et al. (2021)

.

1.1.2 Routine Immunization Programme in Nepal

The immunization program was launched in Nepal in 1977 as an "Expanded Program on Immunization" MoHP (b). Two years later, in 1979, the monovalent vaccine against measles was first introduced in three districts of Nepal as MCV1 and was later expanded to the whole country in 1989 Public Health Update (2019); Suvedi (2005). When the nationwide Supplementary Immunization Activities were implemented in 2012-2013, the national routine immunization schedule was revised, and the measles -rubela (MR) vaccine was introduced. The monovalaent vaccine (introduced in 1989), was scheduled as MCV1 first dose of vaccine at the age of 9 months and MR (introduced in 2013) was scheduled as MCV2 second dose of vaccine at the age of 15 months in 2015 Khanal et al. (2016). A complete dose of the vaccine for measles has been

scheduled since 2015 in Nepal. Furthermore, in 2011, Nepal introduced the concept of "fully immunized villages" to enhance vaccine coverage with the goal of achieving 100% vaccine coverage of all routinely recommended vaccines. As of 2014, 823 villages (21% of 3,915) and 10 districts (13%) had attained full immunization status. However, Nepal aimed to extend this achievement nationwide through routine immunization services by 2017 Public Health Update (2019).

1.1.3 Impact of COVID-19 on Measles Immunization

Since December 2019, the novel coronavirus disease (COVID-19) has rapidly spread worldwide, originating in China. On March 11, 2020, the World Health Organization (WHO) officially declared COVID-19 a pandemic Adhikari et al. (2022). As of September 15, 2023, there have been over 695 million reported cases of COVID-19 and more than 6 million deaths attributed to the disease globally Worldometer (2023). During the COVID-19 pandemic in 2021, vaccination programs were hampered, and only 71 percent of children worldwide received two doses of vaccine, resulting the lowest vaccine coverage since 2008 WHO (2023a, 2022). On the other hand, the World Health Organization (WHO) recommends at least 95 percent vaccination coverage to achieve herd immunity for measles WHO (2022). This situation increases the risk of larger outbreaks worldwide. Eventually, measles outbreaks recorded from July 2023 to December 2023 occurred in Yemen (18,464 cases), Azerbaijan (13,721 cases), Kazakhstan (13,195 cases), India (12,301 cases), Ethiopia (10,060 cases), Russian Federation (7,720 cases), Iraq (7,601 cases), Pakistan (7,027 cases), Kyrgyzstan (5,777 cases), and Indonesia (3,205 cases) Library (2024).

Nepal has also suffered with the COVID-19 pandemic and the government enforced a nationwide lockdown on March 24, 2020, to control the spread of COVID-19. The government of Nepal had set to conduct the MR vaccination campaign in two phases to eradicate measles and rubella from mid-February to mid-April 2020, while the first phase of the campaign was completed and the second phase was disrupted due to the nationwide lockdown. As a result amid the ongoing lockdown, measles outbreaks have been reported including fatality cases in several districts of Nepal including Kathmandu and Lalitpur Poudel (2021).

1.1.4 Measles Virus and Transmission

Measles is caused by the Morbillivirus of family of Paramyxoviridae. It is an enveloped, non-segmented, negative-sense, single-stranded RNA genome of size of length approximately 16,000 nucleotides Guseva et al. (2019). Morphological structure of Measles virus has two regions: Envelop and the Nucleocapsid region. It contains six genes of protein: the fusion (F) protein, haemagglutinin (H) protein and matrix (M) protein are attached in the lipid membrane or in the envelop region however the nucleocapsid (N) protein encapsulates the Nucleocapsid region of the RNA genome, which helps to form ribonucleoprotein (RNP) complex (Figure 4). Other two proteins phosphoprotein (P), and large (L) protein are inside the lipid membrane. The P gene encodes two additional proteins: V protein and C protein which are non structured and are involved in the evasion of host's innate immune response.

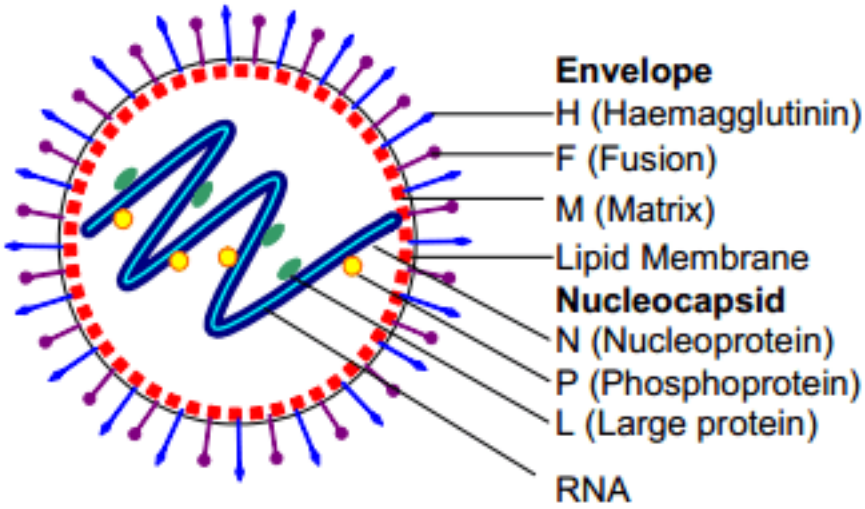

Figure 4: Measles virus: Paramyxovirus,
Source: Okonko et al. (2009)

Usually, respiratory viruses like influenza infect the respiratory tract initially, but the Morbillivirus does not infect the respiratory tract. This infection is a typical respiratory infection, in which immune cells are the main targets rather than respiratory epithelial cells Anelone et al. (2021). Moreover, the main receptor of the measles virus is the Signaling Lymphocytic Activation Molecule Family type I (SLAMF1). The surface of the virus contacts to host receptor through H protein and is responsible for the fusion of the lipid membrane. After the fusion of the lipid membrane, the viral RNA is released into the host cytoplasm. Then the viral genome replicates and transcripts

entirely in the RNP complex (plasma). H and F viral proteins are transported to the plasma membrane and the M protein interacts with RNP complex. The cytoplasmic tails of the H protein and the F protein, the cell membrane, and actin filaments in the host cells are initiated to promote the assembly of the virus and its regulation and its fusion within the cell-to-cell. MV enters the bloodstream through the lymphocytes and then propagates in the lymphoid organs throughout the body. After entering the MV into the tight junction, the immune cells from the basolateral side are infected which is mediated by SLAM, while DC-SIGN supports attaching the MV to DCs, and promotes MV infection and transmission to T-lymphocytes and hence amplifies throughout the body. Lastly, the budding of MV occurs at the apical cell surface and produces airborne MV (Figure 5) Takeda (2008).

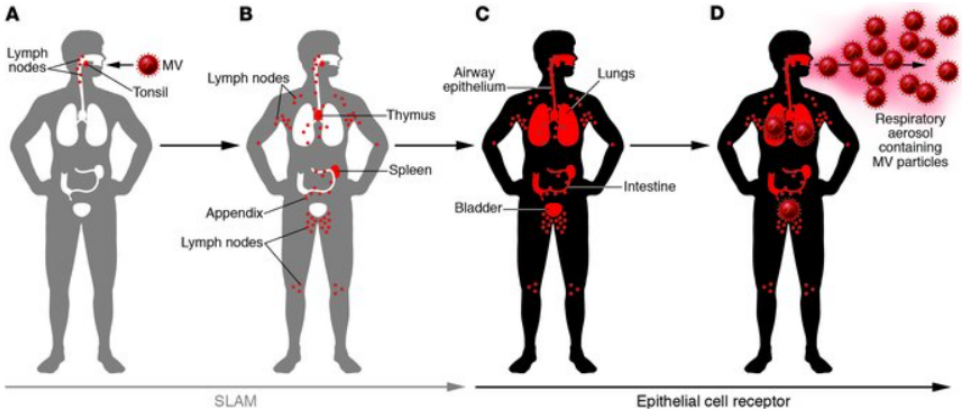

Figure 5: The time course of MV infection and receptor usage.(A) MV enters humans through the respiratory route and initiates its infectious cycle in lymphoid organs in the upper respiratory tract by using SLAM as a receptor. (B) MV-infected lymphocytes enter the bloodstream, and MV propagates in lymphoid organs throughout the body. (C) MV-infected immune cells appear to transmit MV to epithelial cells in various organs (e.g., airway, intestine, bladder). A putative epithelial cell receptor appears to play an important role in MV infection of epithelial cells. (D) MV then replicates in epithelial cells and actively releases progeny viruses into the airway. Consequently, the respiratory aerosols of patients contain large amounts of MV particles. Source: Takeda M.(2008).

1.1.5 Importance of Mathematical Modeling in Epidemiology

Mathematical modeling is essential for developing public health strategies and epidemiological responses by providing insights into transmission dynamics, forecasting outbreaks, and recommending effective control measures Adhikari et al. (2023, 2021); Gautam et al. (2022); Mutua et al. (2015); Pantha et al. (2021); Pokharel et al. (2022,

2024); Vaidya and Wang (2022). It offers critical insights into the complexities of disease transmission, aiding in prediction, resource allocation, and decision-making processes Roberts and Tobias (2000); Shayak et al. (2020). These models help policymakers anticipate outbreak scenarios, allocate healthcare resources effectively, and evaluate the impact of interventions such as social distancing and vaccination campaigns Momoh et al. (2013); Aldila and Asrianti (2019); Manesha et al. (2020); Shayak et al. (2020); Gui-Quan et al. (2020); Tuite et al. (2020). Furthermore, modeling enhances our understanding of disease spread within populations by highlighting crucial factors like the reproduction number, the role of asymptomatic carriers, and the effectiveness of control measures Adhikari et al. (2022); Pokharel et al. (2022). Additionally, mathematical modeling guides vaccine development and distribution strategies, facilitates data interpretation and supports scenario planning Fred (2017). Through continuous refinement and adaptation, these models significantly contribute to our capacity to manage and mitigate the impact of infectious diseases, ultimately saving lives and reducing the societal and economic burden of outbreaks.

The collaboration of mathematical modeling with government strategic planning processes has become prevalent in response to recent outbreaks. For instance, the UK Department of Health relies on the expertise of the Scientific Pandemic Influenza Group on Modeling (SPI-M) to provide guidance on novel respiratory infections Ellen et al. (2021); Dangerfield et al. (2023); Department of Health and Social Care (2018). Notably, during the 2009 H1N1 pandemic, the World Health Organization established a network comprising modeling groups and public health experts to comprehensively address various aspects of the outbreak Matthew et al. (2020); Christina and Christian (2022); Kerkhove and Fergusona (2012). Learning from the on going catatrosphic situation of COVID 19 pandemic, in 2023, a group of researchers introduced the Mathematical Modeling for Infectious Diseases Planning course is aimed at public health professionals in East Africa Ofori et al. (2024). The course outlines its designs and implementation, detailing both challenges and successes, along with lessons learned to inform similar infectious disease training initiatives in the area. The incorporation of mathematical approaches to policy formulation underscores the invaluable insights that modeling and statistical analyses can provide in understanding and effectively managing public health crises. Overall, mathematical modeling of infectious diseases is essential for informing evidence-based public health policies, guiding interventions, and ultimately reducing the burden of infectious diseases on society.

1.2 Objective of the Study

Despite the availability of the vaccine, measles outbreaks in many places of the world have occurred as an endemic. The modeling can help by using epidemiological data to help the policymakers understand the control strategies and help to plan disease eradication. This study focuses on the transmission dynamics of measles with the following objectives:

- To develop the model, and analyze the transmission dynamics of measles concerning monitored and un-monitored vaccination
- To develop the model and analyze the transmission of dynamics of measles in adults and children
- To fit the models to the available data, estimate the crucial parameters and obtain the vaccinated reproduction number R_v, and effective reproduction number R_e

1.3 Literature Review

Mathematical models have been widely employed for over a century to investigate the dynamics of disease transmission in human populations and to forecast risks from epidemiologic data. In recent years, applications of mathematics in infectious diseases have shown remarkably growing trends. We conducted a comprehensive literature review, which we divided into two main sections: the history of epidemic models and models specifically addressing measles transmission.

1.3.1 History of Epidemic Model

In the field of infectious disease modeling, John Graunt is recognized as one of the earliest pioneers. He was among the first to systematically quantify mortality patterns in 1662. His seminal work, "Natural and Political Observations made upon the Bills of Mortality", marked the inception of studying infectious diseases by quantifying mortality cases. Through his analysis of various causes of death, Graunt introduced a method to assess the relative risks associated with different diseases Fred (2017); Daley and Gani (2005); Angélica and Dourado (2021).

Nearly a century later, in 1760, Daniel Bernoulli (1700–1782) made significant strides in epidemiology by delving into vaccination against smallpox. His revolutionary approach involved the calculation of the potential increase in life expectancy resulting from the eradication of smallpox as a cause of death. Bernoulli's initial work was summarized in a brief outline in 1760, followed by a more comprehensive exposition in 1766. Although his methodology initially found more resonance in actuarial literature than in epidemiological circles, it has recently seen broader application and appreciation Bernoulli (1766); Fred (2017); Daley and Gani (2005).

In subsequent years, other notable contributions further advanced the study of infectious diseases. Benjamin Gompertz's development of a logistic growth model in 1825 and John Snow's analysis of the temporal and spatial patterns of cholera in 1855 during the epidemic in London stand out as significant milestones Fred (2017). Additionally, William Budd's study on the spread of typhoid in 1873 and the investigation into the laws governing the rise and fall of epidemics by William Farr in 1840 further enriched the field during the nineteenth century Angélica and Dourado (2021). Similarly, the germ theory of disease, first expressed by Jacob Henle (1809–1885) in 1840 was developed by Robert Koch (1843–1910), Joseph Lister (1827–1912), and Louis Pasteur (1822–1875) in the late nineteenth and early twentieth centuries Fred (2017).

Mathematical epidemiology experienced substantial progress during 20th century. W.H. Hamer presented the idea in 1906 that the transmission of infection ought to be impacted by both the quantity of susceptible individuals and infective individuals Hamer (1906).

In the history of epidemic model, the initial comprehensive mathematical framework for studying infectious diseases, which grabbed a lot of attention in academic circles, was the deterministic compartmental epidemic model introduced in 1927 by Kermack-McKendrick PAS and Juergen (2002); Ogilvy and McKendrick (1991a, 1927, 1991b); McKendrick (1925) and Soper Soper (1929). The model divided the population into compartments, like susceptible, infected, and recovered, and utilized the differential equation to illustrate the transitions between the states has become a fundamental tool for analyzing the dynamics of infectious diseases.

It's notable that during the years spanning 1900 to 1935, renowned public health physicians: Sir R.A. Ross, W.H. Hamer, A.G. McKendrick, and W.O. Kermack developed the foundational principles of compartmental epidemiology, rather than mathematicians Fred (2017); Foppa (2016). Particularly, Sir R.A. Ross made a major

contribution to the epidemic field when he developed the epidemic compartmental model for malaria transmission, incorporating both human and mosquito populations Ross (1911), which was awarded the second Nobel Prize in 1902. The model illustrated how transmission dynamics between mosquitoes and humans, and could be controlled by reducing mosquito populations to a critical threshold. Furthermore, it was the first introduction of the notion of the basic reproduction number, often denoted as R_0, played a crucial role, although they did not explicitly name this threshold value. Two years later MacDonald George (1957), formally identified and defined this threshold in his research on malaria, which has remained a fundamental concept in mathematical epidemiology ever since.

Since the deterministic model is not suitable for the small population, the stochastic model plays a crucial role in disease modeling. The history of the stochastic model was beginning from the 19th century with P.D. En'ko's transmission model in 1889 which is acknowledged by the work of Karl Dietz Foppa (2016). A chain binomial model by, W.H. Frost in 1928 is a groundbreaking stochastic epidemic model H. Andersson (2000). In 1931, M. Greenwood proposed an alternative rendition of the chain binomial model, offering a distinctive perspective within the stochastic epidemic modeling framework. The evolution of stochastic epidemic modeling has seen numerous expansions and updates. In 1999, a book by D.J. Daley and J. Gani provided an extensive overview of some of the more contemporary advancements Giordano et al. (2013). In 1949, Bartlett further refined the comprehension of stochastic disease transmission by describing a stochastic counterpart to the classic Kermack-McKendrick epidemic model Fred (2017) and later in 1956 he applied the stochastic process to measles outbreaks and showed that measles could exhibit periodic outbreaks.

1.3.2 Epidemic Model on Measles Transmission Dynamics

Measles is a highly contagious viral disease with a significant impact on public health, especially in unvaccinated populations. Over the decades, various mathematical models have been developed to understand its transmission dynamics, evaluate control strategies, and guide vaccination policies.

The foundation for modern epidemic modeling was laid by Kermack and McKendrick, who introduced the SIR (Susceptible-Infected-Recovered) model. Their work demonstrated the threshold behavior in epidemics and provided a basic framework for understanding measles dynamics In the subsequent years, Dietz and Schenzle (1985),

Anderson and May (1991) introduced the deterministic model to explore the measles dynamics and impact of vaccination Ogilvy and McKendrick (1991a). Hethcote in 1997, Grenfell and Bolker in 1995 are recognized for the age structure and meta population models Bolker and Grenfell (1995); Hethcote (1997).

Numerous studies have advanced mathematical modeling of measles. For instance, in modeling the measles outbreak among children, researchers incorporated factors such as age groups, spatial and temporal characteristics, and structured metapopulations Cutts et al. (2020); Goufo et al. (2014); Xia et al. (2004); Anderson and May (1992). Metapopulation refers to a collection of populations spatially separated but interconnected, facilitating the movement of individuals between them Colizza and Vespignani (2007).

Deterministic mathematical models such as SIR, SEIR, SVEIR, and SVEIRS, SVEIHR, SVIPR (Where S: Susceptible, V: Vaccinated, I:Infected, H: Hospitalized, P: Pathogen, R:Recovered), fractional derivative models, have been developed to explore various aspects of measles dynamics, including age-structure and immigration-impact Edward et al. (2015); Muhammad et al. (2023); Christopher et al. (2017); Andrea and Andrea (2008); Alemneh and Belay (2023); Kuddus et al. (2021); Mitku and Selam (2017); Peter et al. (2023a, 2022, 2023b); Roberts and Tobias (2000); Song et al. (2019); Trottier and Philippe (2000, 2002). Moreover, some SEIR based models Momoh et al. (2013); Goufo et al. (2014); Ochoche and Gweryina (2019); la Sens et al. (2012) have been developed, including continuous-time linear vaccination-based control strategy, meta-populations, and immunization in pregnant women. These basic models have also been extended to include immunity, vaccination, age-dependent vaccination, time-dependent vaccine efficacy, therapy, quarantine, and treatment Obumneke et al. (2017); Aldila and Asrianti (2019); Edward et al. (2015); Musyoki et al. (2019); Fred et al. (2015); Jaharuddin and Bakhtiar (2020); Wanjau et al. (2019); Massoukou et al. (2018); Memon et al. (2020).

Stochastic models have also been used in the study of measles transmission dynamics. In 2000, David Earn and colleagues used time-series analysis and stochastic modeling to study the impact of vaccination programs on measles dynamics in England and Wales. Their work highlighted the importance of maintaining high vaccination coverage to prevent the resurgence of measles David et al. (2000). Matt Keeling and Bryan Grenfell in 2002 applied stochastic modeling to real-world measles data, incorporating seasonality and spatial heterogeneity Keeling and Grenfell (2002).

1.4 Outline of the Thesis

This study introduces mathematical modeling of measles transmission dynamics to uncover valuable insights. It concentrates on evaluating the impact of control strategies aimed at eradicating the disease in measles-endemic countries like Nepal. The model's validation is based on real data. Furthermore, innovative concepts are put forward to enhance the precision and accuracy of disease dynamics description. The structure of the research is outlined as follows:

In chapter 2 we offer the necessary background in epidemiology and mathematical modeling. Additionally, we introduce a range of theoretical analysis techniques utilized in this dissertation.

In chapter 3, we formulate novel, innovative two deterministic models of measles transmission dynamics. These models assess the impacts of monitored vaccination programs aimed at controlling and eradicating measles, depicting cases among both adults and children. The goal is to evaluate the significance of adult infections in persistent measles cases and the effectiveness of vaccination programs for eradication. Both models are validated with data from measles outbreaks in Nepal, are utilized to estimate the parameter value.

In chapter 4 we present the model analysis including, the existence and dynamics of equilibrium points, computation of vaccinated reproduction number R_v, and effective reproduction number. We establish global asymptotic stability of the disease free equilibrium point when R_v is less than 1, and the persistent nature of the disease when R_v exceeds 1.

In chapter 5, we analyze the models and present their results. Using the monitored vaccination model, simulations are conducted to identify effective monitored vaccination strategies for measles control in Nepal. According to the model predictions, monitored vaccination programs have the potential to mitigate the risk of measles resurgence. The numerical analysis of the adult-child vaccination model yields insights into the vaccination reproduction number (which determines conditions for measles eradication or persistence) and the influence of contact network size. The model analysis demonstrates that while impactful controls can be achieved through vaccines targeted at children, implementing a combined adult-child vaccination program may facilitate the eradication of the disease.

The final chapter 6, presents a summary and conclusion of the main findings, and

discusses the implications of the study and provides recommendations for future research directions.

CHAPTER 2

2. PRELIMINARIES

In this chapter, we introduce, some mathematical and epidemiological prerequisites required for this study concerning infectious diseases. Particularly we introduce some definitions of epidemiological terms, epidemic models and, their development. Moreover, we also introduce some theoretical techniques and analyses which are used in writing this dissertation.

2.1 Basic Terminologies on Disease Modeling

2.1.1 Some Definitions of Epidemiological Terms

Susceptible Individuals

The susceptible individual is epidemiologically defined as the individual, who is at risk of becoming infected by a disease and generally denoted by S.

Exposed Individuals

The exposed class of individuals refer to individuals who have been exposed to an infectious agent but are not yet infectious themselves. An exposed class is defined as an individual who is accessible to contracting a disease and makes a disease-transmitting contact and this class is considered as a disease class that is not infectious and may or may not develop the disease.

Infectious Individuals

An infected individual is someone who has contracted a disease or condition caused by the invasion and multiplication of pathogenic microorganisms, such as bacteria, viruses, fungi, or parasites, within their body. The Infectious individual is an infected can transfer the disease to other susceptible. Infected individuals can't spread the disease and the infectious individual has the main role in the transmission of disease

dynamics. Infected and infectious both are the disease classes.

Recovered Individuals

After the recovery of the infection, the individual belongs to the recovered class. Furthermore, if recovered after the infection gets lifelong immunity that can not be susceptible or it may again be susceptible if recovered can't get immunity.

Epidemic

An unexpected increase in the number of disease cases in a specific geographical area, is a case for the epidemic.

Endemic

When an infectious disease always exists in a particular region then it becomes endemic. Measles is an endemic disease in India, and Nepal.

Pandemic

A pandemic is characterized as the global dissemination of a novel disease during a specific period. Like H1N1 in 1918, H2N2 in 1957, H3N2 in 1968, SARS in 2003, H1N1 in 2003, and COVID-19 are examples of pandemics.

Outbreak

The occurrence of an outbreak of infectious disease in a new area is a sudden increase in the number of cases of the disease.

Latent Individuals and Latent Period

An individual who is infected but not yet capable of transmitting the disease is categorized as a latent individual. Consequently, the latent period refers to the duration between the time of infection and the point at which the individual becomes capable of transmitting the pathogen to another individual.

Incubation Period

The incubation period refers to the duration from the time of exposure to an infectious agent to the onset of the first symptoms of the disease. In infectious diseases, this period represents the time required for the infectious agent to proliferate to a level sufficient to induce symptoms or provide laboratory evidence of infection. It's important to note that the latent period, which is the time between exposure and the ability to transmit the infection to others, does not necessarily coincide with the incubation period.

Incidence

Incidence refers to the number of cases occurring within a specified time frame. Typically, incidence is calculated based on clinical cases, which often leads to an underestimation of the true incidence as it overlooks sub-clinical cases.

Disease-Induced Mortality

Disease-induced mortality is defined as the death per individual due to the disease per unit time, (the death ratio to the entire population per unit time).

Prevalence

Prevalence refers to the proportion of a population that has a particular disease or condition at a specific point in time or over a specified period. It provides a snapshot of how widespread the disease or condition is within the population. Prevalence is usually expressed as a percentage or as the number of cases per a certain number of people (e.g., per 1,000 or 100,000 individuals).

Case Fatality Proportion (CFP)

The ratio of the number of deaths to the number of cases measures the case fatality proportion. For instance, as of June 22, 2021, 4522 people have been diagnosed with CoVID positive, and 41 of them have died. The CFP is 0.009 Martcheva (2008).

Disease-Induced Mortality

Disease-induced mortality is the total death caused by the disease, divided by the entire population per unit time.

2.1.2 Mathematical Derivations and Definitions

2.1.2.1 Eigenvalues, Spectral Radius & Spectral Bound

For a given square matrix A, and v is a non-zero vector then λ is defined eigenvalue of the matrix A corresponding to a non-zerovector v satisfying the condition $A\ v = \lambda\ v$. The spectral radius of A refers to the largest absolute value of the eigenvalues of the matrix A. Let $\lambda_1, \lambda_2, \lambda_3$,... be the eigenvalues of a matrix A, then the spectral radius of A denoted by $\rho(A)$ is defined as:

$$\rho(A) = Max\{\ |\lambda_i|,\ \forall\ i = 1, 2...\}.$$

Spectral bound of a matrix A denoted by $S(A)$ is the largest real part of the eigenvalues.

$$S(A) = Max\{Re(\lambda_i),\ \forall\ i = 1, 2...\}.$$

2.1.2.2 Equilibrium Point

Considering a general autonomous system of ordinary differential equations for a vector valued function f

$$\begin{array}{rcc} \dfrac{dx}{dt} & = & f(x) \\ x & = & (x_1, x_2, ,, x_n),\ f = [f_1, f_2, ,, f_n]^T \end{array} \tag{2.1}$$

Equilibrium point x^* of the system is a point satisfying $\dfrac{dx^*}{dt} = f(x^*) = 0$ i.e. the solution which is independent of time (steady state) Martcheva (2008).

2.1.2.3 Jacobian Matrix

The Jacobian matrix of a system of ordinary differential equations (ODEs) is the matrix of all first-order partial derivatives of the function in the system Martcheva (2008); Diekman et al. (1990). In 2.1 the matrix of all first-order partial derivatives of

the right-hand side of the system 2.1 of equations ($f = (f_1, f_2, ..., f_n)$) to the variable $x = (x_1, x_2, ..., x_n)$ is given as

$$J = \begin{pmatrix} \frac{\partial f_1}{\partial x_1} & \frac{\partial f_1}{\partial x_2} & \cdots & \cdots & \frac{\partial f_1}{\partial x_n} \\ \frac{\partial f_2}{\partial x_1} & \cdots & \cdots & \cdots & \cdots \\ \frac{\partial f_3}{\partial x_1} & \cdots & \cdots & \cdots & \cdots \\ \frac{\partial f_n}{\partial x_1} & \cdots & \cdots & \cdots & \frac{\partial f_n}{\partial x_n}. \end{pmatrix}.$$

2.1.2.4 Basic Reproduction Number

Epidemiologically, the reproduction number symbolized as R_0 quantifies the number of new cases produced from one infectious individual in a population of susceptible individuals throughout the entire infectious period. This metric serves as a critical indicator for understanding the potential spread of an infectious disease. Mathematically, it plays the role of a threshold value for the dynamics of the system. In the field of epidemiology, each infected individual produces, on average, more than one new infection and the disease remains in the population for R_0 greater than one. If R_0 is less than one, then on average, an infected individual generates fewer than one new infected individual throughout its infectious period and the disease dies out Martcheva (2008); Driessche and Watmough (2002). This number in the simple models with a single disease compartment can be expressed as:

R_0 = (number of contacts at a time) × (probability of infection in a contact)
× (duration of infectiousness during epidemics).

However, other models with multiple disease compartments, the next-generation matrix (NGM) method is used in computing the R_0.

2.1.2.5 Effective Reproduction Number

The effective reproduction number, often denoted as R_t, is a crucial epidemiological metric used to quantify the average number of secondary infections generated by each infected individual at a specific point in time during an outbreak or epidemic. Unlike the basic reproduction number (R_0), which represents the average number of secondary infections caused by a single infected individual in a completely susceptible population, the effective reproduction number considers changes in population immunity, behavior, interventions, and other factors influencing transmission dynamics.

In essence, R_t provides insights into the current state of an outbreak by accounting for the evolving conditions that affect transmission. When R_t is greater than one, it indicates that the outbreak is growing, as each infected individual is, on average, infecting more than one new infection. Conversely, when R_t is less than one, the outbreak is declining, as each infected individual is, on average infecting, less than one new infection, leading to eventual control or eradication of the outbreak. When R_t is equal to one, the disease remains endemic within the population N et al. (2019). So the level of R_t needs to be less than one to control the disease in the population.

The effective reproduction number R_t can be estimated as a product of the basic reproduction number R_0 and susceptible population x i.e. $R_t = R_0\ x$.

R_t is a crucial metric for assessing the effectiveness of control measures and guiding public health interventions to mitigate the spread of infectious diseases.

2.1.2.6 Next Generation Matrix

Next-generation matrix refers to a mathematical tool used in the field of epidemiology in modeling the transmission dynamics of infectious diseases particularly, in the case of multiple infectious agents. It's commonly used to predict how a disease might spread within a population and to assess the effectiveness of different control measures.

When dealing with multiple infectious agents, a novel next-generation method, was first proposed in 1990 by Diekmann et al.Diekmann et al. (2010) and later standardized by Van den Driessche and Watmough Driessche and Watmough (2002), provides a useful approach. This technique converts a set of ordinary differential equations (ODEs) or partial differential equations (PDEs) in an infectious disease model into an operator. Within this method, the basic reproduction ratio is precisely derived based on linearization about the disease free-equilibrium point and identified as the principal eigenvalue (spectral radius) of this operator. We follow the method Brauer and CC.Chavez (2012) for detailed formulation.

Considering the compartmental disease model, having n disease compartments and m non-disease compartments.

$$\begin{aligned} \frac{dx_i(t)}{dt} &= \mathcal{F}_i(x,y) - \mathcal{V}_i(x,y), \quad i = 1,2,3,\ldots,n. \\ \frac{dy_j(t)}{dt} &= g_j(x,y) \quad j = 1,2,3,\ldots,m. \end{aligned} \tag{2.2}$$

In this context, $x \in \mathbb{R}^n$ and $y \in \mathbb{R}^m$ and $\mathcal{F}_i(x,y)$ is the new infections into the

i^{th} compartment and $\mathcal{V}_i(x,y) = V_i^-(x) - V_i^+(x)$ is the net flow representing $V_i^-(x)$ the transfer out of and $V_i^+(x)$ the transfer into the i^{th} compartment, satisfying the following assumptions.

I. $\mathcal{F}_i(0,y) = 0$ and $\mathcal{V}_i(0,y) = 0$ for all $y \geq 0, i = 1,2,3,\ldots,n$. All new infections are secondary infections arising from the infected individuals.

II. $\mathcal{F}_i(x,y) \geq 0$ for all $x,y \geq 0, i = 1,2,\ldots,n$. The new infections can not be negative.

III. $\mathcal{V}_i(x,y) \leq 0$ whenever $x_i = 0$, for $i = 1,2,\ldots,n$. The net outflow $\mathcal{V}_i$ from i compartment must be negative for empty compartments.

IV. $\sum_1^n \mathcal{V}_i(x,y) \geq 0$ for all $x,y \geq 0$. The sum represents the total outflow from infected compartments.

V. The disease-free system i.e. $\dfrac{dy_j(t)}{dt} = g_j(0,y) = 0$, has a unique equilibrium, that is locally asymptotically stable. That is all solutions with initial conditions of the form $(0,y)$ approaches a point $(0,y_0)$ as $t \to \infty$ and we refer to it as the disease-free equilibrium.

When introducing a single infected to an initially disease-free population, the initial ability to spread the disease through the population is determined by the linearization of the 2.2 about the disease-free equilibrium point $(0,y_0)$. It is clear that assumption I imply:

$$F_{ij} = \frac{\partial F_i}{\partial x_j}(0,y_0) = V_{ij} = \frac{\partial V_i}{\partial x_j}(0,y_0) = 0,$$

for each pair of (i,j). The system of disease compartments can be expressed as:

$$\frac{dx(t)}{dt} = (F - V)(x), \tag{2.3}$$

Where F and V are $(n \times n)$ matrix of with entries

$$F = \frac{\partial F_i}{\partial x_j}(0,y_0) \text{ and } V = \frac{\partial V_i}{\partial x_j}(0,y_0), \text{ for all } i,j.$$

The ij^{th} entry of the matrix F is the rate at which the infected individual in the state j give rise to the infected individual in i disease compartment. The ij^{th} entry of V^{-1}

is the expected time that a newly infected individual in j will spend in infected state i. As per the assumption the disease-free system

$$\frac{dy_j(t)}{dt} = g_j(0, y) = 0,$$

has a unique asymptotically stable disease-free equilibrium point, the linear stability of the system 2.2 is determined by the linear stability of the matrix $(F - V)$ in 2.3. The number of secondary infections caused by a single infected individual can be determined by multiplying the expected duration of the infectious period by the rate of secondary infections. For the general model with n disease compartments, these values are computed for each compartment.

If there is no secondary infection with non-negative initial condition x_0 representing:

$$\frac{dx(t)}{dt} = -V(x), x(0) = x_0. \tag{2.4}$$

The solution of the 2.4 is $\phi(t, x_0) = e^{-Vt}x_0$. Where the exponential matrix is given as

$$e^A = I + A + \frac{A^2}{2!} + \frac{A^3}{3!}, ... + \frac{A^k}{k!} + ...$$

Clearly,

$$\int_0^\infty \phi(t, x_0)dt = \int_0^\infty e^{-Vt}dt = V^{-1}x_0,$$

where $\phi(t, x_0)$ is the solution of the 2.4, represents the expected time that a newly infected individual will spend in infected state. Thus the ij^{th} entry of the matrix V^{-1} represents the expected time for an individual, initially introduced into the disease-free compartment j spends in the disease compartment i.

$$\int_0^\infty F\phi(t, x_0)dt = FV^{-1}x_0.$$

The matrix FV^{-1} is called Next Generation Matrix Brauer and CC.Chavez (2012) for the system at the disease free equilibrium where it's ij^{th} entry is the expected number of secondary infections in compartment i produced by individuals initially in compartment j. Clearly, the matrix FV^{-1} is non negative and has non negative eigenvalues, its spectral redius $\rho(FV^{-1})$ is the basic reproduction number

$$R_0 = \rho(FV^{-1}).$$

2.1.3 Well-Possedeness

A "well-posed solution" typically refers to a problem that satisfies three criteria:

Existence: At least one solution to the problem within the given specified domain must exist.

Uniqueness: The existing solution must be unique, which ensures that the problem does not produce any other conflicting solutions. In other words, there is only one possible solution for a given initial and boundary conditions.

Stability: The solution to the problem must be stable which means, a small changes in the problem should not result significant changes in the solution.

A mathematical model is said to be well-posed if it satisfies the three fundamental properties or a model well-posed if it has a unique, stable solution within the given initial and boundary condition Giordano et al. (2013); Martcheva (2008).

A properly formulated mathematical model establishes a robust framework for understanding and addressing real-world issues. Models with lacking any of these properties can yield uncertain or untrustworthy outcomes, potentially failing to faithfully represent physical or biological phenomena.

2.1.3.1 Stability of Solutions

Definition of Stability

We consider an equilibrium state $X^* \in \mathbb{R}^n$ for the ordinary differential equation (ODEs):

$$\frac{dX}{dt} = f(X). \tag{2.5}$$

Where vector X represents the state variables and $f(X)$ represents the vector field that describes evolvement of the state over the time.

The equilibrium point X^* is stable if for any small perturbation $\epsilon > 0$ there exists a $\delta > 0$, such that the initial condition $X(0)$ satisfying the condition $\|X^* - X(0)\| < \delta$, then the solution satisfies $\|X^* - X(t)\| < \epsilon$ for all $t \geq 0$.

Local Asymptotic Stability Condition

The equilibrium state (X^*) of the system 2.2 is asymptotically stable if and only if the following conditions hold:

1. The Jacobian matrix J of the system 2.2 at the equilibrium state X^*, for all eigenvalues λ_i of A, is negative.

2. In another way, the spectral radius $\rho(A)$ of the Jacobian matrix A is less than one, i.e., $\rho(A) < 1$.

These criteria guarantee that minor deviations from the equilibrium state (X^*) will diminish over time, and trajectories originating close to the equilibrium state (X^*) will converge to the equilibrium state as $t \to \infty$ Hirsch et al. (2004); Martcheva (2008). This condition established a theorem: .

Theorem 2.1.1 *Martcheva (2008); Driessche and Watmough (2002) Theorem for asymptotically Stable: An equilibrium point of the system of equations is asymptotically stable if all eigenvalues of its jacobian at the equilibrium point have negative real parts and it is unstable if one of eigenvalues has not negative real part.*

2.1.4 Data Fitting & Parameter Estimation

For the validation, the model which is described by the system of ordinary differential equations (ODEs) is fitted to the real data. Through data fitting, certain unknown parameters of the model can be estimated where the ODEs can be solved numerically using MATLAB solvers such as "ode15s" or "ode45." In conjunction with these solvers, optimization functions like "fminsearch" and "fmincon" are employed. The least squares method is commonly utilized for data fitting, aiming to minimize the sum of squared residuals, which quantifies the disparity between the model's predictions and the corresponding values observed in experimental data.

$$J(\Phi^*) = \sum_{k=1}^{n} (h(t_k) - \bar{h}(t_k))^2,$$

where $\Phi^* = (\Phi_1, \Phi_2, ..., \Phi_p)$ is the set of p parameters to be estimated, and h_k is the population obtained from the model while $\bar{h}_k$ is the real time data of the respective population. The total number of data points using in the model fitting is represented by n.

2.1.4.1 Computation of Confidence Intervals

A confidence interval is a statistical range that provides an estimate of the believable values for a population parameter, based on sample data. To establish confidence intervals for the estimated parameters ϕ^*, we calculate the standard errors for the parameters using the approach detailed in chapter 3 of Banks et al. (2014). Initially, we compute the sensitivity matrix Γ for the estimated parameters.

$$\Gamma = \begin{bmatrix} \frac{\partial H_{t_1}}{\partial \Phi_1} & \frac{\partial H_{t_1}}{\partial \Phi_2} & \cdots & \frac{\partial H_{t_1}}{\partial \Phi_p} \\ \frac{\partial H_{t_2}}{\partial \Phi_1} & \frac{\partial H_{t_2}}{\partial \Phi_2} & \cdots & \frac{\partial H_{t_2}}{\partial \Phi_p} \\ \vdots & \vdots & \cdots & \vdots \\ \frac{\partial H_{t_n}}{\partial \Phi_1} & \frac{\partial H_{t_n}}{\partial \Phi_2} & \cdots & \frac{\partial H_{t_n}}{\partial \Phi_p} \end{bmatrix}.$$

Because we cannot express the closed form of $\frac{\partial H_{t_k}}{\partial \Phi_j}$, $j = 1, 2, \ldots, p$, and $k = 1, 2, \ldots, n$ directly from the model we use the subsequent complex-step approximation method to calculate the partial derivatives.

By employing a complex step ih, we examine the Taylor's expansion of H_{t_k},

$$H_{t_k}(\Phi_j + ih) \approx H_{t_k}(\Phi_j) + ihH_{t_k}^{'}(\Phi_j) - \frac{h^2}{2!}H_{t_k}^{''}(\Phi_j) + \ldots,$$

where h is taken to be small positive constant ($h = 10^{-40}$) in our computation and i is the imaginary unit.

Taking out the imaginary part of both sides of the above equation and dividing by h gives

$$H_{t_k}^{'}(\Phi_j) = \frac{\partial H_{t_k-}}{\partial \Phi_j} \approx \frac{Im[H_{t_k}(\Phi_j + ih)]}{h} + O(h^2),$$

where $O(h^2)$ is the terms of order 2 and higher. Then the derivatives are

$$\frac{\partial H_{t_k}}{\partial \Phi_j} \approx D_h^j(H_{t_k}) = \frac{Im\left[H_{t_k}(\Phi_j + ih)\right]}{h},\ j = 1,\ 2,\ \ldots p, \text{ and } k = 1,\ 2,\ \ldots n.$$

$\hat{\Gamma}$ an approximation of the sensitivity matrix is computed by using these Taylors expansion. Then we take $\sqrt{(\sigma^2\{\hat{\Gamma}^T\hat{\Gamma}\}^{-1})_{ii}}$ where, $\sigma^2 \approx \hat{\sigma}^2 = J(\Phi^*)/(n-p)$ and Φ^* represents the fundamental estimated parameter values, serving as the standard deviation for the parameter $\Phi_j, j = 1, 2, \ldots, p$.

2.1.5 Identifiability of the Parameters

There is a significant challenge in the estimation of parameters in the model of biological systems with the nonlinear ordinary differential equation (ODEs). A notable characteristic of biological models is the frequent incorporation of multiple factors that are correlated with each other Maksat et al. (2009); I-Chun and O (2009). Identifiability is one of the critical factor importance in parameter estimation and statistical modeling, particularly within fields such as system identification, machine learning, and data analysis.

A biological model is identifiable, if the parameters ϕ can be uniquly determined from the given sytsem, in other word indentifiabilty defines as a concept of one-to-one mapping between parameters and system input or output Hongyu et al. (2011).

Identifiability is crucial in parameter estimation and statistical modeling, especially in system identification, machine learning, and data analysis. It refers to the ability to uniquely determine model parameters from observed data. When a model is identifiable, each parameter can be estimated without ambiguity, accurately representing the data's underlying relationships. One way to assess identifiability is by using the sensitivity matrix, which measures how variations in model parameters impact the model's output Hongyu et al. (2011).

We have sensitivity matrix Γ in section (2.1.4.1). A model achieves identifiability when the sensitivity matrix attains full rank. In essence, this means that the number of linearly independent rows or columns within the matrix matches the number of parameters to be estimated. If the sensitivity matrix achieves full rank, it signifies the model's identifiability, enabling us to uniquely estimate all parametersJoubert et al. (2018). Conversely, if the sensitivity matrix falls short of full rank, it suggests that certain parameters cannot be identified with the available data and model structure. This circumstance may arise due to redundancy within the model or insufficient data to differentiate specific parameters.

2.1.6 Latin Hypercube Sampling

Latin Hypercube Sampling (LHS) is a systematic method for creating representative samples from multi-dimensional parameter spaces, introduced by Mckay et al. in 1979 McKay et al. (1979). It operates similar to stratified sampling, dividing random distributions into equally probable intervals, from which samples are drawn. The

sample size, denoted by N, is typically recommended to be at least $k + 1$, where k is the number of estimated parameters.

Sensitivity Analysis (SA) quantifies uncertainty in complex models by identifying critical inputs (parameters and initial conditions) and assessing their impact on model outcomes. When inputs are known with little uncertainty, partial derivatives of the output function can be computed. This local SA examines changes in factors near nominal values. However, in fields like biology with highly uncertain inputs, global SA techniques are necessary.

Various SA techniques are tailored to different mathematical and computational models. For models with non-linear, monotonic, effective measures include rank-based metrics like rank correlation coefficient (RCC), partial rank correlation coefficient (PRCC), and standardized rank regression coefficients (SRRC). In general, PRCC emerges as the most efficient and reliable among sampling-based indexes, consistently yielding similar results. It provides a metric for monotonicity after eliminating linear effects from all variables except one.

CHAPTER 3

3. MODELING TRANSMISSION DYNAMICS OF MEASLES IN NEPAL AND ITS CONTROL

In this chapter, we present two novel deterministic models based on the SEIR (Susceptible-Exposed-Infectious-Recovered) model to describe the transmission dynamics of measles in Nepal. The first model evaluates the effect of monitored vaccination programs to control and eliminate measles. This model is parameterized with data from measles outbreaks in Nepal from 2000 to 2019. The second model focuses on measles cases in both adults and children in Nepal. Due to delays in vaccination during the COVID-19 pandemic and ongoing lockdowns, measles outbreaks occurred in different districts. We validate this model by fitting it with real measles incidence cases from November 24, 2022, to March 10, 2023 and estimating crucial parameters. We also present mathematical validation of models.

3.1 Introduction

Monitored vaccination programs may help achieve success in avoiding measles epidemics. Such monitored vaccination programs promote the timely completion of the vaccination, thereby increasing the chance of complete immunity gain. Various factors, including the impact of the COVID-19 pandemic on vaccine coverage, have collectively hampered vaccination programs in 2021. In 2021, a record high of nearly 40 million children missed a measles vaccine dose; 25 million children missed their first dose, and an additional 14.7 million children missed their second dose globally WHO (2022). Note that the World Health Organization (WHO) recommends at least 95 percent vaccination coverage to achieve herd immunity for measles. The world is well under that requirement with only 81 percent of children receiving their first measles-containing vaccine dose, and only 71 percent of children receiving their second one. The decline in vaccine coverage coincides with measles transmission patterns, impacting not only infants but also older age groups Dixon et al. (2021); Unicef for Every Child (2019).

Major challenges for measles control include a lack of a catch-up vaccination program, growing vaccine hesitancy, and insufficient monitoring for elimination and outbreak prevention. In response, the World Health Organization introduced the “Measles and

Rubella Strategic Framework 2021-2030" in 2020, targeting global disease elimination by 2030 WHO (2020, 2023a). After rising outbreaks of measles in 2019, in response, Nepal introduced the National Immunization Program (NIP) in 2020 with a plan for a comprehensive nationwide vaccination campaign targeting children aged 9 to 59 months against both measles and rubella (MR). While the first phase of this campaign was completed as scheduled, the second phase was disrupted by the COVID-19 pandemic, consequently causing measles outbreaks in multiple districts Boss et al. (2022); Thakur et al. (2024). Between January and April 2020, 220 measles cases were reported, with 78% affecting individuals outside the campaign's target age range (9 to 59 months). Notably, 60% of the total cases in the 5–14-year age group were not vaccinated [119]. From November 2022 to March 2023, 690 cases were reported, with approximately 86% of infected individuals aged 15 years and younger, and 58% of the patients were unvaccinated WHO, Disease outbreak news, Item, Measles (2023). Although a rise in number of measles cases has brought attention to the potential threat of severe measles outbreaks, persistent and frequent outbreaks in specific districts, including Morang, Dang, Kapilvastu, Kathmandu, Lalitpur, Dhading, Banke, Kailali, of Nepal pose a severe concern of obstacle to World Health Organisation's (WHO's) global measles eradication plan "Measles and Rubella Strategic Framework 2021-2030"Dall (14 March 2023); Poudel (2019a); WHO (2020, 2023a); WHO, Disease outbreak news, Item, Measles (2023).

In order to achieve the measles eradication goal, the primary focus has been on formulating improved children-vaccination programs. However, it is essential to note that 14% of the infectious cases are unvaccinated adults. These infectious adults originating from the pool of unvaccinated children can act as virus reservoirs in the community and sources for disease outbreaks, causing the obstacle to disease eradication. Implementing a closely monitored vaccination program for both children and adults may be imperative to completely eradicate the disease. Mathematical modeling is a valuable tool for identifying the ideal monitored vaccination programs combined with two different age groups in the context of Nepal. To address these issues, we develop two novel deterministic models to study the transmission dynamics of measles in Nepal. One model incorporates monitored vaccination programs with two classes of vaccinated individuals: one under the monitored program and another without the monitored program. The second model incorporates two age groups: adults and children. The monitored vaccination model is validated using two-decade-long annual measles data, while the other model is validated using two weeks of weekly data and mathematically validate both.

3.2 Modeling: Monitored Vaccination Model

3.2.1 Method

We develop a novel deterministic model, incorporating monitored vaccination programs with two classes of vaccinated individuals, one under the monitored program and another without the monitored program. The model is validated using two-decade-long measles data from Nepal. Our model analysis establishes the local and global stability of disease-free equilibrium, the existence of endemic equilibrium, and the uniform persistence of the disease. Furthermore, we carry out model simulations to properly evaluate the impact of monitored vaccination programs on the short-term and long-term trend of measles transmission in Nepal.

3.2.2 Model Formulation

We develop a transmission dynamics model of measles for the population that includes all the newborns and children under 15 years. As mentioned earlier, implementing a proper vaccination program is often difficult, particularly for children whose parents have poor health knowledge and have fear or skepticism about vaccines. To improve the effectiveness of vaccination programs, we introduce a monitored vaccination program into our model. The program mainly focuses on asserting the completion of vaccines timely and accurately by children under this program. Because of extra care and regular follow-up, the children under this program are expected to have less susceptibility to infection and a higher rate of achieving immunity than those under regular (un-monitored) vaccination programs. To formulate the model, we divide the total population considered (N) into six mutually exclusive compartments: susceptible (S), un-monitored vaccinated (U_V), monitored vaccinated (M_V), exposed (E), infectious (I), and immune (I_M).

The schematic diagram showing the flow of individuals from and to the compartments during the measles transmission dynamics is presented in Figure 6. The dynamical system equations representing the model are as follows:

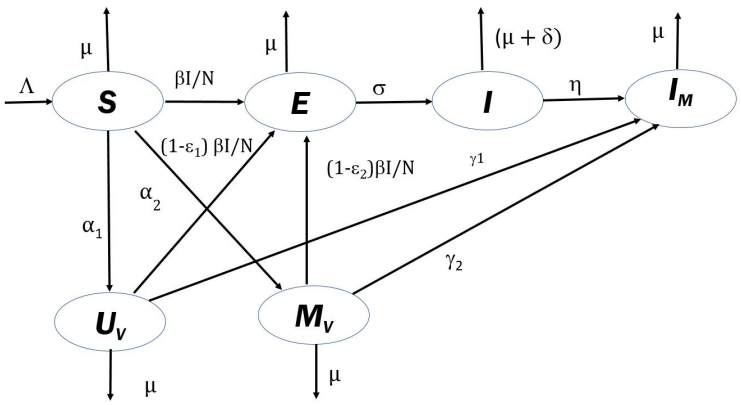

Figure 6: Schematic diagram of the transmission dynamics of measles.

$$\frac{dS}{dt} = \Lambda - \left(\frac{\beta I}{N} + \mu + \alpha_1 + \alpha_2\right) S, \tag{3.1}$$

$$\frac{dU_V}{dt} = \alpha_1 S - \left(\gamma_1 + \mu + \frac{(1-\epsilon_1)\beta I}{N}\right) U_V, \tag{3.2}$$

$$\frac{dM_V}{dt} = \alpha_2 S - \left(\gamma_2 + \mu + \frac{(1-\epsilon_2)\beta I}{N}\right) M_V, \tag{3.3}$$

$$\frac{dE}{dt} = \frac{\beta I S}{N} + \frac{(1-\epsilon_1)\beta I U_V}{N} + \frac{(1-\epsilon_2)\beta I M_V}{N} - (\mu + \sigma)E, \tag{3.4}$$

$$\frac{dI}{dt} = \sigma E - (\mu + \eta + \delta)I, \tag{3.5}$$

$$\frac{dI_M}{dt} = \gamma_1 U_V + \gamma_2 M_V + \eta I - \mu I_M. \tag{3.6}$$

Here, Λ represents the recruitment rate of susceptible, i.e., newly born children. The measles infection occurs with the per capita transmission rate of $\beta I/N$, transferring susceptible individuals to the exposed class. The parameters σ represents the rate of progression of individuals from the exposed class to the infectious class, and η is the recovery rate of infectious individuals from the disease. Since only the children up to the age of 15 years are considered in the study, we assumed μ is the rate at which the children become older than 15 years leaving from the dynamics. We take δ to represent the disease-induced death rate.

The parameters α_1 and α_2 represent the rate of un-monitored vaccination and the monitored vaccination, respectively. As discussed in Pantha et al. Pantha et al. (2021), for practical purposes, the values of α_1 and α_2 for un-monitored and monitored vaccination programs aiming to cover $\zeta_1\%$ and $\zeta_2\%$ of children in t_1 and t_2 years, respectively, can be estimated using $\alpha_1 = -\ln(1-\zeta_1/100)/t_1$ and $\alpha_2 = -\ln(1-\zeta_2/100)/t_2$, respectively. The individual in the monitored vaccinated group is expected to be properly

monitored to ensure the timely completion of the vaccination. In contrast, individuals in the un-monitored vaccinated group have more likelihood of not completing the vaccination in time, possibly delaying the gain of complete immunity. Therefore, we assumed that the un-monitored and monitored vaccinated children become immune at different rates, γ_1 and γ_2, respectively. Our model assumes individuals recovered from natural infection and those completing vaccination have similar immunity. Therefore, we include both of them in the same class, namely the immune class (I_M). The vaccinated children may also be infected, but at lesser infectivity rates $(1-\epsilon_1)\beta$ and $(1-\epsilon_2)\beta$ for un-monitored and monitored vaccinated, respectively. Since the monitoring service providers are expected to counsel individuals in the monitored vaccinated program for timely completion of vaccine and prevention practices, we also expect $0 \leq \epsilon_1 < \epsilon_2 \leq 1$.

3.2.3 Data Source

The publicly available data used in this work is obtained from the official site of the World Health Organization (WHO). The data includes the reported measles cases in Nepal from 2000 to 2019. Since 5% of the reported cases belong to the aged 15 and above WHO (2020), we deducted 5% of the cases from the data. The Crude Birth Rate (CBR) and Infant Mortality Rate (IMR) of Nepal are used from the "Nepal population growth rate 1950–2020" Macrotrends.

3.2.4 Parameter Estimation

Nepal's population under fifteen years was 9,807,000 in 2000 (taken as the base year) and 8,460,000 in 2019 WHO (2020). The actual population size in individual S, U_V, M_V, E, I, I_M, classes is not available. It is recorded that 77% of the population was vaccinated in 2000 (the base year) WHO (2020). For our base case simulation, among the unvaccinated 23% of the total population, we assumed that 22% were in the susceptible class ($S(0) = 2,157,540$). We took 30% of the vaccinated population were in the un-monitored vaccinated class ($U_V(0) = 2,206,575$). Since the monitored vaccination program was not present in 2000, we took $M_V(0) = 0$. From the data, the recorded cases were 8927 (after reducing 5% over 15 years from the total recorded 9397), among which we assume $E(0) = 300$ in the exposed class and $I(0) = 340$ in the infectious class. The remaining population $(N(0) - S(0) - U_V(0) - E(0) - I(0))$ is included in the immune class ($I_M(0) = 5,442,245$).

The recruitment rate ($\Lambda = 612,328$) is the annual average birth rate, which is calculated by using the Crude Birth Rate (CBR) and Infant Mortality Rate (IMR) from the 2000-2019 data Macrotrends. Since only the population below fifteen years is considered in the study, we used $\mu = 1/15 = 0.0667$ per year. It is given that the incubation period of measles is 10–14 days on average Organization; WHO (2019b), and thus the disease progression rate from the exposed class to the infectious class is taken as $\sigma = 1/12 \times 365 \approx 30$ per year. Also, since it takes about 18 days (range between 7 to 23 days) to recover from the disease Organization, we used $\eta = 1/18 \times 365 \approx 20$ per year. As per WHO guidelines, children are vaccinated with the first dose at the age of 9 months and the second dose at 15 months MoHP (a), giving a six-month interval between the two doses. Since the monitored vaccinated individuals (M_V) are expected to complete them in time, we took $\gamma_2 = 0.5$ per year. From the data Knoema (2017); Rathore (2020), we estimated the average disease-induced death rate to be $\delta = 0.01$ per year. The remaining parameters of the model, $\beta,\ \alpha_1,\ \alpha_2,\ \gamma_1,\ \epsilon_1$, and ϵ_2, are estimated by fitting the model to the measles case data from Nepal.

3.2.5 Data Fitting and Model Validation

From the model, the yearly new infections at time t can be calculated using $h(t) = \sigma E(t)$, which we obtained using the numerical solutions of the system (3.1–3.6). Then we estimated the parameters with the help of the nonlinear regression method Motulasky and Christopoulos (2003), which minimizes the following sum of the square residuals:

$$\sum_{k=1}^{n} (h_k - \bar{h_k})^2,$$

where h_k denotes the model predicted yearly new infection, $\bar{h_k}$ denotes yearly new infection data, and n is the number of data points used for the model fitting. For each estimated parameter, we also computed the confidence limits using the standard errors from the sensitivity matrix ($\mathcal{S}$) based on the complex-step derivative technique described in the previous study Adhikari et al. (2021); Banks et al. (2014); Banks and Joyner (2018); Rahman et al. (2019). Our model is consistent with the yearly incidence cases observed in Nepal (Figure 10). In addition, we also show that the model prediction of the cumulative cases agrees well with the cumulative data, thereby validating our model to describe the measles epidemic in Nepal.

We note that while making all six parameters free in the data fitting process, we obtained negative lower limits of some confidence intervals. To tackle this issue, we

needed to fix some of the parameters as done previously Banks et al. (2014); Banks and Joyner (2018); Rahman et al. (2019). Since the parameters α_2 and ϵ_2 are the two least sensitive parameters identified from the sensitivity matrix, $\mathcal{S}$, we fixed $\alpha_2 = 0.02$ per year and $\epsilon_2 = 0.90$ at their best estimate values. We also note that taking the different values of α_2 and ϵ_2 did not significantly affect estimates of other parameters, as expected, because of the least sensitivity. Then, we estimated the remaining only four parameters, $\beta,\ \alpha_1,\ \gamma_1,$ and ϵ_1, from the further data fitting. Here the ratio of the data to the free parameters is 5:1, which lies within the recommended range of 5:1 to 10:1 for a reasonable parameter estimate Schunn and Wallach (2005). Furthermore, to analyze the identifiability of the estimated four parameters, we use the sensitivity-based method H. Miao et al. (2011), in which we obtained the rank of the matrix $\mathcal{S}^T\mathcal{S}$. For our case with four parameters estimated, the obtained full rank (Rank = 4) of the matrix $\mathcal{S}^T\mathcal{S}$ confirms that these four parameters are practically identifiable for the model and the data used in this study. All the computations were carried out in MATLAB (The Math Works. Inc.) using its various routines, including "ode45" (ODE solver) and "fmincon" (minimizer).

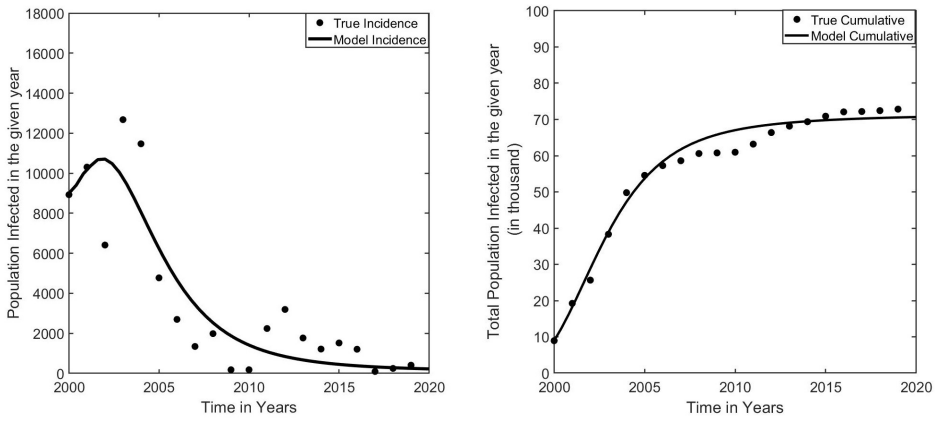

Figure 7: Data fitting and Model validation. (a) The recorded yearly cases of measles in Nepal (dot) along with the best fit of the model (line). (b) The cumulative recorded cases of measles in Nepal (dot) along with the model prediction of the cumulative cases (line).

Our estimates show that the transmission rate (β), the rate of un-monitored vaccination (α_1), the rate of recovery from un-monitored vaccination (γ_1), and the effectiveness of un-monitored vaccination (ϵ_1) are 63.0238 (95% CI: 63.0188–63.0288), 0.31 (95% CI: 0.0902–0.5298), 0.1 (95% CI: 0.0858–0.1142), and 0.5082 (95% CI: 0.4926–0.5238), respectively (Table 1). We note that the confidence interval of the parameter α_1 appears

to be large compared to other parameters for this particular data set. However, we consider this parameter a control parameter and vary widely for the analysis of the vaccination program; thus, one set of confidence intervals does not significantly impact the main results of our study.

Table 1: Values of estimated and fixed parameters.

Parameters $(yr)^{-1}$	Description	Baseline Value	Confidence Interval	Sources
α_2	Monitored vaccination rate	0.02	Fixed	Assumed
α_1	Un-monitored vaccination rate	0.31	[0.0902 0.5298]	Data Fitting
β	Transmission rate	63.02	[63.01 63.03]	Data Fitting
ϵ_1	Effectiveness of un-monitored vacc.	0.51 (Dim.less)	[0.49 0.52]	Data Fitting
ϵ_2	Effectiveness of monitored vacc.	0.9 (Dim.less)	Fixed	Assumed
μ	Removed rate	0.0667	Fixed	Assumed
γ_1	U_V immunity rate	0.1	[0.086 0.12]	Data Fitting
γ_2	M_V immuninity rate	0.5	Fixed	Assumed
σ	Disease progress rate	30	Fixed	WHO (2019b)
η	Recovery rate	20	Fixed	WHO (2019b)
δ	Disease-induced death rate	0.01	Fixed	Knoema (2017)

3.2.6 Positivity and Boundedness

We first establish the biological or epidemiological validation of the model by proving the non-negativity and the boundedness of the solution of the system of equations.

3.2.6.1 Positivity of the Solutions

Theorem 3.2.1 *If* $S(0) > 0,\ U_V(0) \geq 0,\ M_V(0) \geq 0,\ E(0) \geq 0,\ I(0) \geq 0,$ *and* $I_M(0) \geq 0$, *then the set of solution* $\{S(t),\ U_V(t),\ M_V(t),\ E(t),\ I(t),\ I_M(t)\}$ *of the system (3.1–3.6) is positive for all* $t \geq 0$.

Proof: From (3.1), $\dfrac{dS}{dt} > -(\beta I/N + \mu + \alpha_1 + \alpha_2)S$ which implies

$$S(t) > S(0)exp\bigg(-\int_0^t (\beta I(s)/N(s) + \mu + \alpha_1 + \alpha_2)\, ds\bigg).$$

Since $S(0) > 0,\ S(t) > 0,\ \forall t > 0$ confirming the positivity of $S(t)$. Similarly from (3.2–3.6), we have

$$\begin{aligned}
\frac{dU_V}{dt} &\geq -\left(\gamma_1 + \mu + (1-\epsilon_1)\beta I/N\right) U_V, \\
\frac{dM_V}{dt} &\geq -\left(\mu + \gamma_2 + (1-\epsilon_2)\beta I/N\right) M_V, \\
\frac{dE}{dt} &\geq -\left(\mu + \sigma\right) E,\ \frac{dI}{dt} \geq -(\mu + \eta + \delta) I, \\
\text{and}\ \ \frac{dI_M}{dt} &\geq -\mu I_M.
\end{aligned}$$

Then we get

$$\begin{aligned}
U_V(t) \geq & U_V(0) exp\left(-\int_0^t \left((1-\epsilon_1)\beta I(s)/N(s) + \mu + \gamma_1\right) ds\right) \geq 0, \\
M_V(t) \geq & M_V(0) exp\left(-\int_0^t \left((1-\epsilon_2)\ \beta I(s)/N(s) + \mu + \gamma_2\right) ds\right) \geq 0, \\
E(t) \geq & E(0) exp\left(-(\mu+\sigma)t\right) \geq 0,\ I(t) \geq I(0) exp\left(-(\mu+\eta+\delta)t\right) \geq 0, \\
\text{and} I_M(t) \geq & I_M(0) exp\left(-\mu t\right) \geq 0, \forall t > 0,
\end{aligned}$$

for $U_V(0) \geq 0,\ M_V(0) \geq 0,\ E(0) \geq 0,\ I(0) \geq 0$, and $I_M(0) \geq 0$. Therefore, $U_V(t),\ M_V(t),\ E(t),\ I(t),\ I_M(t) \geq 0,\ \forall t > 0$, showing the positivity of the solution set of the system (3.1–3.6). □

3.2.6.2 Boundedness and Invariant Region

Adding all differential equations (3.1–3.6), we get $dN/dt = \Lambda - \mu N - \delta I \leq \Lambda - \mu N$, which provides $N(t) \leq N(0)e^{-\mu t} + \Lambda/\mu(1 - e^{-\mu t})$ and $\limsup_{t\to\infty} N(t) \leq \Lambda/\mu$, showing that the total population is ultimately bounded by Λ/μ. Hence the solution set bounded by Λ/μ is positively invariant in the feasible region

$$\Omega = \left\{(S(t),\ U_V(t),\ M_V(t),\ E(t),\ I(t),\ I_M(t)) \in \mathbb{R}^6_+ : N(t) \leq \Lambda/\mu\right\}.$$

3.3 Modeling: Adult-Child Vaccination Model

We consider measles cases in adults, a more mobile critical group typically not included in regular immunization programs. We introduce a novel deterministic model, incorporating monitored vaccination for children and adults to assess the impact of these adult-child vaccination approaches on measles eradication in Nepal. The model

is validated using fifteen weeks of measles data from Nepal. Our model analysis evaluates the local and global stability of disease-free equilibrium and the existence of at least one endemic equilibrium. We simulate our model to assess the impact of monitored adult-child vaccination programs on reducing measles transmission in Nepal and eventually eradicating the disease over a period of time.

3.3.1 Model Formulation

We categorize the population into two different age groups (0-15 yrs and above 15 yrs) based on the data Dall (14 March 2023) and develop a deterministic mathematical model ($SVEII_m$) to describe the transmission dynamics of measles among those two groups. Since measles can be prevented by complete doses of vaccines and individuals gain lifelong immunity after recovery from infection Edward et al. (2015), we do not consider re-infection in our model. The indices C and A represent the child (0-15 yrs) and adult (above 15) groups, respectively. The group of children and adults are divided into six distinct compartments ($S_C,\ U_C^V,\ M_C^V,\ E_C,\ I_C,\ I_{mC}$) and ($S_A,\ U_A^V,\ V_A,\ E_A,\ I_A,\ I_{mA}$), respectively, as shown in Figure 8. Λ is the recruitment rate of newborns, and ψ is the maturation rate of a child becoming an adult.

Building an effective vaccination program is often difficult, especially when parents lack adequate health knowledge and are skeptical about vaccines. One way to improve the efficacy of immunization is to incorporate a monitored vaccination program so that children who signed up for it receive their immunizations accurately and on time. The unmonitored class includes children not enrolled in the monitored program. The children in this class may frequently skip the complete vaccine doses on time, presumably due to the lack of parents' health consciousness and/or the lack of supervision for proper immunization. On the other hand, the monitored class includes the children enrolled in the monitored program, which ensures enrolled members with supervision for timely immunization of complete doses. Our objective in this study is to develop a model to evaluate such monitored vaccination programs for controlling measles in both children and adults, with the goal of eradicating measles.

In this context, we assume children engaged in the monitored vaccination program exhibit a lower vulnerability to diseases and a greater probability of acquiring immunity due to increased attention and regular supervision, in contrast to children under unsupervised immunization schemes. Consequently, the children eligible for vaccination are divided into two distinct groups: the Un-monitored Vaccination Group (U_A^V),

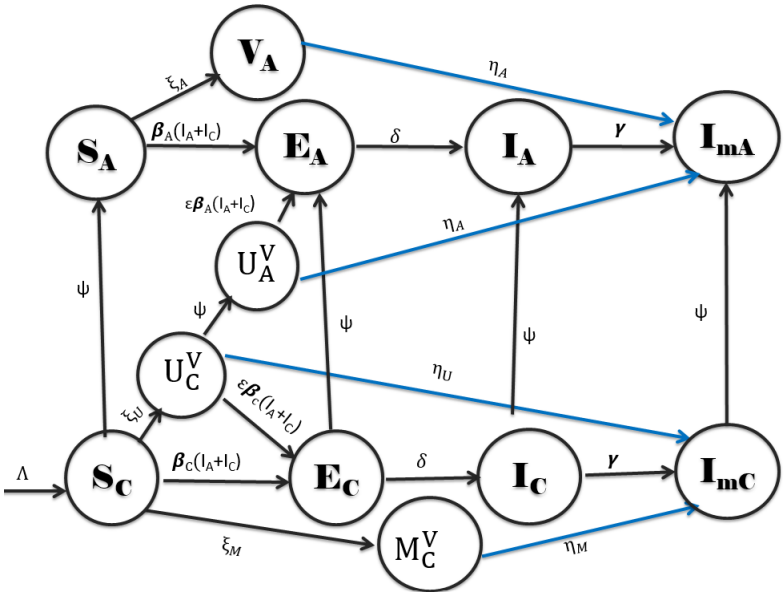

Figure 8: Schematic diagram of the model: The group of children is divided into six distinct compartments: S_C (Susceptible), U_C^V (Un-monitored Vaccinated), M_C^V (Monitored Vaccinated), E_C (Exposed), I_C (Infectious), and I_{mC} (Immune). Similarly, the adult age group is divided into six subgroups ($S_A,\ U_A^V, V_A,\ E_A,\ I_A,\ I_{mA}$).

consisting of vaccinated children undergoing routine vaccination without supervision, and the Monitored Vaccination Group (M_C^V), comprising children vaccinated under supervision to ensure timely administration. In addition, we consider the Adult Vaccination Group (V_A), which consists of vaccinated adults under supervision through the catch-up vaccination program.

Upon successfully receiving both vaccine doses per the recommended schedule, we assume that the Monitored Vaccination Group and Adult Vaccination Group will attain sufficient immunization and become non-susceptible to diseases. η_M and η_A represent the rate of immunization of the Monitored Vaccination Group and Adult Vaccination Group, respectively, and β_C represents the rate of the fully susceptible children becoming infected.

Given the possibility of incomplete administration of vaccine doses within the Un-monitored Vaccination Group, there remains a potential susceptibility to diseases. To capture this infection, we account for disease transmission within this group at a rate of $\epsilon\beta_C$, where $(1-\epsilon)$ represents the vaccine's effectiveness. Additionally, we consider a different infection rate, denoted by β_A, for the adult group, assuming that measles transmission is low among adults. The complete description of the parameters is given in Table 2.

Table 2: Description of the parameters

Symbols	Description
Λ	Recruitment rate to children group
ξ_U, ξ_M	Un-monitored and Monitored children Vaccination rate
ξ_A	Adult Vaccination rate
β_C, β_A	Transmission rate on the children and adults
μ	Natural death rate
γ	Rate of being immune after recovery from infection
ψ	Maturation rate
$(1-\epsilon)$	Effectiveness of the vaccination
η_A	Rate of being immune of Un-monitored vaccinated adults
η_U, η_M	Rate of being immune of Un-monitored, Monitored vaccinated children
δ	Incubation period
d	Disease induced death

The equations of the dynamical system describing measles transmission are as follows:

$$\frac{dS_C}{dt} = \Lambda - (\mu + \xi_M + \xi_U + \psi)\, S_C - \beta_C\, (I_C + I_A)\, S_C, \tag{3.7}$$

$$\frac{dS_A}{dt} = \psi\ S_C - \beta_A\, (I_C + I_A)\, S_A - \mu\ S_A - \xi_A S_A, \tag{3.8}$$

$$\frac{dU_C^V}{dt} = \xi_U\ S_C - \epsilon\beta_C\, (I_C + I_A)\, U_C^V - (\mu + \eta_U + \psi)\, U_C^V, \tag{3.9}$$

$$\frac{dU_A^V}{dt} = \psi U_C^V - \eta_A U_A^V - \beta_A \epsilon\, (I_C + I_A)\, U_A^V - \mu U_A^V, \tag{3.10}$$

$$\frac{dV_A}{dt} = \xi_A S_A - V_A\, (\mu + \eta_A)\,, \tag{3.11}$$

$$\frac{dM_C^V}{dt} = \xi_M S_C - (\mu + \eta_M)\, M_C^V, \tag{3.12}$$

$$\frac{dE_C}{dt} = \beta_C\, (I_C + I_A)\, S_C + \beta_C \epsilon\, (I_C + I_A)\, U_C^V - (\delta + \mu + \psi) E_C, \tag{3.13}$$

$$\frac{dE_A}{dt} = \beta_A\, (I_C + I_A)\, S_A + \beta_A \epsilon\, (I_C + I_A)\, U_A^V + \psi E_C - (\delta + \mu) E_A, \tag{3.14}$$

$$\frac{dI_C}{dt} = \delta E_C - (\gamma + d + \mu + \psi) I_C, \tag{3.15}$$

$$\frac{dI_A}{dt} = \delta E_A + \psi E_C - (\gamma + d + \mu) I_A, \tag{3.16}$$

$$\frac{dI_{mC}}{dt} = \gamma I_C + \eta_M M_C^V - (\mu + \psi) I_{mC} + \eta_U U_C^V, \tag{3.17}$$

$$\frac{dI_{mA}}{dt} = \eta_A (U_A^V + V_A) + \gamma I_A - \mu I_{mA} + \psi I_{mC}. \tag{3.18}$$

3.3.2 Data Source

The publicly available data used in this work is obtained from the official website of the World Health Organization (WHO) World Health Organization (14 March 2023). From November 24, 2022, to March 10, 2023, a total of 690 cases of measles were recorded in western Nepal, spanning outbreaks in seven districts: Banke (327 cases), Surkhet (62 cases), Bardiya (49 cases), Kailali (39 cases), Kanchanpur (27 cases), Bajura (13 cases), and Dang (12 cases). Additionally, three districts in eastern Nepal also reported cases: Mahottari (103 cases), Sunsari (34 cases), and Morang (24 cases). The distribution of measles cases is shown in Figure 9. Among these reported cases, one death was reported, indicating a Case Fatality Rate (CFR) of 0.14% Dall (14 March 2023).

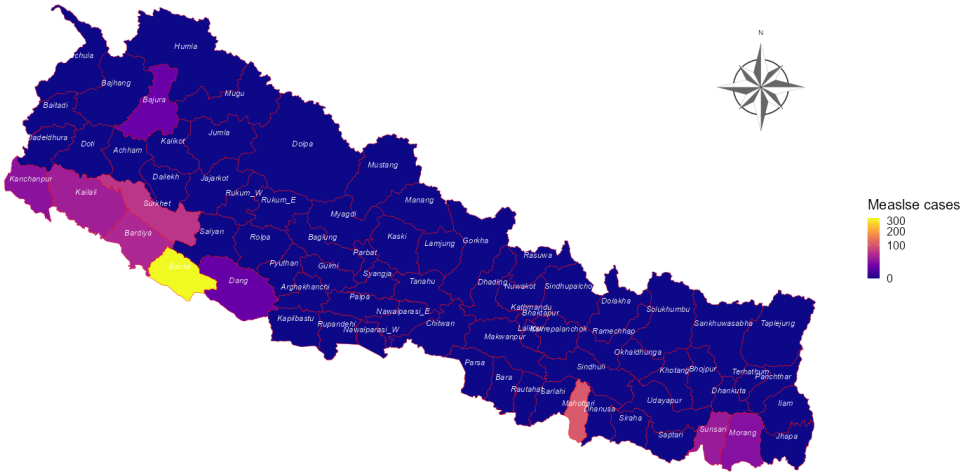

Figure 9: Measles cases in different parts of Nepal from November 24, 2022, to March 10, 2023. The map was created using the cartography package in R 4.3.1.

3.3.3 Data Fitting, Model Validation, and Parameter Estimation

Since measles cases were found only in ten districts of Nepal (Figure 9), we considered the population corresponding to only these ten districts with a total of $N(0) = 6,564,070$ Office. Moreover, as the cases appeared only in a few villages of these ten districts, the whole population is less likely to be in the contact network. Therefore, we assume α is a portion of the total population, so only $\alpha N(0)$ is in the measles transmission contact network. In Nepal, the children population aged up to 14 years is 27.4% Statista (2023), so we assumed 29% of the total population aged up to 15

years and took children and adults initial population

$$N_C(0) = 0.29\alpha N(0) \text{ and } N_A(0) = 0.71\alpha N(0).$$

The vaccinated population in Nepal is about 87 to 93% WHO (2023b), and assuming children are more vaccinated than adults, we took 91% of children and 89% of adults were vaccinated. Thus, we took 9% and 11% of unvaccinated children and adults as respective susceptibles, i.e., $S_C(0) = 0.09\alpha N_C(0)$ and $S_A(0) = 0.11\alpha N_A(0)$. Since there was no adequately monitored vaccination or catch-up program for adult vaccination in Nepal, we took $M_C^V(0) = 50,\ V_A = 0$. Since vaccine effectiveness for measles is 77 to 86% Ichimura et al. (2022); Kumar et al. (2023); Lochlainn et al. (2019), we took 89% as the immune population, giving $I_{mA}(0) = 0.79\alpha N_A(0)$ and $I_{mC}(0) = 0.81\alpha N_C(0)$. The remaining populations are taken as $U_C^V(0)$ and $U_A^V(0)$. Following the magnitude of data, we assume that the outbreak begins with a small number of exposed and infected individuals and took

$$E_C(0) = 5,\ E_A(0) = 3,\ I_C(0) = 2,\ I_A(0) = 1.$$

For this study, individuals under fifteen were categorized as children, giving the maturation rate of $\psi = 1/(15 \times 52) = 0.0013$ per week. Since the average lifespan for Nepal in 2023 is approximately 72 years Macrotrends, we took the natural death rate as $1/(72 \times 52)$ per week. During the period of data collected, no immunization program was in place for adults, so we took both the rate of adult vaccination (ξ_A) and the rate of being immune through adult vaccination (η_A) as zero. We also assume the rate of adults being immune through un-monitored vaccination (η_A) to be zero.

We considered the incubation period for measles to be 10 days (range: 10-14 days) WHO (2023a), implying $\delta = 0.7$ per week. Considering the recovery period from the disease is around 15 days (range: 7-23 days) World Health Organization (2023), we obtain $\gamma = 1/2$ per week. Using the Case Fatality Rate (CFR) of 0.14% in Nepal Dall (14 March 2023); World Health Organization (14 March 2023) in the disease-induced death rate formula

$$d = \frac{-ln(1 - 0.14/100)}{T},$$

given in the previous study Pantha et al. (2021) with $T = 15$ weeks, we obtain $d = 9.3399 \times 10^{-5}$ per week.

In line with WHO guidelines, children receive their first vaccine dose at 9 months of age and the second dose at 15 months MoHP (a), with a six-month interval between

two doses. Accounting for an average vaccine effectiveness of 80 % Min-Shi et al. (1992); WHO (2019a), we adopted $\epsilon = 1 - 0.8 = 0.2$. Since the outbreaks usually remain for a short term of 15 weeks only, as revealed in the data, we can assume that the birth and the death balance each other, i.e., $\Lambda = \mu \times N$.

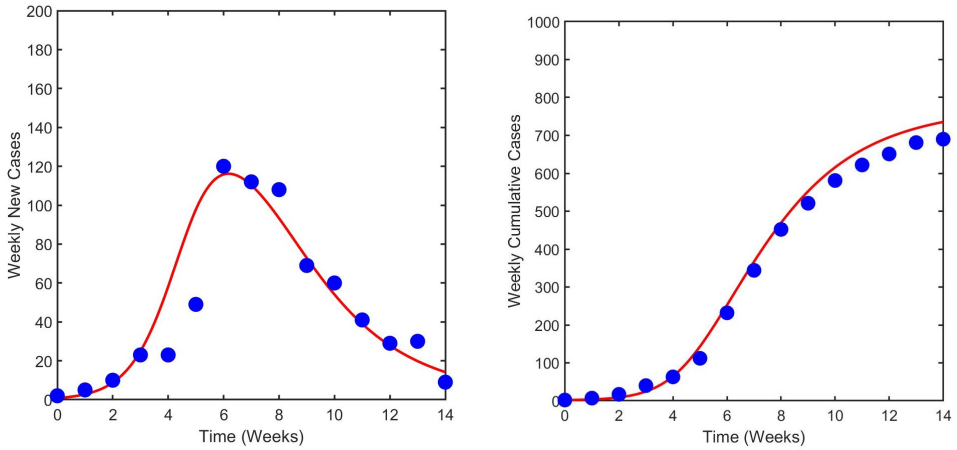

(a) **(b)**

Figure 10: Data fitting and model validation. (a) The recorded weekly cases of measles in Nepal (filled circle) along with the best fit of the model (line). (b) The cumulative recorded measles cases in Nepal (filled circle) along with the model prediction of the cumulative cases (line).

We estimate the parameters β_C, β_A, ξ_U, η_U, η_M, and α by fitting the model with the measles case data from Nepal. From the model, weekly new infections at time t are given by $h(t) = \theta\delta E(t)$, which we obtain using the numerical solutions of the system (3.7-3.18). Here, θ represents the portion of the infection recorded. Then, we estimate the parameters with the help of the nonlinear regression method Motulasky and Christopoulos (2003) that minimizes the following sum of the square residuals:

$$\sum_{k=1}^{15}(h_k - \bar{h}_k)^2,$$

where h_k denotes the model predicted weekly new infection and $\bar{h}_k$ denotes weekly new infection data. All the computations are carried out in MATLAB (The Math Works. Inc.) using its various routines, including "ode45" (ODE solver) and "fmincon" (minimizer).

Our model can fit the data of weekly incidence cases in Nepal well (Figure 10a). In addition, we also show that the model prediction of the cumulative cases agrees well with the cumulative data (Figure 10b), thereby validating our model. The values of

state variables and parameters are given in Table 3 and Table 4, respectively. From our estimation, the transmission rate in children ($\beta_C = 0.00188$) is higher than in adults ($\beta_A = 1.00 \times 10^{-5}$). Despite the low transmission rate among adults, it may still be sufficient to spread the disease and cause obstacles to achieving the mission of measles eradication. Similarly, we obtained the monitored vaccination rate ($\xi_M = 4.777 \times 10^{-6}$) is less than the un-monitored vaccination rate ($\xi_U = 0.0087$), and the rate of being immune from monitored vaccination ($\eta_M = 0.0167$) is higher than the un-monitored vaccination ($\eta_U = 3 \times 10^{-6}$). Our estimates indicate that about 15% of the measles cases were recorded in Nepal ($i.e., \theta = 0.15$) (Table 4).

Table 3: State variables

State Variables	Values	State Variables	Values
$M_C^V(0)$	50	$V_A(0)$	0
$E_C(0)$	5	$E_A(0)$	3
$I_C(0)$	2	$I_A(0)$	1
$S_C(0)$	2,142	$S_A(0)$	6,408
$U_C^V(0)$	2,382	$U_A^V(0)$	5,703
$I_{mC}(0)$	19,271	$I_{mA}(0)$	46,145
$N_C(0)$	23,795	$N_A(0)$	58,256

Table 4: Model parameters

Symbols of Parameters	Values	Source
ξ_U, ξ_M	$0.087, 4.77 \times 10^{-5}$	Data fitting
β_C, β_A	$0.00188, 1.00 \times 10^{-5}$	Data fitting
μ	$1/(72 \times 52)$	Calculated
γ	$1/2$	World Health Organization (2023)
ψ	$1/(15 \times 52)$	Calculated
ϵ	0.2	Min-Shi et al. (1992); WHO (2019a)
η_A	0	Assumed
η_U, η_M	$3 \times 10^{-6}, 0.167$	Data fitting
δ	0.7	World Health Organization (2023)
θ	0.15	Data fitting
d	9.3399×10^{-05}	Calculated
ξ_A	0	Assumed
α	0.01253	Data fitting

3.3.4 Positivity and Boundedness

In the system (3.7 - 3.18), all the state variables are non-negative and should remain non-negative forever since they represent the human population. For the given

non-negative initial conditions, it can be easily verified that system (3.7-3.18) has non-negative solutions at any time t as shown in the following theorem.

Theorem 3.3.1 *If the state variable are non-negative with $S_C > 0$ at time $t = 0$, then the solution set of the system (3.7 - 3.18) is always non-negative and bounded.*

Proof: First, we prove that all the solutions are non-negative. From the system (3.7 - 3.18), we get

$$\begin{aligned}
\frac{dS_C}{dt} &= \Lambda - (\mu + \xi_M + \xi_U + \psi)\, S_C - \beta_C\, (I_C + I_A)\, S_C \\
&> -(\mu + \xi_M + \xi_U + \psi)\, S_C - \beta_C\, (I_C + I_A)\, S_C \\
\Rightarrow S_C &> S_C(0)\, \exp\left(- \int_0^t ((\mu + \xi_M + \xi_U + \psi) + \beta_C\, (I_C + I_A))\, dt \right) \geq 0; \\
\frac{dS_A}{dt} &= \psi\ S_C - \beta_A\, (I_C + I_A)\, S_A - \mu\ S_A - \xi_A\ S_A \\
&> -\beta_A\, (I_C + I_A)\, S_A - \mu\ S_A - \xi_A S_A \\
\Rightarrow S_A &> S_A(0)\, \exp\left(- \int_0^t \beta_A((I_C + I_A) + \mu + \xi_A)\ dt \right) > 0; \\
\frac{dU_C^V}{dt} &= \xi_U\ S_C - \beta_C\ \epsilon\, (I_C + I_A)\, U_C^V\ \ - (\mu + \eta_U + \psi)\, U_C^V \\
&> -\beta_C\ \epsilon\ \ (I_C + I_A)\, U_C^V - (\mu + \eta_U + \psi)\, U_C^V \\
\Rightarrow U_C^V &\geq U_C^V(0)\, \exp \beta_C \epsilon\ \left(- \int_0^t ((I_C + I_A) + (\mu + \eta_U + \psi))\ dt \right) \geq 0;
\end{aligned}$$

$$
\begin{aligned}
\frac{dU_A^V}{dt} &= \psi\ U_C^V - \eta_A\ U_A^V - \beta_A\ \epsilon\,(I_C + I_A)\,U_A^V - \mu\ U_A^V \\
&> -\eta_A\ U_A^V - \beta_A\ \epsilon\ (I_C + I_A)\,U_A^V - \mu\ U_A^V \\
\Rightarrow U_A^V &\geq U_A^V(0)\ \exp\left(-\int_0^t \beta_A\ \epsilon\ (\eta_A + (I_C + I_A) + \mu)\ dt\right) \geq 0; \\
\frac{dV_A}{dt} &= \xi_A S_A - V_A\,(\mu + \eta_A) > -V_A\,(\mu + \eta_A) \\
\Rightarrow V_A &> V_A(0)\ \exp\left(-\int_0^t (\eta_A + \mu)\ dt\right) \geq 0; \\
\frac{dM_C^V}{dt} &= \xi_M\ S_C - (\mu + \eta_M)\,M_C^V \\
&> -(\mu + \eta_M)\,M_C^V \\
\Rightarrow M_C^V &\geq M_C^V(0)\ \exp\left(-\int_0^t ((\mu + \eta_M))\ dt\right) \geq 0; \\
\text{and } \frac{dE_C}{dt} &= \beta_C\,(I_C + I_A)\,S_C + \beta_A\ \epsilon\,(I_C + I_A)\,U_C^V - (\delta + \mu + \psi)E_C \\
&\geq -((\delta + \mu + \psi))E_C \\
\Rightarrow E_C &\geq E_C(0)\ \exp\left(-\int_0^t ((\delta + \mu + \psi))\ dt\right) \geq 0.
\end{aligned}
$$

Similarly, $E_A,\ I_C,\ I_A,\ I_{mC},\ I_{mA}$ are also non-negative. Hence, the solution set $\{S_C, S_A, U_C^V, U_A^V, V_A, M_C^V, E_C, E_A, I_C, I_A, I_{mC}, I_{mA}\}$ of the system (3.7 - 3.18) is always non-negative.

We now prove that these non-negative solutions are bounded. Let $N_h(t)$ be the total human population, i.e., $N_h(t) = S_C(t) + S_A(t) + U_C^V(t) + U_A^V(t) + V_A(t) + M_C^V(t) + E_C(t) + E_A(t) + I_C(t) + I_A(t) + I_{mC}(t) + I_{mA}(t)$. Adding all the equations of the system (3.7 - 3.18), we obtain

$$
\frac{dN_h}{dt} = \Lambda - \mu N_h - d(I_C + I_A) \leq \Lambda - \mu N_h,
$$

which implies

$$
\lim_{t\to\infty} N_h \leq \Lambda/\mu.
$$

Hence, the human population, $N_h(t)$, is ultimately bounded.

Using the above conditions, we have that for any $\alpha > 0$, there exists $t_\alpha > 0$ such that the solution of the system with $t \geq t_\alpha$ lies in the compact set $\Omega = \Omega_h$, where

$$
\Omega_h = \left\{(S_C, S_A, U_C^V, U_A^V, V_A, M_C^V, E_C, E_A, I_C, I_A, I_{mC}, I_{mA}) \in \Re_+^{12} : N_h \leq \Lambda/\mu + \alpha\right\}.
$$

Thus, all the state variables representing the populations are non-negative and bounded.

CHAPTER 4

4. MATHEMATICAL ANALYSIS OF MODELS

In this chapter, we present the mathematical analysis of the models developed in 3. Our model analyses establish the local and global stability of the disease-free equilibrium point for $R_v < 1$, the existence of the endemic equilibrium, and the uniform persistence of the disease for $R_v > 1$. Despite the inability to establish the stability of the endemic equilibrium point in the adult-child vaccination model due to the complexity of the point, we compute the magnitude of the endemic equilibrium. Furthermore, we obtain the vaccinated reproduction number and the effective reproduction number for both cases.

4.1 Analysis of the Monitored Vaccination Model

In this section, we analyze the disease-free equilibrium point and the endemic equilibrium point, as well as their stability with uniform persistence of the monitored vaccination model.

4.1.1 Existence of Equilibria

In this section we discuss the disease-free equilibrium point (DFE) and the endemic equilibrium point of the system (3.1-3.6).

4.1.1.1 Disease Free Equilibrium Point and Formulation of the Vaccinated Reproduction Number

Setting $E = 0$ and $I = 0$ in the system, we obtain DFE: $E^0 = (S^0,\ U_V^0,\ M_V^0,\ 0,\ 0,\ I_M^0)$, where

$$S^0 = \frac{\Lambda}{\alpha_1 + \alpha_2 + \mu},\ U_V^0 = \frac{\alpha_1 \Lambda}{(\alpha_1 + \alpha_2 + \mu)(\gamma_1 + \mu)},$$
$$M_V^0 = \frac{\alpha_2 \Lambda}{(\alpha_1 + \alpha_2 + \mu)(\gamma_2 + \mu)},\ \text{ and } I_M^0 = \frac{\Lambda(\alpha_1\gamma_1(\mu + \gamma_2) + \alpha_2\gamma_2(\mu + \gamma_1))}{\mu(\alpha_1 + \alpha_2 + \mu)(\gamma_1 + \mu)(\gamma_2 + \mu)}.$$

Note that our model implies non-zero immune class I_M^0 at the DFE due to the immunity gained through vaccination.

The vaccinated reproduction number, denoted by R_v, is defined as the average number of secondary cases generated by a single infectious case introduced into the mixed population with susceptible and vaccinated status. Here we formulate the vaccinated reproduction number using the Next Generation method Diekmann and Heesterbeek (2001); Chowell and Hyman (2016); Kuddus et al. (2021); Diekmann et al. (2010); Driessche and Watmough (2002).

Following the Next Generation Matrix method Driessche and Watmough (2002), we divide the system into two groups,

$$\text{infected } \vec{x} = (x_i,\ i = 1, 2) = (E,\ I)$$

$$\text{and uninfected } \ \vec{y} = (y_j,\ j = 1, 2, 3, 4) = (S,\ U_V,\ M_V,\ I_M),$$

as follows:

$$\dot{x}_i = f_i(\vec{x}, \vec{y}) = \mathcal{F}_i(\vec{x}, \vec{y}) - \mathcal{V}_i(\vec{x}, \vec{y}),\ i = 1,\ 2 \text{ and } \ \dot{y}_j = g_j(\vec{x}, \vec{y}),\ j = 1, 2, 3, 4, \quad (4.1)$$

where $\mathcal{F}_i(\vec{x}, \vec{y})$ is the rate of appearance of new infections in the compartment i, and $\mathcal{V}_i(\vec{x}, \vec{y})$ is the difference between the transfer of individuals out of and into the compartment i $(i = 1, 2)$. Here we have

$$\mathcal{F} = \begin{pmatrix} (\beta S + (1-\epsilon_1)\ \beta U_V + (1-\epsilon_2)\ \beta M_V)I/N \\ 0 \end{pmatrix} \text{ and } \mathcal{V} = \begin{pmatrix} (\mu+\sigma)E \\ -\sigma E + (\mu+\eta+\delta)I \end{pmatrix}.$$

It is easy to verify that $\mathcal{F}_i$ and $\mathcal{V}_i$ satisfy the conditions A(1)–A(5) of Driessche and Watmough (2002). As the process provided in Driessche and Watmough (2002), we obtained the Jacobians of $\mathcal{F}$ and $\mathcal{V}$ at the disease free equilibrium point $(D\mathcal{F}(E^0) = F,\ D\mathcal{V}(E^0) = V)$:

$$F = \begin{pmatrix} 0 & (\beta S^0 + (1-\epsilon_1)\ \beta U_V^0 + (1-\epsilon_2)\ \beta M_V^0)/N^0 \\ 0 & 0 \end{pmatrix} \text{ and } V = \begin{pmatrix} \mu+\sigma & 0 \\ -\sigma & \delta+\eta+\mu \end{pmatrix}.$$

Clearly, F is non-negative and V is non singular M-matrix. The next generation matrix FV^{-1} for our model is given by:

$$\begin{pmatrix} \dfrac{\sigma\,(\beta S^0 + (1-\epsilon_1)\ \beta U_V^0 + (1-\epsilon_2)\ \beta M_V^0)}{N^0(\mu+\sigma)(\delta+\eta+\mu)} & \dfrac{(\beta S^0 + (1-\epsilon_1)\ \beta U_V^0 + (1-\epsilon_2)\ \beta M_V^0)}{N^0(\delta+\eta+\mu)} \\ 0 & 0 \end{pmatrix}.$$

Then the vaccinated reproduction number R_v is given by:

$$R_v = \rho(FV^{-1}) = \frac{\beta\sigma\,(S^0 + (1-\epsilon_1)U_V^0 + (1-\epsilon_2)M_V^0)}{N^0(\mu+\sigma)(\delta+\eta+\mu)}.$$

Using the expression of DFE obtained above, we get

$$R_v = \frac{\beta\mu\sigma\left(\alpha_1\left(1-\epsilon_1\right)\left(\gamma_2+\mu\right)+\left(\gamma_1+\mu\right)\left(\alpha_2\left(1-\epsilon_2\right)+\gamma_2+\mu\right)\right)}{\left(\alpha_1+\alpha_2+\mu\right)\left(\gamma_1+\mu\right)\left(\gamma_2+\mu\right)\left(\mu+\sigma\right)(\delta+\eta+\mu)}.$$

Furthermore, as the system (4.1) satisfies all the conditions of (Driessche and Watmough, 2002, Theorem 2), it follows the local stability of the disease-free equilibrium for $R_v < 1$. Moreover, for the verification purpose, we also prove the local stability of DFE by showing the negative real part of eigenvalues in section 4.1.2.1.

4.1.1.2 Endemic Equilibrium Point

Let

$$\lambda^* = \beta I^*/(S^* + U_v^* + M_v^* + E^* + I^* + I_M^*). \tag{4.2}$$

Then solving the full system (3.1–3.6) equated to zero, we get

$$\begin{aligned}
S^* &= \frac{\Lambda}{\alpha_1+\alpha_2+\lambda^*+\mu},\\
U_V^* &= \frac{\alpha_1\Lambda}{Q_1\left(\alpha_1+\alpha_2+\lambda^*+\mu\right)},\\
M_V^* &= \frac{\alpha_2\Lambda}{\left(\gamma_2+\mu\right)\left(\alpha_1+\alpha_2+\mu+\lambda^*(1-\epsilon_2)\right)},\\
E^* &= \frac{\lambda^*\Lambda\left(\alpha_1(1-\epsilon_1)\left(\gamma_2+\lambda^*(1-\epsilon_2)+\mu\right)+Q_1\left(\gamma_2+(\alpha_2+\lambda^*)(1-\epsilon_2)+\mu\right)\right)}{Q_1(\mu+\sigma)\left(\alpha_1+\alpha_2+\lambda^*+\mu\right)\left(\gamma_2+\lambda^*(1-\epsilon_2)+\mu\right)},\\
I^* &= \frac{\lambda^*\Lambda\sigma\left(Q_1\left(\gamma_2+(\alpha_2+\lambda^*)(1-\epsilon_2)+\mu\right)+\alpha_1(1-\epsilon_1)\left(\gamma_2+\lambda^*(1-\epsilon_2)+\mu\right)\right)}{Q_1(\mu+\sigma)\left(\alpha_1+\alpha_2+\lambda^*+\mu\right)(\delta+\eta+\mu)\left(\gamma_2+\lambda^*(1-\epsilon_2)+\mu\right)},\\
I_M^* &= \frac{\Lambda(P_1+P_2P_3)}{Q_1\mu(\mu+\sigma)\left(\alpha_1+\alpha_2+\lambda^*+\mu\right)(\delta+\eta+\mu)\left(\gamma_2+\lambda^*(1-\epsilon_2)+\mu\right)}.
\end{aligned} \tag{4.3}$$

where,

$$\begin{aligned}
Q_1 &= \left(\gamma_1+\lambda^*(1-\epsilon_1)+\mu\right),\\
P_1 &= \alpha_1\left(\gamma_2+(1-\epsilon_2)+\mu\right)\left(\eta(1-\epsilon_1)\lambda^*\sigma-\gamma_1(\mu+\sigma)(\delta+\eta+\mu)\right),\\
P_2 &= \left(\gamma_1+\lambda^*(1-\epsilon_1)+\mu\right),\\
P_3 &= \left(\alpha_2\left(\gamma_2(\mu+\sigma)(\delta+\eta+\mu)+\eta\lambda^*(1-\epsilon_2)\sigma\right)+\eta\lambda^*\sigma\left(\gamma_2+\lambda^*(1-\epsilon_2)+\mu\right)\right).
\end{aligned}$$

Substituting (4.3) into (4.2) and after some simplification, we obtain the following equation in terms of λ^*:

$$\lambda^*(A_3\lambda^{*3}+A_2\lambda^{*2}+A_1\lambda^*+A_0)=0, \tag{4.4}$$

where,

$$
\begin{aligned}
A_3 &= (\delta\mu + (\eta+\mu)(\mu+\sigma))(1-\epsilon_1)(1-\epsilon_2),\\
A_2 &= (1-\epsilon_1)\left((1-\epsilon_2)P + \alpha_1 Q + \alpha_2 Q\right) + (1-\epsilon_2)Q\left(\gamma_1+\mu\right) + Q\left(\gamma_2+\mu\right),\\
A_1 &= (1-\epsilon_1)P\left(\gamma_2+\mu\right) + \left(\gamma_1+\mu\right)\\
&\quad \left((1-\epsilon_2)\left(\alpha_1(\mu+\sigma)(\delta+\eta+\mu) + P + \alpha_2 Q\right) + Q\left(\gamma_2+\mu\right)\right) + (1-\epsilon_1)\\
&\quad \left(\alpha_2\left(\left(\gamma_2+\mu\right)(\mu+\sigma)(\delta+\eta+\mu) - \beta(1-\epsilon_2)\mu\sigma\right) + \alpha_1\left(Q\left(\gamma_2+\mu\right) - \beta(1-\epsilon_2)\mu\sigma\right)\right),\\
A_0 &= (1-R_v)\left(\alpha_1+\alpha_2+\mu\right)\left(\gamma_1+\mu\right)\left(\gamma_2+\mu\right)(\mu+\sigma)(\delta+\eta+\mu),\\
P &= \mu\left((\delta+\eta+\mu)(\mu+\sigma) - \beta\sigma\right),\\
Q &= \delta\mu + (\eta+\mu)(\mu+\sigma).
\end{aligned}
$$

Note that $\lambda^* = 0$ corresponds to the disease-free equilibrium point, and the endemic equilibrium points are given by the solutions of $A_3\lambda^{*3} + A_2\lambda^{*2} + A_1\lambda^* + A_0 = 0$. Here, $A_3 > 0$ and $A_0 < 0$ for $R_v > 1$, so the equation (4.4) has at least one positive root for $R_v > 1$. The positiveness of λ^* implies the positiveness of I^* and E^*. Thus, we conclude that if $R_v > 1$, the system (3.1–3.6) has at least one endemic equilibrium point given by (4.3).

4.1.2 The Global Dynamics Analysis

In this section, we first establish the local and global stability of the disease-free equilibrium when $R_v < 1$ and then prove the persistence of the disease when $R_v > 1$.

4.1.2.1 Local Stability Analysis of the Disease Free Equilibrium Point

Theorem 4.1.1 *The disease-free equilibrium point of the system (3.1–3.6) is locally asymptotically stable if $R_v < 1$ and unstable if $R_v > 1$.*

Proof:

Jacobian of the system (3.1–3.6) at the disease free equilibrium point E^0 is $J = \begin{pmatrix} A_{3\times3} & B_{3\times3} \\ C_{3\times3} & D_{3\times3} \end{pmatrix}$ where,

$$
A_{3\times3} = \begin{pmatrix} -(\alpha_1+\alpha_2+\mu) & 0 & 0 \\ \alpha_1 & -(\gamma_1+\mu) & 0 \\ \alpha_2 & 0 & -(\gamma_2+\mu) \end{pmatrix},
$$

$$B_{3\times3} = \begin{pmatrix} 0 & -\beta S^0/N^0 & 0 \\ 0 & -\beta U_V^0(1-\epsilon_1)/N^0 & 0 \\ 0 & -\beta M_V^0\,(1-\epsilon_2)\,/N^0 & 0 \end{pmatrix},\ C_{3\times3} = \begin{pmatrix} 0 & 0 & 0 \\ 0 & 0 & 0 \\ 0 & \gamma_1 & \gamma_2 \end{pmatrix},$$

$$D_{3\times3} = \begin{pmatrix} -(\mu+\sigma) & \beta\left(S^0 + U_V^0(1-\epsilon_1) + M_V^0(1-\epsilon_2)\right)/N^0 & 0 \\ \sigma & -(\delta+\eta+\mu) & 0 \\ 0 & \eta & -\mu \end{pmatrix}.$$

The eigenvalues of the matrix J are

$$\begin{aligned} &\lambda_1 = -\mu,\ \lambda_2 = -\left(\alpha_1+\alpha_2+\mu\right),\ \lambda_3 = -\left(\gamma_1+\mu\right),\ \lambda_4 = -\left(\gamma_2+\mu\right), \\ &\lambda_5 = \frac{1}{2}\left(-(\delta+\eta+2\mu+\sigma) - \sqrt{(\delta+\eta+2\mu+\sigma)^2 + 4\left(R_v-1\right)(\mu+\sigma)(\delta+\eta+\mu)}\right), \\ &\lambda_6 = \frac{1}{2}\left(-(\delta+\eta+2\mu+\sigma) + \sqrt{(\delta+\eta+2\mu+\sigma)^2 + 4\left(R_v-1\right)(\mu+\sigma)(\delta+\eta+\mu)}\right). \end{aligned} \tag{4.5}$$

Since all the eigenvalues are negative if $R_v < 1$, E^0 is locally asymptotically stable if $R_v < 1$. □

4.1.2.2 Global Stability of Disease Free Equilibrium Point

In the following theorem, we prove that $R_v < 1$ asserts the global stability of the DFE.

Theorem 4.1.2 *If $R_v < 1$, the disease-free equilibrium point E^0 of the system (3.1–3.5) is globally asymptotically stable in $\mathbb{R}^6$.*

Proof: The Jacobian corresponding to (3.4) and (3.5) at the disease-free equilibrium point E^0 is

$$J_0 = \begin{pmatrix} -\mu-\sigma & \dfrac{\beta S^0}{N^0} + \dfrac{(1-\epsilon_1)\ \beta U_V^0}{N^0} + \dfrac{(1-\epsilon_2)\ \beta M_V^0}{N^0} \\ \sigma & -(\delta+\eta+\mu) \end{pmatrix}.$$

The spectral bound of J_0 is defined as: $s(J_0) = \max\{Re(\lambda) : \lambda \text{is an eigenvalue of } J_0\}$. Using the theorem 4.1.1, we conclude:

1. $R_v = 1$ if and only if $s(J_0) = 0$.
2. $R_v < 1$ if and only if $s(J_0) < 0$.
3. $R_v > 1$ if and only if $s(J_0) > 0$.

If $R_v < 1$ then $s(J_0) < 0$. Also, we can obtain a sufficiently small positive number γ such that $s(J_\gamma) < 0$, where

$$J_\gamma = \begin{pmatrix} -\mu - \sigma & \frac{\beta(S^0+\gamma)}{\Lambda/\mu-\gamma} + \frac{(1-\epsilon_1)\beta(U_V^0+\gamma)}{\Lambda/\mu-\gamma} + \frac{(1-\epsilon_2)\beta(M_V^0+\gamma)}{\Lambda/\mu-\gamma} \\ \sigma & -(\delta+\eta+\mu) \end{pmatrix}.$$

From the subsections 3.2.6 and 4.1.1, $N(t) \to \Lambda/\mu$ and $S(t) \to S^0$ as $t \to \infty$ for all $\gamma > 0$. Therefore, there exists $t_1 > 0$ such that $\forall t \geq t_1$, we have $S \leq (S^0+\gamma),\ U_v \leq (U_v^0+\gamma),\ M_v \leq (M_v^0+\gamma),\ N \geq (\Lambda/\mu-\gamma)$. From (3.4) and (3.5), it follows that

$$\begin{aligned}
\frac{dE}{dt} =& \frac{\beta S}{N} I + \frac{(1-\epsilon_1)\ \beta U_V}{N} I + \frac{(1-\epsilon_2)\ \beta M_V}{N} I - (\mu+\sigma)E \\
\leq& \frac{\beta(S^0+\gamma)}{\Lambda/\mu-\gamma} I + \frac{(1-\epsilon_1)\ \beta(U_V^0+\gamma)}{\Lambda/\mu-\gamma} I + \frac{(1-\epsilon_2)\ \beta(M_V^0+\gamma)}{\Lambda/\mu-\gamma} I - (\mu+\sigma)E, \\
\frac{dI}{dt} =& \sigma E - (\mu+\eta+\delta)I. \\
\frac{dE}{dt} &= \frac{\beta(S^0+\gamma)}{\Lambda/\mu-\gamma} I + \frac{(1-\epsilon_1)\ \beta(U_V^0+\gamma)}{\Lambda/\mu-\gamma} I + \frac{(1-\epsilon_2)\ \beta(M_V^0+\gamma)}{\Lambda/\mu-\gamma} I - (\mu+\sigma)E, \\
\frac{dI}{dt} &= \sigma E - (\mu+\eta+\delta)I,\ \ \forall\ t \geq t_1.
\end{aligned} \tag{4.6}$$

Clearly, the system (4.6) has the Jacobian J_γ, which is irreducible with non-negative off-diagonal elements. Then $s(J_\gamma)$ is simple and associated with strongly positive eigenvector $\tilde{v}, \forall\ t \geq t_1$ Smith and Waltman (1995). For any solution $\psi(t)$ of the system (4.6) with non-negative initial value $\psi(0)$, there is a sufficiently large positive number $\zeta > 0$ such that $(E(t_1), I(t_1)) \leq \zeta\tilde{v}$. It is easy to see that $V(t) = \zeta e^{s(J_\gamma)(t-t_1)}\tilde{v}, \forall\ t \geq t_1$ is a solution of (4.6) with $V(t_1) = \zeta\tilde{v}$. Then by the comparison principle (Smith and Waltman, 1995, Theorem B.1), it follows that $(E(t), I(t)) \leq \zeta\tilde{v},\ \ \forall t \geq t_1$. Since $s(J_\gamma) < 0$, we get

$$\lim_{t\to\infty} E(t) = 0,\ \lim_{t\to\infty} I(t) = 0,$$

which implies that (3.1) is asymptotic to the following equation:

$$\begin{aligned}
&\frac{dS}{dt} = \Lambda - (\mu+\alpha_1+\alpha_2)\, S, \\
\Rightarrow\ &S(t) = C_1 e^{-(\mu+\alpha_1+\alpha_2)\,t} + \frac{\Lambda}{(\mu+\alpha_1+\alpha_2)}\left(1 - e^{-(\mu+\alpha_1+\alpha_2)\,t}\right),\ \forall t \geq t_1.
\end{aligned} \tag{4.7}$$

Hence, we get $\lim_{t\to\infty} S(t) = \dfrac{\Lambda}{(\mu+\alpha_1+\alpha_2)}$. Solving the system of differential equations (3.2 & 3.11) together with the help of (3.1), we get

$$U_V = \frac{\alpha_1\Lambda}{(\alpha_1+\alpha_2+\mu)(\gamma_1+\mu)} + c_1 e^{-r_1 t} + c_2 e^{-r_2 t}$$

$$M_V = \frac{\alpha_2 \Lambda}{(\alpha_1 + \alpha_2 + \mu)(\gamma_2 + \mu)} + c_3 e^{-k_1 t} + c_4 e^{-k_2 t},$$

where,

$$r_1 = k_1 = \alpha_1 + \alpha_2 + \mu,\ r_2 = \gamma_1 + \mu,\ \text{and}\ \ k_2 = \gamma_2 + \mu.$$

Thus, we get

$$\lim_{t\to\infty} U_V(t) = \frac{\alpha_1 \Lambda}{(\mu + \alpha_1 + \alpha_2)\,(\gamma_1 + \mu)}, \tag{4.8}$$

$$\lim_{t\to\infty} M_V(t) = \frac{\alpha_2 \Lambda}{(\mu + \alpha_1 + \alpha_2)\,(\gamma_2 + \mu)}. \tag{4.9}$$

In the limiting case, we can further verify that $\lim_{t\to\infty} I_M(t) = I_M^0$. Hence if $R_v < 1$, the disease-free equilibrium point E^0 of the system (3.1–3.5) is globally asymptotically stable. □

4.1.2.3 Uniform Persistence

The disease is endemic if the system is uniformly persistent. The system (3.1–3.6) is said to be uniformly persistent if there exists $\zeta > 0$ such that

$$(S(t),\ U_V(t),\ M_V(t),\ E(t),\ I(t),\ I_M(t)) \in \Gamma$$

satisfying

$$\lim_{t\to\infty} \text{Inf}\ E \geq \zeta,\ \ \lim_{t\to\infty} \text{Inf}\ I \geq \zeta. \tag{4.10}$$

Here it is enough to consider the reduced system (3.1-3.5). We first define the sets

$$\Gamma^o = \{(S, U_V, M_V, E, I) \in \mathbb{R}^5 : I \neq 0 \text{ or } \ E \neq 0\}, \tag{4.11}$$

$$\partial\Gamma^o = \{(S, U_V, M_V, E, I) \in \mathbb{R}^5 : I = 0, E = 0\}. \tag{4.12}$$

We have

$$\Gamma^o \cup \partial\Gamma^o = \Gamma \text{ and } \Gamma^o \cap \partial\Gamma^o = \phi,$$

which implies that $\partial\Gamma^o$ is relatively closed in $\Gamma = (S, U_V, M_V, E, I) \in \mathbb{R}^5$.

To establish the disease persistence for $R_v > 1$, we now prove the following theorem.

Theorem 4.1.3 *If $R_v > 1$, then the system (3.1–3.5) is uniformly persistent with respect to $(\Gamma^0, \partial\Gamma^0)$ in the sense that there is a positive constant $\zeta > 0$ such that every solution $(S(t),\ U_V(t),\ M_V(t),\ E(t),\ I(t))$ of (3.7–3.5) with*

$$(S(0),\ U_V(0),\ M_V(0),\ E(0),\ I(0)) \in \Gamma^0$$

satisfies $\lim_{t\to\infty} Inf\ E \geq \zeta,\ \ \lim_{t\to\infty} Inf\ I \geq \zeta$.

Proof: Let $\psi(t)p$ be the solution function of system (3.1–3.5) with initial value p. We can show the solution $(\psi(t)p),\ t>0$ is uniformly persistent with respect to $(\Gamma^o, \partial\Gamma^o)$ Mutua et al. (2015). For any $(S(0),\ U_V(0),\ M_V(0),\ E(0),\ I(0)) \in \Gamma^0$, (3.1–3.11) provide

$$S(t) = \exp\left(-\int_0^t a(x_1)dx_1\right)\left[\int_0^t \exp\left(\int_0^y a(x_1)dx_1\right) b(y)dy + S(0)\right],$$
$$U_V(t) = \exp\left(-\int_0^t a^*(x_1)dx_1\right)\left[\int_0^t \exp\left(\int_0^y a^*(x_1)dx_1\right) b^*(y)dy + U_V(0)\right],$$
$$M_V(t) = \exp\left(-\int_0^t a^o(x_1)dx_1\right)\left[\int_0^t \exp\left(\int_0^y a^o(x_1)dx_1\right) b^o(y)dy + M_V(0)\right],$$

where $a=\alpha_1+\alpha_2+\mu+\beta I/N,\ b=\Lambda,\ a^*=\gamma_1+\mu+(1-\epsilon_1)\beta I/N,\ b^*=\alpha_1 S,\ a^o=\gamma_2+\mu+(1-\epsilon_2)\beta I/N,$ and $b^o=\alpha_2 S$. Here $\Lambda>0$ implies $S(t)>0$. This follows $U_V(t)>0,\ M_V(t)>0,\ \forall\ t>0$. Thus the non-diseased variables $S(t),\ U_V(t),$ and $M_V(t)$ are positive.

Defining the two sets,

$$M_\partial = \{p \in \partial\Gamma_o : \psi(t)p \in \partial\Gamma_o\},$$
$$\omega(p) = \{q : \psi(t)p \to q \text{ as } t \to \infty\},$$

we claim that $\omega(p)=\{E^0\},\ \forall p \in M_\partial$. If $p(t) \in M_\partial$ then $\psi(t)p \in \partial\Gamma_0$ which implies $I=0$ and $E=0$. From (4.8, 4.9) and (3.1–3.5), as $t\to\infty$ we obtain $S(t), U_V(t)$, and $M_V(t)$ approaching to

$$\frac{\Lambda}{(\mu+\alpha_1+\alpha_2)},\ \frac{\Lambda\alpha_1}{(\mu+\alpha_1+\alpha_2)(\gamma_1+\mu)},\ \text{and}\ \frac{\Lambda\alpha_2}{(\mu+\alpha_1+\alpha_2)(\gamma_2+\mu)},\ \text{respectively,}$$

which is the equilibrium point E^0. Hence $\omega(p)=\{E^0\},\ \forall p \in M_\partial$.

Using the theorem 4.1.2 (Condition 3, $R_v>1$ for $s(J_0)>0$), we can get a sufficiently small $\rho>0$ such that the perturbation J_ρ on J_0 satisfies $s(J_\rho)>0$, (see Mutua et al. (2015),(Kato, 1976, Section II.5.8)) for $R_v>1$, where

$$J_\rho = \begin{pmatrix} -\mu-\sigma & \dfrac{\beta\ (S^0-\rho)}{\Lambda/\mu+\rho} + \dfrac{(1-\epsilon_1)\ \beta\ (U_V^0-\rho)}{\Lambda/\mu+\rho} + \dfrac{(1-\epsilon_2)\ \beta\ (M_V^0-\rho)}{\Lambda/\mu+\rho} \\ \sigma & -\delta-\eta-\mu \end{pmatrix}.$$

Now we claim that disease-free equilibrium point E^0 is uniform weak repeller with any solution $\psi(t)$. For this we need to show

$$\lim_{t\to\infty}\ \text{Sup}\ \left\|\psi(t)p - E^0\right\| \geq \rho, \forall\ p \in \Gamma^0.$$

On contrary, suppose there exists a $p_0 \in \Gamma^0$ such that $\lim_{t\to\infty} \text{Sup } \|\psi(t)p_0 - E^0\| < \rho$. From the subsections 3.2.6 and 4.1.1, $N(t) \to \Lambda/\mu$ and $S(t) \to S^0$ as $t \to \infty$ implying that for all $\rho > 0$ there exists $t_2 > 0$ such that $\forall t \geq t_2$,

$$S \geq (S^0 - \rho),\ U_V \geq (U_V^0 - \rho),\ M_V \geq (M_V^0 - \rho),\ N \leq (\Lambda/\mu + \rho).$$

Then (3.4) and (3.5) follows that,

$$\begin{aligned}
\frac{dE}{dt} =& \frac{\beta S}{N} I + \frac{(1-\epsilon_1)\ \beta U_V}{N} I + \frac{(1-\epsilon_2)\ \beta M_V}{N} I - (\mu+\sigma)E \\
\geq& \frac{\beta(S^0-\rho)}{\Lambda/\mu+\rho} I + \frac{(1-\epsilon_1)\ \beta(U_V^0-\rho)}{\Lambda/\mu+\rho} I + \frac{(1-\epsilon_2)\ \beta(M_V^0-\rho)}{\Lambda/\mu+\rho} I - (\mu+\sigma)E, \\
\frac{dI}{dt} =& \sigma E - (\mu+\eta+\delta)I.
\end{aligned}$$

We consider the following auxiliary equations:

$$\begin{aligned}
\frac{dE}{dt} &= \frac{\beta(S^0-\rho)}{\Lambda/\mu+\rho} I + \frac{(1-\epsilon_1)\ \beta(U_v^0-\rho)}{\Lambda/\mu+\rho} I + \frac{(1-\epsilon_2)\ \beta(M_v^0-\rho)}{\Lambda/\mu+\rho} I - (\mu+\sigma)E, \\
\frac{dI}{dt} &= \sigma E - (\mu+\eta+\delta)I.
\end{aligned} \tag{4.13}$$

Here, J_ρ is the Jacobian of the system (4.13), is irreducible with non-negative off-diagonal elements, then $s(J_\rho)$ is simple and associated with strongly positive eigenvector $\tilde{v}, \forall\ t \geq t_2$, $(E(t_2), I(t_2)) > 0$. Thus there is a positive number $\xi > 0$ such that $(E(t_2), I(t_2)) \geq \xi\tilde{v}$ holds. It is easy to see that $V = \xi e^{s(J_\rho)(t-t_2)}\tilde{v},\ \ \forall\ t \geq t_2$ is a solution of (4.13) with $V(t_2) = \xi\tilde{v}$. Hence by comparison principle (Smith and Waltman, 1995, Theorem B.1), we get

$$(E(t), I(t)) \geq \xi e^{s(J_\rho)(t-t_2)}\tilde{v},\ \ \forall\ t \geq t_2.$$

Also, for $R_v > 1$, we have $s(J_\rho) > 0$, implying $\lim_{t\to\infty} E(t) = \infty$, $\lim_{t\to\infty} I(t) = \infty$, which is a contradiction. This proves that the solution repels from E^0. It follows that forward orbit of any solutions in M_∂ converges to E^0 is isolated in $\mathbb{R}^5$.

Now, we define a stable set of E^0:

$$W^s(E^0) = \{p \in \Gamma :\ d(\psi(t)p, E^0) \to 0 \text{ as } t \to \infty\}.$$

Clearly, $W^s(E^0) \cap \Gamma^0 = \emptyset$. It follows that there is no cycle in M_∂ from E^0 to E^0. Applying (Zhao, 2017, Theorem 1.3.1), we conclude that the system (3.1–3.5) is uniformly persistent, i.e., there exists $\zeta > 0$ satisfying (4.10). □

4.2 Mathematical Analysis of the Adult-Child Vaccination Model

The analysis of equilibria points and stability of disease free equilibrium point for the adult-child vaccination model is presented in this section. Moreover, it also presents the bifurcation diagram.

4.2.1 Disease-free Equilibrium and Reproduction number

Here, we derive the expression of the disease-free and endemic equilibrium points. Taking $E_C^0 = 0,\ E_A^0 = 0,\ I_C^0 = 0,\ I_A^0 = 0$, we obtain the disease-free equilibrium: $E^0 = (S_C^0,\ S_A^0,\ (U_C^V)^0,\ (U_A^V)^0, V_A^0,\ (M_C^V)^0,\ 0,\ 0,\ 0,\ 0,\ I_{mC}^0,\ I_{mA}^0)$, where

$$
\begin{aligned}
S_C^0 &= \frac{\Lambda}{\mu + \xi_M + \xi_U + \psi},\\
S_A^0 &= \frac{\Lambda\psi}{(\xi_A + \mu)\,(\mu + \xi_M + \xi_U + \psi)},\\
(U_C^V)^0 &= \frac{\Lambda\xi_U}{Z\,(\mu + \xi_M + \xi_U + \psi)},\\
(U_A^V)^0 &= \frac{\Lambda\psi\xi_U}{Z(\eta_A + \mu)\,(\mu + \xi_M + \xi_U + \psi)},\\
V_A^0 &= \frac{\Lambda\psi\xi_A}{(\eta_A + \mu)(\xi_A + \mu)\,(\mu + \xi_M + \xi_U + \psi)},\\
(M_C^V)^0 &= \frac{\Lambda\xi_M}{Z_1\,(\mu + \xi_M + \xi_U + \psi)},\\
I_{mC}^0 &= \frac{\Lambda\,(\eta_M\,(\xi_M Z + \eta_U\xi_U) + \mu\eta_U\xi_U)}{ZZ_1(\mu + \psi)\,(\mu + \xi_M + \xi_U + \psi)},\\
I_{mA}^0 &= \frac{\Lambda\psi\,(ZZ_1\eta_A\,(\xi_A(\mu + \psi) + \mu\,(Z_1\xi_M + \eta_M\xi_U)) + \mu^2\,(Z_1\eta_U\xi_U + Z\eta_M\xi_M))}{ZZ_1\mu^2(\mu + \psi)\,(\eta_A + \mu)\,(\mu + \xi_M + \xi_U + \psi)},\\
\text{and } Z &= (\mu + \eta_U + \psi)\,,\ Z_1 = (\mu + \eta_M)\,.
\end{aligned}
$$

Given that a significant portion of the population has already been vaccinated, we adopt a similar approach to our previous study Pokharel et al. (2022) in defining the vaccinated reproduction number, R_v. This is done considering the presence of the vaccinated population, as opposed to an entire population susceptible to infection. The vaccinated reproduction number, R_v, represents the average number of secondary cases resulting from introducing a single infectious case into the mixed population, which comprises individuals with both susceptible and vaccinated status. To calculate R_v,

we utilize the Next Generation Matrix method described in previous studies Diekmann and Heesterbeek (2001); Diekmann et al. (2010); Driessche and Watmough (2002).

Following the Next Generation Matrix method Driessche and Watmough (2002), we divide the system into two groups, infected $\vec{x} = (x_i, i = 1, 2, 3, 4) = (E_C,\ E_A,\ I_C,\ I_A)$ and uninfected $\vec{y} = (y_j, j = 1, 2, 3, 4, 5, 6, 7, 8) = (S_C,\ S_A,\ U_C^V,\ U_A^V,\ V_A,\ M_C^V,\ I_{mC},\ I_{mA})$. We then set $\dot{x_i} = f_i(\vec{x}, \vec{y}) = \mathcal{F}_i(x, y) - \mathcal{V}_i(x, y)$ for $i = 1, 2..4$ and $\dot{y_j} = g_j(\vec{x}, \vec{y})$ for $j = 1, 2..., 8$, where $\mathcal{F}_i(x, y)$ is the rate of appearance of new infections in the compartment i and $\mathcal{V}_i(x, y)$ is the difference between the transfer of individuals out of and into the compartment i for $i = 1, 2, 3, 4$. Here we have

$$\mathcal{F} = \begin{pmatrix} \beta_C(I_C + I_A)S_C \\ \beta_A(I_C + I_A)S_A \\ 0 \\ 0 \end{pmatrix} \text{ and } \mathcal{V} = \begin{pmatrix} -(I_C + I_A)\beta_C U_C^V \epsilon + (\delta + \mu + \psi)E_C, \\ -(I_C + I_A)\beta_A U_A^V \epsilon - E_C\psi + E_A(\delta + \mu), \\ -E_C\delta + I_C(\gamma + d + \mu + \psi), \\ -E_A\delta - I_C\psi + I_A(\gamma + d + \mu), \end{pmatrix}.$$

It is straightforward to confirm that the conditions A(1)-A(5) mentioned in Driessche and Watmough (2002) are satisfied by the sets $\mathcal{F}_i$ and $\mathcal{V}_i$ for $i = 1, 2, 3, 4$. We derive the Jacobian matrices of $\mathcal{F}$ and $\mathcal{V}$ at disease-free equilibrium point (E^0), yielding $D\mathcal{F}(E^0) = F$ and $D\mathcal{V}(E^0) = V$ as follows:

$$F = \begin{pmatrix} 0 & 0 & \beta_C S_C^0 + \beta_C (U_C^V)^0 \epsilon & \beta_C S_C^0 + \beta_C (U_C^V)^0 \epsilon \\ 0 & 0 & \beta_A S_A^0 + \beta_A (U_A^V)^0 \epsilon & \beta_A S_A^0 + \beta_A (U_A^V)^0 \epsilon \\ 0 & 0 & 0 & 0 \\ 0 & 0 & 0 & 0 \end{pmatrix},$$

$$V = \begin{pmatrix} \delta + \mu + \psi & 0 & 0 & 0 \\ -\psi & \delta + \mu & 0 & 0 \\ -\delta & 0 & \gamma + d + \mu + \psi & 0 \\ 0 & -\delta & -\psi & \gamma + d + \mu \end{pmatrix},$$

$$V^{-1} = \begin{pmatrix} \frac{1}{\delta + \mu + \psi} & 0 & 0 & 0 \\ \frac{\psi}{(\delta + \mu)(\delta + \mu + \psi)} & \frac{1}{\delta + \mu} & 0 & 0 \\ \frac{\delta^2 + \delta\mu}{L} & 0 & \frac{1}{\gamma + d + \mu + \psi} & 0 \\ \frac{\delta\psi(\gamma + \delta + d + 2\mu + \psi)}{L(\gamma + d + \mu)} & \frac{\delta}{(\delta + \mu)(\gamma + d + \mu)} & \frac{\psi}{(\gamma + d + \mu)(\gamma + d + \mu + \psi)} & \frac{1}{\gamma + d + \mu} \end{pmatrix},$$

where $L = (\delta + \mu)(\delta + \mu + \psi)(\gamma + d + \mu + \psi)$. Since F is a non-negative and V is a non-singular M-matrix, the next generation matrix FV^{-1} exists, and its spectral

radius $\rho(FV^{-1})$ gives the vaccinated reproduction number R_v. Therefore,

$$R_v = \frac{\delta\left(\beta_C S_C^0 + \beta_A S_A^0 + \epsilon\beta_C (U_C^V)^0 + \epsilon\beta_A (U_A^V)^0\right)}{(\delta+\mu)(\gamma+d+\mu)}$$

$$= \frac{\delta\Lambda\left(\beta_C\epsilon\xi_U\left(\eta_A+\mu\right)\left(\xi_A+\mu\right) + \beta_A\psi\epsilon\xi_U\left(\xi_A+\mu\right) + \beta_C Z\left(\eta_A+\mu\right)\left(\xi_A+\mu\right) + \beta_A\psi Z\left(\eta_A+\mu\right)\right)}{Z(\delta+\mu)\left(\eta_A+\mu\right)\left(\xi_A+\mu\right)\left(\gamma+d+\mu\right)\left(\mu+\xi_M+\xi_U+\psi\right)}.$$

We also compute the time-dependent effective reproduction number, denoted by R_e. The R_e value aids us in monitoring whether the epidemic at a given time t is exhibiting an upward trend ($R_e > 1$) or a downward trend ($R_e < 1$). In our model, the effective reproduction number is determined by the following expression:

$$R_e = \frac{\delta\left(\beta_C S_C(t) + \beta_A S_A(t) + \epsilon\beta_C U_C^V(t) + \epsilon\beta_A U_A^V(t)\right)}{(\delta+\mu)(\gamma+d+\mu)}.$$

4.2.2 Stability of Disease free Equilibrium

4.2.2.1 Local Stability

The Jacobian J_0 of the system (3.7 - 3.18) at the disease free equilibrium E^0 is given by $J_0 = [A_{12\times6}\ B_{12\times6}]$, where $A_{12\times6} =$

$$\begin{pmatrix}
-\mu-\xi_M-\xi_U-\psi & 0 & 0 & 0 & 0 & 0 \\
\psi & -\mu-\xi_A & 0 & 0 & 0 & 0 \\
\xi_U & 0 & -\mu-\eta_U-\psi & 0 & 0 & 0 \\
0 & 0 & \psi & -\eta_A-\mu & 0 & 0 \\
0 & \xi_A & 0 & 0 & -\eta_A-\mu & 0 \\
\xi_M & 0 & 0 & 0 & 0 & -\mu-\eta_M \\
0 & 0 & 0 & 0 & 0 & 0 \\
0 & 0 & 0 & 0 & 0 & 0 \\
0 & 0 & 0 & 0 & 0 & 0 \\
0 & 0 & 0 & 0 & 0 & 0 \\
0 & 0 & \eta_U & 0 & 0 & \eta_M \\
0 & 0 & 0 & \eta_A & \eta_A & 0
\end{pmatrix},$$

$$B_{12\times 6} = \begin{pmatrix} 0 & 0 & -\beta_C S_C & -\beta_C S_C & 0 & 0 \\ 0 & 0 & -\beta_A S_A & -\beta_A S_A & 0 & 0 \\ 0 & 0 & -\beta_C U_C^V\ \epsilon & -\beta_C U_C^V\ \epsilon & 0 & 0 \\ 0 & 0 & -\beta_A U_A^V\ \epsilon & -\beta_A U_A^V\ \epsilon & 0 & 0 \\ 0 & 0 & 0 & 0 & 0 & 0 \\ 0 & 0 & 0 & 0 & 0 & 0 \\ -\delta-\mu-\psi & 0 & \beta_C S_C + \beta_C U_C^V \epsilon & \beta_C S_C + \beta_C U_C^V \epsilon & 0 & 0 \\ \psi & -\delta-\mu & \beta_A S_A + \beta_A U_A^V\ \epsilon & \beta_A S_A + \beta_A U_A^V \epsilon & 0 & 0 \\ \delta & 0 & -\gamma-d-\mu-\psi & 0 & 0 & 0 \\ 0 & \delta & \psi & -\gamma-d-\mu & 0 & 0 \\ 0 & 0 & \gamma & 0 & -\mu-\psi & 0 \\ 0 & 0 & 0 & \gamma & \psi & -\mu \end{pmatrix}.$$

Let $\lambda_i, i = 1, 2, ..., 12$, be eigenvalues of the matrix J_0. Then $\lambda_1 = -\mu,\ \lambda_2 = -(\mu + \xi_A),\ \lambda_3 = -(\mu + \psi),\ \lambda_4 = -(\mu + \eta_M),\ \lambda_5 = -(\mu + \eta_A), \lambda_6 = -(\mu + \eta_A),\ \lambda_7 = -(\mu + \eta_U + \psi)$,
$\lambda_8 = -(\mu + \xi_M + \xi_U + \psi),\ \lambda_9 = -(\gamma + d + \mu + \psi),\ \lambda_{10} = -(\delta + \mu + \psi)$,
$\lambda_{11} = -\frac{1}{2}\left(d + \delta + 2\mu + \gamma + \sqrt{(\gamma + d + \delta + 2\mu)^2 - 4\,(1 - R_v)\,(\delta + \mu)(\gamma + d + \mu)}\right)$,
$\lambda_{12} = -\frac{1}{2}\left(d + \delta + 2\mu + \gamma - \sqrt{(\gamma + d + \delta + 2\mu)^2 - 4\,(1 - R_v)\,(\delta + \mu)(\gamma + d + \mu)}\right)$.

All eigenvalues are negative except λ_{12}, which is also negative for $R_v < 1$. Thus, we can conclude that the disease-free equilibrium point is locally asymptotically stable for $R_v < 1$.

In the epidemiological sense, the locally asymptotically stability of the disease-free equilibrium for $R_v < 1$ implies that the measles dynamics initiated with a small number of infections introduced in the community approaches to the measles-free state over time when the vaccinated reproduction number remains less than one. In other words, the vaccinated reproduction number being less than unity assures that the disease outbreak will die out when a small population perturbation occurs with the introduction of a small number of infections, which is usually the case at the beginning of infection. Such a condition allows us to design a vaccination policy that assures $R_v < 1$, thereby avoiding the outbreak. However, local stability does not ensure outbreak control under all conditions or if the system is perturbed significantly.

4.2.2.2 Global Stability

In this section, we show that $R_v < 1$ also asserts the global stability of the disease-free equilibrium E^0 as stated in the following theorem.

Theorem 4.2.1 *The disease-free equilibrium* (E^0) *is globally stable when* $R_v < 1$.

Here, we determine the global stability of (E^0) using the results presented in a previous study Chávez et al. (2002). First, the system (3.7 - 3.18) is written as $dX/dt = F(X,Y)$, $dY/dt = G(X,Y)$, with $G(X,0) = 0$, where $X \in R^8$ and $Y \in R^4$ represent the uninfected and infected compartments, respectively. Then satisfying the following two conditions implies the global asymptotically stability of the system around disease-free equilibrium point $E^0 = (X^*, 0)$:

1. For $dX/dt = F(X,0)$, X^* is globally stable, (where $X^* \in R^8$ at disease free state) and
2. $\hat{G}(X,Y) = BY - G(X,Y) \geq 0$, for $(X,Y) \in R^{12}$, where B is the Jacobian of the infected system at the disease-free equilibrium E^0.

Clearly, the system

$$\frac{dX}{dt} = \begin{pmatrix} \Lambda - S_C\left(\mu + \xi_M + \xi_U + \psi\right) \\ S_C\,\psi - \mu S_A \\ S_C\xi_U - U_C^V\left(\mu + \eta_U + \psi\right) \\ U_C^V\psi - U_A^V(\mu + \eta_A) \\ \xi_A S_A - V_A\left(\mu + \eta_A\right), \\ S_C\xi_M - M_C^V\left(\mu + \eta_M\right) \\ M_C^V\eta_M - I_{mC}(\mu + \psi) + U_C^V\eta_U \\ (U_A^V + V_A)\eta_A - \mu I_{mA} + I_{mC}\,\psi \end{pmatrix}$$

is globally asymptotically stable at X^*. The matrix of the infected compartments is given as:

$$G = \begin{pmatrix} \left(I_C + I_A\right)\beta_C S_C + \left(I_C + I_A\right)\beta_C U_C^V\epsilon - (\delta + \mu + \psi)E_C \\ \left(I_C + I_A\right)\beta_A S_A + \left(I_C + I_A\right)\beta_A U_A^V\epsilon + E_C\psi - E_A(\delta + \mu) \\ E_C\delta - I_C(\gamma + d + \mu + \psi) \\ E_A\delta + I_C\psi - I_A(\gamma + d + \mu) \end{pmatrix}.$$

The Jacobian of the matrix G at the disease-free equilibrium is $B=$

$$\begin{pmatrix} -\delta - \mu - \psi & 0 & \beta_C\left(S_C\right)^0 + \beta_C\left(U_C^V\right)^0\epsilon & \beta_C\left(S_C\right)^0 + \beta_C\left(U_C^V\right)^0\epsilon \\ \psi & -\delta - \mu & \beta_A\left(S_A\right)^0 + \beta_A\left(U_A^V\right)^0\epsilon & \beta_A\left(S_A\right)^0 + \beta_A\left(U_A^V\right)^0\epsilon \\ \delta & 0 & -\gamma - d - \mu - \psi & 0 \\ 0 & \delta & \psi & -\gamma - d - \mu \end{pmatrix}.$$

$$Y = \begin{pmatrix} E_C \\ E_A \\ I_C \\ I_A \end{pmatrix},$$

$$BY = \begin{pmatrix} -E_C(\delta+\mu+\psi) + (I_C+I_A)\,\beta_C\,(S_C)^{\,0} + (I_C+I_A)\,\beta_C\left(U_C^V\right)^{0}\epsilon \\ -E_A(\delta+\mu) + (I_C+I_A)\,\beta_A\,(S_A)^{\,0} + (I_C+I_A)\,\beta_A\left(U_A^V\right)^{0}\epsilon + E_C\psi \\ E_C\delta - I_C(\gamma+d+\mu+\psi) \\ -I_A(\gamma+d+\mu) + E_A\delta + I_C\psi \end{pmatrix},$$

where Y is a (4×1) matrix with elements (E_C, E_A, I_C, I_A). Then $BY - G$ or $\hat{G} =$

$$\begin{pmatrix} (I_C+I_A)\,\beta_C\left(\left(\dfrac{\Lambda}{\mu+\xi_M+\xi_U+\psi} - S_C\right) + \epsilon\left(\dfrac{\Lambda\xi_U}{Z\,(\mu+\xi_M+\xi_U+\psi)} - U_C^V\right)\right) \\ (I_C+I_A)\,\beta_A\left(\epsilon\left(\dfrac{\Lambda\psi\xi_U}{Z\,(\eta_A+\mu)\,(\mu+\xi_M+\xi_U+\psi)} - U_A^V\right) + \left(\dfrac{\Lambda\psi}{(\mu+\xi_A)\,(\mu+\xi_M+\xi_U+\psi)} - S_A\right)\right) \\ 0 \\ 0 \end{pmatrix}.$$

From the system of equations (3.7-3.18), we ultimately obtain

$$\begin{aligned} S_C &\le \frac{\Lambda}{\mu+\xi_M+\xi_U+\psi}, \\ S_A &\le \frac{\Lambda\psi}{(\mu+\xi_A)\,(\mu+\xi_M+\xi_U+\psi)}, \\ U_C^V &\le \frac{\Lambda\xi_U}{Z\,(\mu+\xi_M+\xi_U+\psi)}, \\ U_A^V &\le \frac{\Lambda\psi\xi_U}{Z\,(\eta_A+\mu)\,(\mu+\xi_M+\xi_U+\psi)}. \end{aligned}$$

Clearly $(BY-G)$ is the non-negative matrix for $R_v < 1$, so the disease free equilibrium point is globally asymptotically stable when $R_v < 1$.

Epidemiologically, our theorem establishing the global stability of the disease-free equilibrium implies that the disease can't establish sustained transmission within the population for any, even significantly large, initial number of infections as long as $R_v < 1$. The global stability of the disease-free equilibrium point of our model helps to maintain and implement preventive strategies such as vaccination programs for disease control.

Suppose $E^* = \left(S_C^*,\ S_A^*,\ (U_C^V)^*,\ (U_A^V)^*,\ V_A^*,\ (M_C^V)^*,\ E_C^*,\ E_A^*,\ I_C^*,\ I_A^*, I_{mC}^*,\ I_{mA}^*\right)$ be an endemic equilibrium of the system. Let, $I^* = I_C^* + I_A^*$, then solving the system (3.7

- 3.18), we get

$$
\begin{aligned}
S_C^* &= \frac{\Lambda}{\beta_C I^* + \mu + \xi_M + \xi_U + \psi}, \\
S_A^* &= \frac{\Lambda\psi}{(\beta_A I^* + \mu + \xi_A)\,(\beta_C I a^* + \mu + \xi_M + \xi_U + \psi)}, \\
(U_C^V)^* &= \frac{\Lambda\xi_U}{(\beta_C I^* + \mu + \xi_M + \xi_U + \psi)\,(\beta_C I^*\epsilon + Z)}, \\
(U_A^V)^* &= \frac{\Lambda\psi\xi_U}{(\eta_A + \beta_A I^*\epsilon + \mu)\,(\beta_C I^* + \mu + \xi_M + \xi_U + \psi)\,(\beta_C I^*\epsilon + Z)}, \\
V_A^* &= \frac{\Lambda\psi\xi_A}{(\eta_A + \mu)\,(\beta_A I^* + \mu + \xi_A)\,(\beta_C I^* + \mu + \xi_M + \xi_U + \psi)}, \\
(M_C^V)^* &= \frac{\Lambda\xi_M}{(\mu + \eta_M)\,(\beta_C I^* + \mu + \xi_M + \xi_U + \psi)}, \\
E_C^* &= \frac{\beta_C I^*\Lambda\,(\beta_C I^*\epsilon + \epsilon\ \xi_U + Z)}{(\delta + \mu + \psi)\,(\beta_C I^* + \mu + \xi_M + \xi_U + \psi)\,(\beta_C I^*\epsilon + Z)}, \\
I_C^* &= \frac{\beta_C\delta I^*\Lambda\,(\beta_C I^*\epsilon + \epsilon\ \xi_U + Z)}{(\delta + \mu + \psi)(\gamma + d + \mu + \psi)\,(\beta_C I^* + \mu + \xi_M + \xi_U + \psi)\,(\beta_C I^*\epsilon + Z)}.
\end{aligned}
$$

4.2.3 Endemic Equilibrium

Obtaining the endemic point in the infectious disease modeling is crucial to understanding the long-term disease dynamics. For many situations with imperfect vaccination programs, which is likely the current condition in Nepal, the endemic equilibrium provides the epidemic's severity. The epidemic level, at least, informs important policy guidelines for disease control if not eradicated.

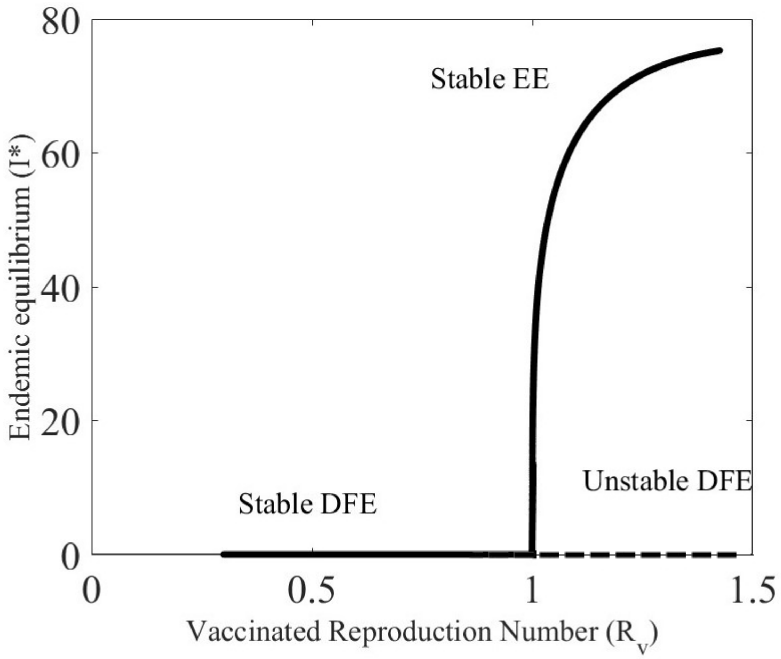

Figure 11: Forward Bifurcation Diagram: Forward bifurcation at $R_v = 1$, the disease free equilibrium is stable for $R_v < 1$. The disease free is unstable and endemic equilibrium is stable for $R_v > 1$.

Here, $E_A^*,\ I_A^*,\ I_{mC}^*,\ I_{mA}^*$ are positive when $R_v > 1$ (see supplementary file). After manipulating the equations of the system at diseased equilibrium we obtained the equation given as:

$$(A_4(I^*)^4 + A_3(I^*)^3 + A_2(I^*)^2 + A_1 I^* + A_0)I^* = 0, \tag{4.14}$$

where,

$$A_4 = \beta_C^2 \beta_A^2 \epsilon^2 (\delta + \mu)(\gamma + d + \mu),$$
$$A_0 = (1 - R_v)\,(\delta + \mu)\,(\eta_A + \mu)\,(\xi_A + \mu)\,(\gamma + d + \mu)\,(\mu + \eta_U + \psi)\,(\mu + \xi_M + \xi_U + \psi)\,,$$

and $A_1,\ A_2,\ A_3$ are provided in supplementary file. Note that $I^* = 0$ corresponds to the disease-free equilibrium E^0. Since $A_0 < 0$ when $R_v > 1$ and $A_4 > 0$, then by Vieta's Theorem, there exists at least one positive I^* and the system has at least one endemic equilibrium when $R_v > 1$.

We can compute the magnitude of endemic equilibrium by solving Eq. (4.14). We were unable to establish the stability of the endemic equilibrium analytically due to the complexity brought by the higher-order equations with nonlinearity. However, we performed numerical analysis for the stability of the endemic equilibrium and

presented results as a bifurcation diagram with the existence and stability of the endemic equilibrium for $R_v > 1$ (Fig. 11), for which the disease-free equilibrium is unstable.

CHAPTER 5

5. NUMERICAL RESULTS

In this chapter, we present the results of model simulations. Using the monitored vaccination model, we identify strategies for the successful control of measles in Nepal and predict that monitored vaccination programs can help control the potential resurgence of the disease. Analysis of the adult-child vaccination model shows that impactful control can be achieved by children-focused vaccines, and a combined adult-child vaccination program may help ensure the eradication of the disease. The results highlight that while children are the primary targets for measles outbreaks, a small infection in adults may act as a reservoir for measles, causing obstacles to eradication. Impactful control can be achieved by children-focused vaccines, and a combined adult-child vaccination program may help ensure the eradication of the disease.

5.1 Numerical Results of Monitored Vaccination Model

5.1.1 Basic Dynamics of Measles in Nepal

We first present the properties of basic dynamics of measles in Nepal, particularly vaccinated reproduction numbers and long-term dynamics.

5.1.1.1 Computation of the Reproduction Numbers

Using the estimated parameters (Table 2), we obtain the reproduction number of measles in the presence of vaccination in Nepal to be $R_v = 1.0098$. While $R_v > 1$ is consistent with the currently ongoing endemic of measles, the actual magnitude we observed is significantly lower than the previously estimated reproduction number between 5 and 18 in other places for Disease Control and Prevention (2020). The low value of R_v is expected as its estimate is based on the parameters influenced by the vaccination program. We now compute the time-dependent effective reproduction number, R_t, which describes the time-varying average number of secondary cases.

The value of R_t allows us to track whether the epidemic at time t is in an increasing ($R_t > 1$) or decreasing ($R_t < 1$) trend. For our model, the effective reproduction number is given by

$$R_t = \frac{\beta\sigma\left(S(t) + U_V(t)(1-\epsilon_1) + M_V(t)(1-\epsilon_2)\right)}{N(t)(\mu+\sigma)(\delta+\eta+\mu)}.$$

Using the estimated parameters (Table 2), we obtained the pattern of R_t as shown in Figure 12. As predicted by our model, the value of the effective reproduction number remains less than unity, indicating the epidemic is in decreasing trend until 2030, after which R_t increases and remains greater than unity until 2095, showing the increasing trend of the disease in the period 2030–2095 (Figure 12).

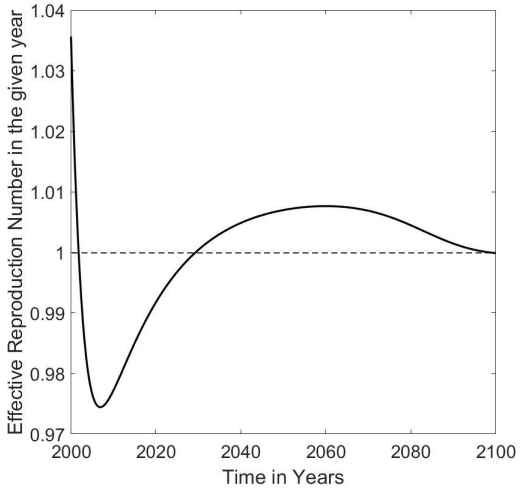

Figure 12: Effective Reproduction Number (R_t). The model predicted effective reproduction number, (R_t), for measles epidemic in Nepal. The value of the effective reproduction number $R_t < 1$, until 2030, after which increases and $R_t > 1$ until 2095.

5.1.1.2 Longterm Dynamics

In this section, we present our model prediction for the long-term dynamics of measles transmission in Nepal. If the current trend continues, there will still be 178 cases in 2023 (Figure 13), indicating an obstacle to the measles elimination program set by the government of Nepal. Our model predicts that the cases remain at a significantly low level until 2033 but persist at a low level without being eradicated. After 2033, the resurgence of the outbreak will begin and reach the peak value (7670) in 2097. The dynamic is relatively slow, reaching a steady-state only after about 2100. The resurgence of measles in Nepal predicted by our model supports the worldwide trend

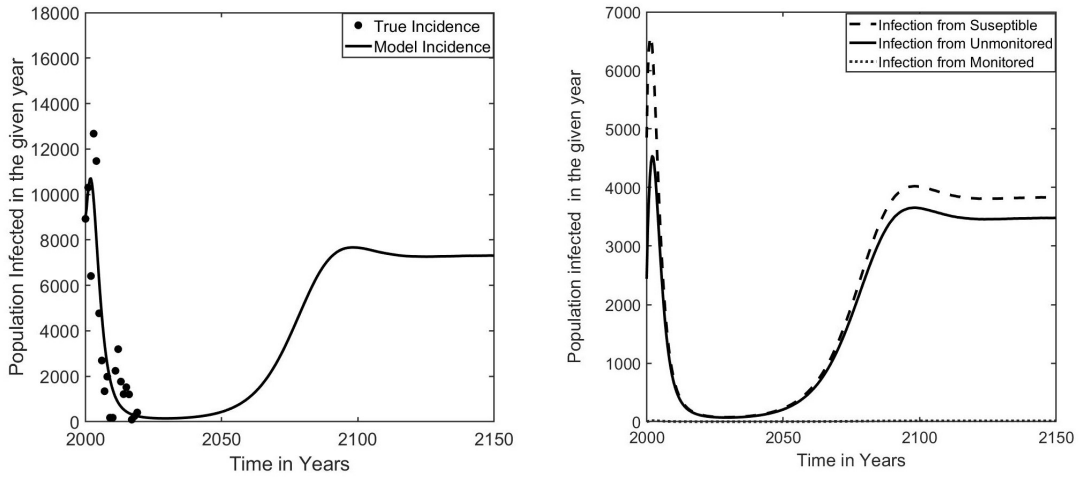

(a) **(b)**

Figure 13: (a) Longterm dynamics predicted by the model. The model prediction of the longterm dynamics of yearly new measles cases in Nepal. (b) Infections from the different classes. The model prediction of the longterm dynamics of yearly new measles cases in Nepal contributed by susceptible, un-monitored vaccinated, and monitored vaccinated classes.

of the epidemic, which shows an eventual resurgence in many places such as the UK, the US (31 states including New York), and the Philippines. We also predict the contribution of susceptible (unvaccinated), un-monitored vaccinated, and monitored vaccinated to the resurgence of the measles cases. As per our model prediction, the major contribution to the resurgence is from the susceptible and the un-monitored vaccinated groups. Note that the un-monitored vaccinated group can be significantly high in Nepal, as shown by the data that while 92% are vaccinated with MCV1, only about 76% are vaccinated with MCV2 in 2019 WHO (2020). Therefore, proper implementation of the monitored vaccination program may be needed to avoid the resurgence of the disease.

5.1.2 Sensitivity Analysis

This section includes sensitivity index of parameters and sensitivity of parameters in global space to R_v and to the disease dynamics: peak infection and time of peak infection.

5.1.2.1 Sensitivity of Parameters to R_v

We first observe the local sensitivity of R_v to each of the parameters. For this, we obtain the sensitivity index S_x, given by

$$S_x = \left(\frac{x}{R_v}\right)\left(\frac{\partial R_v}{\partial x}\right),$$

where x is the parameter of which the sensitivity is to be obtained. Based on S_x, we found that R_v is highly sensitive to β. The parameter γ_1 also affects R_v more than the other parameters, and the ϵ_2 affects less while the effect of σ and α_2 are negligible (Figure 14).

We also extend the analysis to the global sensitivity by using Latin Hypercube Sampling (LHS) Marino et al. (2008), taking 1000 sample points from the global parameter space. We compute the partial rank correlation coefficients to identify the most influential parameters. We observed that in the global parameter space, the parameters ϵ_1, α_1, and β are the most strongly effective to R_v, followed by $\alpha_2, \epsilon_2, \gamma_1$, and σ, while γ_2 is less effective (Figure 14).

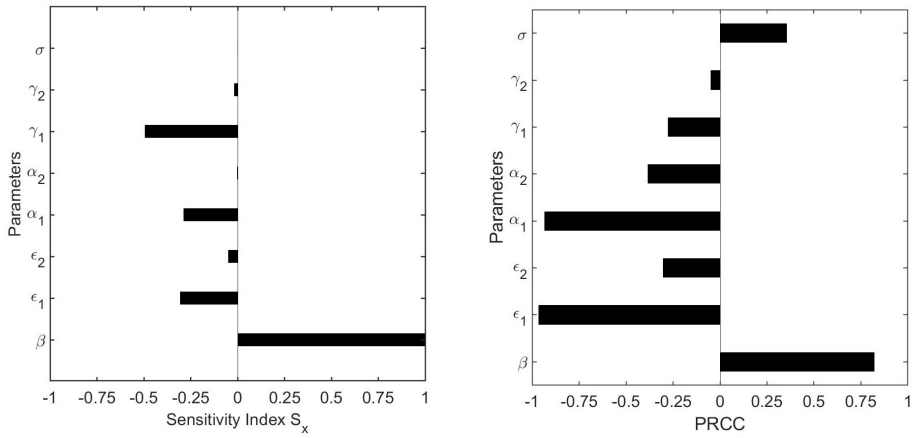

(a) **(b)**

Figure 14: (a) Local sensitivity of parameters to R_v. The sensitivity index, S_x, showing the level of change in R_v with respect to the parameters. Note that the sensitivity index S_x of $\sigma = 0.0022$ and $\alpha_2 = -0.06$ are negligible, and thus difficult to visualize in the figure. (b) Global sensitivity of R_v. Partial Rank Correlation Coefficients for R_v from LHS method.

5.1.2.2 Sensitivity of Parameters to the Dynamics

In this section, we use Latin Hypercube Sampling Marino et al. (2008) from the global parameter space to identify the sensitivity level of the peak value of the infected class and that of the time at the peak of the epidemic. The computed partial rank correlation coefficient corresponding to each parameter is presented in Figure 15. Our analysis shows that the peak value of the infected class is highly correlated to β (positive correlation). The peak value is moderately affected by α_1, α_2, γ_1, and σ and is weakly correlated to the parameters γ_2, ϵ_2, and ϵ_1 (Figure 15). Similarly, the peak time of the epidemic is mostly affected by the parameters β and ϵ_1, while it is less influenced by the parameters α_1 and γ_1. The parameters $\sigma, \gamma_2, \alpha_2$, and ϵ_2 have the least effect on the peak time.

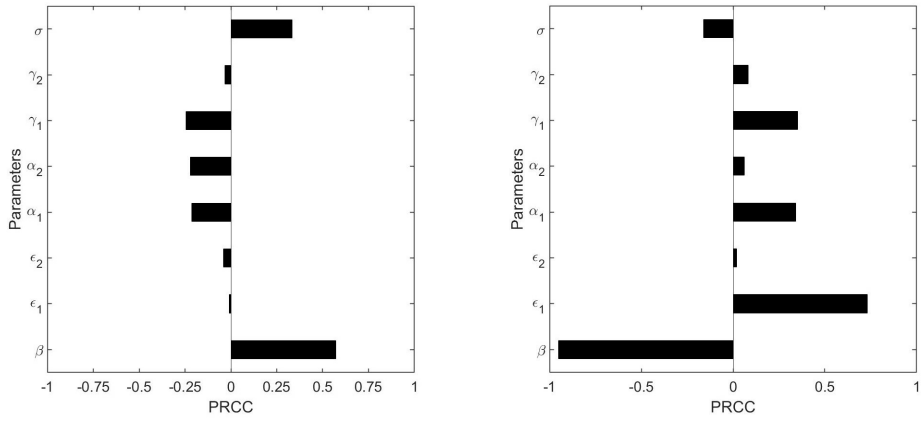

Figure 15: (a) Global sensitivity of the peak level of infected class. The partial rank correlation coefficients for sensitivity of peak level of infected class based on Latin Hypercube sampling. **(b) Global sensitivity of the peak time.** The partial rank correlation coefficients for sensitivity for the peak time based on Latin Hypercube sampling.

5.1.3 Effects of Monitored and Un-monitored Vaccination

We use five parameters, the un-monitored vaccination rate (α_1), the monitored vaccination rate (α_2), the immunization rate of un-monitored vaccination (γ_1), the effectiveness of un-monitored vaccination (ϵ_1), and the effectiveness of monitored vaccination (ϵ_2) to evaluate the effects of the vaccination programs.

5.1.3.1 Effects on the Measles Eradication

Note that $R_v < 1$ can be associated with a condition required to eradicate the disease (Section 4.1.2). We now use our R_v formulation to identify vaccine-related parameters that can reduce R_v below one (Figure 16). We found that at the current level of α_1, either the monitored vaccination rate α_2 needs to rise by 250% ($\alpha_2 \geq .07$) or the effectiveness of un-monitored vaccination ϵ_1 needs to rise by 4% ($\epsilon_1 \geq 0.52$) to make $R_v < 1$. On the other hand, with the current effectiveness of monitored vaccination (ϵ_2), the effectiveness of un-monitored vaccination (ϵ_1) needs to be greater than 0.52 to make $R_v < 1$ (Figure 16).

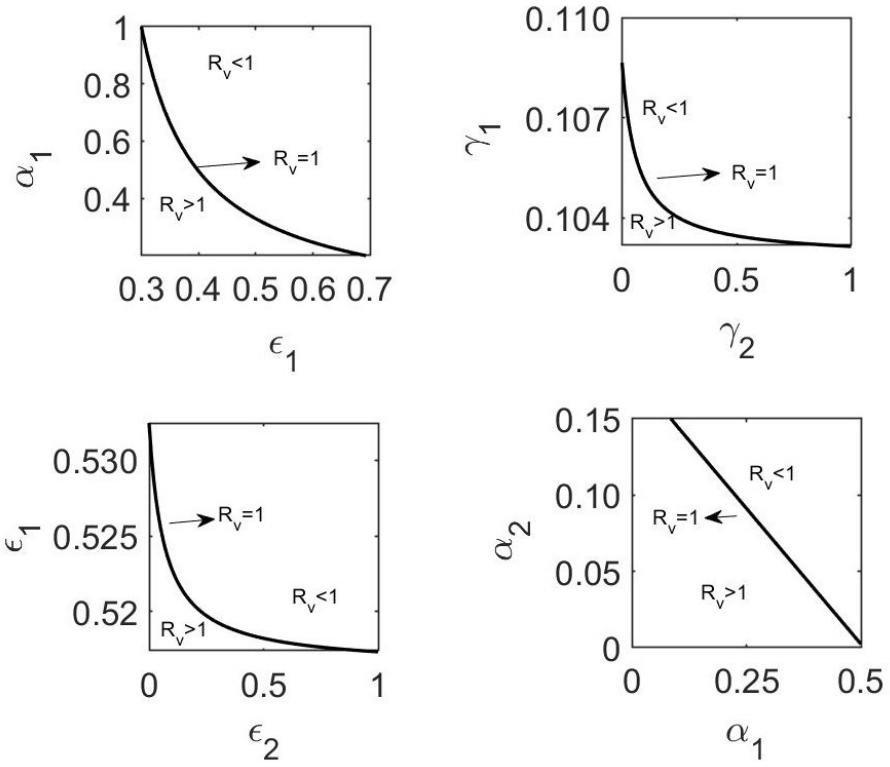

Figure 16: Effects of vaccination on R_v. The contour line (the solid line) corresponding to $R_v = 1$ in the parameter space plane with each two of the un-monitored vaccination rate (α_1), monitored vaccination rate (α_2), the effectiveness of un-monitored vaccination (ϵ_1), effectiveness of monitored vaccination (ϵ_2), immunization rates of un-monitored vaccination (γ_1) and immunization rate of monitored vaccination (γ_2).

If the un-monitored vaccination rate (α_1) is increased by 20% ($\alpha_1 \approx 0.42$ per year), the activity of the monitored vaccination program can be somewhat relaxed at the current level of $\alpha_2 \approx 0.02$ per year for $R_v < 1$. On the other hand, if α_1 is decreased by 26% ($\alpha_1 \approx 0.23$ per year), the activity of the monitored vaccination program needs

to be raised, making the level of α_2 exceed more than 0.1 per year to achieve $R_v < 1$.

5.1.3.2 Effects on the Dynamics

In the absence of monitored vaccination, the model predicts that the cases will rise and reach the peak value of 85,750 in 2038 for $\alpha_2 = 0$. With the reduction of un-monitored vaccination by 50% or $\alpha_1 = 0.15$, our model predicts that the cases will rise and reach the peak value of 647,300 in 2028 (Figure 17). If the immunity rate of un-monitored vaccination is decreased by 50%, i.e., $\gamma_1 = 0.05$, the cases rise, leading to the peak value of about 452,800 in 2030. Similarly, if the effectiveness of un-monitored vaccination is decreased by 20% ($\epsilon_1 = 0.4$), the cases may rise and reach the peak value of 268,200 in 2027.

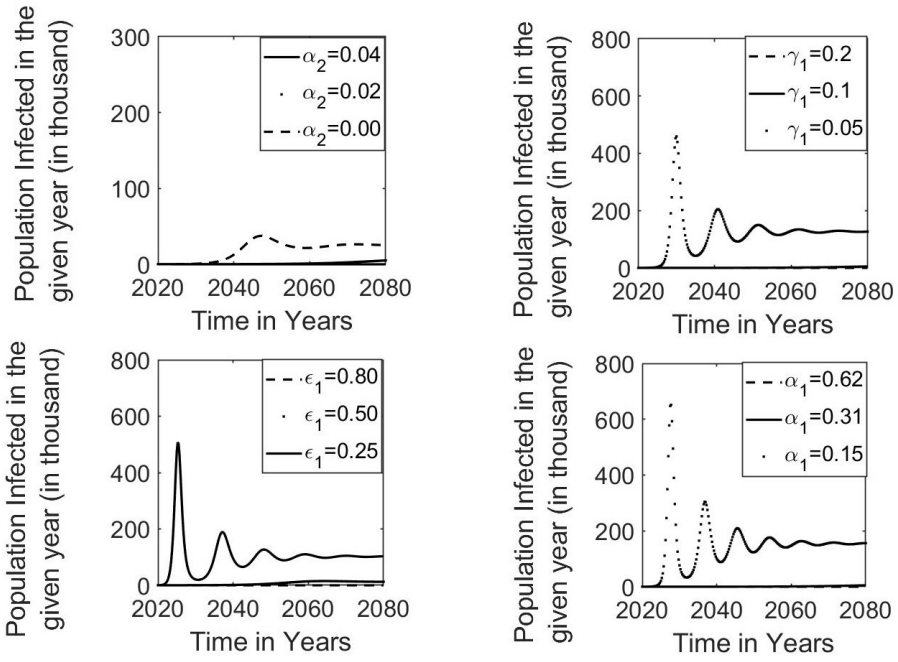

Figure 17: Effects of vaccination on the dynamics. Model prediction of dynamics in the present scenario and various level of un-monitored vaccination rate (α_1), its immunization rate (γ_1), and the effectiveness (ϵ_1) and the monitored vaccination rate (α_2).

5.1.3.3 Effects on the Steady State

We explore how the different levels of vaccination-related parameters, α_1, α_2, $\gamma_1, \gamma_2, \epsilon_1$, and ϵ_2 (Figure 18) affect the level of steady-state of new infections (Figure 18). As expected, an increase in the vaccination rate decreases the steady-state level

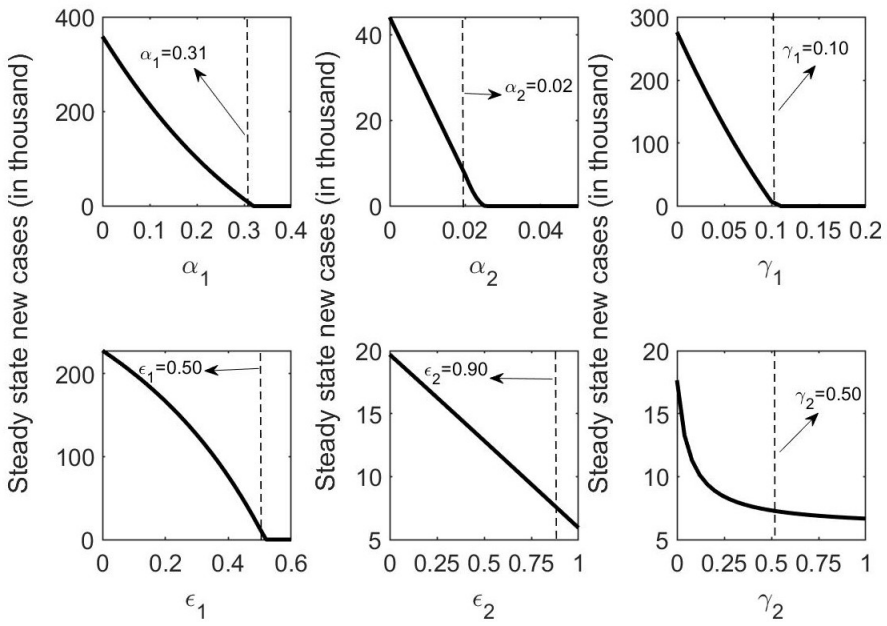

Figure 18: Effects of vaccination on the steady state. Model predicted new cases at the steady state for the various vaccination rates α_1, α_2, immunized rate γ_1, γ_2 and effectiveness of un- monitored and monitored vaccination program ϵ_1, and ϵ_2, respectively.

of new infections. Based on our model prediction, the current level of vaccination results in 7,312 new cases at a steady state. To sufficiently reduce the steady-state level of new infections, the rate of un-monitored vaccination should be increased by 6.5% ($\alpha_1 = 0.33$), or the rate of monitored vaccination should be increased by 50% ($\alpha_2 = 0.03$). Similarly, the immunizing rate of un-monitored vaccine needs to be increased by 100% ($\gamma_1 = 0.2$), or its effectiveness needs to be increased by 20% ($\epsilon_1 = 0.6$) to bring the steady-state level of new infections to a sufficiently low level.

Furthermore, the reduction of 6.5% of the un-monitored vaccination rate (α_1) increases the steady-state new cases by 206% (22.35 thousand), showing the high impact of the vaccination rate. Also, lowering the monitored vaccination rate (α_2) by 50% increases the steady-state level of new cases by approximately 250% (25.56 thousand). Similarly, decreasing the immunity rate of un-monitored vaccination (γ_1) by 10% increases the steady-state new cases by about 300% (29.1 thousand) while reducing the effectiveness of monitored vaccination (ϵ_2) by 18% increases the steady-state new cases by 30% (9.528 thousand).

5.2 Conclusion

In recent years, the frequent outbreaks of measles in developing and developed countries have become a significant obstacle to achieving the goal of elimination. Mainly, unvaccinated children are the victims of the disease Patel et al. (2020); Sitaula et al. (2010); UN, News (2020). Despite the Supplementary Immunization Activities (SIAs), most of the population is not vaccinated in some districts of Nepal, including Rautahat, Kapilvastu, Morang, and Bajura. Furthermore, many of those initiating the vaccination does not complete the vaccine doses correctly, making them not completely protected. Because of the resurgence of measles in Nepal since 2017 New Spotlight online (2019); Poudel (2019a), WHO's deadline for the elimination goal has been extended to 2023 Rathore (2020). We developed a novel deterministic model validated by the data from Nepal to evaluate the monitored vaccination programs.

We thoroughly analyzed our model to formulate the vaccinated reproduction number ($R_v > 1$), the stability analysis, and the disease persistence theory. Using the model and the available data from the official websites of WHO, we estimated key parameters related to the un-monitored vaccination. Moreover, we performed a global sensitivity analysis using Latin Hypercube Sampling from the wider parameter space. Our model predicts that the measles elimination goal can be achieved if the monitored vaccination rate is increased by 50% ($\alpha_2 = 0.03$) or the un-monitored vaccination rate is increased by 6.5% ($\alpha_1 = 0.33$). The elimination goal can also be achieved by the high effectiveness of the un-monitored vaccine (i.e., with $\epsilon_1 \geq 0.53$). However, if the current trend continues, our model predicts that the measles will persist causing an obstacle to the measles elimination goal of Nepal. Furthermore, our model predicts that without any additional interventions, measles transmission will continue with a rise in the epidemic after 2033 (Figure 13). Our model also predicts that the major contributor to the measles resurgence in Nepal is susceptible (unvaccinated) and un-monitored vaccinated groups, emphasizing the need for the expedition of monitored-vaccination programs. The epidemic dynamics in Nepal is quite slow, reaching the peak only in about 2097 (Figure 13). The observed slow dynamics is consistent with the previous study Horrocks and Bauc (2020).

We acknowledge some limitations of our study. The parameter estimations are based on the limited data of yearly incidence cases (2000–2019). Moreover, measles is a short-term disease recovered within a month, so the daily or weekly more detailed and accurate data can help improve the prediction of our model. We could obtain the closed

form of the unique endemic equilibrium but are unable to perform a detailed analysis of the endemic equilibrium. Instead, we established the disease persistence criteria. The homogeneous mixing assumed among the children of Nepal can be improved by the model with an appropriate network of contact among children.

In summary, we develop a model of measles transmission in the context of Nepal, where monitoring is critical for the successful implementation of the vaccination program. Our thorough analysis and the detailed numerical simulations of the model can provide helpful information for policymakers to design ideal monitored-vaccination programs to achieve the elimination goal of measles from Nepal.

5.3 Numerical Simulations of Adult-Child Vaccination Model

In this section we present the sensitivity analysis, impact of monitored vaccination program on disease increase-decrease trend, reduction of diseae burden and impact of the contact network. Additionally, this section also present the implications of the infections in adults to disease eradiacation program.

5.3.1 Parameter Sensitivity Analysis

5.3.1.1 Sensitivity of R_v

We quantify the local sensitivity of R_v to each of the parameters $\beta_C,\ \beta_A,\ \psi,\ \gamma,\ d,\ \delta,\ \epsilon,\ \mu,\ \eta_A,\ \eta_U,\ \eta_M,\ \xi_M,\ \xi_U$, and ξ_A. For this, we obtained the sensitivity index, S_x, for each parameter x using the relationship:

$$S_x = \left(\frac{x}{R_v}\right)\left(\frac{\partial R_v}{\partial x}\right).$$

Based on the sensitivity index S_x, we found that the parameter γ affects R_v the most compared to the other parameters. The second parameter affecting R_v is β_C, followed by the parameters $\epsilon,\ \psi,\ \mu,\ \xi_U,$ and β_A, while the effects of $d,\ \delta,\ \eta_A,\ \eta_M,\ \xi_A,\ \eta_M$ and ξ_M to R_v are negligible (Figure 19 a).

We also performed the global sensitivity analysis by using the Latin Hypercube Sampling (LHS) technique Marino et al. (2008) with 1000 samples of parameter sets from a wider parameter range of $\pm 25\%$ of the base value of each parameter.

We compute the partial rank correlation coefficients (PRCC) to identify the most influential parameter to R_v. We observed that the parameters γ, β_C, ϵ, and ψ are the most sensitive parameters for R_v, which are followed by μ, ξ_U, and β_A, and the rest of the parameters are less effective (Figure 19 b). Both local and global analyses show that R_v is mostly influenced by the parameters γ, β_C, and ϵ.

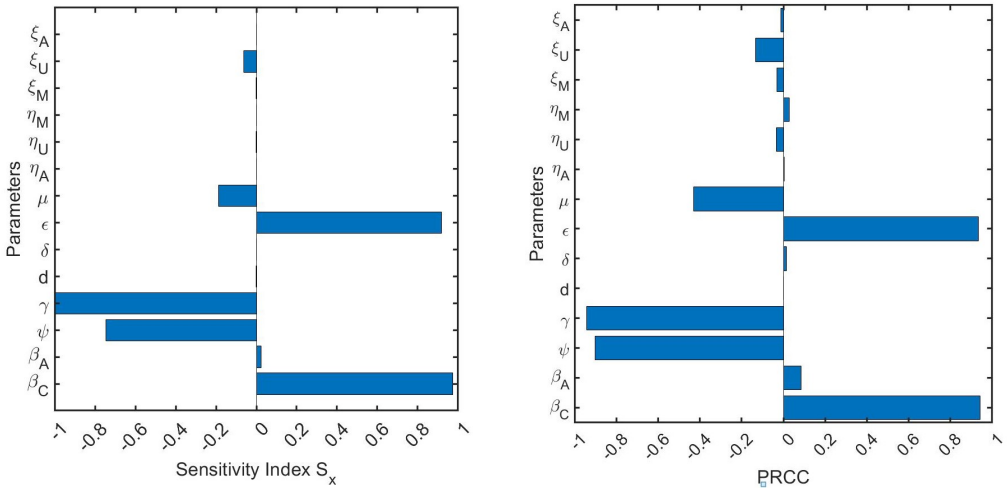

Figure 19: (a) Local sensitivity of parameters to R_v. The sensitivity index, S_x, showing the level of change in R_v with respect to the parameters. Note that the sensitivity index S_x of $d, \delta, \eta_A, \eta_U, \eta_M, \xi_A$ and ξ_M are negligible and difficult to visualize in the figure.(b) Global sensitivity of R_v. Partial Rank Correlation Coefficients for R_v from LHS method.

5.3.1.2 Sensitivity of Measles Dynamics

We also used the Latin Hypercube Sampling Marino et al. (2008) method to explore the global sensitivity of the measles dynamics represented by the peak infection and the time to peak in adults, children, and combined. The computed partial rank correlation coefficient corresponding to each parameter is presented in Figure 20. Our analysis shows that the peak value of the infected class I_A is highly influenced by γ, β_A, ϵ, and δ followed by β_C and then by ξ_U while the remaining parameters are less effective (Figure 20a). Also, the peak value of the infected class I_C is highly influenced by β_C, ϵ, δ, and γ, followed by ξ_U and other parameters are less effective (Figure 20b). Similarly, the peak value of the infected class of children and adults combined is influenced by the parameters β_C, ϵ, δ, γ, followed by ξ_U. In contrast, the remaining parameters are less effective (Figure 20c).

The time to peak infection is mostly affected by the parameters β_C, δ, and γ, followed by ϵ and ξ_M. The rest of the parameters in I_A and I_C less influences it. Similarly, the time to peak for combined infection is mainly affected by δ, β_C, γ, and ϵ, followed by ξ_M, while the remaining parameters are less effective (Figure 20 f).

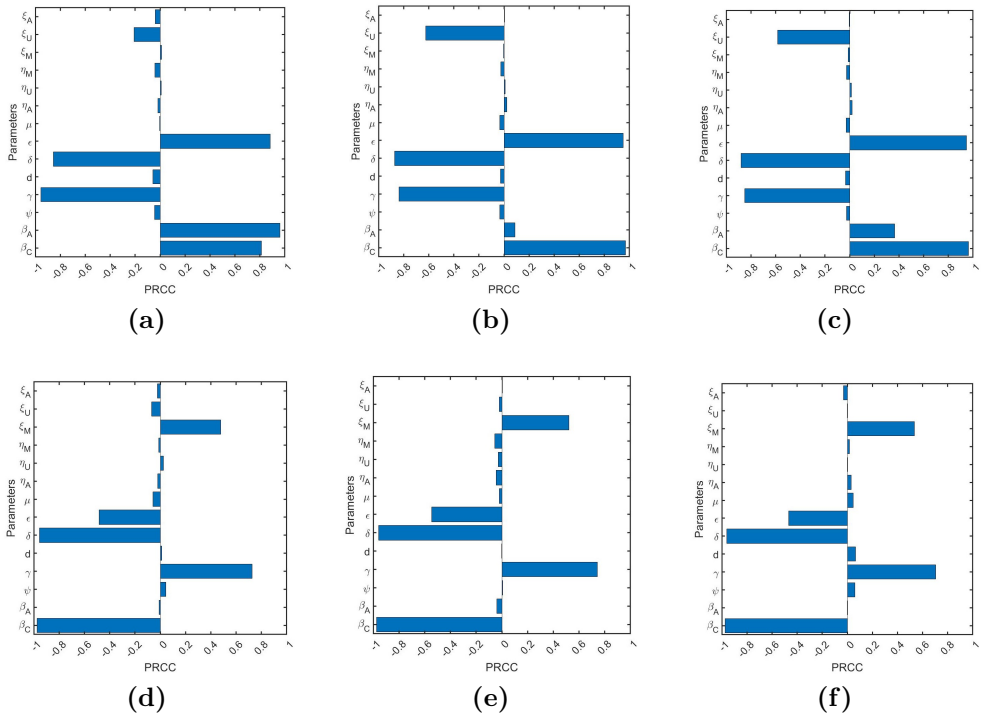

Figure 20: Sensitivity of measles dynamics. Global sensitivity of the parameters to peak value and time of peak infection for adult I_A (a, d), children I_C (b, e), and combined child and adult (c, f). The partial rank correlation coefficients for sensitivity are based on 1000 Latin Hypercube Sample sets of parameters.

5.3.2 Impact of the Contact Network on Infection

While we estimated the base contact network in the data context, the contact network may change depending on the situation. Therefore, we now explore the effects of the contact network on the total number of infections and its peak value for each infected class. An increase in children's contact network by 5, 10, and 15 times the base case results in the rise of peak infection of children by 8, 16, and 21 times, respectively, and an increase in the total children infection by 4, 7, and 8 times, respectively (Figure 21a). Similarly, the same increment level in the adult contact network results in the increment of the total infection by 28, 85, and 133 times and the peak infection by 28, 92, and 166 times, respectively (Figure 21b). An increment in the contact network

of all populations by 5, 10, and 15 times results in an increment of approximately 8, 17, and 23 times in the peak infection and 7, 16, and 23 times in the total infection, respectively (Figure 21c).

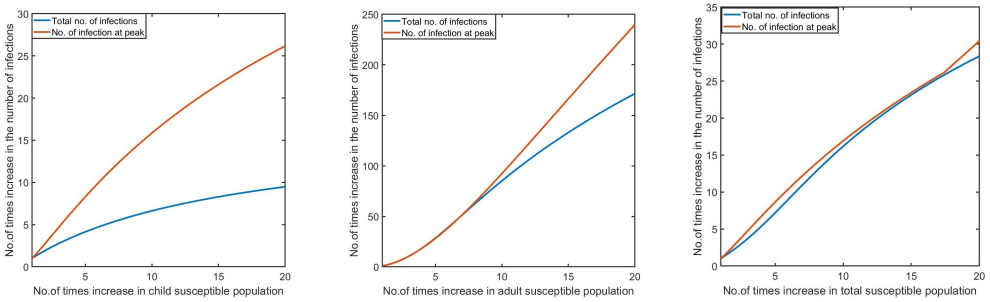

(a) **(b)** **(c)**

Figure 21: The total number of infections and peak infection on the variation of the contact network of (a) children, (b) adults, and (c) total (children and adults).

5.3.3 Impact of Monitored Vaccine Program

5.3.3.1 On Disease Increase-Decrease Trend

Here, we examine the profound role of vaccine coverage in the increase-decrease trend of the disease, i.e., reducing the effective reproduction number (R_e) below one. We evaluate the effect of both timeliness and extension of vaccination coverage in achieving the goal of $R_e < 1$ (decreasing trend). Our findings show that complete vaccine coverage within the first two weeks of outbreaks yields remarkable outcomes in lowering the effective reproduction number. Achieving a vaccination coverage of over 90% among children within two weeks decreases the effective reproduction number to below 1 in just two weeks. In contrast, when vaccine coverage is limited to only 20%, this critical threshold is reached only after six weeks (Figure 22a).

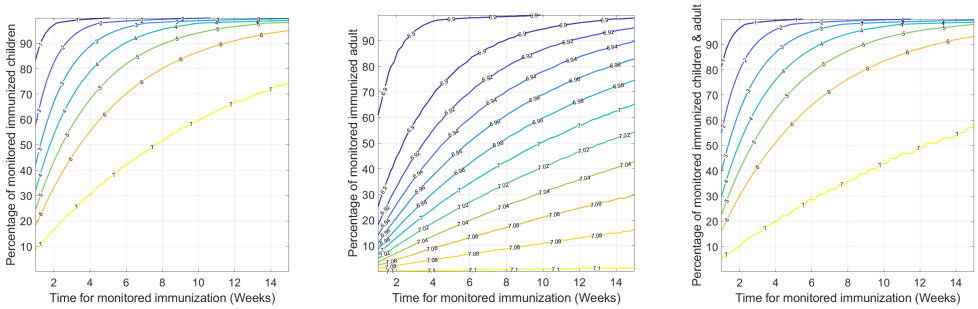

(a) **(b)** **(c)**

Figure 22: Time (in weeks) for the effective reproduction number to be less than one when (a) only children are immunized, (b) only adults are immunized, and (c) children and adults are immunized.

Our model predicts that a vaccination campaign focused only on adults may not be sufficient to reduce the effective reproduction number to below one within a reasonable time frame. As depicted in Figure (22b), the complete vaccine coverage of adults within two weeks slightly lowers the effective reproduction number in about seven weeks. The vaccination distributed among the combined population is less effective than the vaccination entirely given to children. In this case, the threshold can be lowered to below one in one week by 90% of vaccine coverage within three weeks, while it takes six weeks for 30% of coverage within two weeks (Figure 22c).

5.3.3.2 On the Reduction of Disease Burden

We also explore the impact of vaccine coverage over a specific period on reducing measles cases and the maximum weekly cases. Our modeling reveals a significant variation in the effects of vaccine coverage across distinct age groups (Figure 23). 20% of children vaccination within two weeks can reduce about 85% of the total measles cases and 85% of the maximum weekly cases, while 90% of children vaccination within six weeks can reduce more than 90% of the total measles cases and more than 90% of the maximum weekly cases (Figure 23a, 23b). In contrast, 20% of adult vaccinations within two weeks can reduce only 10% of the total cases and only 5% of the maximum weekly cases. Even 90% of the adult vaccinations within six weeks can reduce only 12% of the total cases and only 7% of the maximum weekly cases (Figure 23c, 23d).

90% of combined adult-child vaccination within two weeks reduces about 80% of the total measles cases and 80% of the maximum weekly cases (Figure 23e, 23f). These results highlight that the effectiveness of vaccination in diminishing measles prevalence

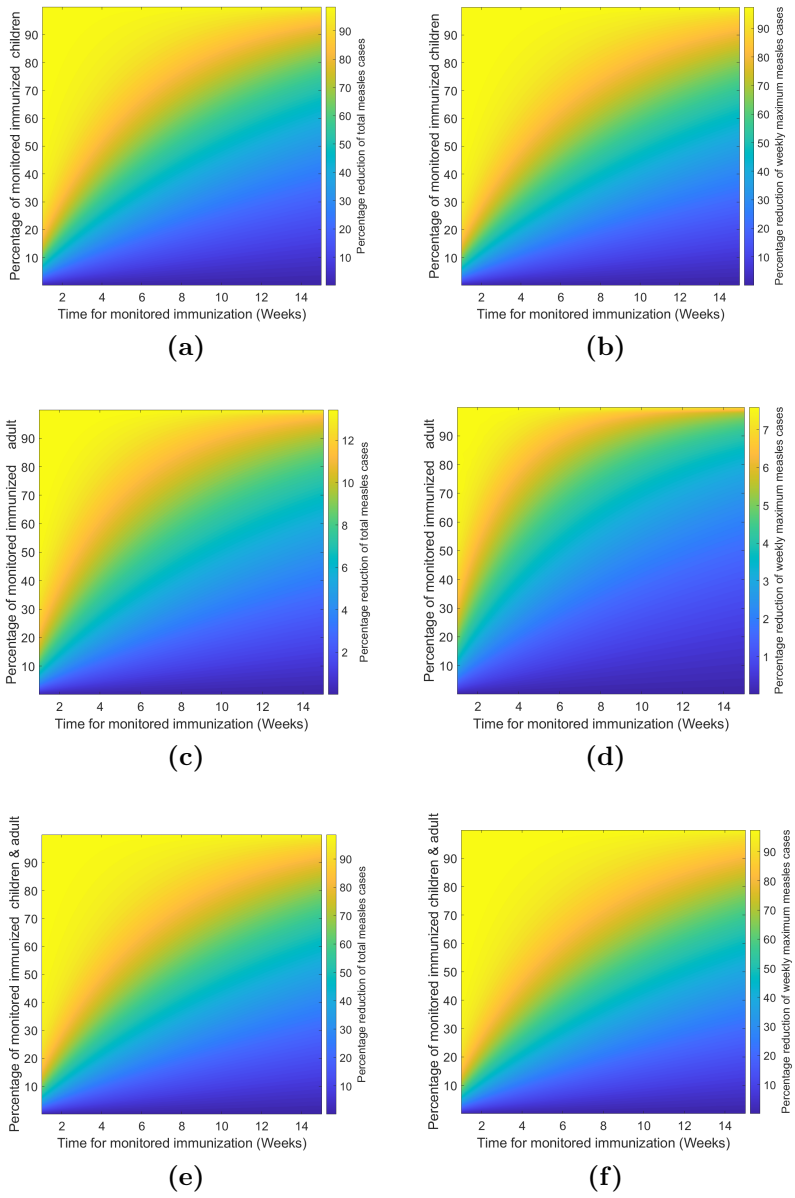

Figure 23: Impact of the coverage of monitored children vaccination on the percentage reduction of (a) the total measles cases and (b) weekly maximum new cases of measles, adult vaccination on the percentage reduction of (c) the total measles cases and (d) weekly maximum new cases of measles, the children and adult vaccination on the percentage reduction of (e) the total measles cases and (f) weekly maximum new cases of measles.

is notably more pronounced in vaccination programs focused on children (Figure 23a) than adults (Figure 23c). However, it is worth noting that even though the adult vaccination may reduce the burden negligibly compared to childhood vaccination, it still plays a vital role in controlling the disease, especially for eradication, since adults may act as a potential reservoir source for persistent disease transmission.

5.3.4 Infections in Adults: Implications to Disease Eradication

As found above, vaccination focused on adults only has the negligible benefit of reducing the disease burden compared to vaccination focused on children. However, persistent infection in adults may pose an obstacle to measles eradication. Therefore, we further performed a deeper analysis to explore whether a realistic adult infection-related parameter range exists that may cause an obstacle to eradication. To examine this, we identified the region corresponding to the disease eradication ($R_v < 1$) and disease persistence ($R_v > 1$) in the ξ_M-ξ_A parameter space of children and adults vaccination rates (Figure 24).

As illustrated in Figure 24, with the parameter range $3 \leq \xi_M \leq 17(\times 10^{-5})$ and $0 \leq \xi_A \leq 10(\times 10^{-4})$, we observe that there exists a realistic parameter range (space below $R_v = 1$ curve in Figure 24) for which $R_v > 1$. This indicates that unless the child vaccination rate is sufficiently large, the value of R_v may remain above one due to some persistent infection in adults. In this case, introducing adult vaccination on top of the child vaccination can reduce R_v below one. Therefore, in the situation when children-focused vaccination is not sufficiently large enough, which is likely the case in developing countries like Nepal, persistent infection in adults can be a major hurdle for disease eradication, and considering adult-focused vaccination along with children's vaccination becomes critical for global disease eradication.

5.4 Conclusion

In recent years, measles outbreaks have occurred frequently in many places of the globe. The threat of measles is growing due to the expansion of immunity gaps, COVID-19's disruption of routine immunization, and the lack of planned global vaccination campaigns. The reduction of vaccination is also attributed to various factors, including societal and educational impacts and religious barriers. In Nepal, the decline in

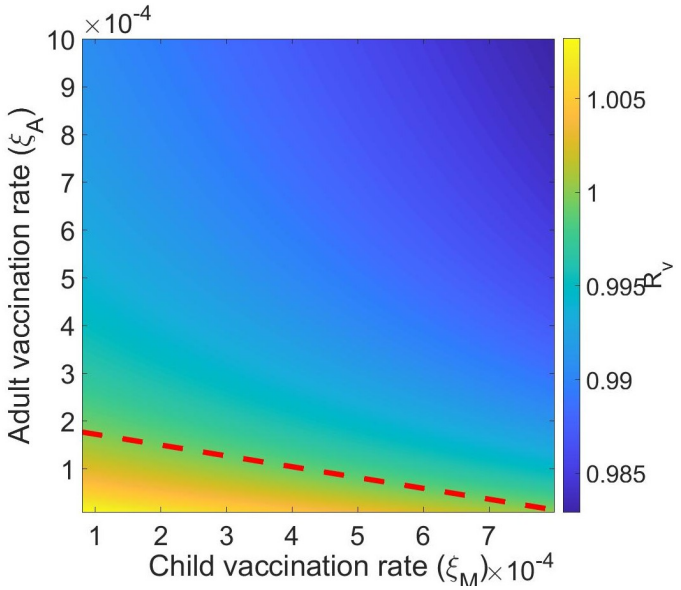

Figure 24: Value of R_v for combinations of children and adults vaccination rates (ξ_M-ξ_A parameter space). The dashed red line corresponds to $R_v = 1$.

vaccination coverage corresponds to the patterns of measles epidemics. While a higher proportion of cases are observed in young infants and older children, a small number of cases have frequently been observed in Nepalese adults WHO, Disease outbreak news, Item, Measles (2023), implying that the unvaccinated adults may serve as a virus reservoir to cause obstacles to WHO's eradication goal. The model developed in this study with both children and adult groups is essential to identify the ideal monitored vaccination strategy for both adults and children to ensure the global eradication of measles.

Using our model validated by the measles case data of different regions of Nepal from November 24, 2022, to March 10, 2023World Health Organization (14 March 2023), we estimated the measles-vaccinated reproduction number in Nepal to be $R_v = 11.677$. The value of R_v is much higher than one, indicating that significant efforts need to be put into the vaccination program in Nepal to meet WHO's global eradication goal. Most notably, our model predicts a critical adult vaccination level required in combination with a partially successful children's vaccination program to bring R_v less than one. Therefore, our study underscores the need for combined adult and children vaccination for measles eradication, in contrast to the often ignored adult group in vaccination programs.

We explored the effect of the contact network size on measles epidemics. We found that increasing contact networks ultimately increases the total and weekly measles

cases in children and adults. Interestingly, the increase in measles burden is more pronounced due to the rise of contact networks among adults than children, mainly when the increased level is more than ten times the base case. This result further highlights the importance of adult vaccination, which lowers the adult susceptible population, thereby reducing the total infection and weekly infection.

We also examined the impact of vaccine coverage on disease trends (Figure 22) and the disease burden (Figure 23). Our model helps identify a reasonable level of child-adult vaccine coverage to ensure the decreasing trend of measles (i.e., $R_e < 1$). For example, 90% in three weeks or 30% in two weeks of vaccine coverage can bring R_e less than one in one day or six days, respectively. Similarly, our model allows us to properly evaluate the vaccination program for reducing the disease burden. For example, an 80% reduction in the total measles cases and an 80% reduction in the maximum weekly cases can be achieved by covering 90% adult and child population within two weeks of vaccination. Our results show that the vaccine focused entirely on children can reduce the disease burden more than that distributed among both children and adults, highlighting the significance of prioritizing childhood vaccine coverage as a primary strategy for reducing disease burden. However, as discussed above, adult vaccination should not be overlooked as it may have a critical role in disease eradication. Our result is consistent with the previous studies Aldila and Asrianti (2019); Garba et al. (2017); Jaharuddin and Bakhtiar (2020); Lessler et al. (2016); Pokharel et al. (2022).

We acknowledge some limitations of our study. The parameter estimations were based on the limited data of weekly incidence cases. The lack of granular data and information could have hindered the achievement of more accurate outcomes. Although we successfully derived the closed form of the distinct endemic equilibrium, we were unable to complete a thorough analysis of this equilibrium due to model complexities. For example, we couldn't achieve the stability condition of endemic equilibrium, while we only explored the stability of endemic equilibrium through numerical methods. We have ignored the potential effects of spatial heterogeneity on disease transmission and assumed a homogenous mixed population. Spatial heterogeneity may play a role in disease transmission, especially in the spread of measles in some specific districts of Nepal. Further study on the cost-effectiveness analysis based on the country's financial status would benefit the optimal policy design to achieve the measles eradication goal.

In summary, we developed a novel model of measles transmission in the context of Nepal, incorporating the two different age groups, children (under 15) and adults (15 and above). Our model demonstrates that the adult group is a potential reservoir

of measles, causing obstacles to eradicating the disease. Our results suggest that implementing the adult vaccines along with the children's vaccine is critical for achieving WHO's global measles eradication goal. A well-planned adult-child combination of monitored vaccination programs may be necessary to facilitate the ambitious objective of eradicating measles from Nepal.

CHAPTER 6

6. SUMMARY AND CONCLUSION

The primary objectives of this study are to construct comprehensive mathematical models for analyzing the transmission dynamics of measles, investigate impact of monitored vaccination on chidren and adults group in transmission dynamics, particularly within Nepal, and assess potential control measures. Furthermore, the study aims to validate the developed mathematical models using real data in Nepal, enabling the estimation of critical parameters, disease threshold values the vaccinated reproduction number (R_v) and the time-varying effective reproduction number (R_e). This validation enhances our understanding of the disease's spread and informs important of proper vaccination.

6.1 Summary

In chapter 2, the study establishes the groundwork by presenting fundamental background information on epidemiology and mathematical modeling and, introduces key theoretical analysis techniques utilized throughout the dissertation. Chapter 3 is dedicated to crafting two deterministic mathematical models, their validation, and the estimation of crucial parameters. One model accounts for measles yearly cases from 2000 to 2019 in Nepal, considering monitored and unmonitored vaccination. Another model, incorporating adults and children, examines the impact of adult and child vaccination in eradicating the disease. Real data is utilized for model validation and parameter estimation. Chapter 4 focuses on the mathematical analysis of the models developed in chapter 3 and establishes the existence and dynamics of equilibrium points, as well as the vaccinated and effective reproduction numbers.

Our thorough analysis and numerical simulations in chapter 5 provides policymakers with crucial insights for designing effective monitored vaccination programs to eradicate measles in Nepal. Our model analysis highlights adults as a potential reservoir for measles, underscoring the importance of integrating adult vaccination with child immunization to meet the WHO's global eradication goal. Coordinating monitored vaccination efforts for both adults and children is essential for achieving the ambitious aim of eliminating measles from Nepal.

In the course of this research, several key tools and methods were utilized to enhance the robustness and reliability of our models. For optimizing the model, this work employed the nonlinear least square method to estimate the parameters. These methodologies enable us to precisely determine the most appropriate parameter values by fitting them with real data. This comprehensive approach refines our models while simultaneously providing a robust assessment of parameter uncertainty. We also utilize identifiability of the estimated parameters. This step is crucial in validating the model and confirming that the parameters can be accurately determined from the available data, thereby enhancing the model's credibility. To analyze global sensitivity, we employed Latin Hypercube Sampling (LHS). This statistical method allowed us to efficiently sample the parameter space and assess the impact of various parameters on the model's outcomes. By identifying the most influential parameters, LHS provided insights into which factors are most critical for measles transmission and control, thereby guiding targeted intervention strategies. In this work, we use MATLAB (The MathWorks, Inc.), for the numerical simulations.

We acknowledge limitations in our study, including parameter estimations based on limited data and the assumption of homogeneous mixing among children in Nepal. Incorporating a contact network model and obtaining more granular data could improve accuracy.

6.2 Conclusion

This work focuses on realistic vaccination scenarios, developing epidemic models that highlight the complex dynamics of measles transmission and the critical role of vaccination in controlling and eradicating the disease. We prioritize capturing the interaction of influential factors within real-world scenarios, incorporating variables such as behavioral responses, health education, immunization planning, and the impact of vaccination.

This dissertation presents formulation of two epidemic models to describe measles transmission in Nepal. One model incorporates vaccination scenarios and health education, while another one emphasizes the importance of considering both child-adult vaccination in measles eradication programs. Desertation includes the validation of the models with real measles cases in Nepal and the estimation of the parameters. The work also focuses on mathematical analysis and, numerical analysis with simulations. The mathematical analysis includes the existence of equilibria, their dynamics, computation

of vaccinated reproduction number, and effective reproduction number.

The numerical analysis of monitored and unmonitored vaccination programs reveals that monitoring vaccination is critical for the successful implementation of the vaccination program. These findings provide valuable information for policymakers to design effective monitored vaccination programs to eliminate the disease. The approach of two different age groups results in representations of disease dynamics that accurately reflect the importance of the proper child vaccination as well as combined adult and child vaccination for the eradication of the disease. Moreover, the two models provide valuable insights into the dynamics of disease transmission in vaccinated populations. The monitored vaccination model suggests a stable endemic situation, while the adult-child vaccination model indicates a need for more aggressive control measures to prevent an epidemic. Understanding these dynamics is crucial for effective public health planning and intervention.

In conclusion, this work advocates for a comprehensive vaccination strategy that includes monitored vaccination programs, and both adult-child vaccination programs. Utilizing these approaches, public health authorities can strengthen measles control efforts and advance toward eradication. The application of robust statistical and analytical tools has established a solid foundation for our findings.

6.3 Suggestion for Future Direction

In the future research we propose the following domains for additional investigation into the dynamics of the epidemic for potential public health interventions and help the policy makers:

- Continuing this work to refine models and explore the impact of various vaccination strategies in different epidemiological and socio-economic contexts. This will ensure that vaccination programs are both effective and adaptable, ultimately leading to a measles-free world.
- Developing a within host model to study the transmission dynamics of virus within a host.
- Understanding the impact of vaccination on measles transmission involves examining factors such as vaccine efficacy, vaccine coverage rates, and the potential for

immunity to decrease over time. By utilizing epidemic models to analyze these factors, we can evaluate role of vaccination toward the eradication of measles.

- By using the epidemical model, additional examination of the cost-effectiveness analysis, considering the financial status of the country, enhances the development of an optimal policy to attain the goal of measles eradication.

References

K. Adhikari, R. Gautam, A. Pokharel, KN. Uprety, and NK. Vaidya. Transmission dynamics of covid-19 in nepal: Mathematical model uncovering effective controls. *Journal of Theoretical Biology*, **521**:110680, 2021. ISSN 0022-5193. doi: https://doi.org/10.1016/j.jtbi.2021.110680.

K. Adhikari, R. Gautam, A. Pokharel, M. Dhimal, K.N. Uprety, and N. K Vaidya. Insight into delta variant dominated second wave of COVID-19 in Nepal. *Epidemics*, **2022**:100642, 2022. doi: https://doi.org/10.1016/j.epidem.2022.100642.

K. Adhikari, R. Gautam, A. Pokharel, M. Dhimal, K.N. Uprety, and NK. Vaidya. Data-driven models for the risk of infection and hospitalization during a pandemic: Case study on covid-19 in nepal. *Journal of Theoritical Biology*, **574**:111622, 2023.

D. Aldila and D. Asrianti. A deterministic model of measles with imperfect vaccination and quarantine intervention:. *International Conference on Mathematics: Pure, Applied and Computation*, **1218**:012044–012054, 2019. doi: 10.1088/1742-6596/1218/1/012044.

H. Tessema Alemneh and A. Mesele Belay. Modelling, analysis, and simulation of measles disease transmission dynamics,. *Discrete Dynamics in Nature and Society*, **2023**, 2023. doi: https://doi.org/10.1155/2023/9353540.

R. Anderson and R May. *Infectious Diseases of Humans: Dynamics and Control:*. Oxford University Press, Oxford, 1992.

F. Andrea and P. Andrea. Threshold behaviour of a SIR epidemic model with age structure and immigration. *Journal of mathematical biology*, **57**:1–27, 08 2008. doi: 10.1007/s00285-007-0143-1.

Anet JN. Anelone, J Edward Hancock, N. Klein, K. Peter, and S. Spurgeon K. Control theory helps to resolve the measles paradox. *R. Soc.Open Sci.*, **8**, 2021. doi: https://doi.org/10.1098/rsos.201891.

S. Mata Angélica and S.M.P. Dourado. Mathematical modeling applied to epidemics: an overview. *São Paulo J. Math. Sci*, **15**:1025–1044, 2021. doi: https://doi.org/10.1007/s40863-021-00268-7.

HT. Banks and ML. Joyner. Information content in data sets: a review of methods for interrogation and model comparison:. *J. Inverse Ill-Posed Probl.*, **26**:423–452, 2018. doi: https://doi.org/10.1515/jiip-2017-0096.

HT. Banks, S. Hu, and WC. Thompson. *Modeling and inverse problems in the presence of uncertainty*. CRC Press, Taylor and Francis Group, A Chapman and Hall Book, 2014.

D. Bernoulli. Essai d'une nouvelle analyse de la mortalité cause par la petite vérole et des avantages de l'inoculation pour la prévenir. histoire de l'académie royale des sciences avec les mémoires de mathématique:. *History of Actuarial Science*, **8**:1766, 1766.

B. Bolker and B. Grenfell. Space, persistence and dynamics of measles epidemics:. *Philosophical Transactions: Biological Sciences*, **348**(1325:):309–320, 1995.

AS. Boss, P. Rai, BP. Gupta, R. Pradhan, M. Lacoul, S. Shakya, and et al. Nepal measles outbreak response immunization during covid-19: A risk-based intervention strategy:. *Vaccine*, **40**(20):2884–2893, 2022.

F. Brauer and CC.Chavez. *Mathematical models in population biology and epidemiology:*. Springer, 2012.

B.Zadrozny and E. Edwards. Anti-vaccine groups take dangerous online harassment into the real world:, 2019.

Child Health Division, DoHS,MoHP. National immunization program reaching every child, comprehensive multi-year plan 2068-2072 (2011- 2016). Technical report, MoHP, 2011.

G. Chowell and JM. Hyman. *Mathematical and Statistical Modeling for Emerging and Re-emerging Infectious Diseases*. Springer, 2016. ISBN 978-3-319-40413-4 (eBook). doi: 10.1007/978-3-319-40413-4.

P. Christina and A Y. Christian. Role of mathematical modelling in future pandemic response policy. *BMJ*, **378**, 2022. doi: 10.1136/bmj-2022-070615.

FJ. Christopher, S. Katriona, and C. Spencer et al. Measles outbreak response decision-making under uncertainty: a retrospective analysis :. *J. R. Soc. Interface*, **15**, 2017. URL `http://doi.org/10.1098/rsif.2017.0575R`.

CC. Chávez, F. Zhilan, and W. Huang. On the computation of r0 and its role in global stability. *IMA Volumes in Mathematics and Its Applications*, **125**:229–250, 2002. doi: https://doi.org/10.1007/978-1-4757-3667-0_13.

V. Colizza and A. Vespignani. Invasion threshold in heterogeneous metapopulation networks:. *Phys. Rev. Lett.*, **99**, 2007. doi: https://doi.org/10.1103/PhysRevLett.99.148701.

FT Cutts, Ea Dansereau, MJ Ferrari, M Hanson, KA McCarthy, CJE Metcalf, and et al. Using models to shape measles control and elimination strategies in low- and middle-income countries: A review of recent applications. *Vaccine*, **38**(5):979–992, 2020. doi: 10.1016/j.vaccine.2019.11.020.

DJ Daley and J Gani. *Epidemic Modeling: An Introduction:*. Cambridge University Press, 2005. doi: https://doi.org/10.1017/CBO9780511608834.

Chris Dall. Nepal hit by measles outbreak, 14 March 2023. URL `https://www.who.int/emergencies/disease-outbreak-news/item/2023-DON446`.

CE. Dangerfield, ID Abrahams, C. Budd, M. Butchers, ME. Cates, AR. Champneys, and et al. Getting the most out of maths: How to coordinate mathematical modelling research to support a pandemic, lessons learnt from three initiatives that were part of the COVID-19 response in the UK. *Journal of Theoretical Biology*, **557**:111332, 2023.

JD. Earn David, P. Rohani, M. Bolker Benjamin, and Bryan T. Grenfell. A simple model for complex dynamical transitions in epidemics:. *Science*, **287**(5453:):667–670, 2000.

Department of Health and Social Care. *SPI-M modelling summary for pandemic influenza, Edition. Nov,*. GOV. UK, 2018. URL `https://assets.publishing.service.gov.uk/government/uploads/system/uploads/attachment_data/file/756738/SPI-M_modelling_summary_final.pdf`.

O. Diekman, HJA. Peter, and AJM Johan. On the definition and the computation of the basic reproduction ratio R0 in models for infectious diseases in heterogeneous populations:. *Journal of mathematical biology*, **28**:365–382, 1990.

O. Diekmann and JA Peter Heesterbeek. Mathematical epidemiology of infectious diseases: Model building, analysis and interpretation:. *International Journal of Epidemiology*, **30**(1):186–186, 2001. doi: https://doi.org/10.1093/ije/30.1.186.

O. Diekmann, H. Johan Andre Peter, and M .ohan AJ. The construction of next-generation matrices for compartmental epidemic models:. *J. R. Soc. Interface*, **7**, 2010. doi: https://doi.org/10.1098/rsif.2009.0386.

Lake County General Health District. Measles, 2023. URL `https://www.lcghd.org/measles/`.

MG. Dixon, M. Ferrari, S. Antoni, and et.al. Progress toward regional measles elimination worldwide, 2000–2020:. *Morbidity and Mortality Weekly Report*, **70**(45), 2021.

P. van den Driessche and J. Watmough. Reproduction numbers and sub-threshold endemic equilibria for compartmental models of disease transmission:. *Mathematical Biosciences*, **180**, 2002. doi: https://doi.org/10.1016/S0025-5564(02)00108-6.

A Train Education. Measles epidemic: Overcoming vaccine prejudice. Technical report, 2024. URL `https://www.atrainceu.com/content/2-history-and-pathology-measles`.

S. Edward, E. Kitengeso Raymond, T. Kiria Gabriel, N. Felician, G. Mwema Godfrey, and P. Mafarasa Arbogast. A mathematical model for control and elimination of the transmission dynamics of measles. *Applied and computational mathematics*, **4**: 396–408, 09 2015. doi: 10.11648/j.acm.20150406.12.

B.-P. Ellen, D. Leon, J. Thibaut, and P. Lorenzo. Modelling that shaped the early COVID-19 pandemic response in the UK:, 2021.

I M Foppa. *A historical introduction to mathematical modeling of infectious diseases: Seminal Papers in Epidemiology:*. Academic Press, 2016.

Centers for Disease Control and Prevention. Measles symptoms and complications, 2020. URL `https://www.cdc.gov/measles/symptoms/index.html`.

B. Fred. Mathematical epidemiology: Past, present, and future:. *Infectious Disease Modelling*, **2**(2):113–127, 2017.

M. Ongau Fred, J. Sigey, Jeconiah A. Okello, and et al. Mathematical modeling on the control of measles by vaccination: Case study of kisii county, kenya:. *The SIJ Transactions on Computer Science Engineering & its Applications (CSEA)*, **2**:38–46, 2015. doi: 10.9756/SIJCSEA/V2I4/0203150101.

SM. Garba, MA. Safi, and S. Usaini. Mathematical model for assessing the impact of vaccination and treatment on measles transmission dynamics. *Mathematical Methods in the Applied Science*, **40**(18), 2017. doi: https://doi.org/10.1002/mma.4462.

R. Gautam, A. Pokharel, K. Adhikari, KN. Uprety, and NK. Vaidya. Modeling malaria transmission in nepal: impact of imported cases through cross-border mobility:. *Journal of Biological Dynamics*, **16**(1):528–564, 2022. doi: 10.1080/17513758.2022.2096935.

M. George. The epidemiology and control of malaria:. *The Epidemiology and Control of Malaria.*, 1957.

FR. Giordano, WP. Fox, and SB. Horton. *A first course in mathematical modeling:*. Cengage Learning, 2013.

EF. Doungmo Goufo, Noutchie SC. Oukouomi, and S. Mugisha. A fractional seir epidemic model for spatial and temporal spread of measles in metapopulations:. *Abstract and Applied Analysis*, **2014**:6, 2014. doi: 10.1155/2014/781028.

B. Guarino and S. Lena H. New york anti-vaccine event attracts pro-vaccine protests amid measles outbreak, 2019.

S. Gui-Quan, W. Shi-Fu, L. Ming-Tao, L. Li, Z. Juan, Z. Wei, J. Zhen, and F. Guo-Lin. Transmission dynamics of COVID-19 in Wuhan, China: effects of lockdown and medical resources:. *Nonlinear Dynamics*, **101**:1981–1993, 2020.

S. Guseva, S. Milles, M. Blackledge, and Rob WH. Ruigrok. The nucleoprotein and phosphoprotein of measles virus:. *Front Microbiol*, **10**:1832, 2019. doi: 10.3389/fmicb.2019.01832.

T. Britton H. Andersson. *Stochastic Epidemic Models and Their Statistical Analysis:*. Lecture Notes in Statistics 151. Springer-Verlag New York, 1 edition, 2000. ISBN 978-0-387-95050-1,978-1-4612-1158-7. URL `http://gen.lib.rus.ec/book/index.php?md5=2afc15af9e933514e050ecaa62d39eda`.

X. Xia H. Miao, A. S. Perelson, and H. Wu. On identifiability of nonlinear ode models and applications in viral dynamics:. *SIAM Rev.*, **53**:3–39, 2011. doi: https://doi.org/10.1137/090757009.

WH. Hamer. The milroy lectures on epidemic disease in england—the evidence of variability and persistence of type:. *The Lancet*, **1**, 1906. doi: 1906;167:733738.

HW. Hethcote. An age-structured model for pertussis transmission. *Mathematical Bioscience*, **145**:89–136, 1997.

MW. Hirsch, S. Smale, and RL. Devane. *Dfferential Equation, Dynamical Systems and an Introduction to Chaos:*. Elsever, 2004.

M. Hongyu, X. Xiaohua, P. Alan S, and W. Hulin. On identifiability of nonlinear ODE models and applications in viral dynamics:. *SIAM review*, **53**(1):3–39, 2011.

J. Horrocks and CT. Bauc. Algorithmic discovery of dynamic models from infectious disease data:. *Sci. Rep.*, 10:7061, 2020. doi: https://doi.org/10.1038/s41598-020-63877-w.

C. I-Chun and V. Eberhard O. Recent developments in parameter estimation and structure identification of biochemical and genomic systems:. *Mathematical biosciences*, **219**(2):57–83, 2009.

Y. Ichimura, M. Yamauchi, N. Yoshida, S. Miyano, and et al. Effectiveness of immunization activities on measles and rubella immunity among individuals in east sepik, papua new guinea: A cross-sectional stud:y. *PMC- IJID*, **3**, 2022. doi: 10.1016/j.ijregi.2022.03.001.

Jaharuddin and T. Bakhtiar. Control policy mix in measles transmission dynamics using vaccination, therapy, and treatment. *International Journal of Mathematics and Mathematical Sciences*, **2020**:20, 2020. doi: 10.1155/2020/1561569.

AB. Joshi. Measles deaths in nepal: estimating the national cases in fatality ratio:. *Bull World Health Organ 2009*, **87**(6):405–484, 2009. doi: 10.2471/BLT.07.050427.

D Joubert, JD Stigter, and J Molenaar. Determining minimal output sets that ensure structural identifiability:. *PLoS One*, **13**(11):1–19, 2018.

KB. Karki, M. Dhimal, A. Raj Pandey, B Bista, and .et al. Measles outbreak in kapilvastu, nepal: An outbreak investigation 2016. Technical report, Nepal Health Research Council, 2016.

T. Kato. *Perturbation theory for linear operators*. Springer-Verlag, Berlin Heidelberg, 1976.

MJ. Keeling and Bryan T. Grenfell. Understanding the persistence of measles: reconciling theory, simulation and observation. *Proceedings of the Royal Society B: Biological Sciences*, **269**(1489), 2002.

MD Van Kerkhove and N M Fergusona. Epidemic and intervention modelling: a scientific rationale for policy decisions? lessons from the 2009 influenza pandemic:. *Bulletin of the World Health Organization*, **90**(4):306–310, 2012.

S. Khanal, TR. Sedain, GR. Choudary, JN. Giri, RB., R. Pant, and et al. Progress toward measles elimination - nepal, 2007–2014. *CDC Morbidity and Mortality Weekly Report (MMWR):*, **65**(8:):206–210., 2016. doi: http://dx.doi.org/10.15585/mmwr.mm6508a3externalicon.

Knoema. Nepal- deaths due to measles among children aged < 5 years, 2017. URL `https://knoema.com/atlas/Nepal/topics/Health/Deaths-among-children-under-5-by-cause/Deaths-due-to-measles`.

MA. Kuddus, M. Mohiuddin, and A. Rahman. Mathematical analysis of a measles transmission dynamics model in bangladesh with double dose vaccination,. *Sci Rep.*, **11**(1):16571, 2021. doi: 10.1038/s41598-021-95913-8.

S. Selva Kumar, A-M. Hartner, A. Chandran, K A.M. Gaythorpe, X. Li, and et al. Evaluating effective measles vaccine coverage in the malaysian population accounting for between-dose correlation and vaccine efficacy. *BMC Public Health*, **23**(2351), 2023. doi: https://doi.org/10.1186/s12889-023-17082-9.

M. De la Sens, A. Quesadas, A. Ibeas, and R. Nistal. An observed-based vaccination lawfor a seir epidemic model:. *International Journal of Computer Theory and Engineering*, **4**(3), 2012. doi: 10.7763/IJCTE.2012.V4.488.

J. Lessler, C. Jessica E. Metcalf, Felicity T. Cutts, Bryan, and T. Grenfell. Impact on epidemic measles of vaccination campaigns triggered by disease outbreaks or serosurveys: A modeling study. *PLoS Med*, **13**(10), 2016. doi: https://doi.org/10.1371/journal.pmed.1002144.

Memorial Sloan Kettering Cancer Center Library. Global measles outbreaks, 2024. URL `https://libguides.mskcc.org/publichealth/MeaslesOutbreaksGlobal`.

LM Nic Lochlainn, B de Gier, N van der Maas, PM Strebel, T Goodman, RS van Binnendijk, and et.al. Immunogenicity, effectiveness, and safety of measles vaccination in infants younger than 9 months: a systematic review and meta-analysis. *Lancet Infect Dis*, **11**:1235–124, 2019. doi: 10.1016/S1473-3099(19)30395-0.

Macrotrends. Nepal population 1950-2020. URL `https://www.macrotrends.net/countries/NPL/nepal/population`.

A. Maksat, F-N Yves, A. Kaandorp Jaap, and G. Blom Joke. Systems biology: parameter estimation for biochemical models:. *The FEBS journal*, **276**(4):886–902, 2009.

P. Manesha, K. Malavika, B. Kerri, David N Hackney, and R. Kimberlyn M. Forecasting the impact of coronavirus disease during delivery hospitalization: an aid for resource utilization:. *American Journal of Obstetrics & Gynecology MFM*, **2**(3):100127, 2020.

S. Marino, Ia B. Hogue, Christian J. Ray, and Denise E. Kirschner. A methodology for performing global uncertainty and sensitivity analysis in systems biology. **254** (1):178–196, 2008. doi: 10.1016/j.jtbi.2008.04.011.

M. Martcheva. *An Introduction to Mathematical Epidemiology:*. Springer, 2008. ISBN 978-1-4899-7611-6. doi: 10.1007/978-1-4899-7612-3.

RY. M'pika Massoukou, Noutchie S. Clovis Oukouomi, and R. Guiem. Global dynamics of an sveir model with age-dependent vaccination, infection, and latency:. *Abstract and Applied Analysis*, **2018**:21, 2018. doi: org/10.1155/2018/8479638.

B. Matthew, D. Fredrick Scott, F. Julia, George D. George, Hammond A., Hall I., Haw D., and et al. Coordinating the real-time use of global influenza activity data for better public health planning:. *Influenza and Other Respiratory Viruses*, **14**(2): 105–110, 2020.

MD. McKay, R.J. Beckman, and W.J. Conover. A comparison of three methods for selecting values of input variables in the analysis of output from a computer code:. *Technometrics*, **21**(2:):239–245, 1979. doi: https://doi.org/10.2307/1268522.

A. G McKendrick. Applications of mathematics to medical problems:. *Proceedings of the Edinburgh Mathematical Society*, **44**:98–130, 1925.

Z. Memon, S. Qureshi, and B. Rasool Memon. Mathematical analysis for a new nonlinear measles epidemiological system using real incidence data from pakistan. *Eur. Phys. J. Plus*, (135):378, 2020. doi: 10.1140/epjp/s13360-020-00392-x.

L. Min-Shi, K. Chwan-Chuen, J. Jia-Yuh, and et al. Seroepidemiology and evaluation of passive surveillance during 1988–1989 measles outbreak in taiwan. *International Journal of Epidemiology*, **21**(6):1165–1174, 1992. doi: https://doi.org/10.1093/ije/21.6.1165.

Mitku and Selam. Mathematical modeling and simulation study for the control and transmission dynamics of measles:. *American Journal of Applied Mathematics*, **5**: 99–107, 2017. doi: 10.11648/j.ajam.20170504.11.

MoHP. Government of nepal, ministry of health and population, national immunization programme, a. URL `https://mohp.gov.np/program/national-immunisation-programme/en`.

MoHP. National immunization programme. Technical report, Government of Nepal, Ministry of Health and Population Child Health Division, Department of Health Services (DoHS), b. URL `http://www.chd.gov.np`.

A. Atte Momoh, M. Olanrewaju Ibrahim, IJ. Uwanta, and SB. Manga. Mathematical model for control of measles epidemiology:. *Inter. J. Pure Appl. Math*, **67**:707–718, 2013. doi: 10.1016/S0031-8914(53)80099-6.

H. Motulasky and A. Christopoulos. *Fitting Model to Biological Data Using Linear and Non Linear Regression. A Practical Guide to Curve Fitting:*. Graph Pad Software Inc.San Diego,CA, 2003. URL `www.graphpad.com`.

F. Muhammad, S. Aamir, A. Ali, B. Dumitru, and S. Manuel De la. Modelling and analysis of a measles epidemic model with the constant proportional caputo operator,. *Symmetry*, **15**(2), 2023. doi: 10.3390/sym15020468.

E. Mueni Musyoki, R. Ndung'u, and S. Osman. A mathematical model for the transmission of measles with passive immunity. *International Journal of Scientific Research in Mathematical and Statistical Sciences*, **6**(2):01–08, 2019.

JM. Mutua, F.-Bin Wang, and NK. Vaidya. Modeling malaria and typhoid fever co-infection dynamics. *Mathematical Biosciences*, **264**:128 – 144, 2015. ISSN 0025-5564. doi: https://doi.org/10.1016/j.mbs.2015.03.014.

T. Robin N, E S. Jake, RD. van Gaalen, and et al. Improved inference of time-varying reproduction numbers during infectious disease outbreaks:. *Epidemics*, **29**:100356, 2019.

New Spotlight online. Number of measles cases in nepal increased by more than two times in 2018, April 2019. URL `https://www.spotlightnepal.com/2019/04/25/number-measles-cases-nepal-increased/`.

NYC. Measles, 2019. URL https://www1.nyc.gov/site/doh/health/health-topics/measles.page.

C. Obumneke, II. Adamu, and S Timothy Ado. Mathematical model of the dynamics of measles under the combined effect of vaccination and measles therapy:. *International Journal of Science and Technology*, **6**:118–173, 2017.

J. Ochoche and RI. Gweryina. A mathematical model of measles with vaccination and two phases of infectiousness:. *Journal of Mathematics*, **10**(1):95–105, 2019. doi: 10.9790/5728-101495105.

National Statistics Office. National population and housing census 2021 (national report). URL https://censusnepal.cbs.gov.np/results.

SK. Ofori, E.A. Dankwa, E. Ngwakongni, A. Amberbir, A. Bekele, and et al. Evidence-based decision making: Infectious disease modeling training for policymakers in East Africa. *Annal of Global Health*, **90**(22), 2024.

K. William Ogilvy and A. G McKendrick. A contribution to the mathematical theory of epidemics:. *Proceedings of the royal society of london. Series A, Containing papers of a mathematical and physical character*, **115**(772):700–721, 1927.

K. William Ogilvy and A. G McKendrick. Contributions to the mathematical theory of epidemics–I. 1927:. *Bulletin of mathematical biology*, **53**(1-2):33–55, 1991a.

K. William Ogilvy and AG McKendrick. Contributions to the mathematical theory of epidemics - iii. further studies of the problem of endemicity:. *Bulletin of mathematical biology*, **53**(1-2):89–118, 1991b.

Iheanyi Okonko, Ayoteju Ogun, Adedeji, Babalola, Udeze Augustine, Babatunde Motayo, Adewale, Garba, Fowotade Adeola, A. Adekolurejo, O. A, and Obioma Mejeha. The role of laboratory confirmations and molecular epidemiology in global eradication of measles. *AFRICAN JOURNAL OF BIOTECHNOLOGY*, 8:7319–31, 12 2009.

World Health Organization. Nepal - deaths due to measles among children aged <5 years. URL https://www.who.int/immunization/monitoring_surveillance/burden/vpd/WHO_SurveillanceVaccinePreventable_11_Measles_R1.pdf?ua=1.

B. Pantha, S. Giri, HR. Joshi, and NK. Vaidya. Modeling transmission dynamics of rabies in nepal:. *Infect. Dis. Model*, **6**:284–301, 2021. doi: 10.1016/j.idm.2020.12.009.

J. Niall PAS and M. Juergen. Updating the accounts: global mortality of the 1918-1920" spanish" influenza pandemic. *Bulletin of the History of Medicine*, pages 105–115, 2002.

MK. Patel, JL. Goodson, JP. Alexander Jr, and et al. Progress toward regional measles elimination - worldwide, 2000–2019. *Morbidity and Mortality Weekly Report (MMWR)*, **60**(45), 2020.

O. James Peter, M M. Ojo, R. Viriyapong, and F. Abiodun Oguntolu. Mathematical model of measles transmission dynamics using real data from nigeria,. *Journal of Difference Equations and Applications,*, **28**(6):753–770, 2022. doi: 10.1080/10236198.2022.2079411.

O. James Peter, N. Dwi Fahrani, Fatmawati, Windarto, and C.W. Chukwu. A fractional derivative modeling study for measles infection with double dose vaccination,. *Healthcare Analytics*, **4**:100231, 2023a. ISSN 2772-4425. doi: https://doi.org/10.1016/j.health.2023.100231.

O. James Peter, S. Qureshi, M. M. Ojo, R. Viriyapong, and A. Soomro. Mathematical dynamics of measles transmission with real data from pakistan:. *Model. Earth Syst. Environ*, **9**:1545–1558, 2023b. doi: https://doi.org/10.1007/s40808-022-01564-7.

A. Pokharel, K. Adhikari, R. Gautam, KN. Uprety, and N K. Vaidya. Modeling transmission dynamics of measles in nepal and its control with monitored vaccination program:. *Mathematical Biosciences and Engineering*, **19**(8), 2022. doi: 10.3934/mbe.2022397.

A. Pokharel, K. Adhikari, R. Gautam, KN. Uprety, and NK. Vaidya. Modeling measles transmission in adults and children: Implications to vaccination for eradication:. *Infectious Disease Modelling*, **9**(4:):1007–1026, 2024. doi: https://doi.org/10.1016/j.idm.2024.04.012.

A. Poudel. Low vaccine coverage rate, floating population leading to repeat measles outbreaks,, May 2019a. URL `https://reliefweb.int/report/nepal/low-vaccine-coverage-rate-floating-population-leading-repeat-measles-outbreaks`.

A. Poudel. Measles outbreak in morang, dang and kapilvastu raises concern:, April 2019b. URL https://kathmandupost.com/national/2019/04/30/measles-outbreak-in-morang-dang-and-kapilvastu-raises-concern.

A. Poudel. Routin immunization:, 2020. URL http://arjunmaske.blogspot.com/2014/09/how-to-measlestransmission.html.

A. Poudel. Measles outbreaks reported in five districts including in kathmandu and lalitpur in last one month:, April 2021. URL https://kathmandupost.com/national/2020/04/29/measles-outbreaks-reported-in-five-districts-including-in-kathmandu-and-lalitpu

M. Poudel. Unidentified disease claims lives of six kids;, 2016. URL https://kathmandupost.com/national/2016/01/20/unidentified-disease-claims-lives-of-six-kids.

Public Health Update. The national immunization programme (national immunization schedule), nepal, 2019. URL https://publichealthupdate.com/national-immunization-schedule/.

M. Rahman, K. Bekele-Maxwell, LL. Cates, HT. Banks, and NK. Vaidya. Modeling zika virus transmission dynamics: parameter estimates, disease characteristics, and prevention. *Sci. Rep.*, **9**:10575, 2019. doi: https://doi.org/10.1038/s41598-019-46218-4.

HS. Rathore. Measles outbreak kills two children and infects over 150 in chepang settlements of dhading district, 2020. URL https://kathmandupost.com/province-no-3/2020/04/06/measles-outbreak-kills-two-children-and-infects-over-150-in-chepang-\settlements-of-dhading-district.

MG. Roberts and MI. Tobias. Predicting and preventing measles epidemics in New Zealand: Application of a mathematical model. *Epidemiology and infection*, **124**: 279–287, 2000. doi: 10.1017/S0950268899003556.

R. Ross. *The prevention of malaria:*. John Murray, 1911.

CD. Schunn and DP. Wallach. Evaluating goodness-of-fit in comparison of models to data. pages 115–135, 2005.

B. Shayak, M. Sharma, H. Richard, AK. Singh, and A. Misra. Transmission dynamics of COVID-19 and impact on public health policy. *MedRxiv*, pages 2020–03, 2020.

S. Sitaula, GR. Awasthi, JB. Thapa, and KP et al. Joshi. Measles outbreak among unvaccinated children in bajura. *JNMA J Nepal Med Assoc*, **50**(180):273–6, 2010. URL https://pubmed.ncbi.nlm.nih.gov/22049889/.

HL. Smith and P. Waltman. *The Theory of the Chemostat*. Cambridge University Press, 1995. ISBN 0-521-47027-7.

X. Song, Y. Jiang, and H. Wei. Analysis of a saturation incidence sveirs epidemic model with pulse and two time delay:. *Applied Mathematics and Computation*, **214**, 2019. doi: https://doi.org/10.1016/j.amc.2009.04.005.

HE. Soper. The interpretation of periodicity in disease prevalence:. *Journal of the Royal Statistical Society*, **92**(1):34–73, 1929.

Statista. Share of children in total population in nepal from 2013 to 2022, 2023. URL https://www.statista.com/statistics/678090/nepal-children-as-a-percentage-of-the-population/.

Lena H. Sun and B. Guarino. Anti-vaxxers target communities battling measles, 2019. URL https://www.washingtonpost.com/national/health-science/antivaxxers-go-viral-in-communities-battling-measles/2019/05/20/a476417c-78d7-11e9-bd25-c989555e7766_story.html.

N. Sunuwar, S. Katuwal, S. Yadav, and et al. The interruption of administering routine measles vaccine in nepal: A point of contention during and post the coronavirus disease 2019 pandemic? *International Journal of Scientific Study*, (4):124–128, 2021.

BK Suvedi. Twenty-five years of immunization program in nepal. *Kathmandu Univ Med J (KUMJ)*, 3(1), 2005.

M. Takeda. Measles virus breaks through epithelial cell barriers to achieve transmission. *J Clin Invest*, **118**(7), 2008. doi: https://doi.org/10.1172/JCI36251.

CK. Thakur, N. Gupta, N. Pokhrel, S. Adhikari, M. Dhimal, and P. Gyanwali. Stumbling blocks on the path to measles-free nepal: impact of the covid-19 pandemic:. *Trop Med Health*, **52**(10), 2024. doi: https://doi.org/10.1186/s12889-023-17082-9.

H. Trottier and P. Philippe. Deterministic modeling of infectious diseases: Theory and methods:. *The Internet Journal of Infectious Diseases*, **1**(2), 2000. doi: 10.1016/S0031-8914(53)80099-6.

H. Trottier and P. Philippe. Deterministic modeling of infectious diseases: Measles cycles and the role of births and vaccination:. *The Internet Journal of Infectious Diseases*, **2**(2), 2002. doi: 10.5580/fe9.

AR. Tuite, DN. Fisman, and AL. Greer. Mathematical modelling of covid-19 transmission and mitigation strategies in the population of ontario, canada:. *CMAJ*, **192** (19):E497–E505, 2020.

UN, News. Measles cases hit 23-year high last year, killing 200,000 as vaccination stalls, who says, 2020.

Unicef for Every Child. More than 140,000 die from measles as cases surge worldwide, 2019. URL https://www.who.int/news/item/05-12-2019-more-than-140-000-die-from-measles-as-cases-surge-worldwide#:~:text=Worldwide%20more%20than%20140%2C000%20people,devastating%20outbreaks%20in%20all%20regions.

S. Uprety. Meanwhile a measles outbreak in nepal, delays in vaccination during lockdown infects more with measles than does coronavirus nationwide:, May 2020. URL https://www.nepalitimes.com/here-now/meanwhile-a-measles-outbreak-in-nepal/.

NK. Vaidya and F-B. Wang. Persistence of mosquito vector and dengue: Impact of seasonal and diurnal temperature variations:. *Discrete and Continuous Dynamical Systems - B*, **27**(1):393–420, 2022. ISSN 1531-3492. doi: 10.3934/dcdsb.2021048.

MJ. Wanjau, R. Titus, and C. Isaac. Mathematical modeling of the transmission dynamics of measles under the effect of vaccination:. *IOSR Journal of Mathematics*, **15**(4):10–19, 2019.

WHO. Measles: Towards elimination in nepal, 2019a. URL https://www.who.int/southeastasia/news/feature-stories/detail/measles-towards-elimination-in-nepal.

WHO. Measles, 2019b. URL https://www.who.int/news-room/fact-sheets/detail/measle.

WHO. Measles and rubella strategic framework 2021–2030, 2020. URL https://www.who.int/publications/i/item/measles-and-rubella-strategic-framework-2021-2030.

WHO. Who vaccine-preventable diseases: monitoring system. 2019 global summary. Technical report, World Health Organization, 2020. URL https://apps.who.int/immunization_monitoring/globalsummary.

WHO. Nearly 40 million children are dangerously susceptible to growing measles threat, 2022. URL https://www.who.int/news/item/23-11-2022-nearly-40-million-children-are-dangerously-susceptible-to-growing-me

WHO. Measles, 2023a. URL https://www.who.int/news-room/fact-sheets/detail/measles.

WHO. Measles reported cases and incidence, 2023b. URL https://immunizationdata.who.int/pages/incidence/MEASLES.html?CODE=Global+NPL&YEAR=.

WHO, Disease outbreak news, Item, Measles. Measles-nepal, 2023. URL https://www.cidrap.umn.edu/measles/nepal-hit-measles-outbreak.

A. William, H. Jennifer, M. Lynne, and W. Charles. Epidemiology and prevention of vaccine-preventable diseases 13th edition:. 13 edition, 2015. URL https://www.cdc.gov/vaccines/pubs/pinkbook/downloads/meas.pdf.

World Health Organization. Measles - nepal, 14 March 2023. URL https://www.who.int/emergencies/disease-outbreak-news/item/2023-DON446.

World Health Organization. Measles – global situation, 2019. URL https://www.who.int/emergencies/disease-outbreak-news/item/2019-DON211.

World Health Organization. Measles, 2023. URL https://www.who.int/news-room/fact-sheets/detail/measles.

Worldometer. Coronavirus Pandemic, 2023. URL https://www.worldometers.info/coronavirus.

Y. Xia, O. N. Bjørnstad, and B.T. Grenfell. Measles metapopulation dynamics: a gravity model for epidemiological coupling and dynamics:. *Am. Nat.*, **164**(2): 267–281, 2004.

X-Q. Zhao. *Dynamical Systems in Population Biology*. Springer, 2017. ISBN 978-3-319-56433-3. doi: 10.1007/978-3-319-56433-3.

Appendix

Publications

1. **Pokharel A.** , Adhikari K., Gautam R., Uprety KN., and Vaidya NK. Modeling measles transmission in adults and children: Implications to vaccination for eradication: Infectious Disease Modelling, (2024), 9(4:):1007–1026, 2024.

2. **Pokharel A**, Adhikari K, Gautam R, Uprety KN, Vaidya NK, Campus A, Campus RR. Modeling transmission dynamics of measles in Nepal and its control with monitored vaccination program. *Math Biosci Eng.* 2022;19(8):8554-79.

3. **Pokharel A.**, Adhikari K., Gautam R. 2024. Modelling the Impact of Vaccination on the Control of Measles in Nepal, *The Nepali Mathematical Sciences Report* (2024),41(1), 15–34, doi; https://doi.org10.3126/nmsr.v41i1.67453.

4. Adhikari K., Gautam R., **Pokharel A.**, Uprety KN., and Vaidya NK.. Transmission dynamics of covid-19 in nepal: Mathematical model uncovering effective controls:. Journal of Theoretical Biology, 521:110680, 2021. ISSN 0022-5193. doi: https: //doi.org/10.1016/j.jtbi.2021.110680.

5. Adhikari K., Gautam R., **Pokharel A.**, Dhimal M., Uprety KN., and Vaidya NK.. Insight into delta variant dominated second wave of COVID-19 in Nepal. Epidemics, page 100642, 2022. doi: https://doi.org/10.1016/j.epidem.2022.100642.

6. Adhikari K., Gautam R., **Pokharel A.**, Uprety KN., and Vaidya NK.. Data-driven models for the risk of infection and hospitalization during a pandemic: Case study on covid-19 in nepal. Journal of Theoritical Biology, 574:111622, 2023.

7. Gautam, R., **Pokharel, A.**, Adhikari, K., Uprety, K.N. and Vaidya, N.K., 2022. Modeling malaria transmission in Nepal: impact of imported cases through cross- border mobility. Journal of Biological Dynamics, 16(1),528-564. https://doi.org/10.1080/17513758.2022.2096935

8. Gautam, R., Adhikari,K., **Pokharel A.**, Uprety, K.N., & Vaidya, N.K., 2024. Role of cross-border mobility on the backward bifurcation of malaria transmission model: Implications for malaria control in Nepal.Nonlinear Analysis: Real World Applications, Volume 81,104173. https://authors.elsevier.com/sd/article/S1468-1218(24)00113-5

9. Chanda NB, Adhikari K, Gautam R, **Pokharel A.**, Uprety KN, Estimating effects of nonpharmaceutical interventions of COVID-19 in Sudurpaschim province, Nepal. *Journal of Institute of Science and Technology*, Vol. 28 No. 1 (2023), DOI: https://doi.org/10.3126/jist.v28i1.49044.

10. **Pokharel A.**, Adhikari K., Gautam R. 2024. Modelling the Impact of Vaccination on the Control of Measles in Nepal, T*he Nepali Mathematical Sciences Report* (2024),41(1), 15–34, doi; https://doi.org10.3126/nmsr.v41i1.67453.

11. Gautam Dwarika., Gautam R.,.,Adhikari K., **Pokharel A.**, Uprety KN., Transmission Dynamics of Dengue Disease in the Rupandehi District of Nepal. Journal of Nepal Mathematical Society (JNMS), (2024), June.

12. Gautam, R., Adhikari, K., **Pokharel A.**, Ghosh,B., Schwartz,E. J., Uprety, K.N. and Vaidya, N.K., 2022. Modeling malaria transmission with relapse delay: Impact on elimination plan of low endemic countries. (Submitted)

Conferences/Workshops/Seminars

1. **Presentation:**. "An In-Host Model of Measles Virus Infection" in National Conference on Mathematics & Its Applications (NCMA-2022) (11-13 June, 2022, Ilam).

2. **Facilitator:** Data Visualization in Epidemic models. Infectious diseases workshop on "Mathematical Modeling for Epidemic Control and prevention" (21-24, June 2022). Nepal health research council.

3. **Participation:** The 13th Conference on Dynamical Systems Applied to Biology and Natural Sciences (DSABNS 2022) Mathematical and Theoretical Biology Group (MTB), Feb. 8- 11, 2022.

4. **Presentation:** "Mathematical Modeling of Transmission Dynamics and Control of Measles in Nepal", in the 3rd International Conference on Frontiers of Science and Technology-2021 (ICFST-2021) India, August 13-14, 2021.

5. **Presentation:** "Transmission Dynamics of Measles and Control through Vaccination Campaign in Nepal" on International Conference on Analysis and its Applications (ICAA)- 2021, Nepal, organized by Nepal Mathematical Society, April 9 – 11, 2021.

6. **Presntation:** "Transmission Dynamics of Measles and Control through Vaccination Campaign in Nepal" in International Conference on Analysis and Applications (April 9-11, 2021). Organized by Nepal Mathematical Society.

7. **Presentation** "Modeling the Impact of Vaccination on theTransmission Dynamics of Measles in Nepal", Virtual SMB 2021, Annual Meeting Jun 13-17, 2021, Society for Mathematical Biology.

8. **Presentation:** "Transmission Dynamics of Measles and Control through Vaccination Campaign", International Conference on Applied Mathematics and Computational Sciences, 2019, DIT, Deharadun India, October 17-19, 2019.

Scholarly Awards/Honors

- **PhD Research Fellowship:** GRAID (Graduate Research Assistantships in Developing Countries) Program, International Mathematical Union (IMU). Fellowship period: 06/01/2020 – 05/31/2024.

- **NMS-Fellowship-2020:** Nepal Mathematical Society.

Mathematical Biosciences and Engineering

http://www.aimspress.com/journal/mbe

MBE, 19(8): 8554–8579.
DOI: 10.3934/mbe.2022397
Received: 24 February 2022
Revised: 22 April 2022
Accepted: 24 May 2022
Published: 10 June 2022

Research article

Modeling transmission dynamics of measles in Nepal and its control with monitored vaccination program

Anjana Pokharel[1], Khagendra Adhikari[2], Ramesh Gautam[3], Kedar Nath Uprety[4] and Naveen K. Vaidya[5,6,7,*]

[1] Padma Kanya Multiple Campus, Tribhuvan University, Kathmandu, Nepal
[2] Amrit Campus, Tribhuvan University, Kathmandu, Nepal
[3] Ratna Rajya Laxmi Campus, Tribhuvan University, Kathmandu, Nepal
[4] Central Department of Mathematics, Tribhuvan University, Kathmandu, Nepal
[5] Department of Mathematics and Statistics, San Diego State University, San Diego, CA, USA
[6] Computational Science Research Center, San Diego State University, San Diego, CA, USA
[7] Viral Information Institute, San Diego State University, San Diego, CA, USA

* **Correspondence:** Email: nvaidya@sdsu.edu.

Abstract: Measles is one of the highly contagious human viral diseases. Despite the availability of vaccines, measles outbreak frequently occurs in many places, including Nepal, partly due to the lack of compliance with vaccination. In this study, we develop a novel transmission dynamics model to evaluate the effects of monitored vaccination programs to control and eliminate measles. We use our model, parameterized with the data from the measles outbreak in Nepal, to calculate the vaccinated reproduction number, R_v, of measles in Nepal. We perform model analyses to establish the global asymptotic stability of the disease-free equilibrium point for $R_v < 1$ and the uniform persistence of the disease for $R_v > 1$. Moreover, we perform model simulations to identify monitored vaccination strategies for the successful control of measles in Nepal. Our model predicts that the monitored vaccination programs can help control the potential resurgence of the disease.

Keywords: mathematical model; measles; Nepal; stability and persistence analysis; vaccination

1. Introduction

Measles is one of the acute and highly contagious viral diseases found as early as the 7th century [1]. It is transmitted either by direct contact with infectious droplets or by airborne spread [2, 3], mainly among children under five years. Before developing vaccines, measles epidemics used to occur every

2 to 5 years, resulting in an annual 20 to 30 million infections and at least 1 million deaths worldwide [4, 5]. Measles incidence and related deaths decreased globally during 2000–2016 [6, 7]. However, the measles cases have begun to increase again after 2017. The number of cases in 2019 reached the highest in the past 23 years. The death due to measles also increased by 22% in 2017 and climbed up to 50% in 2019 [6, 7].

Measles can be successfully prevented with two doses of vaccines received at the recommended ages of 9 months (first dose) and 15 months (second dose) [8]. However, due to various reasons, such as poor health systems, lack of access to vaccination, and fear or skepticism about vaccines, the proper implementation of vaccination programs has been a huge issue. Improper and insufficient vaccines have presumably caused frequent measles outbreaks in developed and developing countries, including Nepal. In 2017, the global coverage of the vaccine's first dose was about 85%, significantly lower than the 95% recommended by the WHO to achieve herd immunity [5]. Even among developed countries, such as the United States, France, United Kingdom, Argentina, Italy, Japan, Canada, Germany, Australia, and Chile, the vaccine coverage has not met the WHO-recommended threshold for herd immunity [5]. Efforts by the anti-vaccine activists in the world [9, 10] might have partially contributed to the low vaccine coverage and eventually to occasional outbreaks, such as the one in New York in 2018–2019 [11, 12].

In Nepal, the monovalent vaccine, known as MCV1, against measles was first introduced in three districts in 1979. It was later expanded to the whole country in 1989 [13–15]. Measles was one of the major causes of childhood death before 2007, presumably because of the low coverage of MCV1. After the MCV1 coverage was increased from 81% to 88% during 2007-2014 along with Supplementary Immunization Activities (SIAs), the suspected measles incidence declined by 13% [14–19]. However, the measles cases began to increase in Nepal in 2017 (99, 247, and 430 measles cases in 2017, 2018, and 2019, respectively) [20, 21]. In 2019 measles outbreaks occurred in Morang, Dang, Kapilvastu, Kathmandu, and Lalitpur districts [20–23]. Notably, a frequent measles outbreak has been reported in districts with low vaccine coverage like Kapilvastu, where 95% of children were not vaccinated in 2016 [24–26]. Even in vaccinated people, the protection level may be reduced due to improper vaccination timing and incomplete doses. Monitored vaccination programs may help achieve success in avoiding measles epidemics. Such monitored vaccination programs promote the timely completion of the vaccination, thereby increasing the chance of complete immunity gain. Mathematical modeling is a valuable tool for identifying the ideal monitored vaccination programs in the context of Nepal.

Many SIR (susceptible, infected, recovered) based deterministic models, including age-structure and immigration-impact, have already been developed for the transmission dynamics of measles [27–32]. Moreover, some SEIR (susceptible, exposed, infected, recovered) based models [33–36] have been developed, including continuous-time linear vaccination-based control strategy, meta-populations, and immunization in pregnant women. These basic models have also been extended to include immunity, vaccination, age-dependent vaccination, time-dependent vaccine efficacy, therapy, quarantine, and treatment [2, 37–44]. However, modeling has not been extensively explored to study monitored vaccination programs, especially in the context of Nepal.

Regarding measles in Nepal, some descriptive, analytic, and retrospective studies [14, 45–47] have provided insights into the progress in measles control, the Case Fatality Rate (CFR) of measles, and the genetic type of the Asian measles virus. Many of these studies have incorporated the vaccination but lack a monitored vaccination program. In this study, we develop a novel deterministic model,

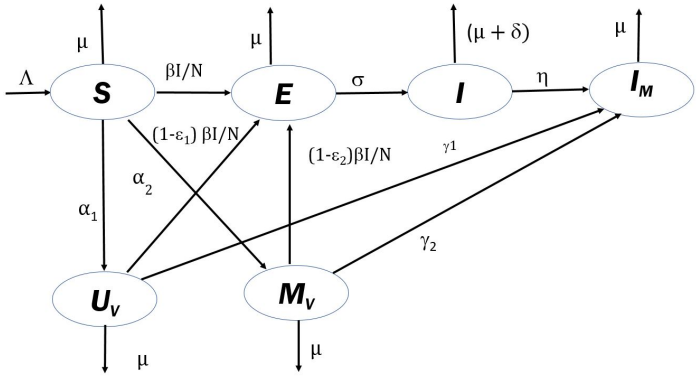

Figure 1. Schematic diagram of the transmission dynamics of measles.

incorporating monitored vaccination programs with two classes of vaccinated individuals, one under the monitored program and another without the monitored program. The model is validated using two-decade-long measles data from Nepal. Our model analysis establishes the local and global stability of disease-free equilibrium, the existence of endemic equilibrium, and the uniform persistence of the disease. Furthermore, we carry out model simulations to properly evaluate the impact of monitored vaccination programs on the short-term and long-term trend of measles transmission in Nepal.

2. Mathematical model

We develop a transmission dynamics model of measles for the population that includes all the newborns and children under 15 years. As mentioned earlier, implementing a proper vaccination program is often difficult, particularly for children whose parents have poor health knowledge and have fear or skepticism about vaccines. To improve the effectiveness of vaccination programs, we introduce a monitored vaccination program into our model. The program mainly focuses on asserting the completion of vaccines timely and accurately by children under this program. Because of extra care and regular follow-up, the children under this program are expected to have less susceptibility to infection and a higher rate of achieving immunity than those under regular (un-monitored) vaccination programs. To formulate the model, we divide the total population considered (N) into six mutually exclusive compartments: susceptible (S), un-monitored vaccinated (U_V), monitored vaccinated (M_V), exposed (E), infectious (I), and immune (I_M).

The schematic diagram showing the flow of individuals from and to the compartments during the measles transmission dynamics is presented in Figure 1. The dynamical system equations representing the model are as follows:

$$\frac{dS}{dt} = \Lambda - \left(\frac{\beta I}{N} + \mu + \alpha_1 + \alpha_2\right) S, \tag{2.1}$$

$$\frac{dU_V}{dt} = \alpha_1 S - \left(\gamma_1 + \mu + \frac{(1-\varepsilon_1)\beta I}{N}\right) U_V, \tag{2.2}$$

$$\frac{dM_V}{dt} = \alpha_2 S - \left(\gamma_2 + \mu + \frac{(1-\varepsilon_2)\beta I}{N}\right) M_V, \tag{2.3}$$

$$\frac{dE}{dt} = \frac{\beta IS}{N} + \frac{(1-\varepsilon_1)\beta IU_V}{N} + \frac{(1-\varepsilon_2)\beta IM_V}{N} - (\mu+\sigma)E, \tag{2.4}$$

$$\frac{dI}{dt} = \sigma E - (\mu+\eta+\delta)I, \tag{2.5}$$

$$\frac{dI_M}{dt} = \gamma_1 U_V + \gamma_2 M_V + \eta I - \mu I_M. \tag{2.6}$$

Here, Λ represents the recruitment rate of susceptible, i.e., newly born children. The measles infection occurs with the per capita transmission rate of $\beta I/N$, transferring susceptible individuals to the exposed class. The parameters σ represents the rate of progression of individuals from the exposed class to the infectious class, and η is the recovery rate of infectious individuals from the disease. Since only the children up to the age of 15 years are considered in the study, we assumed μ is the rate at which the children become older than 15 years leaving from the dynamics. We take δ to represent the disease-induced death rate.

The parameters α_1 and α_2 represent the rate of un-monitored vaccination and the monitored vaccination, respectively. As discussed in Pantha et al. [49], for practical purposes, the values of α_1 and α_2 for un-monitored and monitored vaccination programs aiming to cover $\zeta_1\%$ and $\zeta_2\%$ of children in t_1 and t_2 years, respectively, can be estimated using $\alpha_1 = -\ln(1-\zeta_1/100)/t_1$ and $\alpha_2 = -\ln(1-\zeta_2/100)/t_2$, respectively. The individual in the monitored vaccinated group is expected to be properly monitored to ensure the timely completion of the vaccination. In contrast, individuals in the un-monitored vaccinated group have more likelihood of not completing the vaccination in time, possibly delaying the gain of complete immunity. Therefore, we assumed that the un-monitored and monitored vaccinated children become immune at different rates, γ_1 and γ_2, respectively. Our model assumes individuals recovered from natural infection and those completing vaccination have similar immunity. Therefore, we include both of them in the same class, namely the immune class (I_M). The vaccinated children may also be infected, but at lesser infectivity rates $(1-\varepsilon_1)\beta$ and $(1-\varepsilon_2)\beta$ for un-monitored and monitored vaccinated, respectively. Since the monitoring service providers are expected to counsel individuals in the monitored vaccinated program for timely completion of vaccine and prevention practices, we also expect $0 \leq \varepsilon_1 < \varepsilon_2 \leq 1$.

3. Parameter estimation, data fitting, and model validation

3.1. Data source

The publicly available data used in this work is obtained from the official site of the World Health Organization (WHO) [48]. The data includes the reported measles cases in Nepal from 2000 to 2019. Since 5% of the reported cases belong to the aged 15 and above [48], we deducted 5% of the cases from the data. The Crude Birth Rate (CBR) and Infant Mortality Rate (IMR) of Nepal are used from the "Nepal population growth rate 1950–2020" [50].

3.2. Parameter estimation

Nepal's population under fifteen years was 9,807,000 in 2000 (taken as the base year) and 8,460,000 in 2019 [48]. The actual population size in individual S, U_V, M_V, E, I, I_M, classes is not available. It is recorded that 77% of the population was vaccinated in 2000 (the base year) [48]. For our base

case simulation, among the unvaccinated 23% of the total population, we assumed that 22% were in the susceptible class ($S(0) = 2,157,540$). We took 30% of the vaccinated population were in the unmonitored vaccinated class ($U_V(0) = 2,206,575$). Since the monitored vaccination program was not present in 2000, we took $M_V(0) = 0$. From the data, the recorded cases were 8927 (after reducing 5% over 15 years from the total recorded 9397), among which we assume $E(0) = 300$ in the exposed class and $I(0) = 340$ in the infectious class. The remaining population $(N(0) - S(0) - U_V(0) - E(0) - I(0))$ is included in the immune class ($I_M(0) = 5,442,245$).

The recruitment rate ($\Lambda = 612,328$) is the annual average birth rate, which is calculated by using the Crude Birth Rate (CBR) and Infant Mortality Rate (IMR) from the 2000-2019 data [50]. Since only the population below fifteen years is considered in the study, we used $\mu = 1/15 = 0.0667$ per year. It is given that the incubation period of measles is 10–14 days on average [4, 51], and thus the disease progression rate from the exposed class to the infectious class is taken as $\sigma = 1/12 \times 365 \approx 30$ per year. Also, since it takes about 18 days (range between 7 to 23 days) to recover from the disease [51], we used $\eta = 1/18 \times 365 \approx 20$ per year. As per WHO guidelines, children are vaccinated with the first dose at the age of 9 months and the second dose at 15 months [8], giving a six-month interval between the two doses. Since the monitored vaccinated individuals (M_V) are expected to complete them in time, we took $\gamma_2 = 0.5$ per year. From the data [52, 53], we estimated the average disease-induced death rate to be $\delta = 0.01$ per year. The remaining parameters of the model, β, α_1, α_2, γ_1, ε_1, and ε_2, are estimated by fitting the model to the measles case data from Nepal.

3.3. Data fitting and model validation

From the model, the yearly new infections at time t can be calculated using $h(t) = \sigma E(t)$, which we obtained using the numerical solutions of the system (2.1–2.6). Then we estimated the parameters with the help of the nonlinear regression method [54], which minimizes the following sum of the square residuals:

$$\sum_{k=1}^{n} (h_k - \bar{h_k})^2,$$

where h_k denotes the model predicted yearly new infection, $\bar{h_k}$ denotes yearly new infection data, and n is the number of data points used for the model fitting. For each estimated parameter, we also computed the confidence limits using the standard errors from the sensitivity matrix ($\mathscr{S}$) based on the complex-step derivative technique described in the previous study [55–58]. Our model is consistent with the yearly incidence cases observed in Nepal (Figure 2). In addition, we also show that the model prediction of the cumulative cases agrees well with the cumulative data, thereby validating our model to describe the measles epidemic in Nepal.

We note that while making all six parameters free in the data fitting process, we obtained negative lower limits of some confidence intervals. To tackle this issue, we needed to fix some of the parameters as done previously [55–57]. Since the parameters α_2 and ε_2 are the two least sensitive parameters identified from the sensitivity matrix, $\mathscr{S}$, we fixed $\alpha_2 = 0.02$ per year and $\varepsilon_2 = 0.90$ at their best estimate values. We also note that taking the different values of α_2 and ε_2 did not significantly affect estimates of other parameters, as expected, because of the least sensitivity. Then, we estimated the remaining only four parameters, β, α_1, γ_1, and ε_1, from the further data fitting. Here the ratio of the data to the free parameters is 5:1, which lies within the recommended range of 5:1 to 10:1 for a reasonable parameter estimate [59]. Furthermore, to analyze the identifiability of the estimated four

parameters, we use the sensitivity-based method [60], in which we obtained the rank of the matrix $\mathscr{S}^T\mathscr{S}$. For our case with four parameters estimated, the obtained full rank (Rank = 4) of the matrix $\mathscr{S}^T\mathscr{S}$ confirms that these four parameters are practically identifiable for the model and the data used in this study. All the computations were carried out in MATLAB (The Math Works. Inc.) using its various routines, including "ode45" (ODE solver) and "fmincon" (minimizer).

Our estimates show that the transmission rate (β), the rate of un-monitored vaccination (α_1), the rate of recovery from un-monitored vaccination (γ_1), and the effectiveness of un-monitored vaccination (ε_1) are 63.0238 (95% CI: 63.0188–63.0288), 0.31 (95% CI: 0.0902–0.5298), 0.1 (95% CI: 0.0858–0.1142), and 0.5082 (95% CI: 0.4926–0.5238), respectively (Table 1). We note that the confidence interval of the parameter α_1 appears to be large compared to other parameters for this particular data set. However, we consider this parameter a control parameter and vary widely for the analysis of the vaccination program; thus, one set of confidence intervals does not significantly impact the main results of our study.

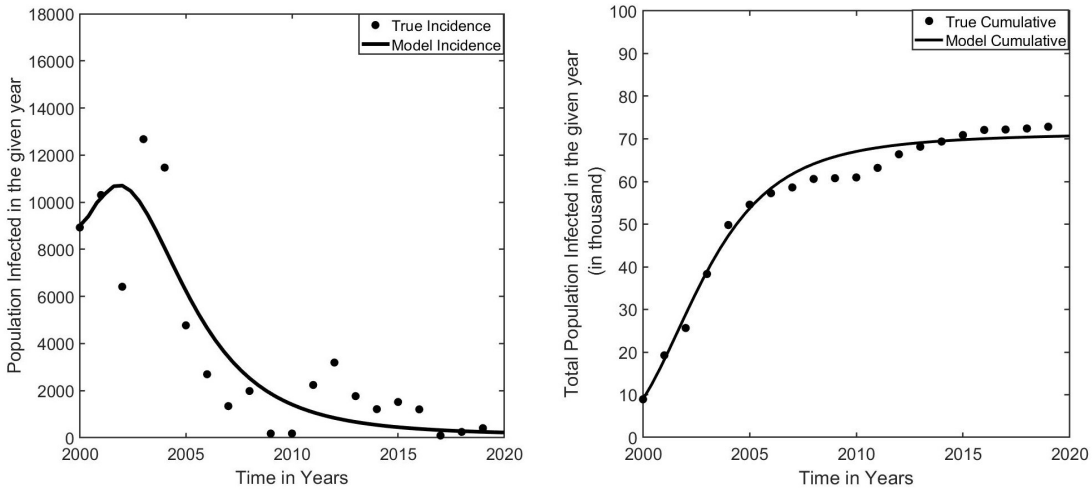

Figure 2. Data fitting and Model validation. (a) The recorded yearly cases of measles in Nepal (dot) along with the best fit of the model (line). (b) The cumulative recorded cases of measles in Nepal (dot) along with the model prediction of the cumulative cases (line).

4. Model analysis

4.1. Basic properties of model

We first establish the biological or epidemiological validation of the model by proving the non-negativity and the boundedness of the solution of the system of equations.

Table 1. Values of estimated and fixed parameters.

Parameters $(yr)^{-1}$	Description	Baseline Value	Confidence Interval	Sources
α_2	Monitored vaccination rate	0.02	Fixed	Assumed
α_1	Un-monitored vaccination rate	0.31	[0.0902 0.5298]	Data Fitting
β	Transmission rate	63.02	[63.01 63.03]	Data Fitting
ε_1	Effectiveness of un-monitored vacc.	0.51 (Dim.less)	[0.49 0.52]	Data Fitting
ε_2	Effectiveness of monitored vacc.	0.9 (Dim.less)	Fixed	Assumed
μ	Removed rate	0.0667	Fixed	Assumed
γ_1	U_V immunity rate	0.1	[0.086 0.12]	Data Fitting
γ_2	M_V immuninity rate	0.5	Fixed	Assumed
σ	Disease progress rate	30	Fixed	[4]
η	Recovery rate	20	Fixed	[4]
δ	Disease-induced death rate	0.01	Fixed	[52]

4.1.1. Positivity of the solutions

Theorem 4.1. *If $S(0) > 0$, $U_V(0) \geq 0$, $M_V(0) \geq 0$, $E(0) \geq 0$, $I(0) \geq 0$, and $I_M(0) \geq 0$, then the set of solution $\{S(t), U_V(t), M_V(t), E(t), I(t), I_M(t)\}$ of the system (2.1–2.6) is positive for all $t \geq 0$.*

Proof. From (2.1), $\frac{dS}{dt} > -(\beta I/N + \mu + \alpha_1 + \alpha_2)S$, which implies $S(t) > S(0)exp\left(-\int_0^t (\beta I(s)/N(s) + \mu + \alpha_1 + \alpha_2)\,ds\right)$. Since $S(0) > 0$, $S(t) > 0$, $\forall t > 0$ confirming the positivity of $S(t)$. Similarly from (2.2–2.6), we have $\frac{dU_V}{dt} \geq -(\gamma_1 + \mu + (1-\varepsilon_1)\beta I/N)\,U_V$, $\frac{dM_V}{dt} \geq -(\mu + \gamma_2 + (1-\varepsilon_2)\beta I/N)M_V$, $\frac{dE}{dt} \geq -(\mu + \sigma)E$, $\frac{dI}{dt} \geq -(\mu + \eta + \delta)I$, and $\frac{dI_M}{dt} \geq -\mu I_M$. Then we get $U_V(t) \geq U_V(0)exp\left(-\int_0^t ((1-\varepsilon_1)\beta I(s)/N(s) + \mu + \gamma_1)\,ds\right) \geq 0$, $M_V(t) \geq M_V(0)exp\left(-\int_0^t ((1-\varepsilon_2)\,\beta I(s)/N(s) + \mu + \gamma_2)\,ds\right) \geq 0$, $E(t) \geq E(0)exp\,(-(\mu+\sigma)t) \geq 0$, $I(t) \geq I(0)exp\,(-(\mu+\eta+\delta)t) \geq 0$, and $I_M(t) \geq I_M(0)exp\,(-\mu t) \geq 0, \forall t > 0$ for $U_V(0) \geq 0$, $M_V(0) \geq 0$, $E(0) \geq 0$, $I(0) \geq 0$, and $I_M(0) \geq 0$. Therefore, $U_V(t)$, $M_V(t)$, $E(t)$, $I(t)$, $I_M(t) \geq 0$, $\forall t > 0$, showing the positivity of the solution set of the system (2.1–2.6). □

4.1.2. Boundedness and invariant region

Adding all differential equations (2.1–2.6), we get $dN/dt = \Lambda - \mu N - \delta I \leq \Lambda - \mu N$, which provides $N(t) \leq N(0)e^{-\mu t} + \Lambda/\mu(1 - e^{-\mu t})$ and $\limsup_{t\to\infty} N(t) \leq \Lambda/\mu$, showing that the total population is

ultimately bounded by Λ/μ. Hence the solution set bounded by Λ/μ is positively invariant in the feasible region

$$\Omega = \left\{ (S(t),\, U_V(t),\, M_V(t),\, E(t),\, I(t),\, I_M(t)) \in \mathbb{R}^6_+ : N(t) \leq \Lambda/\mu \right\}.$$

4.2. Existence of Equilibria

In this section we discuss the disease-free equilibrium point (DFE) and the endemic equilibrium point of the system (2.1–2.6).

4.2.1. Disease free equilibrium point and formulation of the vaccinated reproduction number

Setting $E = 0$ and $I = 0$ in the system, we obtain DFE: $E^0 = (S^0,\ U_V^0,\ M_V^0,\ 0,\ 0,\ I_M^0)$, where $S^0 = \dfrac{\Lambda}{\alpha_1+\alpha_2+\mu}$, $U_V^0 = \dfrac{\alpha_1\Lambda}{(\alpha_1+\alpha_2+\mu)(\gamma_1+\mu)}$, $M_V^0 = \dfrac{\alpha_2\Lambda}{(\alpha_1+\alpha_2+\mu)(\gamma_2+\mu)}$, and $I_M^0 = \dfrac{\Lambda(\alpha_1\gamma_1(\mu+\gamma_2)+\alpha_2\gamma_2(\mu+\gamma_1))}{\mu(\alpha_1+\alpha_2+\mu)(\gamma_1+\mu)(\gamma_2+\mu)}$. Note that our model implies non-zero immune class I_M^0 at the DFE due to the immunity gained through vaccination.

The vaccinated reproduction number, denoted by R_v, is defined as the average number of secondary cases generated by a single infectious case introduced into the mixed population with susceptible and vaccinated status. Here we formulate the vaccinated reproduction number using the Next Generation method [61–65].

Following the Next Generation Matrix method [62], we divide the system into two groups, infected $\vec{x} = (x_i,\ i = 1,2) = (E,\ I)$ and uninfected $\vec{y} = (y_j,\ j = 1,2,3,4) = (S,\ U_V,\ M_V,\ I_M)$, as follows:

$$\dot{x}_i = f_i(\vec{x},\vec{y}) = \mathscr{F}_i(\vec{x},\vec{y}) - \mathscr{V}_i(\vec{x},\vec{y}),\ i = 1,\ 2 \text{ and } \dot{y}_j = g_j(\vec{x},\vec{y}),\ j = 1,2,3,4, \tag{4.1}$$

where $\mathscr{F}_i(\vec{x},\vec{y})$ is the rate of appearance of new infections in the compartment i, and $\mathscr{V}_i(\vec{x},\vec{y})$ is the difference between the transfer of individuals out of and into the compartment i ($i = 1,2$). Here we have

$$\mathscr{F} = \begin{pmatrix} (\beta S + (1-\varepsilon_1)\,\beta U_V + (1-\varepsilon_2)\,\beta M_V)I/N \\ 0 \end{pmatrix} \text{ and } \mathscr{V} = \begin{pmatrix} (\mu+\sigma)E \\ -\sigma E + (\mu+\eta+\delta)I \end{pmatrix}.$$

It is easy to verify that $\mathscr{F}_i$ and $\mathscr{V}_i$ satisfy the conditions A(1)–A(5) of [62]. As the process provided in [62], we obtained the Jacobians of $\mathscr{F}$ and $\mathscr{V}$ at the disease free equilibrium point ($D\mathscr{F}(E^0) = F,\ D\mathscr{V}(E^0) = V$):

$$F = \begin{pmatrix} 0 & (\beta S^0 + (1-\varepsilon_1)\,\beta U_V^0 + (1-\varepsilon_2)\,\beta M_V^0)/N^0 \\ 0 & 0 \end{pmatrix} \text{ and } V = \begin{pmatrix} \mu+\sigma & 0 \\ -\sigma & \delta+\eta+\mu \end{pmatrix}.$$

Clearly, F is non-negative and V is non singular M-matrix. The next generation matrix for our model is given by:

$$FV^{-1} = \begin{pmatrix} \dfrac{\sigma\left(\beta S^0 + (1-\varepsilon_1)\,\beta U_V^0 + (1-\varepsilon_2)\,\beta M_V^0\right)}{N^0(\mu+\sigma)(\delta+\eta+\mu)} & \dfrac{(\beta S^0 + (1-\varepsilon_1)\,\beta U_V^0 + (1-\varepsilon_2)\,\beta M_V^0)}{N^0(\delta+\eta+\mu)} \\ 0 & 0 \end{pmatrix}.$$

Then the vaccinated reproduction number R_v is given by:

$$R_v = \rho(FV^{-1}) = \frac{\beta\sigma\left(S^0 + (1-\varepsilon_1)U_V^0 + (1-\varepsilon_2)M_V^0\right)}{N^0(\mu+\sigma)(\delta+\eta+\mu)}.$$

Using the expression of DFE obtained above, we get

$$R_v = \frac{\beta\mu\sigma\left(\alpha_1(1-\varepsilon_1)(\gamma_2+\mu) + (\gamma_1+\mu)(\alpha_2(1-\varepsilon_2)+\gamma_2+\mu)\right)}{(\alpha_1+\alpha_2+\mu)(\gamma_1+\mu)(\gamma_2+\mu)(\mu+\sigma)(\delta+\eta+\mu)}.$$

Furthermore, as the system (4.1) satisfies all the conditions of [62, Theorem 2], it follows the local stability of the disease-free equilibrium for $R_V < 1$. Moreover, for the verification purpose, we also prove the local stability of DFE by showing the negative real part of eigenvalues in Subsection 4.3.1 below.

4.2.2. Endemic equilibrium point

Let

$$\lambda^* = \beta I^*/(S^* + U_v^* + M_v^* + E^* + I^* + I_M^*). \tag{4.2}$$

Then solving the full system (2.1–2.6) equated to zero, we get

$$\begin{aligned}
S^* &= \frac{\Lambda}{\alpha_1+\alpha_2+\lambda^*+\mu},\\
U_V^* &= \frac{\alpha_1\Lambda}{Q_1(\alpha_1+\alpha_2+\lambda^*+\mu)},\\
M_V^* &= \frac{\alpha_2\Lambda}{(\gamma_2+\mu)(\alpha_1+\alpha_2+\mu+\lambda^*(1-\varepsilon_2))},\\
E^* &= \frac{\lambda^*\Lambda(\alpha_1(1-\varepsilon_1)(\gamma_2+\lambda^*(1-\varepsilon_2)+\mu)+Q_1(\gamma_2+(\alpha_2+\lambda^*)(1-\varepsilon_2)+\mu))}{Q_1(\mu+\sigma)(\alpha_1+\alpha_2+\lambda^*+\mu)(\gamma_2+\lambda^*(1-\varepsilon_2)+\mu)},\\
I^* &= \frac{\lambda^*\Lambda\sigma(Q_1(\gamma_2+(\alpha_2+\lambda^*)(1-\varepsilon_2)+\mu)+\alpha_1(1-\varepsilon_1)(\gamma_2+\lambda^*(1-\varepsilon_2)+\mu))}{Q_1(\mu+\sigma)(\alpha_1+\alpha_2+\lambda^*+\mu)(\delta+\eta+\mu)(\gamma_2+\lambda^*(1-\varepsilon_2)+\mu)},\\
I_M^* &= \frac{\Lambda(P_1+P_2P_3)}{Q_1\mu(\mu+\sigma)(\alpha_1+\alpha_2+\lambda^*+\mu)(\delta+\eta+\mu)(\gamma_2+\lambda^*(1-\varepsilon_2)+\mu)}.
\end{aligned} \tag{4.3}$$

where,

$$\begin{aligned}
Q_1 &= (\gamma_1+\lambda^*(1-\varepsilon_1)+\mu),\\
P_1 &= \alpha_1(\gamma_2+(1-\varepsilon_2)+\mu)(\eta(1-\varepsilon_1)\lambda^*\sigma-\gamma_1(\mu+\sigma)(\delta+\eta+\mu)),\\
P_2 &= (\gamma_1+\lambda^*(1-\varepsilon_1)+\mu),\\
P_3 &= (\alpha_2(\gamma_2(\mu+\sigma)(\delta+\eta+\mu)+\eta\lambda^*(1-\varepsilon_2)\sigma)+\eta\lambda^*\sigma(\gamma_2+\lambda^*(1-\varepsilon_2)+\mu)).
\end{aligned}$$

Substituting (4.3) into (4.2) and after some simplification, we obtain the following equation in terms of λ^*:

$$\lambda^*(A_3\lambda^{*3}+A_2\lambda^{*2}+A_1\lambda^*+A_0) = 0, \tag{4.4}$$

where,

$$
\begin{aligned}
A_3 &= (\delta\mu + (\eta+\mu)(\mu+\sigma))(1-\varepsilon_1)(1-\varepsilon_2),\\
A_2 &= (1-\varepsilon_1)\left((1-\varepsilon_2)P + \alpha_1 Q + \alpha_2 Q\right) + (1-\varepsilon_2)Q(\gamma_1+\mu) + Q(\gamma_2+\mu),\\
A_1 &= (1-\varepsilon_1)P(\gamma_2+\mu) + (\gamma_1+\mu)\left((1-\varepsilon_2)\left(\alpha_1(\mu+\sigma)(\delta+\eta+\mu) + P + \alpha_2 Q\right) + Q(\gamma_2+\mu)\right)\\
&\quad + (1-\varepsilon_1)\left(\alpha_2\left((\gamma_2+\mu)(\mu+\sigma)(\delta+\eta+\mu) - \beta(1-\varepsilon_2)\mu\sigma\right) + \alpha_1\left(Q(\gamma_2+\mu) - \beta(1-\varepsilon_2)\mu\sigma\right)\right),\\
A_0 &= (1-R_v)(\alpha_1+\alpha_2+\mu)(\gamma_1+\mu)(\gamma_2+\mu)(\mu+\sigma)(\delta+\eta+\mu),\\
P &= \mu\left((\delta+\eta+\mu)(\mu+\sigma) - \beta\sigma\right),\\
Q &= \delta\mu + (\eta+\mu)(\mu+\sigma).
\end{aligned}
$$

Note that $\lambda^* = 0$ corresponds to the disease-free equilibrium point, and the endemic equilibrium points are given by the solutions of $A_3\lambda^{*3} + A_2\lambda^{*2} + A_1\lambda^* + A_0 = 0$. Here, $A_3 > 0$ and $A_0 < 0$ for $R_v > 1$, so the equation (4.4) has at least one positive root for $R_v > 1$. The positiveness of λ^* implies the positiveness of I^* and E^*. Thus, we conclude that if $R_v > 1$, the system (2.1–2.6) has at least one endemic equilibrium point given by (4.3).

4.3. The global dynamics analysis

In this section, we first establish the local and global stability of the disease-free equilibrium when $R_v < 1$ and then prove the persistence of the disease when $R_v > 1$.

4.3.1. Local stability analysis of the disease free equilibrium point

Theorem 4.2. *The disease-free equilibrium point of the system (2.1–2.6) is locally asymptotically stable if $R_v < 1$ and unstable if $R_v > 1$.*

Proof. Jacobian of the system (2.1–2.6) at the disease free equilibrium point is $J = \begin{pmatrix} A_{3\times3} & B_{3\times3} \\ C_{3\times3} & D_{3\times3} \end{pmatrix}$ where,

$$
A_{3\times3} = \begin{pmatrix} -(\alpha_1+\alpha_2+\mu) & 0 & 0 \\ \alpha_1 & -(\gamma_1+\mu) & 0 \\ \alpha_2 & 0 & -(\gamma_2+\mu) \end{pmatrix},\ B_{3\times3} = \begin{pmatrix} 0 & -\beta S^0/N^0 & 0 \\ 0 & -\beta U_V^0(1-\varepsilon_1)/N^0 & 0 \\ 0 & -\beta M_V^0(1-\varepsilon_2)/N^0 & 0 \end{pmatrix},
$$

$$
C_{3\times3} = \begin{pmatrix} 0 & 0 & 0 \\ 0 & 0 & 0 \\ 0 & \gamma_1 & \gamma_2 \end{pmatrix},\ D_{3\times3} = \begin{pmatrix} -(\mu+\sigma) & \beta\left(S^0 + U_V^0(1-\varepsilon_1) + M_V^0(1-\varepsilon_2)\right)/N^0 & 0 \\ \sigma & -(\delta+\eta+\mu) & 0 \\ 0 & \eta & -\mu \end{pmatrix}.
$$

The eigenvalues of the matrix J are

$$
\begin{aligned}
&\lambda_1 = -\mu,\ \lambda_2 = -(\alpha_1+\alpha_2+\mu),\ \lambda_3 = -(\gamma_1+\mu),\ \lambda_4 = -(\gamma_2+\mu),\\
&\lambda_5 = \frac{1}{2}\left(-(\delta+\eta+2\mu+\sigma) - \sqrt{(\delta+\eta+2\mu+\sigma)^2 + 4(R_v-1)(\mu+\sigma)(\delta+\eta+\mu)}\right),\\
&\lambda_6 = \frac{1}{2}\left(-(\delta+\eta+2\mu+\sigma) + \sqrt{(\delta+\eta+2\mu+\sigma)^2 + 4(R_v-1)(\mu+\sigma)(\delta+\eta+\mu)}\right). \qquad (4.5)
\end{aligned}
$$

Since all the eigenvalues are negative if $R_v < 1$, E^0 is locally asymptotically stable if $R_v < 1$. □

4.4. Global stability of disease free equilibrium point

In the following theorem, we prove that $R_v < 1$ asserts the global stability of the DFE.

Theorem 4.3. *If $R_v < 1$, the disease-free equilibrium point E^0 of the system (2.1–2.5) is globally asymptotically stable in $\mathbb{R}^6$.*

Proof. The Jacobian corresponding to (2.4) and (2.5) at the disease-free equilibrium point E^0 is

$$J_0 = \begin{pmatrix} -\mu-\sigma & \dfrac{\beta S^0}{N^0} + \dfrac{(1-\varepsilon_1)\,\beta U_V^0}{N^0} + \dfrac{(1-\varepsilon_2)\,\beta M_V^0}{N^0} \\ \sigma & -(\delta+\eta+\mu) \end{pmatrix}.$$

The spectral bound of J_0 is defined as: $s(J_0) = max\{Re(\lambda) : \lambda \text{is an eigenvalue of } J_0\}$. Using the theorem 4.2, we conclude:

1. $R_v = 1$ if and only if $s(J_0) = 0$.
2. $R_v < 1$ if and only if $s(J_0) < 0$.
3. $R_v > 1$ if and only if $s(J_0) > 0$.

If $R_v < 1$ then $s(J_0) < 0$. Also, we can obtain a sufficiently small positive number γ such that $s(J_\gamma) < 0$, where

$$J_\gamma = \begin{pmatrix} -\mu-\sigma & \dfrac{\beta(S^0+\gamma)}{\Lambda/\mu-\gamma} + \dfrac{(1-\varepsilon_1)\beta(U_V^0+\gamma)}{\Lambda/\mu-\gamma} + \dfrac{(1-\varepsilon_2)\beta(M_V^0+\gamma)}{\Lambda/\mu-\gamma} \\ \sigma & -(\delta+\eta+\mu) \end{pmatrix}.$$

From the subsections 4.1 and 4.2, $N(t) \to \Lambda/\mu$ and $S(t) \to S^0$ as $t \to \infty$ for all $\gamma > 0$. Therefore, there exists $t_1 > 0$ such that $\forall t \geq t_1$, we have $S \leq (S^0+\gamma)$, $U_v \leq (U_v^0+\gamma)$, $M_v \leq (M_v^0+\gamma)$, $N \geq (\Lambda/\mu-\gamma)$. From (2.4) and (2.5), it follows that

$$\begin{aligned} \frac{dE}{dt} =& \frac{\beta S}{N} I + \frac{(1-\varepsilon_1)\,\beta U_V}{N} I + \frac{(1-\varepsilon_2)\,\beta M_V}{N} I - (\mu+\sigma)E \\ \leq& \frac{\beta(S^0+\gamma)}{\Lambda/\mu-\gamma} I + \frac{(1-\varepsilon_1)\,\beta(U_V^0+\gamma)}{\Lambda/\mu-\gamma} I + \frac{(1-\varepsilon_2)\,\beta(M_V^0+\gamma)}{\Lambda/\mu-\gamma} I - (\mu+\sigma)E, \\ \frac{dI}{dt} =& \sigma E - (\mu+\eta+\delta)I. \end{aligned}$$

$$\begin{aligned} \frac{dE}{dt} &= \frac{\beta(S^0+\gamma)}{\Lambda/\mu-\gamma} I + \frac{(1-\varepsilon_1)\,\beta(U_V^0+\gamma)}{\Lambda/\mu-\gamma} I + \frac{(1-\varepsilon_2)\,\beta(M_V^0+\gamma)}{\Lambda/\mu-\gamma} I - (\mu+\sigma)E, \\ \frac{dI}{dt} &= \sigma E - (\mu+\eta+\delta)I, \ \forall\, t \geq t_1. \end{aligned} \tag{4.6}$$

Clearly, the system (4.6) has the Jacobian J_γ, which is irreducible with non-negative off-diagonal elements. Then $s(J_\gamma)$ is simple and associated with strongly positive eigenvector $\tilde{v}$, $\forall\, t \geq t_1$ [66]. For any solution $\psi(t)$ of the system (4.6) with non-negative initial value $\psi(0)$, there is a sufficiently large positive number $\zeta > 0$ such that $(E(t_1), I(t_1)) \leq \zeta\tilde{v}$. It is easy to see that $V(t) = \zeta e^{s(J_\gamma)(t-t_1)}\tilde{v}, \forall\, t \geq t_1$ is a solution of (4.6) with $V(t_1) = \zeta\tilde{v}$. Then by the comparison principle [66, Theorem B.1], it follows that $(E(t), I(t)) \leq \zeta\tilde{v}$, $\forall t \geq t_1$. Since $s(J_\gamma) < 0$, we get

$$\lim_{t\to\infty} E(t) = 0, \ \lim_{t\to\infty} I(t) = 0,$$

which implies that (2.1) is asymptotic to the following equation:

$$\frac{dS}{dt} = \Lambda - (\mu + \alpha_1 + \alpha_2) S,$$
$$\Rightarrow S(t) = C_1 e^{-(\mu+\alpha_1+\alpha_2)t} + \frac{\Lambda}{(\mu+\alpha_1+\alpha_2)} \left(1 - e^{-(\mu+\alpha_1+\alpha_2)t}\right), \ \forall t \geq t_1.$$

Hence, we get $\lim_{t\to\infty} S(t) = \frac{\Lambda}{(\mu+\alpha_1+\alpha_2)}$. Solving the system of differential equations (2.2 & 2.3) together with the help of (2.1), we get

$$U_V = \frac{\alpha_1\Lambda}{(\alpha_1+\alpha_2+\mu)(\gamma_1+\mu)} + c_1 e^{-r_1 t} + c_2 e^{-r_2 t}, \ M_V = \frac{\alpha_2\Lambda}{(\alpha_1+\alpha_2+\mu)(\gamma_2+\mu)} + c_3 e^{-k_1 t} + c_4 e^{-k_2 t},$$

where,

$$r_1 = k_1 = \alpha_1 + \alpha_2 + \mu, \ r_2 = \gamma_1 + \mu, \text{ and } \ k_2 = \gamma_2 + \mu.$$

Thus, we get

$$\lim_{t\to\infty} U_V(t) = \frac{\alpha_1\Lambda}{(\mu+\alpha_1+\alpha_2)(\gamma_1+\mu)}, \tag{4.7}$$

$$\lim_{t\to\infty} M_V(t) = \frac{\alpha_2\Lambda}{(\mu+\alpha_1+\alpha_2)(\gamma_2+\mu)}. \tag{4.8}$$

In the limiting case, we can further verify that $\lim_{t\to\infty} I_M(t) = I_M^0$. Hence if $R_v < 1$, the disease-free equilibrium point E^0 of the system (2.1–2.5) is globally asymptotically stable. □

4.4.1. Uniform persistence

The disease is endemic if the system is uniformly persistent. The system (2.1–2.6) is said to be uniformly persistent if there exists $\zeta > 0$ such that $(S(t),\ U_V(t),\ M_V(t),\ E(t),\ I(t),\ I_M(t)) \in \Gamma$ satisfying

$$\lim_{t\to\infty} \text{Inf}\, E \geq \zeta, \ \lim_{t\to\infty} \text{Inf}\, I \geq \zeta. \tag{4.9}$$

Here it is enough to consider the reduced system (2.1-2.5). We first define the sets

$$\Gamma^o = \{(S, U_V, M_V, E, I) \in \mathbb{R}^5 : I \neq 0 \text{ or } \ E \neq 0\}, \tag{4.10}$$

$$\partial\Gamma^o = \{(S, U_V, M_V, E, I) \in \mathbb{R}^5 : I = 0, E = 0\}. \tag{4.11}$$

We have

$$\Gamma^o \cup \partial\Gamma^o = \Gamma \text{ and } \Gamma^o \cap \partial\Gamma^o = \phi,$$

which implies that $\partial\Gamma^o$ is relatively closed in $\Gamma = (S, U_V, M_V, E, I) \in \mathbb{R}^5$.

To establish the disease persistence for $R_v > 1$, we now prove the following theorem.

Theorem 4.4. *If $R_v > 1$, then the system (2.1–2.5) is uniformly persistent with respect to $(\Gamma^0, \partial\Gamma^0)$ in the sense that there is a positive constant $\zeta > 0$ such that every solution $(S(t),\ U_V(t),\ M_V(t),\ E(t),\ I(t))$ of (2.1–2.5) with $(S(0),\ U_V(0),\ M_V(0),\ E(0),\ I(0)) \in \Gamma^0$ satisfies $\lim_{t\to\infty} Inf\, E \geq \zeta, \ \lim_{t\to\infty} Inf\, I \geq \zeta$.*

Proof. Let $\psi(t)p$ be the solution function of system (2.1–2.5) with initial value p. We can show the solution $(\psi(t)p),\ t>0$ is uniformly persistent with respect to $(\Gamma^o, \partial\Gamma^o)$ [67]. For any $(S(0),\ U_V(0),\ M_V(0),\ E(0),\ I(0)) \in \Gamma^0$, (2.1–2.3) provide

$$S(t) = \exp\left(-\int_0^t a(x_1)dx_1\right)\left[\int_0^t \exp\left(\int_0^y a(x_1)dx_1\right) b(y)dy + S(0)\right],$$
$$U_V(t) = \exp\left(-\int_0^t a^*(x_1)dx_1\right)\left[\int_0^t \exp\left(\int_0^y a^*(x_1)dx_1\right) b^*(y)dy + U_V(0)\right],$$
$$M_V(t) = \exp\left(-\int_0^t a^o(x_1)dx_1\right)\left[\int_0^t \exp\left(\int_0^y a^o(x_1)dx_1\right) b^o(y)dy + M_V(0)\right],$$

where $a = \alpha_1+\alpha_2+\mu+\beta I/N,\ b=\Lambda,\ a^* = \gamma_1+\mu+(1-\varepsilon_1)\beta I/N,\ b^* = \alpha_1 S,\ a^o = \gamma_2+\mu+(1-\varepsilon_2)\beta I/N$, and $b^o = \alpha_2 S$. Here $\Lambda>0$ implies $S(t)>0$. This follows $U_V(t)>0$, $M_V(t)>0$, $\forall\, t>0$. Thus the non-diseased variables $S(t),\ U_V(t)$, and $M_V(t)$ are positive.

Defining the two sets,

$$M_\partial = \{p \in \partial\Gamma_o : \psi(t)p \in \partial\Gamma_o\},$$
$$\omega(p) = \{p : \psi(t)x_n \to p \text{ as } t\to\infty\},$$

we claim that $\omega(p) = \{E^0\},\ \forall p \in M_\partial$. If $p(t) \in M_\partial$ then $\psi(t)p \in \partial\Gamma_0$ which implies $I=0$ and $E=0$. From (4.7, 4.8) and (2.1–2.5), as $t\to\infty$ we obtain $S(t), U_V(t)$, and $M_V(t)$ approaching to

$$\frac{\Lambda}{(\mu+\alpha_1+\alpha_2)},\ \frac{\Lambda\alpha_1}{(\mu+\alpha_1+\alpha_2)(\gamma_1+\mu)},\ \text{and}\ \frac{\Lambda\alpha_2}{(\mu+\alpha_1+\alpha_2)(\gamma_2+\mu)},\ \text{respectively,}$$

which is the equilibrium point E^0. Hence $\omega(p) = \{E^0\},\ \forall p \in M_\partial$.

Using the theorem 4.3 (Condition 3, $R_v>1$ for $s(J_0)>0$), we can get a sufficiently small $\rho>0$ such that the perturbation J_ρ on J_0 satisfies $s(J_\rho)>0$, (see [67], [68, Section II.5.8]) for $R_v>1$, where

$$J_\rho = \begin{pmatrix} -\mu-\sigma & \dfrac{\beta\,(S^0-\rho)}{\Lambda/\mu+\rho} + \dfrac{(1-\varepsilon_1)\,\beta\,(U_V^0-\rho)}{\Lambda/\mu+\rho} + \dfrac{(1-\varepsilon_2)\,\beta\,(M_V^0-\rho)}{\Lambda/\mu+\rho} \\ \sigma & -\delta-\eta-\mu \end{pmatrix}.$$

Now we claim that disease-free equilibrium point E^0 is uniform weak repeller with any solution $\psi(t)$. For this we need to show

$$\lim_{t\to\infty}\ \text{Sup}\ \left\|\psi(t)p - E^0\right\| \geq \rho, \forall\ p \in \Gamma^0.$$

On contrary, suppose there exists a $p_0 \in \Gamma^0$ such that $\lim\limits_{t\to\infty}\ \text{Sup}\ \left\|\psi(t)p_0 - E^0\right\| < \rho$. From the subsections 4.1 and 4.2, $N(t)\to\Lambda/\mu$ and $S(t)\to S^0$ as $t\to\infty$ implying that for all $\rho>0$ there exists $t_2>0$ such that $\forall t\geq t_2$, $S\geq(S^0-\rho)$, $U_v\geq(U_v^0-\rho)$, $M_v\geq(M_v^0-\rho)$, $N\leq(\Lambda/\mu+\rho)$. Then (2.4) and (2.5) follows that,

$$\begin{aligned}\frac{dE}{dt} &= \frac{\beta S}{N}I + \frac{(1-\varepsilon_1)\,\beta U_V}{N}I + \frac{(1-\varepsilon_2)\,\beta M_V}{N}I - (\mu+\sigma)E \\ &\geq \frac{\beta(S^0-\rho)}{\Lambda/\mu+\rho}I + \frac{(1-\varepsilon_1)\,\beta(U_v^0-\rho)}{\Lambda/\mu+\rho}I + \frac{(1-\varepsilon_2)\,\beta(M_v^0-\rho)}{\Lambda/\mu+\rho}I - (\mu+\sigma)E,\end{aligned}$$

$$\frac{dI}{dt} = \sigma E - (\mu + \eta + \delta)I.$$

We consider the following auxiliary equations:

$$\begin{aligned} \frac{dE}{dt} &= \frac{\beta(S^0-\rho)}{\Lambda/\mu+\rho}I + \frac{(1-\varepsilon_1)\,\beta(U_v^0-\rho)}{\Lambda/\mu+\rho}I + \frac{(1-\varepsilon_2)\,\beta(M_v^0-\rho)}{\Lambda/\mu+\rho}I - (\mu+\sigma)E, \\ \frac{dI}{dt} &= \sigma E - (\mu+\eta+\delta)I. \end{aligned} \tag{4.12}$$

Here, J_ρ is the Jacobian of the system (4.12), is irreducible with non-negative off-diagonal elements, then $s(J_\rho)$ is simple and associated with strongly positive eigenvector $\tilde{v}, \forall\ t \geq t_2$, $(E(t_2), I(t_2)) > 0$. Thus there is a positive number $\xi > 0$ such that $(E(t_2), I(t_2)) \geq \xi\tilde{v}$ holds. It is easy to see that $V = \xi e^{s(J_\rho)(t-t_2)}\tilde{v},\ \forall\ t \geq t_2$ is a solution of (4.12) with $V(t_2) = \xi\tilde{v}$. Hence by comparison principle [66, Theorem B.1], we get

$$(E(t), I(t)) \geq \xi e^{s(J_\rho)(t-t_2)}\tilde{v},\ \forall\ t \geq t_2.$$

Also, for $R_v > 1$, we have $s(J_\rho) > 0$, implying $\lim_{t\to\infty} E(t) = \infty$, $\lim_{t\to\infty} I(t) = \infty$, which is a contradiction. This proves that the solution repels from E^0. It follows that forward orbit of any solutions in M_∂ converges to E^0 is isolated in $\mathbb{R}^5$.

Now, we define a stable set of E^0:

$$W^s(E^0) = \{p \in \Gamma :\ d(\psi(t)p, E^0) \to 0 \text{ as } t \to \infty\}.$$

Clearly, $W^s(E^0) \cap \Gamma^0 = \emptyset$. It follows that there is no cycle in M_∂ from E^0 to E^0. Applying [69, Theorem 1.3.1], we conclude that the system (2.1–2.5) is uniformly persistent, i.e., there exists $\zeta > 0$ satisfying (4.9). □

5. Numerical results

5.1. Basic dynamics of measles in Nepal

We first present the properties of basic dynamics of measles in Nepal, particularly vaccinated reproduction numbers and long-term dynamics.

5.1.1. Computation of the reproduction numbers

Using the estimated parameters (Table 1), we obtain the reproduction number of measles in the presence of vaccination in Nepal to be $R_v = 1.0098$. While $R_v > 1$ is consistent with the currently ongoing endemic of measles, the actual magnitude we observed is significantly lower than the previously estimated reproduction number between 5 and 18 in other places [70]. The low value of R_v is expected as its estimate is based on the parameters influenced by the vaccination program. We now compute the time-dependent effective reproduction number, R_t, which describes the time-varying average number of secondary cases. The value of R_t allows us to track whether the epidemic at time t is in an increasing ($R_t > 1$) or decreasing ($R_t < 1$) trend. For our model, the effective reproduction number is given by

$$R_t = \frac{\beta\sigma\,(S(t) + U_V(t)(1-\varepsilon_1) + M_V(t)(1-\varepsilon_2))}{N(t)(\mu+\sigma)(\delta+\eta+\mu)}.$$

Using the estimated parameters (Table 1), we obtained the pattern of R_t as shown in Figure 3. As predicted by our model, the value of the effective reproduction number remains less than unity, indicating the epidemic is in decreasing trend until 2030, after which R_t increases and remains greater than unity until 2095, showing the increasing trend of the disease in the period 2030–2095 (Figure 3).

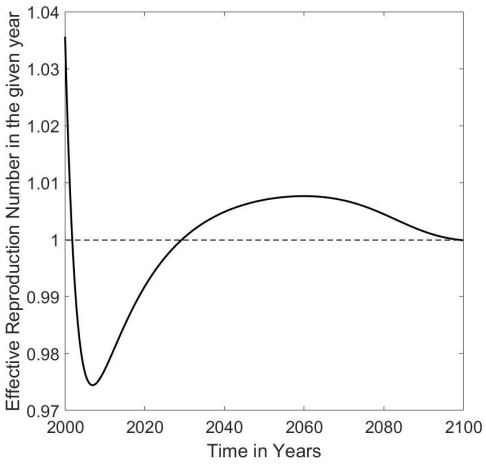

Figure 3. Effective Reproduction Number (R_t). The model predicted effective reproduction number, (R_t), for measles epidemic in Nepal.

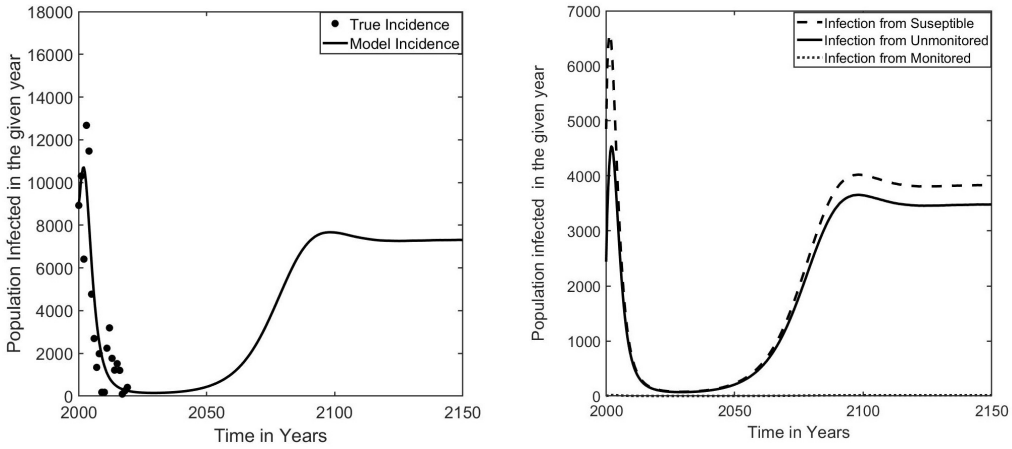

Figure 4. (a) Longterm dynamics predicted by the model. The model prediction of the longterm dynamics of yearly new measles cases in Nepal. (b) Infections from the different classes. The model prediction of the longterm dynamics of yearly new measles cases in Nepal contributed by susceptible, un-monitored vaccinated, and monitored vaccinated classes.

5.1.2. Longterm dynamics

In this section, we present our model prediction for the long-term dynamics of measles transmission in Nepal. If the current trend continues, there will still be 178 cases in 2023 (Figure 4), indicating an obstacle to the measles elimination program set by the government of Nepal. Our model predicts that the cases remain at a significantly low level until 2033 but persist at a low level without being eradicated. After 2033, the resurgence of the outbreak will begin and reach the peak value (7670) in 2097. The dynamic is relatively slow, reaching a steady-state only after about 2100. The resurgence of measles in Nepal predicted by our model supports the worldwide trend of the epidemic, which shows an eventual resurgence in many places such as the UK, the US (31 states including New York), and the Philippines. We also predict the contribution of susceptible (unvaccinated), un-monitored vaccinated, and monitored vaccinated to the resurgence of the measles cases. As per our model prediction, the major contribution to the resurgence is from the susceptible and the un-monitored vaccinated groups. Note that the un-monitored vaccinated group can be significantly high in Nepal, as shown by the data that while 92% are vaccinated with MCV1, only about 76% are vaccinated with MCV2 in 2019 [48]. Therefore, proper implementation of the monitored vaccination program may be needed to avoid the resurgence of the disease.

5.2. Sensitivity analysis

5.2.1. Sensitivity of parameters to R_v

We first observe the local sensitivity of R_v to each of the parameters. For this, we obtain the sensitivity index S_x, given by

$$S_x = \left(\frac{x}{R_v}\right)\left(\frac{\partial R_v}{\partial x}\right),$$

where x is the parameter of which the sensitivity is to be obtained. Based on S_x, we found that R_v is highly sensitive to β. The parameter γ_1 also affects R_v more than the other parameters, and the ε_2 affects less while the effect of σ and α_2 are negligible (Figure 5).

We also extend the analysis to the global sensitivity by using Latin Hypercube Sampling (LHS) [71], taking 1000 sample points from the global parameter space. We compute the partial rank correlation coefficients to identify the most influential parameters. We observed that in the global parameter space, the parameters ε_1, α_1, and β are the most strongly effective to R_v, followed by $\alpha_2, \varepsilon_2, \gamma_1$, and σ, while γ_2 is less effective (Figure 5).

5.2.2. Sensitivity of parameters to the dynamics

In this section, we use Latin Hypercube Sampling [71] from the global parameter space to identify the sensitivity level of the peak value of the infected class and that of the time at the peak of the epidemic. The computed partial rank correlation coefficient corresponding to each parameter is presented in Figure 6. Our analysis shows that the peak value of the infected class is highly correlated to β (positive correlation). The peak value is moderately affected by α_1, α_2, γ_1, and σ and is weakly correlated to the parameters γ_2, ε_2, and ε_1 (Figure 6). Similarly, the peak time of the epidemic is mostly affected by the parameters β and ε_1, while it is less influenced by the parameters α_1 and γ_1. The parameters $\sigma, \gamma_2, \alpha_2$, and ε_2 have the least effect on the peak time.

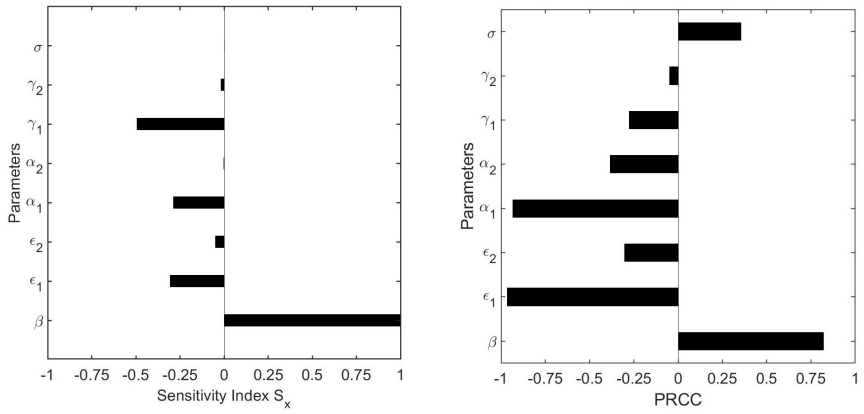

Figure 5. (a) Local sensitivity of parameters to R_v. The sensitivity index, S_x, showing the level of change in R_v with respect to the parameters. Note that the sensitivity index S_x of $\sigma = 0.0022$ and $\alpha_2 = -0.06$ are negligible, and thus difficult to visualize in the figure. (b) Global sensitivity of R_v. Partial Rank Correlation Coefficients for R_v from LHS method.

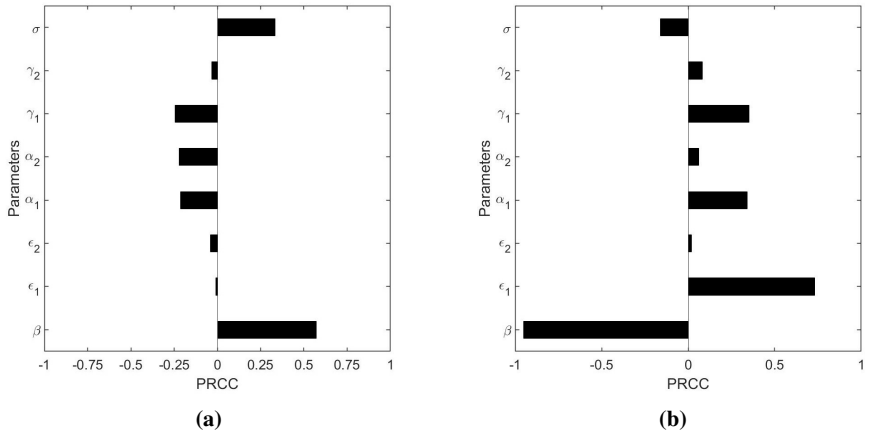

Figure 6. (a) Global sensitivity of the peak level of infected class. The partial rank correlation coefficients for sensitivity of peak level of infected class based on Latin Hypercube sampling. (b) Global sensitivity of the peak time. The partial rank correlation coefficients for sensitivity for the peak time based on Latin Hypercube sampling.

5.3. Effects of monitored and un-monitored vaccination

We use five parameters, the un-monitored vaccination rate (α_1), the monitored vaccination rate (α_2), the immunization rate of un-monitored vaccination (γ_1), the effectiveness of un-monitored vaccination (ε_1), and the effectiveness of monitored vaccination (ε_2) to evaluate the effects of the vaccination programs.

5.3.1. Effects on the measles eradication

Note that $R_v < 1$ can be associated with a condition required to eradicate the disease (Section 4.3). We now use our R_v formulation to identify vaccine-related parameters that can reduce R_v below one (Figure 7). We found that at the current level of α_1, either the monitored vaccination rate α_2 needs to rise by 250% ($\alpha_2 \geq .07$) or the effectiveness of un-monitored vaccination ε_1 needs to rise by 4% ($\varepsilon_1 \geq 0.52$) to make $R_v < 1$. On the other hand, with the current effectiveness of monitored vaccination (ε_2), the effectiveness of un-monitored vaccination (ε_1) needs to be greater than 0.52 to make $R_v < 1$ (Figure 7).

If the un-monitored vaccination rate (α_1) is increased by 20% ($\alpha_1 \approx 0.42$ per year), the activity of the monitored vaccination program can be somewhat relaxed at the current level of $\alpha_2 \approx 0.02$ per year for $R_v < 1$. On the other hand, if α_1 is decreased by 26% ($\alpha_1 \approx 0.23$ per year), the activity of the monitored vaccination program needs to be raised, making the level of α_2 exceed more than 0.1 per year to achieve $R_v < 1$.

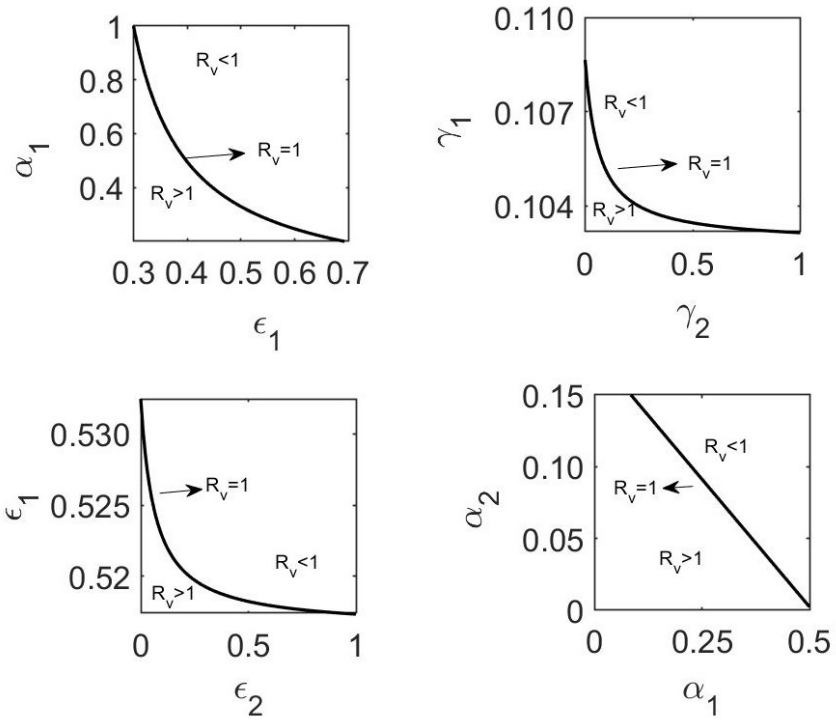

Figure 7. Effects of vaccination on R_v. The contour line (the solid line) corresponding to $R_v = 1$ in the parameter space plane with each two of the un-monitored vaccination rate (α_1), monitored vaccination rate (α_2), the effectiveness of un-monitored vaccination (ε_1), effectiveness of monitored vaccination (ε_2), immunization rates of un-monitored vaccination (γ_1) and immunization rate of monitored vaccination (γ_2).

5.3.2. Effects on the dynamics

In the absence of monitored vaccination, the model predicts that the cases will rise and reach the peak value of 85,750 in 2038 for $\alpha_2 = 0$. With the reduction of un-monitored vaccination by 50% or $\alpha_1 = 0.15$, our model predicts that the cases will rise and reach the peak value of 647,300 in 2028 (Figure 8). If the immunity rate of un-monitored vaccination is decreased by 50%, i.e., $\gamma_1 = 0.05$, the cases rise, leading to the peak value of about 452,800 in 2030. Similarly, if the effectiveness of un-monitored vaccination is decreased by 20% ($\varepsilon_1 = 0.4$), the cases may rise and reach the peak value of 268,200 in 2027.

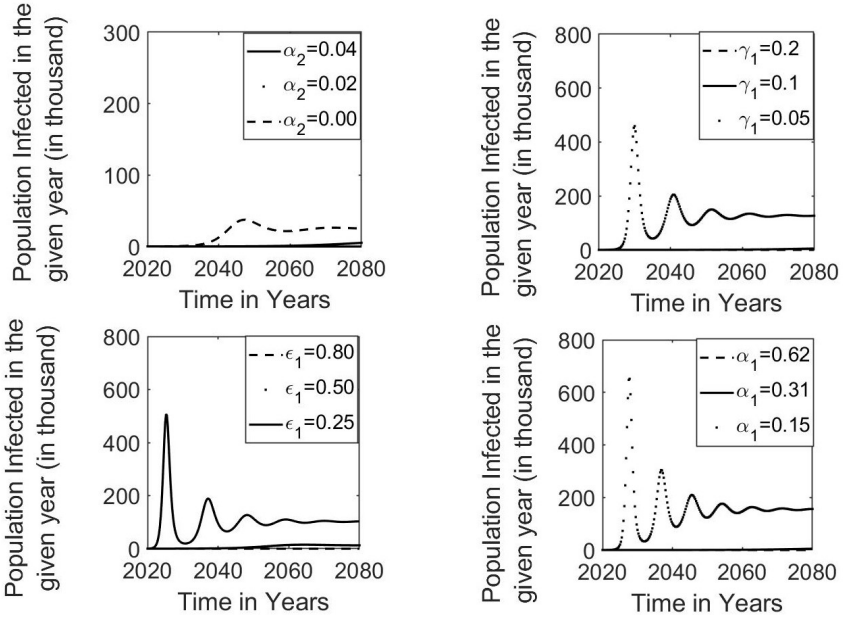

Figure 8. Effects of vaccination on the dynamics. Model prediction of dynamics in the present scenario and various level of un-monitored vaccination rate (α_1), its immunization rate (γ_1), and the effectiveness (ε_1) and the monitored vaccination rate (α_2).

5.3.3. Effects on the steady state

We explore how the different levels of vaccination-related parameters, α_1, α_2, $\gamma_1, \gamma_2, \varepsilon_1$, and ε_2, (Figure 9) affect the level of steady-state of new infections (Figure 9). As expected, an increase in the vaccination rate decreases the steady-state level of new infections. Based on our model prediction, the current level of vaccination results in 7,312 new cases at a steady state. To sufficiently reduce the steady-state level of new infections, the rate of un-monitored vaccination should be increased by 6.5% ($\alpha_1 = 0.33$), or the rate of monitored vaccination should be increased by 50% ($\alpha_2 = 0.03$). Similarly, the immunizing rate of un-monitored vaccine needs to be increased by 100% ($\gamma_1 = 0.2$), or its effectiveness needs to be increased by 20% ($\varepsilon_1 = 0.6$) to bring the steady-state level of new infections to a sufficiently low level.

Furthermore, the reduction of 6.5% of the un-monitored vaccination rate (α_1) increases the steady-state new cases by 206% (22.35 thousand), showing the high impact of the vaccination rate. Also,

lowering the monitored vaccination rate (α_2) by 50% increases the steady-state level of new cases by approximately 250% (25.56 thousand). Similarly, decreasing the immunity rate of un-monitored vaccination (γ_1) by 10% increases the steady-state new cases by about 300% (29.1 thousand) while reducing the effectiveness of monitored vaccination (ε_2) by 18% increases the steady-state new cases by 30% (9.528 thousand).

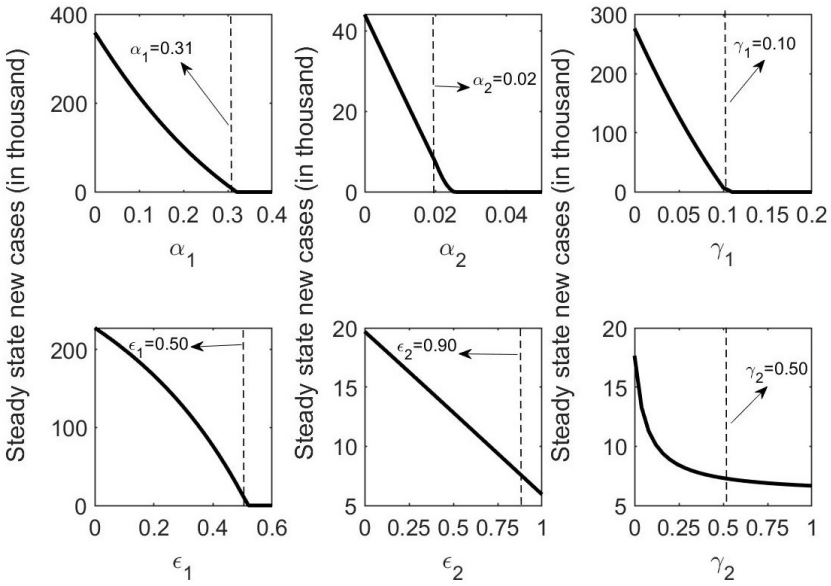

Figure 9. Effects of vaccination on the steady state. Model predicted new cases at the steady state for the various vaccination rates α_1, α_2, immunized rate γ_1, γ_2 and effectiveness of un-monitored and monitored vaccination program ε_1, and ε_2, respectively.

6. Conclusions

In recent years, the frequent outbreaks of measles in developing and developed countries have become a significant obstacle to achieving the goal of elimination. Mainly, unvaccinated children are the victims of the disease [6, 7, 26]. Despite the Supplementary Immunization Activities (SIAs), most of the population is not vaccinated in some districts of Nepal, including Rautahat, Kapilvastu, Morang, and Bajura. Furthermore, many of those initiating the vaccination does not complete the vaccine doses correctly, making them not completely protected. Because of the resurgence of measles in Nepal since 2017 [20, 21], WHO's deadline for the elimination goal has been extended to 2023 [53]. We developed a novel deterministic model validated by the data from Nepal to evaluate the monitored vaccination programs.

We thoroughly analyzed our model to formulate the vaccinated reproduction number ($R_v > 1$), the stability analysis, and the disease persistence theory. Using the model and the available data from the official websites of WHO, we estimated key parameters related to the un-monitored vaccination. Moreover, we performed a global sensitivity analysis using Latin Hypercube Sampling from the wider parameter space. Our model predicts that the measles elimination goal can be achieved if the monitored

vaccination rate is increased by 50% ($\alpha_2 = 0.03$) or the un-monitored vaccination rate is increased by 6.5% ($\alpha_1 = 0.33$). The elimination goal can also be achieved by the high effectiveness of the un-monitored vaccine (i.e., with $\varepsilon_1 \geq 0.53$). However, if the current trend continues, our model predicts that the measles will persist causing an obstacle to the measles elimination goal of Nepal. Furthermore, our model predicts that without any additional interventions, measles transmission will continue with a rise in the epidemic after 2033 (Figure 4). Our model also predicts that the major contributor to the measles resurgence in Nepal is susceptible (unvaccinated) and unmonitored vaccinated groups, emphasizing the need for the expedition of monitored-vaccination programs. The epidemic dynamics in Nepal is quite slow, reaching the peak only in about 2097 (Figure 4). The observed slow dynamics is consistent with the previous study [72].

We acknowledge some limitations of our study. The parameter estimations are based on the limited data of yearly incidence cases (2000–2019). Moreover, measles is a short-term disease recovered within a month, so the daily or weekly more detailed and accurate data can help improve the prediction of our model. We could obtain the closed form of the unique endemic equilibrium but are unable to perform a detailed analysis of the endemic equilibrium. Instead, we established the disease persistence criteria. The homogeneous mixing assumed among the children of Nepal can be improved by the model with an appropriate network of contact among children.

In summary, we develop a model of measles transmission in the context of Nepal, where monitoring is critical for the successful implementation of the vaccination program. Our thorough analysis and the detailed numerical simulations of the model can provide helpful information for policymakers to design ideal monitored-vaccination programs to achieve the elimination goal of measles from Nepal.

Acknowledgments

This research was supported by the GRAID (Graduate Research Assistantships in Developing Countries) awards from the International Mathematical Union (IMU). AP acknowledges the Nepal Mathematical Society (NMS) for the NMS Ph.D. Fellowship Award 2020. KA acknowledges the Nepal Academy of Science and Technology (NAST) for Ph.D. Fellowship and the Nepal Mathematical Society (NMS) for the NMS Ph.D. Fellowship award 2020. RG acknowledges the University Grants Commission (UGC) for Ph.D. Fellowship and Nepal Mathematical Society (NMS) for the NMS Ph.D. Fellowship Award 2020. The work of NKV was supported by NSF grants DMS-1951793 and DEB-2030479 from the National Science Foundation of the USA and the UGP award from San Diego State University.

Conflict of interest

The authors declare there is no conflict of interest.

References

1. J. Hamborsky, A. Kroger, S. Wolfe , *Epidemiology and prevention of vaccine-preventable diseases*, 13th ed. Washington D.C. Public Health Foundation, 2015.
2. E. Stephen, K. Raymond, K. Gabriel, F. Nestory, M. Godfrey, M. Arbogast, A mathematical model

for control and elimination of the transmission dynamics of measles, *Appl. Comput. Math.*, **4** (2015), 396–408. https://doi.org/10.11648/j.acm.20150406.12

3. *Center for Disease Control and Prevention (CDC)*, Measles epidemic: Overcoming vaccine prejudice (History of measles outbreaks), *A Train Education*, available from: https://www.atrainceu.com/content/2-history-and-pathology-measles (accessed on 8 February 2021).
4. *World Health Organization*, Measles, available from: https://www.who.int/news-room/fact-sheets/detail/measles, (accessed on 10 March 2021).
5. UNICEF, *UNICEF for every child*, Over 20 million children worldwide missed out on measles vaccine annually in past 8 years, creating a pathway to current global outbreaks, available from: https://www.unicef.org/nepal/press-releases/over-20-million-children-worldwide-missed-out-measles-vaccine-annually-\past-8-years (accessed on 28 March 2020).
6. *United Nations: UN News*, Measles cases hit 23-year high last year, killing 200,000 as vaccination stalls, WHO says, available from: https://news.un.org/en/story/2020/11/1077482 (accessed on 10 March 2020).
7. M. K. Patel, J. L. Goodson, J. P. Alexander Jr, K. Kretsinger, S. V. Sodha, C. Steulet, et al., Progress toward regional measles elimination– worldwide, 2000–2019, *Morb. Mortal. Wkly. Rep.*, **69** (2020), 1700. https://doi.org/10.15585/mmwr.mm6848a1
8. *Government of Nepal, Ministry of Health and Population*, National immunization programme, available from: https://www.mohp.gov.np/eng/program/child-health-services/nip (accessed on 28 March 2021).
9. L. H. Sun, B. Guarino, Anti-vaxxers target communities battling measles, available from: https://www.washingtonpost.com/national/health-science/antivaxxers-go-viral-in-communities-battling-measles/2019/05/20/a476417c-78d7-11e9-bd25-c989555e7766_story.html (accessed: 20 April 2020).
10. B. Zadrozny, E. Edwards, Anti-vaccine groups take dangerous online harassment into the real world, available from: https://www.nbcnews.com/health/kids-health/anti-vaccine-groups-take-dangerous-harassment-offline-real-world-n1096461 (accessed on 20 April 2020).
11. *New York City (NYC) Health*, Measles, available from: https://www1.nyc.gov/site/doh/health/health-topics/measles.page (accessed on 10 August 2020).
12. B. Guarino, L. H. Sun, New York anti-vaccine event attracts pro-vaccine protests amid measles outbreak, available from: https://www.washingtonpost.com/health/2019/06/05/brooklyn-anti-vaccine-event-attracts-pro-vaccine-protests-amid-measles\-outbreak/, (accessed on 20 April 2020).
13. *Public Health Update*, National immunization schedule, Nepal (Updated), available from: https://publichealthupdate.com/national-immunization-schedule-nepal/ (accessed on 10 March 2020).
14. S. Khanal, T. R. Sedai, G. R. Choudary, J. N. Giri, R. Bohara, R. Pant, et al., Progress toward measles elimination — Nepal, 2007–2014, *Morb. Mortal. Wkly. Rep.*, **65** (2016), 206–210. https://doi.org/10.15585/mmwr.mm6508a3

15. B. K. Suvedi, Twenty-five years of immunization program in Nepal, *Kathmandu Univ. Med. J.*, **3** (2005), 4.

16. *Government of Nepal, Ministry of Health and Population Child Health Division, Department of Health Services (DoHS)*, National immunization programme, available from: http://www.chd.gov.np (accessed on 10 March 2020).

17. *Child Health Division, DoHS, MoHP*, National immunization program, reaching every child, comprehensive multi-year plan 2068–2072 (2011–2016), MoHP, Nepal (2011).

18. A. Poudel, Routin immunization: How to Measles Transmission, (2014), available from: http://arjunmaske.blogspot.com/2014/09/how-to-measlestransmission.html (accessed on 12 August 2020).

19. A. Poudel, Measles outbreak in Morang, Dang and Kapilvastu raises concern, available from: https://kathmandupost.com/national/2019/04/30/measles-outbreak-in-morang-dang-and-kapilvastu-raises-concern (accessed on 12 September 2020).

20. A. Poudel, Low vaccine coverage rate, floating population leading to repeat measles outbreaks, available from: https://reliefweb.int/report/nepal/low-vaccine-coverage-rate-floating-population-leading-repeat-measles-outbreaks (accessed on 12 September 2020).

21. *New Spotlight Online*, Number Of Measles Cases In Nepal Increased by more than two times in 2018, available from: https://www.spotlightnepal.com/2019/04/25/number-measles-cases-nepal-increased/ (accessed on 25 March 2020).

22. A. Poudel, Measles outbreaks reported in five districts including in Kathmandu and Lalitpur in last one month, available from: https://kathmandupost.com/national/2020/04/29/measles-outbreaks-reported-in-five-districts-including-in-kathmandu-and-lalitpur\-in-last-one-month, (accessed on 5 March 2021).

23. S. Uprety, Meanwhile, a measles outbreak in Nepal, available from: https://www.nepalitimes.com/here-now/meanwhile-a-measles-outbreak-in-nepal/ (accessed on 28 March 2021).

24. K. B. Karki, M. Dhimal, A. R. Pandey, B. Bista, A. Pandey, B. R. Giri, et al., *Measles outbreak in Kapilvastu, Nepal: an outbreak investigation*, Nepal Health Research Council, Ramshah Path, Kathmandu, Nepal, 2016.

25. M. Poudel, Unidentified disease claims lives of six kids, available from: https://kathmandupost.com/national/2016/01/20/unidentified-disease-claims-lives-of-six-kids (accessed on 10 September 2020).

26. S. Sitaula, G. R. Awasthi, J. B. Thapa, K. P Joshi, A. Ramaiya, Measles outbreak among unvaccinated children in Bajura, *JNMA J. Nepal Med. Assoc.*, **50** (2010), 273–276. https://doi.org/10.31729/jnma.48

27. H. Trottier, P. Philippe, Deterministic modeling of infectious diseases: measles cycles and the role of births and vaccination, *Internet J. Infect. Dis.*, **2** (2002), 8 page.

28. H. Trottier, P. Philippe, Deterministic modeling of infectious diseases: theory and methods, *Internet J. Infect. Dis.*, **1** (2000), 3.

29. S. N. Mitku, Mathematical modeling and simulation study for the control and transmission dynamics of measles, *Am. J. Appl. Math.*, **5** (2017), 99–107. https://doi.org/10.11648/j.ajam.20170504.11

30. M. G. Robert, M. I. Tobias, Predicting and preventing measles epidemics in New Zealand, *Epidemiol. Infect.*, **124** (2000), 279–287. https://doi.org/10.11648/j.ajam.20170504.11

31. A. Franceschetti, A. Pugliese, Threshold behaviour of a SIR epidemic model with age structure and immigration, *J. Math. Biol.*, **57** (2008), 1–27. https://doi.org/10.1007/s00285-007-0143-1

32. J. F. Christopher, S. Katriona, C. Spencer, C. M. Jose, G. Christopher, G. James, et al., Measles outbreak response decision-making under uncertainty: a retrospective analysis, *J. R. Soc. Interface*, **15** (2017), 20170575. http://doi.org/10.1098/rsif.2017.0575R

33. A. A. Momoh, M. O. Ibrahim, I. J. Uwanta, S. B. Manga, Mathematical model for control of measles epidemiology, *Inter. J. Pure Appl. Math.*, **67** (2013), 707–718. https://doi.org/10.12732/ijpam.v87i5.4

34. M. D. la Sens, A. Quesadas, A. Ibeas, R. Nistal, An observed-based vaccination law for a SEIR epidemic model, *Int. J. Comput. Theory Eng.*, **4** (2012), 1–32. http://doi.org/10.7763/IJCTE.2012.V4.488

35. E. F. Doungmo Goufo, S. C. Oukouomi Noutchie, S. Mugisha, A fractional SEIR epidemic model for spatial and temporal spread of measles in metapopulations, *Abstr. Appl. Anal.*, **2014** (2014), 6. https://doi.org/10.1155/2014/781028

36. J. Ochoche, R. Gweryina, A mathematical model of measles with vaccination and two phases of infectiousness, *J. Math.*, **10** (2019), 95–105. https://doi.org/10.9790/5728-101495105

37. E. M, Musyoki, R. Ndung'u, S. Osman, A mathematical model for the transmission of measles with passive immunity, *Int. J. Res. Math. Stat. Sci.*, **6** (2019), 1–8. https://doi.org/10.26438/ijsrmss/v6i2.18

38. M. Fred, J. Sigey, J. A. Okello, J. Okwoyo, G. J. Kang'ethe, Mathematical modeling on the control of measles by vaccination: case study of KISII County Kenya, *SIJ Trans. Comput. Sci. Eng. Appl. (CSEA)*, **2** (2015), 38–46. https://doi.org/10.9756/SIJCSEA/V2I4/0203150101

39. O. Christopher, A. I. Ibrahim, A. S. Timothy, Mathematical model of the dynamics of measles under the combined effect of vaccination and measles therapy, *Int. J. Sci. Technol.*, **6** (2017), 118–173.

40. M. J. Wanjau, R. Titus, C. Isaac, Mathematical modeling of the transmission dynamics of measles under the effect of vaccination, *IOSR J. Math.*, **15** (2019), 10–19.

41. R. Y. M'pika Massoukou, S. C. Oukouomi Noutchie, R. Guiem, Global dynamics of an SVEIR model with age-dependent vaccination, infection, and latency, *Abstr. Appl. Anal.*, **2018** (2018), 1–21. https://doi.org/10.1155/2018/8479638

42. T. Bakhtiar, Control policy mix in measles transmission dynamics using vaccination, therapy, and treatment, *Int. J. Math. Math. Sci.*, **2020** (2020), 1–20.

43. Z. Memon, S. Qureshi, B. R. Memon, Mathematical analysis for a new nonlinear measles epidemiological system using real incidence data from Pakistan, *Eur. Phys. J. Plus*, **135** (2020), 1–21. https://doi.org/10.1140/epjp/s13360-020-00392-x

44. D. Aldila, D. Asrianti, A deterministic model of measles with imperfect vaccination and quarantine intervention, *Int. Conf. Mathematics: Pure, Appl. Computat.*, **1218** (2019), 012044–012054. https://doi.org/10.1088/1742-6596/1218/1/012044

45. *Centers for Disease Control and Prevention (CDC)*, Progress in measles control–Nepal, 2000-2006, *MMWR Morb. Mortal Wkly Rep.*, **56** (2007), 1028–1031.

46. A. T. Truong, M. N. Mulders, D. C. Gautam, W. Ammerlaan, R. L. de Swart, C. C. King, et al., Genetic analysis of Asian measles virus strains–new endemic genotype in Nepal, *Virus Res.*, **76** (2001), 71–78. https://doi.org/10.1016/S0168-1702(01)00255-6

47. A. B. Joshi, Measles deaths in Nepal: estimating the national cases in fatality ratio, *Bull World Health Organ*, **87** (2009), 405–484. https://doi.org/10.2471/BLT.07.050427

48. *World Health Organization*, WHO vaccine-preventable diseases: monitoring system. 2020 global summary, 2019, available from: `https://apps.who.int/immunization_monitoring/globalsummary` (accessed on 28 march 2020).

49. B. Pantha, S. Giri, H. R. Joshi, N. K.Vaidya, Modeling transmission dynamics of rabies in Nepal, *Infect. Dis. Model.*, **6** (2021), 284–301. https://doi.org/10.1016/j.idm.2020.12.009

50. *Macrotrends*, Nepal Population 1950–2020, available from: `https://www.macrotrends.net/countries/NPL/nepal/population` (accessed on 2 October 2020).

51. *World Health Organization*, Nepal - Deaths due to measles among children aged <5 years, available from: `https://www.who.int/immunization/monitoring_surveillance/burden/vpd/WHO_SurveillanceVaccinePreventable_11_Measles_R1.pdf?ua=1` (accessed on 2 October 2020).

52. *World Data Atlas*, Nepal-Deaths due to measles among children aged < 5 years, available from: `https://knoema.com/atlas/Nepal/topics/Health/Deaths-among-children-under-5-by-cause/Deaths-due-to-measles` (accessed on 3 October 2020).

53. H. S. Rathore, Measles outbreak kills two children and infects over 150 in Chepang settlements of Dhading district, available from: `https://kathmandupost.com/province-no-3/2020/04/06/measles-outbreak-kills-two-children-and-infects-over-150-in-chepang-\settlements-of-dhading-district` (accessed on 3 October 2020).

54. H. Motulasky, A. Christopoulos, *Fitting Model to Biological Data Using Linear and Non Linear Regression. A Practical Guide to Curve Fitting*, Graph Pad Software Inc.San Diego, CA, (2003), `www.graphpad.com` https://doi.org/10.5206/mase/10847 .

55. M. Rahman, K. Bekele-Maxwell, L. L. Cates, H. T. Banks, N. K. Vaidya, Modeling zika virus transmission dynamics: parameter estimates, disease characteristics, and prevention, *Sci. Rep.*, **9** (2019), 10575. https://doi.org/10.1038/s41598-019-46218-4

56. H. T. Banks, S. Hu, W. C. Tompson, *Modeling and inverse problems in the presence of uncertainty*, CRC Press, Taylor and Francis Group, A Chapman and Hall Book, 2014.

57. H. T. Banks, M. L. Joyner, Information content in data sets: a review of methods for interrogation and model comparison, *J. Inverse Ill-Posed Probl.*, **26** (2018), 423–452. https://doi.org/10.1515/jiip-2017-0096

58. K. Adhikari, R. Gautam, A. Pokharel, K. N. Uprety, N. K. Vaidya, Transmission dynamics of COVID-19 in Nepal: Mathematical model uncovering effective control, *J. Theor. Biol.*, **521** (2021), 110680. https://doi.org/10.1016/j.jtbi.2021.110680
59. C. D. Schunn, D. P. Wallach, Evaluating goodness-of-fit in comparison of models to data, *Psychologie der Kognition: Reden and Vorträge anlässlich der Emeritierung von Werner Tack*, (2005), 115–135.
60. H. Miao, X. Xia, A. S. Perelson, H. Wu, On identifiability of nonlinear ODE models and applications in viral dynamics, *SIAM Rev.*, **53** (2011), 3–39. https://doi.org/10.1137/090757009
61. O. Diekmann, J. A. P. Heesterbeek, *Mathematical Epidemiology of Infectious Diseases: Model Building, Analysis and Interpretation*, Wiley, New York, 1999.
62. P. van den Driessche, J. Watmough, Reproduction numbers and sub-threshold endemic equilibria for compartmental models of disease transmission, *Math. Biosci.*, **180** (2002), 29–48. https://doi.org/10.1016/S0025-5564(02)00108-6
63. G. Chowell, J. M. Hyman, *Mathematical and statistical modeling for emerging and re-emerging infectious diseases*, Springer International Publishing Switzerland, 2016.
64. O. Diekmann, J. A. P. Heesterbeek, M. G. Roberts, The construction of next-generation matrices for compartmental epidemic models, *J. R. Soc. Interface*, **7** (2010), 873–885. https://doi.org/10.1098/rsif.2009.0386
65. M. A. Kuddus, M. Mohiuddin, A. Rahman, Mathematical analysis of a measles transmission dynamics model in Bangladesh with double dose vaccination, *Sci. Rep.*, **11** (2021), 1–16. https://doi.org/10.1038/s41598-021-95913-8
66. H. L. Smith, P. Waltman, *The theory of the chemostat*, Cambridge University Press, 1995.
67. J. M. Mutua, F. Bin Wang, N. K. Vaidya, Modeling malaria and typhoid fever co-infection dynamics, *Math. Biosci.*, **264** (2015), 128–144. https://doi.org/10.1016/j.mbs.2015.03.014
68. T. Kato, *Perturbation theory for linear operators* , Springer-Verlag, Berlin Heidelberg, 1976.
69. X. Q. Zhao, *Dynamical systems in population biology*, Springer International Publishing, 2017.
70. *Centers for Disease Control and Prevention*, Measles symptoms and complications, available from: `https://www.cdc.gov/measles/symptoms/index.html` (accessed on 10 September 2020).
71. S. Marino, I. B. Hogue, C. J. Ray, D. E. Kirschner, A methodology for performing global uncertainty and sensitivity analysis in systems biology, *J. Theor. Biol.*, **254** (2008), 178–196. https://doi.org/10.1016/j.jtbi.2008.04.011
72. J. Horrocks, C. T. Bauc, Algorithmic discovery of dynamic models from infectious disease data, *Sci. Rep.*, **10** (2020), 7061. https://doi.org/10.1038/s41598-020-63877-w

AIMS Press

Infectious Disease Modelling 9 (2024) 1007–1026

Contents lists available at ScienceDirect

Infectious Disease Modelling

journal homepage: www.keaipublishing.com/idm

Modeling measles transmission in adults and children: Implications to vaccination for eradication

Anjana Pokharel [a, b], Khagendra Adhikari [b, c], Ramesh Gautam [b, d], Kedar Nath Uprety [b, e], Naveen K. Vaidya [b, f, g, h, *]

[a] Padma Kanya Multiple Campus, Tribhuvan University, Kathmandu, Nepal
[b] Mathematical Biology Research Center, Kathmandu, Nepal
[c] Amrit Campus, Tribhuvan University, Kathmandu, Nepal
[d] Ratna Rajya Laxmi Campus, Tribhuvan University, Kathmandu, Nepal
[e] Central Department of Mathematics, Tribhuvan University, Kathmandu, Nepal
[f] Department of Mathematics and Statistics, San Diego State University, San Diego, CA, USA
[g] Computational Science Research Center, San Diego State University, San Diego, CA, USA
[h] Viral Information Institute, San Diego State University, San Diego, CA, USA

ARTICLE INFO

Article history:
Received 2 February 2024
Received in revised form 17 April 2024
Accepted 29 April 2024
Available online 4 May 2024
Handling Editor: Dr. Raluca Eftimie

2010 MSC:
34K20
34L30
92B05
92D30

Keywords:
Measles eradication
Measles reservoir
Adult-child vaccination
Adults and children groups
Nepal

ABSTRACT

Despite the availability of successful vaccines, measles outbreaks have occurred frequently in recent years, presumably due to the lack of proper vaccination implementation. Moreover, measles cases in adult groups, albeit small in number, indicate that the previously neglected adult group may need to be brought into vaccine coverage to achieve WHO's goal of measles eradication from the globe. In this study, we develop a novel transmission dynamics model to describe measles cases in adults and children to evaluate the role of adult infection in persistent measles cases and vaccination programs for eradication. Analysis of our model, validated by measles cases from outbreaks in Nepal, provides the vaccination reproduction number (conditions for measles eradication or persistence) and the role of contact network size. Our results highlight that while children are primary targets for measles outbreaks, a small number of infections in adults may act as a reservoir for measles, causing obstacles to eradication. Furthermore, our model analysis shows that while impactful controls can be achieved by children-focused vaccines, a combined adult-child vaccination program may help assert eradication of the disease.

1. Introduction

Measles, a disease caused by the morbillivirus, remains a major global health concern. Despite the availability of effective vaccines, measles outbreaks occur frequently, especially among children, and the infection causes severe complications in infected individuals. According to WHO, measles vaccination averted around 56 million deaths due to this disease during the 21-year time (between 2000 and 2021) (WHO, 2023a). However, in 2021, there were 128,000 recorded deaths due to measles, occurring primarily among unvaccinated or partially vaccinated children, highlighting the need for more focused prevention efforts to bring the global measles cases down (WHO, 2023a).

* Corresponding author. Mathematical Biology Research Center, Kathmandu, Nepal.
E-mail address: nvaidya@sdsu.edu (N.K. Vaidya).
Peer review under responsibility of KeAi Communications Co., Ltd.

https://doi.org/10.1016/j.idm.2024.04.012

Various factors, including limited access to healthcare systems, vaccine hesitancy driven by skepticism, and the impact of the COVID-19 pandemic on vaccine coverage, have collectively hampered vaccination programs in 2021. In 2021, a record high of nearly 40 million children missed a measles vaccine dose; 25 million children missed their first dose, and an additional 14.7 million children missed their second dose (WHO, 2022). The world data is well under that, with only 81% of children receiving their first measles-containing vaccine dose, and only 71% of children receiving their second one. Note that the World Health Organization (WHO) recommends at least 95 percent vaccination coverage to achieve herd immunity for measles (Unicef for Every Child, 2019).

The decline in vaccine coverage coincides with measles transmission patterns, impacting not only infants but also older age groups (Meredith et al., 2021). Major challenges for measles control include a lack of a catch-up vaccination program, growing vaccine hesitancy, and insufficient monitoring for elimination and outbreak prevention. In response, the World Health Organization introduced the "Measles and Rubella Strategic Framework 2021–2030" in 2020, targeting global disease elimination by 2030 (WHO, 2020; WHO, 2023a).

In Nepal, measles vaccination was introduced in 1979, but until 2007, national MCV1 coverage remained below 85 percent, resulting in childhood mortality due to measles. From 2007 to 2014, MCV1 coverage increased from 81% in 2007 to 88% in 2014 (WHO, 2023b). As a result, a remarkable reduction of 98% in measles cases was achieved by 2017 (Sekhar et al., 2022). However, the cases rose in 2018–2019 by 66% (from 260 to 431) (WHO, 2023c). In response, the National Immunization Program (NIP) was introduced in 2020 with a plan for a comprehensive nationwide vaccination campaign targeting children aged 9–59 months against both measles and rubella (MR). While the first phase of this campaign was completed as scheduled, the second phase was disrupted by the COVID-19 pandemic, consequently causing measles outbreaks in multiple districts (Sekhar et al., 2022; Thakur et al., 2024). Between January and April 2020, 220 measles cases were reported, with 78% affecting individuals outside the campaign's target age range (9–59 months). Notably, 60% of the total cases in the 5–14 year age group were not vaccinated (Sekhar et al., 2022).

Recently, from November 2022 to March 2023, 690 cases were reported, with approximately 86% of infected individuals aged 15 years and younger, and 58% of the patients were unvaccinated (WHO, 2023d). While a rising number of measles cases has brought attention to the potential threat of severe measles outbreaks, persistent and frequent outbreaks in specific districts, including Morang, Dang, Kapilvastu, Kathmandu, Lalitpur, Dhading, Banke, Kailali, of Nepal pose a severe concern of obstacle to World Health Organisation's (WHO's) global measles eradication plan "Measles and Rubella Strategic Framework 2021–2030" (Dall, 2023; Poudel, 2019; WHO, 2020; WHO, 2023a; WHO, 2023d). In order to achieve the measles eradication goal, the primary focus has been on formulating improved children-vaccination programs. However, it is essential to note that 14% of the infectious cases are unvaccinated adults. Notably, these infectious adults originating from the pool of unvaccinated children can act as virus reservoirs in the community and sources for disease outbreaks, despite the control in the children group, causing the obstacle to disease eradication. Therefore, implementing a closely monitored vaccination program combined for both children and adults may be imperative to devise a program for completely eradicating the disease.

Mathematical models play a vital role in understanding transmission dynamics, forecasting outbreaks, and proposing effective control strategies (Adhikari et al., 2021; Adhikari et al., 2022; Gautam et al., 2022; Mutua, Wang, & Vaidya, 2015; Vaidya & Wang, 2022). Therefore, mathematical modeling can be a valuable tool for studying measles transmission in children and adult subgroups with different degrees of interactions between intragroup and intergroup populations residing in the same community. Numerous mathematical models have been developed for measles, including SIR, SEIR, SVEIR and SVEIRS, SVEIHR, fractional derivative models, to explore various aspects of measles dynamics (Edward et al., 2015; Farman et al., 2023; Haileyesus & Asnakew, 2023; Kuddus et al., 2021; Peter et al., 2022, 2023a, 2023b; Roberts, 2000; Song et al., 2019; Trottier & Philippe, 2000). Specifically in the context of Nepal, previous studies have discussed progress in measles control, case fatality rates, and the genetic type of the Asian measles virus, most incorporating vaccination (Joshi, 2009; Khanal, 2016; Poudel, 2019; Truong et al., 2001). In Pokharel et al. (2022), we introduced a deterministic model to examine the effect of monitored and un-monitored vaccination in children of Nepal (Pokharel et al., 2022). However, none of the previous models has considered the adult group, presumably the critical group for the global eradication of measles.

In this study, we consider measles cases in adults, a more mobile critical group typically not included in regular immunization programs. We introduce a novel deterministic model, incorporating monitored vaccination for children and adults to assess the impact of these adult-child vaccination approaches on measles eradication in Nepal. The model is validated using fifteen weeks of measles data from Nepal. Our model analysis evaluates the local and global stability of disease-free equilibrium and the existence of at least one endemic equilibrium. We simulate our model to assess the impact of monitored adult-child vaccination programs on reducing measles transmission in Nepal and eventually eradicating the disease over a period of time.

2. Model formulation

2.1. Data source

The publicly available data used in this work is obtained from the official website of the World Health Organization (WHO) (WHO-Nepal, 2023a). From November 24, 2022, to March 10, 2023, a total of 690 cases of measles were recorded in western Nepal, spanning outbreaks in seven districts: Banke (327 cases), Surkhet (62 cases), Bardiya (49 cases), Kailali (39 cases), Kanchanpur (27 cases), Bajura (13 cases), and Dang (12 cases). Additionally, three districts in eastern Nepal also reported

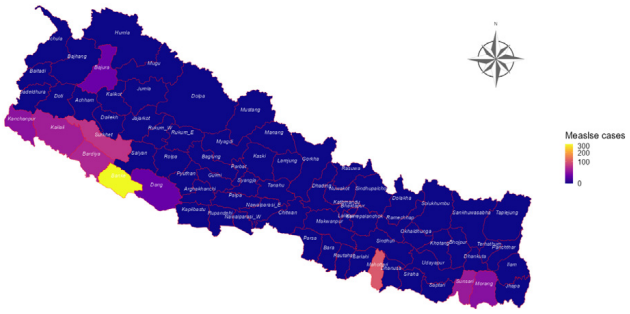

Fig. 1. Measles Cases in Nepal. Measles cases in different parts of Nepal from November 24, 2022, to March 10, 2023. The map was created using the cartography package in R 4.3.1.

cases: Mahottari (103 cases), Sunsari (34 cases), and Morang (24 cases). The distribution of measles cases is shown in Fig. 1. Among these reported cases, one death was reported, indicating a Case Fatality Rate (CFR) of 0.14% (Dall, 2023).

2.2. Transmission dynamics model

We categorize the population into two different age groups (0–15 yrs and above 15 yrs) based on the data (Dall, 2023) and develop a deterministic mathematical model ($SVEII_m$) to describe the transmission dynamics of measles among those two groups. Since measles can be prevented by complete doses of vaccines and individuals gain lifelong immunity after recovery from infection (Edward et al., 2015), we do not consider re-infection in our model. The indices C and A represent the child (0–15 yrs) and adult (above 15) groups, respectively. The group of children and adults are divided into six distinct compartments $(S_C,\ U_C^V,\ M_C^V,\ E_C,\ I_C,\ I_{mC})$ and $(S_A,\ U_A^V,\ V_A,\ E_A,\ I_A,\ I_{mA})$, respectively, as shown in Fig. 2. Λ is the recruitment rate of newborns, and ψ is the maturation rate of a child becoming an adult.

Building an effective vaccination program is often difficult, especially when parents lack adequate health knowledge and are skeptical about vaccines. One way to improve the efficacy of immunization is to incorporate a monitored vaccination program so that children who signed up for it receive their immunizations accurately and on time. The unmonitored class includes children not enrolled in the monitored program. The children in this class may frequently skip the complete vaccine doses on time, presumably due to the lack of parents' health consciousness and/or the lack of supervision for proper immunization. On the other hand, the monitored class includes the children enrolled in the monitored program, which ensures enrolled members with supervision for timely immunization of complete doses. Our objective in this study is to develop a model to evaluate such monitored vaccination programs for controlling measles in both children and adults, with the goal of eradicating measles.

In this context, we assume children engaged in the monitored vaccination program exhibit a lower vulnerability to diseases and a greater probability of acquiring immunity due to increased attention and regular supervision, in contrast to children under unsupervised immunization schemes. Consequently, the children eligible for vaccination are divided into two distinct groups: the Un-monitored Vaccination Group (U_A^V), consisting of vaccinated children undergoing routine vaccination without supervision, and the Monitored Vaccination Group (M_C^V), comprising children vaccinated under supervision to

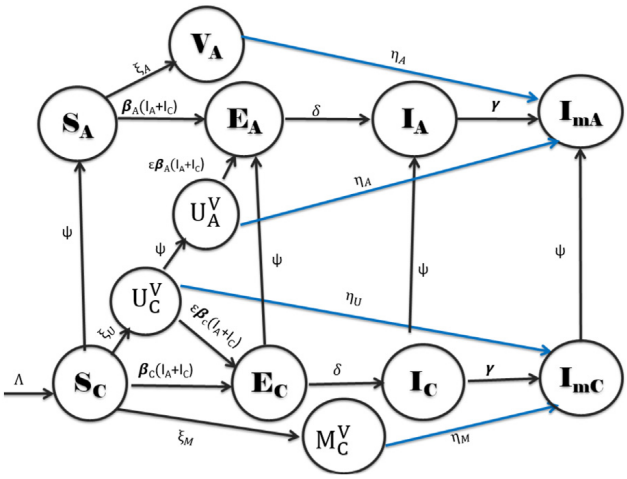

Fig. 2. Schematic diagram of the model: The group of children is divided into six distinct compartments: S_C (Susceptible), U_C^V (Un-monitored Vaccinated), M_C^V (Monitored Vaccinated), E_C (Exposed), I_C (Infectious), and I_{mC} (Immune). Similarly, the adult age group is divided into six subgroups $(S_A,\ U_A^V, V_A,\ E_A,\ I_A,\ I_{mA})$.

Table 1
Description of the parameters.

Symbols	Description
Λ	Recruitment rate to children group
ξ_U, ξ_M	Un-monitored and Monitored children Vaccination rate
ξ_A	Adult Vaccination rate
β_C, β_A	Transmission rate on the children and adults
μ	Natural death rate
γ	Rate of being immune after recovery from infection
ψ	Maturation rate
$(1-\epsilon)$	Effectiveness of the vaccination
η_A	Rate of being immune of Un-monitored vaccinated adults
η_U, η_M	Rate of being immune of Un-monitored, Monitored vaccinated children
δ	Incubation period
d	Disease induced death

ensure timely administration. In addition, we consider the Adult Vaccination Group (V_A), which consists of vaccinated adults under supervision through the catch-up vaccination program.

Upon successfully receiving both vaccine doses per the recommended schedule, we assume that the Monitored Vaccination Group and Adult Vaccination Group will attain sufficient immunization and become non-susceptible to diseases. η_M and η_A represent the rate of immunization of the Monitored Vaccination Group and Adult Vaccination Group, respectively, and β_C represents the rate of the fully susceptible children becoming infected.

Given the possibility of incomplete administration of vaccine doses within the Un-monitored Vaccination Group, there remains a potential susceptibility to diseases. To capture this infection, we account for disease transmission within this group at a rate of $\epsilon\beta_C$, where $(1-\epsilon)$ represents the vaccine's effectiveness. Additionally, we consider a different infection rate, denoted by β_A, for the adult group, assuming that measles transmission is low among adults. The complete description of the parameters is given in Table 1.

The equations of the dynamical system describing measles transmission are as follows:

$$\frac{dS_C}{dt} = \Lambda - (\mu + \xi_M + \xi_U + \psi)S_C - \beta_C(I_C + I_A)S_C, \tag{1}$$

$$\frac{dS_A}{dt} = \psi\ S_C - \beta_A(I_C + I_A)S_A - \mu\ S_A - \xi_A S_A, \tag{2}$$

$$\frac{dU_C^V}{dt} = \xi_U\ S_C - \epsilon\beta_C(I_C + I_A)U_C^V - (\mu + \eta_U + \psi)U_C^V, \tag{3}$$

$$\frac{dU_A^V}{dt} = \psi U_C^V - \eta_A U_A^V - \beta_A\epsilon(I_C + I_A)U_A^V - \mu U_A^V, \tag{4}$$

$$\frac{dV_A}{dt} = \xi_A S_A - V_A(\mu + \eta_A), \tag{5}$$

$$\frac{dM_C^V}{dt} = \xi_M S_C - (\mu + \eta_M)M_C^V, \tag{6}$$

$$\frac{dE_C}{dt} = \beta_C(I_C + I_A)S_C + \beta_C\epsilon(I_C + I_A)U_C^V - (\delta + \mu + \psi)E_C, \tag{7}$$

$$\frac{dE_A}{dt} = \beta_A(I_C + I_A)S_A + \beta_A\epsilon(I_C + I_A)U_A^V + \psi E_C - (\delta + \mu)E_A, \tag{8}$$

$$\frac{dI_C}{dt} = \delta E_C - (\gamma + d + \mu + \psi)I_C, \tag{9}$$

$$\frac{dI_A}{dt} = \delta E_A + \psi E_C - (\gamma + d + \mu)I_A, \tag{10}$$

$$\frac{dI_{mC}}{dt} = \gamma I_C + \eta_M M_C^V - (\mu + \psi)I_{mC} + \eta_U U_C^V, \tag{11}$$

$$\frac{dI_{mA}}{dt} = \eta_A(U_A^V + V_A) + \gamma I_A - \mu I_{mA} + \psi I_{mC}. \tag{12}$$

3. Model analysis

3.1. Positivity and boundedness of the solutions

In the system (1–12), all the state variables are non-negative and should remain non-negative forever since they represent the human population. For the given non-negative initial conditions, it can be easily verified that system (1-12) has non-negative solutions at any time t as shown in the following theorem.

Theorem 3.1. *If the state variable are non-negative with $S_C > 0$ at time $t = 0$, then the solution set of the system (1 - 12) is always non-negative and bounded.*

Proof:
First, we prove that all the solutions are non-negative. From the system (1–12), we get

$$\begin{aligned}
\frac{dS_C}{dt} &= \Lambda - (\mu + \xi_M + \xi_U + \psi)S_C - \beta_C(I_C + I_A)S_C \\
&> -(\mu + \xi_M + \xi_U + \psi)S_C - \beta_C(I_C + I_A)S_C \\
\Rightarrow S_C &> S_C(0)\exp\left(-\int_0^t ((\mu + \xi_M + \xi_U + \psi) + \beta_C(I_C + I_A))\,dt\right) \geq 0; \\
\frac{dS_A}{dt} &= \psi\, S_C - \beta_A(I_C + I_A)S_A - \mu\, S_A - \xi_A\, S_A \\
&> -\beta_A(I_C + I_A)S_A - \mu\, S_A - \xi_A S_A \\
\Rightarrow S_A &> S_A(0)\exp\left(-\int_0^t \beta_A((I_C + I_A) + \mu + \xi_A)\,dt\right) > 0; \\
\frac{dU_C^V}{dt} &= \xi_U\, S_C - \beta_C\,\epsilon(I_C + I_A)U_C^V - (\mu + \eta_U + \psi)U_C^V \\
&> -\beta_C\,\epsilon\,(I_C + I_A)U_C^V - (\mu + \eta_U + \psi)U_C^V \\
\Rightarrow U_C^V &\geq U_C^V(0)\exp\beta_C\epsilon\left(-\int_0^t ((I_C + I_A) + (\mu + \eta_U + \psi))\,dt\right) \geq 0; \\
\frac{dU_A^V}{dt} &= \psi\, U_C^V - \eta_A\, U_A^V - \beta_A\,\epsilon(I_C + I_A)U_A^V - \mu\, U_A^V \\
&> -\eta_A\, U_A^V - \beta_A\,\epsilon\,(I_C + I_A)U_A^V - \mu\, U_A^V \\
\Rightarrow U_A^V &\geq U_A^V(0)\exp\left(-\int_0^t \beta_A\,\epsilon\,(\eta_A + (I_C + I_A) + \mu)\,dt\right) \geq 0; \\
\frac{dV_A}{dt} &= \xi_A S_A - V_A(\mu + \eta_A) > -V_A(\mu + \eta_A) \\
\Rightarrow V_A &> V_A(0)\exp\left(-\int_0^t (\eta_A + \mu)\,dt\right) \geq 0; \\
\frac{dM_C^V}{dt} &= \xi_M\, S_C - (\mu + \eta_M)M_C^V \\
&> -(\mu + \eta_M)M_C^V \\
\Rightarrow M_C^V &\geq M_C^V(0)\exp\left(-\int_0^t ((\mu + \eta_M))\,dt\right) \geq 0; \\
\text{and } \frac{dE_C}{dt} &= \beta_C(I_C + I_A)S_C + \beta_A\,\epsilon(I_C + I_A)U_C^V - (\delta + \mu + \psi)E_C \\
&\geq -((\delta + \mu + \psi))E_C \\
\Rightarrow E_C &\geq E_C(0)\exp\left(-\int_0^t ((\delta + \mu + \psi))\,dt\right) \geq 0.
\end{aligned}$$

Similarly, $E_A, I_C, I_A, I_{mC}, I_{mA}$ are also non-negative. Hence, the solution set $\{S_C, S_A, U_C^V, U_A^V, V_A, M_C^V, E_C, E_A, I_C, I_A, I_{mC}, I_{mA}\}$ of system (1–12) is always non-negative.

We now prove that these non-negative solutions are bounded. Let $N_h(t)$ be the total human population, i.e., $N_h(t) = S_C(t) + S_A(t) + U_C^V(t) + U_A^V(t) + V_A(t) + M_C^V(t) + E_C(t) + E_A(t) + I_C(t) + I_A(t) + I_{mC}(t) + I_{mA}(t)$. Adding all the equations of the system (1–12), we obtain

$$\frac{dN_h}{dt} = \Lambda - \mu N_h - d(I_C + I_A) \leq \Lambda - \mu N_h,$$

which implies

$$\lim_{t\to\infty} N_h \leq \Lambda/\mu.$$

Hence, the human population, $N_h(t)$, is ultimately bounded.

Using the above conditions, we have that for any $\alpha > 0$, there exists $t_\alpha > 0$ such that the solution of the system with $t \geq t_\alpha$ lies in the compact set $\Omega = \Omega_h$, where $\Omega_h = \left\{\left(S_C, S_A, U_C^V, U_A^V, V_A, M_C^V, E_C, E_A, I_C, I_A, I_{mC}, I_{mA}\right) \in \Re_+^{12} : N_h \leq \Lambda/\mu + \alpha\right\}$. Thus, all the state variables representing the populations are non-negative and bounded.

3.2. Disease-free equilibrium and reproduction number

Here, we derive the expression of the disease-free and endemic equilibrium points. Taking $E_C^0 = 0$, $E_A^0 = 0$, $I_C^0 = 0$, $I_A^0 = 0$, we obtain the disease-free equilibrium: $E^0 = (S_C^0,\ S_A^0,\ (U_C^V)^0,\ (U_A^V)^0, V_A^0,\ (M_C^V)^0,\ 0,\ 0,\ 0,\ 0,\ I_{mC}^0,\ I_{mA}^0)$, where

$$\begin{aligned}
S_C^0 &= \frac{\Lambda}{\mu + \xi_M + \xi_U + \psi},\\
S_A^0 &= \frac{\Lambda\psi}{(\xi_A + \mu)(\mu + \xi_M + \xi_U + \psi)},\\
\left(U_C^V\right)^0 &= \frac{\Lambda\xi_U}{Z(\mu + \xi_M + \xi_U + \psi)},\\
\left(U_A^V\right)^0 &= \frac{\Lambda\psi\xi_U}{Z(\eta_A + \mu)(\mu + \xi_M + \xi_U + \psi)},\\
V_A^0 &= \frac{\Lambda\psi\xi_A}{(\eta_A + \mu)(\xi_A + \mu)(\mu + \xi_M + \xi_U + \psi)},\\
\left(M_C^V\right)^0 &= \frac{\Lambda\xi_M}{Z_1(\mu + \xi_M + \xi_U + \psi)},\\
I_{mC}^0 &= \frac{\Lambda(\eta_M(\xi_M Z + \eta_U\xi_U) + \mu\eta_U\xi_U)}{ZZ_1(\mu + \psi)(\mu + \xi_M + \xi_U + \psi)},\\
I_{mA}^0 &= \frac{\Lambda\psi\left(ZZ_1\eta_A(\xi_A(\mu + \psi) + \mu(Z_1\xi_M + \eta_M\xi_U)) + \mu^2(Z_1\eta_U\xi_U + Z\eta_M\xi_M)\right)}{ZZ_1\mu^2(\mu + \psi)(\eta_A + \mu)(\mu + \xi_M + \xi_U + \psi)},\\
\text{and } Z &= (\mu + \eta_U + \psi),\ Z_1 = (\mu + \eta_M).
\end{aligned}$$

Given that a significant portion of the population has already been vaccinated, we adopt a similar approach to our previous study (Pokharel et al., 2022) in defining the vaccinated reproduction number, R_v. This is done considering the presence of the vaccinated population, as opposed to an entire population susceptible to infection. The vaccinated reproduction number, R_v, represents the average number of secondary cases resulting from introducing a single infectious case into the mixed population, which comprises individuals with both susceptible and vaccinated status. To calculate R_v, we utilize the Next Generation Matrix method described in previous studies (Diekmann & Heesterbeek, 2001; van den Driessche & Watmough, 2002; Diekmann, Heesterbeek, & Roberts, 1992).

Following the Next Generation Matrix method (van den Driessche & Watmough, 2002), we divide the system into two groups, infected $\vec{x} = (x_i, i = 1,2,3,4) = (E_C,\ E_A,\ I_C,\ I_A)$ and uninfected $\vec{y} = (y_j, j = 1,2,3,4,5,6,7,8) = (S_C,\ S_A,\ U_C^V,\ U_A^V,\ V_A,\ M_C^V,\ I_{mC},\ I_{mA})$. We then set $\dot{x}_i = f_i(\vec{x}, \vec{y}) = \mathcal{F}_i(x,y) - \mathcal{V}_i(x,y)$ for $i = 1, 2..4$ and $\dot{y}_j = g_j(\vec{x}, \vec{y})$ for $j = 1, 2 \ldots, 8$, where $\mathcal{F}_i(x,y)$ is the rate of appearance of new infections in the compartment i and $\mathcal{V}_i(x,y)$ is the difference between the transfer of individuals out of and into the compartment i for $i = 1, 2, 3, 4$. Here we have

$$\mathcal{F} = \begin{pmatrix} \beta_C(I_C + I_A)S_C + (I_C + I_A)\beta_C U_C^V \epsilon \\ \beta_A(I_C + I_A)S_A + (I_C + I_A)\beta_A U_A^V \epsilon \\ 0 \\ 0 \end{pmatrix} \text{ and } \mathcal{V} = \begin{pmatrix} (\delta + \mu + \psi)E_C \\ -E_C\psi + E_A(\delta + \mu) \\ -E_C\delta + I_C(\gamma + d + \mu + \psi) \\ -E_A\delta - I_C\psi + I_A(\gamma + d + \mu) \end{pmatrix}.$$

It is straightforward to confirm that the conditions A(1)-A(5) mentioned in van den Driessche & Watmough (2002) are satisfied by the sets $\mathcal{F}_i$ and $\mathcal{V}_i$ for $i = 1, 2, 3, 4$. We derive the Jacobian matrices of $\mathcal{F}$ and $\mathcal{V}$ at disease-free equilibrium point (E^0), yielding $D\mathcal{F}(E^0) = F$ and $D\mathcal{V}(E^0) = V$ as follows:

$$F = \begin{pmatrix} 0 & 0 & \beta_C S_C^0 + \beta_C (U_C^V)^0 \epsilon & \beta_C S_C^0 + \beta_C (U_C^V)^0 \epsilon \\ 0 & 0 & \beta_A S_A^0 + \beta_A (U_A^V)^0 \epsilon & \beta_A S_A^0 + \beta_A (U_A^V)^0 \epsilon \\ 0 & 0 & 0 & 0 \\ 0 & 0 & 0 & 0 \end{pmatrix},$$

$$V = \begin{pmatrix} \delta + \mu + \psi & 0 & 0 & 0 \\ -\psi & \delta + \mu & 0 & 0 \\ -\delta & 0 & \gamma + d + \mu + \psi & 0 \\ 0 & -\delta & -\psi & \gamma + d + \mu \end{pmatrix},$$

$$V^{-1} = \begin{pmatrix} \frac{1}{\delta + \mu + \psi} & 0 & 0 & 0 \\ \frac{\psi}{(\delta + \mu)(\delta + \mu + \psi)} & \frac{1}{\delta + \mu} & 0 & 0 \\ \frac{\delta^2 + \delta\mu}{L} & 0 & \frac{1}{\gamma + d + \mu + \psi} & 0 \\ \frac{\delta\psi(\gamma + \delta + d + 2\mu + \psi)}{L(\gamma + d + \mu)} & \frac{\delta}{(\delta + \mu)(\gamma + d + \mu)} & \frac{\psi}{(\gamma + d + \mu)(\gamma + d + \mu + \psi)} & \frac{1}{\gamma + d + \mu} \end{pmatrix},$$

where $L = (\delta + \mu)(\delta + \mu + \psi)(\gamma + d + \mu + \psi)$. Since F is a non-negative and V is a non-singular M-matrix, the next generation matrix FV^{-1} exists, and its spectral radius $\rho(FV^{-1})$ gives the vaccinated reproduction number R_v. Therefore,

$$R_v = \frac{\delta\left(\beta_C S_C^0 + \beta_A S_A^0 + \epsilon\beta_C (U_C^V)^0 + \epsilon\beta_A (U_A^V)^0\right)}{(\delta + \mu)(\gamma + d + \mu)}$$

$$= \frac{\delta\Lambda(\beta_C\epsilon\xi_U(\eta_A + \mu)(\xi_A + \mu) + \beta_A\psi\epsilon\xi_U(\xi_A + \mu) + \beta_C Z(\eta_A + \mu)(\xi_A + \mu) + \beta_A\psi Z(\eta_A + \mu))}{Z(\delta + \mu)(\eta_A + \mu)(\xi_A + \mu)(\gamma + d + \mu)(\mu + \xi_M + \xi_U + \psi)}.$$

We also compute the time-dependent effective reproduction number, denoted by R_e. The R_e value aids us in monitoring whether the epidemic at a given time t is exhibiting an upward trend ($R_e > 1$) or a downward trend ($R_e < 1$). In our model, the effective reproduction number is determined by the following expression:

$$R_e = \frac{\delta\left(\beta_C S_C(t) + \beta_A S_A(t) + \epsilon\beta_C U_C^V(t) + \epsilon\beta_A U_A^V(t)\right)}{(\delta + \mu)(\gamma + d + \mu)}.$$

3.3. Stability of disease free equilibrium E^0

3.3.1. Local stability of disease free equilibrium E^0

The Jacobian J_0 of the system (1–12) at the disease free equilibrium E^0 is given by $J_0 = [A_{12\times 6}\, B_{12\times 6}]$, where

$$A_{12\times 6}=\begin{pmatrix} -\mu-\xi_M-\xi_U-\psi & 0 & 0 & 0 & 0 & 0\\ \psi & -\mu-\xi_A & 0 & 0 & 0 & 0\\ \xi_U & 0 & -\mu-\eta_U-\psi & 0 & 0 & 0\\ 0 & 0 & \psi & -\eta_A-\mu & 0 & 0\\ 0 & \xi_A & 0 & 0 & -\eta_A-\mu & 0\\ \xi_M & 0 & 0 & 0 & 0 & -\mu-\eta_M\\ 0 & 0 & 0 & 0 & 0 & 0\\ 0 & 0 & 0 & 0 & 0 & 0\\ 0 & 0 & 0 & 0 & 0 & 0\\ 0 & 0 & 0 & 0 & 0 & 0\\ 0 & 0 & \eta_U & 0 & 0 & \eta_M\\ 0 & 0 & 0 & \eta_A & \eta_A & 0 \end{pmatrix},$$

$$B_{12\times 6}=\begin{pmatrix} 0 & 0 & -\beta_C S_C & -\beta_C S_C & 0 & 0\\ 0 & 0 & -\beta_A S_A & -\beta_A S_A & 0 & 0\\ 0 & 0 & -\beta_C U_C^V\,\epsilon & -\beta_C U_C^V\,\epsilon & 0 & 0\\ 0 & 0 & -\beta_A U_A^V\,\epsilon & -\beta_A U_A^V\,\epsilon & 0 & 0\\ 0 & 0 & 0 & 0 & 0 & 0\\ 0 & 0 & 0 & 0 & 0 & 0\\ -\delta-\mu-\psi & 0 & \beta_C S_C+\beta_C U_C^V\epsilon & \beta_C S_C+\beta_C U_C^V\epsilon & 0 & 0\\ \psi & -\delta-\mu & \beta_A S_A+\beta_A U_A^V\,\epsilon & \beta_A S_A+\beta_A U_A^V\epsilon & 0 & 0\\ \delta & 0 & -\gamma-d-\mu-\psi & 0 & 0 & 0\\ 0 & \delta & \psi & -\gamma-d-\mu & 0 & 0\\ 0 & 0 & \gamma & 0 & -\mu-\psi & 0\\ 0 & 0 & 0 & \gamma & \psi & -\mu \end{pmatrix}.$$

Let λ_i, $i = 1, 2, \ldots 12$, be eigenvalues of the matrix J_0. Then $\lambda_1 = -\mu$, $\lambda_2 = -(\mu + \xi_A)$, $\lambda_3 = -(\mu + \psi)$, $\lambda_4 = -(\mu + \eta_M)$, $\lambda_5 = -(\mu + \eta_A)$, $\lambda_6 = -(\mu + \eta_A)$, $\lambda_7 = -(\mu + \eta_U + \psi)$,

$\lambda_8 = -(\mu + \xi_M + \xi_U + \psi)$, $\lambda_9 = -(\gamma + d + \mu + \psi)$, $\lambda_{10} = -(\delta + \mu + \psi)$,

$$\lambda_{11} = -\tfrac{1}{2}\left(d+\delta+2\mu+\gamma+\sqrt{(\gamma+d+\delta+2\mu)^2-4(1-R_v)(\delta+\mu)(\gamma+d+\mu)}\right),$$

$$\lambda_{12} = -\tfrac{1}{2}\left(d+\delta+2\mu+\gamma-\sqrt{(\gamma+d+\delta+2\mu)^2-4(1-R_v)(\delta+\mu)(\gamma+d+\mu)}\right).$$ All eigenvalues are negative except λ_{12}, which is also negative for $R_v < 1$. Thus, we can conclude that the disease-free equilibrium point is locally asymptotically stable for $R_v < 1$.

In the epidemiological sense, the locally asymptotically stability of the disease-free equilibrium for $R_v < 1$ implies that the measles dynamics initiated with a small number of infections introduced in the community approaches to the measles-free state over time when the vaccinated reproduction number remains less than one. In other words, the vaccinated reproduction number being less than unity assures that the disease outbreak will die out when a small population perturbation occurs with the introduction of a small number of infections, which is usually the case at the beginning of infection. Such a condition allows us to design a vaccination policy that assures $R_v < 1$, thereby avoiding the outbreak. However, local stability does not ensure outbreak control under all conditions or if the system is perturbed significantly.

3.3.2. Global stability of the disease-free equilibrium E^0

In this section, we show that $R_v < 1$ also asserts the global stability of the disease-free equilibrium E^0 as stated in the following theorem.

Theorem 3.2. *The disease-free equilibrium E^0 is globally stable when $R_v < 1$.*

Here, we determine the global stability of E^0 using the results presented in a previous study (Castillo-Chávez et al., 2002). First, system (1–12) is written as $dX/dt = F(X, Y)$, $dY/dt = G(X, Y)$, with $G(X, 0) = 0$, where $X \in R^8$ and $Y \in R^4$ represent the uninfected and infected compartments, respectively. Then satisfying the following two conditions implies the global asymptotically stability of the system around disease-free equilibrium point $E^0 = (X^*, 0)$:

1. For $dX/dt = F(X, 0)$, X^* is globally stable, (where $X^* \in R^8$ at disease free state) and
2. $\hat{G}(X,Y) = BY - G(X,Y) \geq 0$, for $(X, Y) \in R^{12}$, where B is the Jacobian of the infected system at the disease-free equilibrium E^0.

Clearly, the system

$$\frac{dX}{dt} = \begin{pmatrix} \Lambda - S_C(\mu + \xi_M + \xi_U + \psi) \\ S_C\,\psi - \mu S_A \\ S_C\xi_U - U_C^V(\mu + \eta_U + \psi) \\ U_C^V\psi - U_A^V(\mu + \eta_A) \\ \xi_A S_A - V_A(\mu + \eta_A), \\ S_C\xi_M - M_C^V(\mu + \eta_M) \\ M_C^V\eta_M - I_{mC}(\mu + \psi) + U_C^V\eta_U \\ (U_A^V + V_A)\eta_A - \mu I_{mA} + I_{mC}\,\psi \end{pmatrix}$$

is globally asymptotically stable at X^*. The matrix of the infected compartments is given as:

$$G = \begin{pmatrix} (I_C + I_A)\beta_C S_C + (I_C + I_A)\beta_C U_C^V\epsilon - (\delta + \mu + \psi)E_C \\ (I_C + I_A)\beta_A S_A + (I_C + I_A)\beta_A U_A^V\epsilon + E_C\psi - E_A(\delta + \mu) \\ E_C\delta - I_C(\gamma + d + \mu + \psi) \\ E_A\delta + I_C\psi - I_A(\gamma + d + \mu) \end{pmatrix}.$$

The Jacobian of the matrix G at the disease-free equilibrium is $B =$

$$\begin{pmatrix} -\delta - \mu - \psi & 0 & \beta_C(S_C)^0 + \beta_C\left(U_C^V\right)^0\epsilon & \beta_C(S_C)^0 + \beta_C\left(U_C^V\right)^0\epsilon \\ \psi & -\delta - \mu & \beta_A(S_A)^0 + \beta_A\left(U_A^V\right)^0\epsilon & \beta_A(S_A)^0 + \beta_A\left(U_A^V\right)^0\epsilon \\ \delta & 0 & -\gamma - d - \mu - \psi & 0 \\ 0 & \delta & \psi & -\gamma - d - \mu \end{pmatrix}.$$

$$Y = \begin{pmatrix} E_C \\ E_A \\ I_C \\ I_A \end{pmatrix},$$

$$BY = \begin{pmatrix} -E_C(\delta + \mu + \psi) + (I_C + I_A)\beta_C(S_C)^0 + (I_C + I_A)\beta_C\left(U_C^V\right)^0\epsilon \\ -E_A(\delta + \mu) + (I_C + I_A)\beta_A(S_A)^0 + (I_C + I_A)\beta_A\left(U_A^V\right)^0\epsilon + E_C\psi \\ E_C\delta - I_C(\gamma + d + \mu + \psi) \\ -I_A(\gamma + d + \mu) + E_A\delta + I_C\psi \end{pmatrix},$$

where Y is a (4×1) matrix with elements (E_C, E_A, I_C, I_A). Then $BY - G$ or $\hat{G} =$

$$\begin{pmatrix} (I_C + I_A)\beta_C\left(\left(\frac{\Lambda}{\mu + \xi_M + \xi_U + \psi} - S_C\right) + \epsilon\left(\frac{\Lambda\xi_U}{Z(\mu + \xi_M + \xi_U + \psi)} - U_C^V\right)\right) \\ (I_C + I_A)\beta_A\left(\epsilon\left(\frac{\Lambda\psi\xi_U}{Z(\eta_A + \mu)(\mu + \xi_M + \xi_U + \psi)} - U_A^V\right) + \left(\frac{\Lambda\psi}{(\mu + \xi_A)(\mu + \xi_M + \xi_U + \psi)} - S_A\right)\right) \\ 0 \\ 0 \end{pmatrix}.$$

From the system of equations 1–12, we ultimately obtain

$$S_C \leq \frac{\Lambda}{\mu+\xi_M+\xi_U+\psi}, S_A \leq \frac{\Lambda\psi}{(\mu+\xi_A)(\mu+\xi_M+\xi_U+\psi)}, U_C^V \leq \frac{\Lambda\xi_U}{Z(\mu+\xi_M+\xi_U+\psi)}, \text{and } U_A^V \leq \frac{\Lambda\psi\xi_U}{Z(\eta_A+\mu)(\mu+\xi_M+\xi_U+\psi)}.$$

Clearly $(BY - G)$ is the non-negative matrix for $R_v < 1$, so the disease free equilibrium point is globally asymptotically stable when $R_v < 1$.

Epidemiologically, our theorem establishing the global stability of the disease-free equilibrium implies that the disease can't establish sustained transmission within the population for any, even significantly large, initial number of infections as long as $R_v < 1$. The global stability of the disease-free equilibrium point of our model helps to maintain and implement preventive strategies such as vaccination programs for disease control.

3.4. Endemic equilibrium

Obtaining the endemic point in the infectious disease modeling is crucial to understanding the long-term disease dynamics. For many situations with imperfect vaccination programs, which is likely the current condition in Nepal, the endemic equilibrium provides the epidemic's severity. The epidemic level, at least, informs important policy guidelines for disease control if not eradicated.

Suppose $E^* = \left(S_C^*,\ S_A^*,\ (U_C^V)^*,\ (U_A^V)^*,\ V_A^*,\ (M_C^V)^*,\ E_C^*,\ E_A^*,\ I_C^*,\ I_A^*, I_{mC}^*,\ I_{mA}^*\right)$ be an endemic equilibrium of the system. Let, $I^* = I_C^* + I_A^*$. Then solving system (1–12), we get

$$\begin{aligned}
S_C^* &= \frac{\Lambda}{\beta_C I^* + \mu + \xi_M + \xi_U + \psi},\\
S_A^* &= \frac{\Lambda\psi}{(\beta_A I^* + \mu + \xi_A)(\beta_C I a^* + \mu + \xi_M + \xi_U + \psi)},\\
\left(U_C^V\right)^* &= \frac{\Lambda\xi_U}{(\beta_C I^* + \mu + \xi_M + \xi_U + \psi)(\beta_C I^*\epsilon + Z)},\\
\left(U_A^V\right)^* &= \frac{\Lambda\psi\xi_U}{(\eta_A + \beta_A I^*\epsilon + \mu)(\beta_C I^* + \mu + \xi_M + \xi_U + \psi)(\beta_C I^*\epsilon + Z)},\\
V_A^* &= \frac{\Lambda\psi\xi_A}{(\eta_A+\mu)(\beta_A I^* + \mu + \xi_A)(\beta_C I^* + \mu + \xi_M + \xi_U + \psi)},\\
\left(M_C^V\right)^* &= \frac{\Lambda\xi_M}{(\mu+\eta_M)(\beta_C I^* + \mu + \xi_M + \xi_U + \psi)},\\
E_C^* &= \frac{\beta_C I^* \Lambda(\beta_C I^*\epsilon + \epsilon\ \xi_U + Z)}{(\delta+\mu+\psi)(\beta_C I^* + \mu + \xi_M + \xi_U + \psi)(\beta_C I^*\epsilon + Z)},\\
I_C^* &= \frac{\beta_C \delta I^* \Lambda(\beta_C I^*\epsilon + \epsilon\ \xi_U + Z)}{(\delta+\mu+\psi)(\gamma+d+\mu+\psi)(\beta_C I^* + \mu + \xi_M + \xi_U + \psi)(\beta_C I^*\epsilon + Z)}.
\end{aligned}$$

Here, $E_A^*,\ I_A^*,\ I_{mC}^*,\ I_{mA}^*$ are positive when $R_v > 1$ (see supplementary file). After manipulating the equations of the system at diseased equilibrium we obtained the equation given as:

$$(A_4(I^*)^4 + A_3(I^*)^3 + A_2(I^*)^2 + A_1 I^* + A_0)I^* = 0, \tag{13}$$

where,

$$\begin{aligned}
A_4 &= \beta_C^2\beta_A^2\epsilon^2(\delta+\mu)(\gamma+d+\mu),\\
A_0 &= (1-R_v)(\delta+\mu)(\eta_A+\mu)(\xi_A+\mu)(\gamma+d+\mu)(\mu+\eta_U+\psi)(\mu+\xi_M+\xi_U+\psi),
\end{aligned}$$

and A_1, A_2, A_3 are provided in supplementary file. Note that $I^* = 0$ corresponds to the disease-free equilibrium E^0. Since $A_0 < 0$ when $R_v > 1$ and $A_4 > 0$, then by Vieta's Theorem, there exists at least one positive I^* and the system has at least one endemic equilibrium when $R_v > 1$.

We can compute the magnitude of endemic equilibrium by solving Eq. (13). We were unable to establish the stability of the endemic equilibrium analytically due to the complexity brought by the higher-order equations with nonlinearity. However, we performed numerical analysis for the stability of the endemic equilibrium and presented results as a bifurcation diagram

with the existence and stability of the endemic equilibrium for $R_v > 1$ (Fig. 3), for which the disease-free equilibrium is unstable.

4. Numerical simulations

4.1. Data fitting, model validation, and parameter estimation

Since measles cases were found only in ten districts of Nepal (Fig. 1), we considered the population corresponding to only these ten districts with a total of $N(0) = 6,564,070$ (N. S. Office, 2021). Moreover, as the cases appeared only in a few villages of these ten districts, the whole population is less likely to be in the contact network. Therefore, we assume α is a portion of the total population, so only $\alpha N(0)$ is in the measles transmission contact network. In Nepal, the children population aged up to 14 years is 27.4% (Statista, 2023), so we assumed 29% of the total population aged up to 15 years and took $N_C(0) = 0.29\alpha N(0)$ and $N_A(0) = 0.71\alpha N(0)$.

The vaccinated population in Nepal is about 87–93% (WHO, 2023c), and assuming children are more vaccinated than adults, we took 91% of children and 89% of adults were vaccinated. Thus, we took 9% and 11% of unvaccinated children and adults as respective susceptibles, i.e., $S_C(0) = 0.09\alpha N_C(0)$ and $S_A(0) = 0.11\alpha N_A(0)$. Since there was no adequately monitored vaccination or catch-up program for adult vaccination in Nepal, we took $M_C^V(0) = 50,\ V_A = 0$. Since vaccine effectiveness for measles is 77–86% (Ichimura et al., 2022; Kumar et al., 2023; Lochlainn et al., 2019), we took 89% as the immune population, giving $I_{mA}(0) = 0.79\alpha N_A(0)$ and $I_{mC}(0) = 0.81\alpha N_C(0)$. The remaining populations are taken as $U_C^V(0)$ and $U_A^V(0)$. Following the magnitude of data, we assume that the outbreak begins with a small number of exposed and infected individuals and took $E_C(0) = 5$, $E_A(0) = 3$, $I_C(0) = 2$, $I_A(0) = 1$.

For this study, individuals under 15 were categorized as children, giving the maturation rate of $\psi = 1/(15 \times 52) = 0.0013$ per week. Since the average lifespan for Nepal in 2023 is approximately 72 years (Macrotrends), we took the natural death rate as $1/(72 \times 52)$ per week. During the period of data collected, no immunization program was in place for adults, so we took both the rate of adult vaccination (ξ_A) and the rate of being immune through adult vaccination (η_A) as zero. We also assume the rate of adults being immune through un-monitored vaccination (η_A) to be zero.

We considered the incubation period for measles to be 10 days (range: 10–14 days) (WHO, 2023a), implying $\delta = 0.7$ per week. Considering the recovery period from the disease is around 15 days (range: 7–23 days) (WHO-Nepal, 2023b), we obtain $\gamma = 1/2$ per week. Using the Case Fatality Rate (CFR) of 0.14% in Nepal (Dall, 2023; WHO-Nepal, 2023a) in the disease-induced death rate formula $d = \frac{-ln(1-0.14/100)}{T}$ given in the previous study (Pantha, Giri, Joshi, & Vaidya, 2021) with $T = 15$ weeks, we obtain $d = 9.3399 \times 10^{-5}$ per week.

In line with WHO guidelines, children receive their first vaccine dose at 9 months of age and the second dose at 15 months (MoHP, 2024), with a six-month interval between two doses. Accounting for an average vaccine effectiveness of 80 % (Min-Shi et al., 2009; WHO-Measles, 2019), we adopted $\epsilon = 1 - 0.8 = 0.2$. Since the outbreaks usually remain for a short term of 15 weeks only, as revealed in the data, we can assume that the birth and the death balance each other, i.e., $\Lambda = \mu \times N$.

We estimate the parameters β_C, β_A, ξ_U, η_U, η_M, and α by fitting the model with the measles case data from Nepal. From the model, weekly new infections at time t are given by $h(t) = \theta\delta E(t)$, which we obtain using the numerical solutions of system (1-

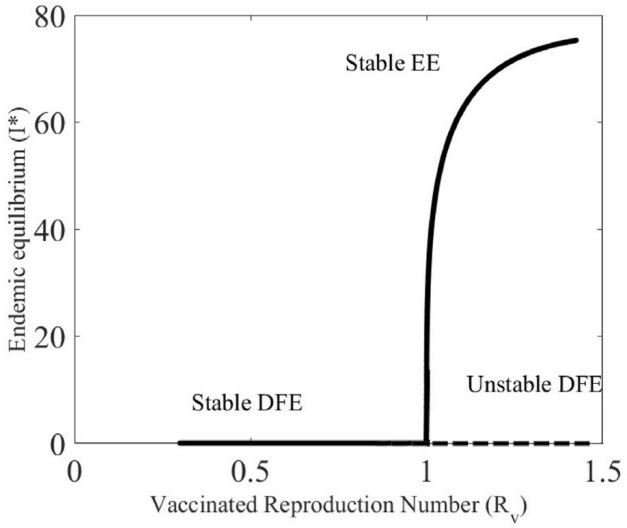

Fig. 3. Forward bifurcation at $R_v = 1$. The disease free equilibrium is stable for $R_v < 1$. The disease free is unstable and endemic equilibrium is stable for $R_v > 1$.

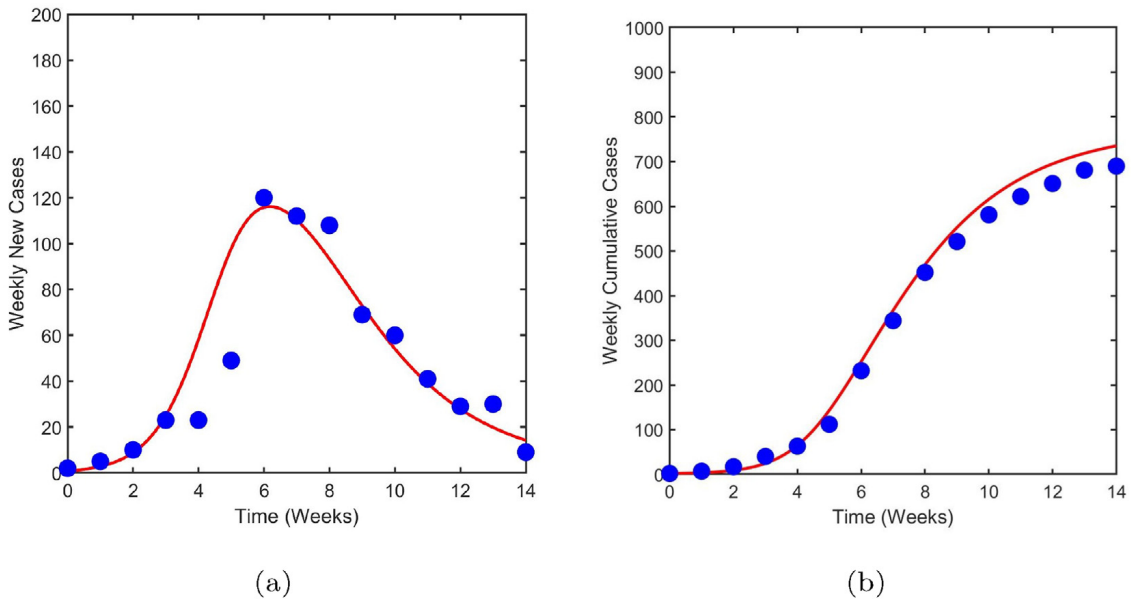

Fig. 4. Data fitting and model validation. (a) The recorded weekly cases of measles in Nepal (filled circle) along with the best fit of the model (line). (b) The cumulative recorded measles cases in Nepal (filled circle) along with the model prediction of the cumulative cases (line).

12). Here, θ represents the portion of the infection recorded. Then, we estimate the parameters with the help of the nonlinear regression method (Motulasky & Arthur, 2003) that minimizes the following sum of the square residuals:

$$\sum_{k=1}^{15} (h_k - \bar{h}_k)^2,$$

where h_k denotes the model predicted weekly new infection and $\bar{h}_k$ denotes weekly new infection data. All the computations are carried out in MATLAB (The Math Works. Inc.) using its various routines, including “ode45” (ODE solver) and “fmincon” (minimizer).

Our model can fit the data of weekly incidence cases in Nepal well (Fig. 4a). In addition, we also show that the model prediction of the cumulative cases agrees well with the cumulative data (Fig. 4b), thereby validating our model. The values of state variables and parameters are given in Table 2 and Table 3, respectively. From our estimation, the transmission rate in children ($\beta_C = 0.00188$) is higher than in adults ($\beta_A = 1.00 \times 10^{-5}$). Despite the low transmission rate among adults, it may still be sufficient to spread the disease and cause obstacles to achieving the mission of measles eradication. Similarly, we obtained the monitored vaccination rate ($\xi_M = 4.777 \times 10^{-6}$) is less than the un-monitored vaccination rate ($\xi_U = 0.0087$), and the rate of being immune from monitored vaccination ($\eta_M = 0.0167$) is higher than the un-monitored vaccination ($\eta_U = 3 \times 10^{-6}$). Our estimates indicate that about 15% of the measles cases were recorded in Nepal (*i.e.*, $\theta = 0.15$) (Table 3).

4.2. Parameter sensitivity analysis

4.2.1. Sensitivity of R_v

We quantify the local sensitivity of R_v to each of the parameters β_C, β_A, ψ, γ, d, δ, ϵ, μ, η_A, η_U, η_M, ξ_M, ξ_U, and ξ_A. For this, we obtained the sensitivity index, S_x, for each parameter x using the relationship:

$$S_x = \left(\frac{x}{R_v}\right)\left(\frac{\partial R_v}{\partial x}\right).$$

Based on the sensitivity index S_x, we found that the parameter γ affects R_v the most compared to the other parameters. The second parameter affecting R_v is β_C, followed by the parameters ϵ, ψ, μ, ξ_U, and β_A, while the effects of d, δ, η_A, η_M, ξ_A, η_M and ξ_M to R_v are negligible (Fig. 5a).

We also performed the global sensitivity analysis by using the Latin Hypercube Sampling (LHS) technique (Simeone, Hogue, Ray, & Kirschner, 2008) with 1000 samples of parameter sets from a wider parameter range of ±25% of the base value of each parameter. We compute the partial rank correlation coefficients (PRCC) to identify the most influential parameter to R_v. We observed that the parameters γ, β_C, ϵ, and ψ are the most sensitive parameters for R_v, which are followed

Table 2
State variables.

State Variables	Values	State Variables	Values
$M_C^V(0)$	50	$V_A(0)$	0
$E_C(0)$	5	$E_A(0)$	3
$I_C(0)$	2	$I_A(0)$	1
$S_C(0)$	2142	$S_A(0)$	6408
$U_C^V(0)$	2382	$U_A^V(0)$	5703
$I_{mC}(0)$	19,271	$I_{mA}(0)$	46,145
$N_C(0)$	23,795	$N_A(0)$	58,256

Table 3
Model parameters.

Symbols of Parameters	Values	Source
ξ_U, ξ_M	0.087, 4.77×10^{-5}	Data fitting
β_C, β_A	0.00188, 1.00×10^{-5}	Data fitting
μ	$1/(72 \times 52)$	Calculated
γ	1/2	WHO-Nepal (2023b)
ψ	$1/(15 \times 52)$	Calculated
ϵ	0.2	[46, 47]
η_A	0	Assumed
η_U, η_M	3×10^{-6}, 0.167	Data fitting
δ	0.7	WHO-Nepal (2023b)
θ	0.15	Data fitting
d	9.3399×10^{-05}	Calculated
ξ_A	0	Assumed
α	0.01253	Data fitting

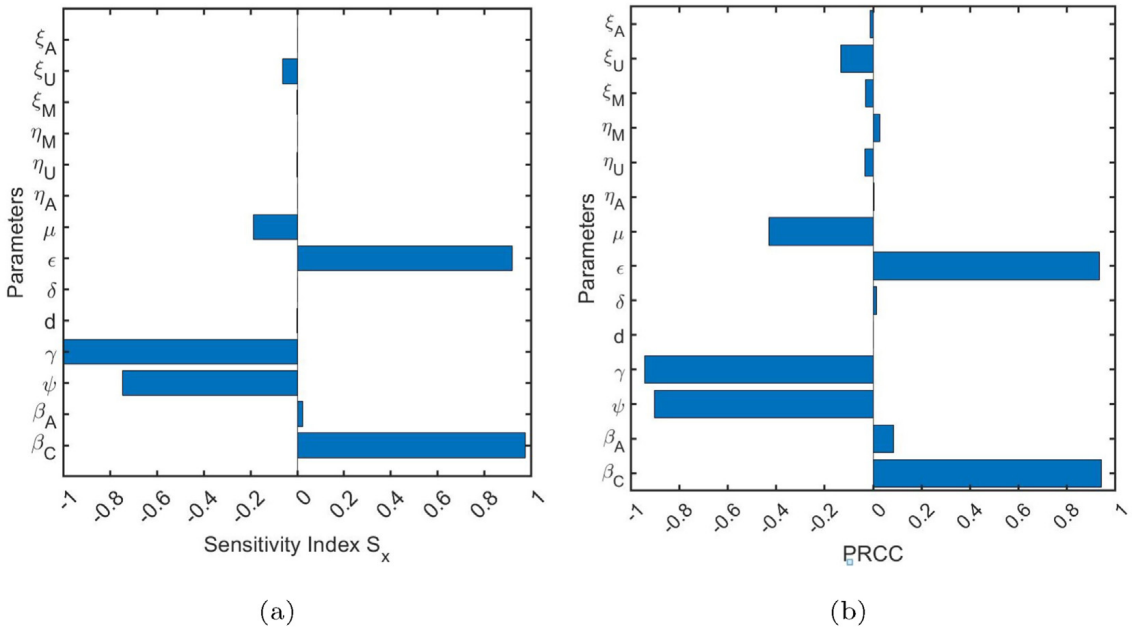

Fig. 5. (a) Local sensitivity of parameters to R_v. The sensitivity index, S_x, showing the level of change in R_v with respect to the parameters. Note that the sensitivity index S_x of d, δ, η_A, η_U, η_M, ξ_A and ξ_M are negligible and difficult to visualize in the figure. **(b) Global sensitivity of** R_v. Partial Rank Correlation Coefficients for R_v from LHS method.

by μ, ξ_U, and β_A, and the rest of the parameters are less effective (Fig. 5b). Both local and global analyses show that R_v is mostly influenced by the parameters γ, β_C, and ϵ.

4.2.2. Sensitivity of measles dynamics

We also used the Latin Hypercube Sampling (Simeone, Hogue, Ray, & Kirschner, 2008) method to explore the global sensitivity of the measles dynamics represented by the peak infection and the time to peak in adults, children, and combined. The computed partial rank correlation coefficient corresponding to each parameter is presented in Fig. 6. Our analysis shows

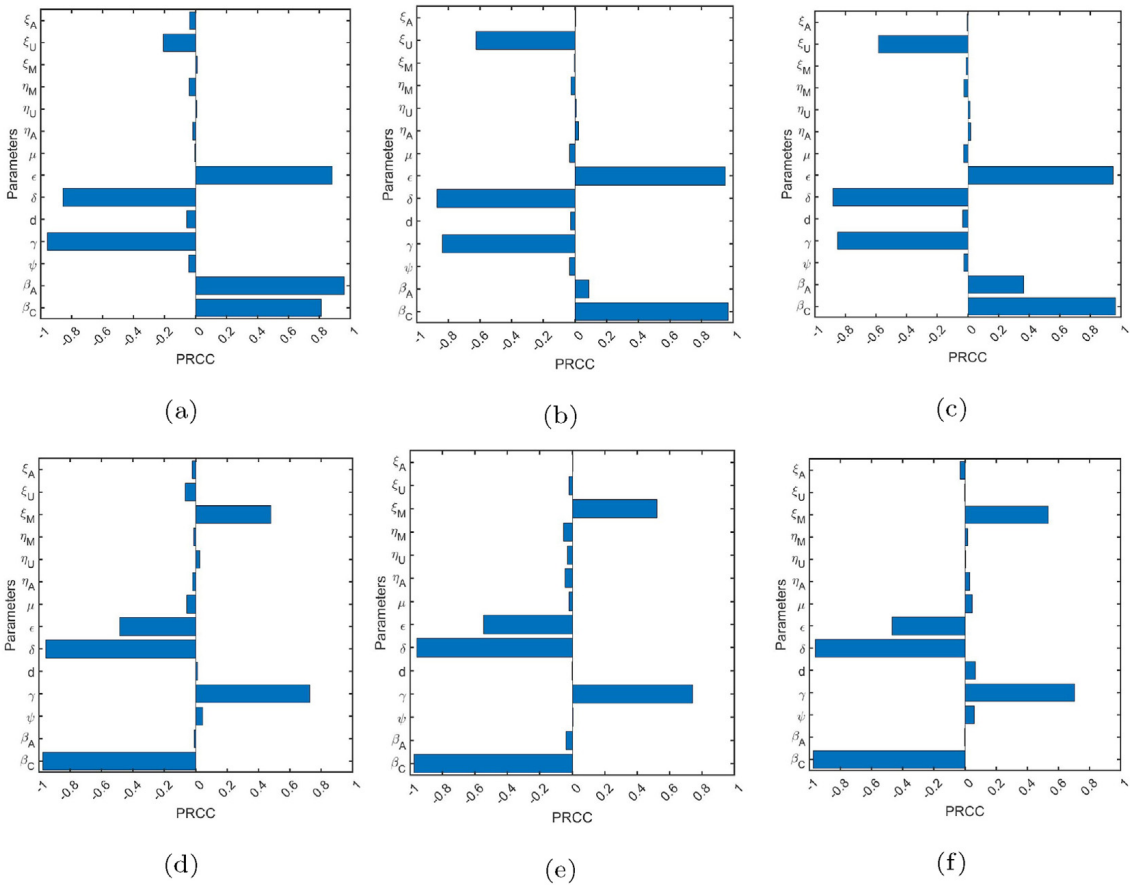

Fig. 6. Sensitivity of measles dynamics. Global sensitivity of the parameters to peak value and time to peak infection for adult I_A (a, d), children I_C (b, e), and combined child and adult (c, f). The partial rank correlation coefficients for sensitivity are based on 1000 Latin Hypercube Sample sets of parameters.

that the peak value of the infected class I_A is highly influenced by γ, β_A, ϵ, and δ followed by β_C and then by ξ_U while the remaining parameters are less effective (Fig. 6a). Also, the peak value of the infected class I_C is highly influenced by β_C, ϵ, δ, and γ, followed by ξ_U and other parameters are less effective (Fig. 6b). Similarly, the peak value of the infected class of children and adults combined is influenced by the parameters β_C, ϵ, δ, γ, followed by ξ_U. In contrast, the remaining parameters are less effective (Fig. 6c).

The time to peak infection is mostly affected by the parameters β_C, δ, and γ, followed by ϵ and ξ_M. The rest of the parameters in I_A and I_C less influences it. Similarly, the time to peak for combined infection is mainly affected by δ, β_C, γ, and ϵ, followed by ξ_M, while the remaining parameters are less effective (Fig. 6f).

4.3. Impact of the contact network on infection

While we estimated the base contact network in the data context, the contact network may change depending on the situation. Therefore, we now explore the effects of the contact network on the total number of infections and its peak value for each infected class. An increase in children's contact network by 5, 10, and 15 times the base case results in the rise of peak infection of children by 8, 16, and 21 times, respectively, and an increase in the total children infection by 4, 7, and 8 times, respectively (Fig. 7a). Similarly, the same increment level in the adult contact network results in the increment of the total infection by 28, 85, and 133 times and the peak infection by 28, 92, and 166 times, respectively (Fig. 7b). An increment in the contact network of all populations by 5, 10, and 15 times results in an increment of approximately 8, 17, and 23 times in the peak infection and 7, 16, and 23 times in the total infection, respectively (Fig. 7c).

4.4. Impact of monitored vaccine program

4.4.1. On disease increase-decrease trend

Here, we examine the profound role of vaccine coverage in the increase-decrease trend of the disease, i.e., reducing the effective reproduction number (R_e) below one. We evaluate the effect of both timeliness and extension of vaccination

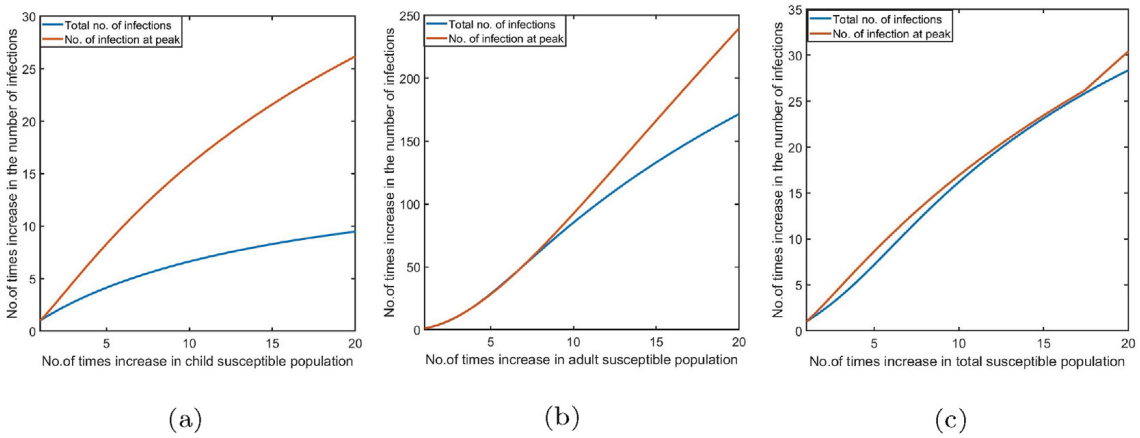

Fig. 7. Effects of the contact network size. The total number of infections and peak infection on the variation of the contact network of (a) children, (b) adults, and (c) total (children and adults).

coverage in achieving the goal of $R_e < 1$ (decreasing trend). Our findings show that complete vaccine coverage within the first two weeks of outbreaks yields remarkable outcomes in lowering the effective reproduction number. Achieving a vaccination coverage of over 90% among children within two weeks decreases the effective reproduction number to below 1 in just two weeks. In contrast, when vaccine coverage is limited to only 20%, this critical threshold is reached only after six weeks (Fig. 8a).

Our model predicts that a vaccination campaign focused only on adults may not be sufficient to reduce the effective reproduction number to below one within a reasonable time frame. As depicted in Fig. 8b, the complete vaccine coverage of adults within two weeks slightly lowers the effective reproduction number in about seven weeks. The vaccination distributed among the combined population is less effective than the vaccination entirely given to children. In this case, the threshold can be lowered to below one in one week by 90% of vaccine coverage within three weeks, while it takes six weeks for 30% of coverage within two weeks (Fig. 8c).

4.4.2. On the reduction of disease burden

We also explore the impact of vaccine coverage over a specific period on reducing measles cases and the maximum weekly cases. Our modeling reveals a significant variation in the effects of vaccine coverage across distinct age groups (Fig. 9). 20% of children vaccination within two weeks can reduce about 85% of the total measles cases and 85% of the maximum weekly cases, while 90% of children vaccination within six weeks can reduce more than 90% of the total measles cases and more than 90% of the maximum weekly cases (Fig. 9a and b). In contrast, 20% of adult vaccinations within two weeks can reduce only 10% of the total cases and only 5% of the maximum weekly cases. Even 90% of the adult vaccinations within six weeks can reduce only 12% of the total cases and only 7% of the maximum weekly cases (Fig. 9c and d).

90% of combined adult-child vaccination within two weeks reduces about 80% of the total measles cases and 80% of the maximum weekly cases (Fig. 9e and f). These results highlight that the effectiveness of vaccination in diminishing measles

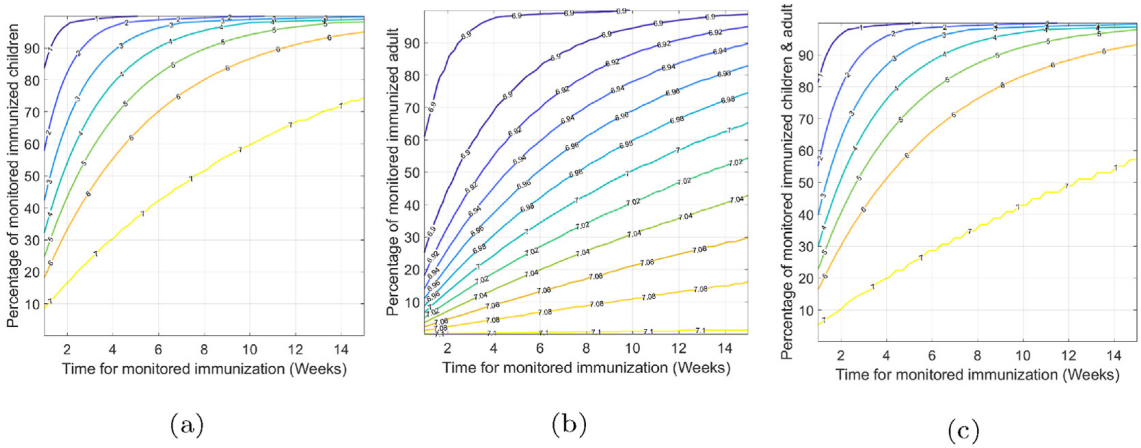

Fig. 8. Time for R_e<1. Time (in weeks) for the effective reproduction number to be less than one when (a) only children are immunized, (b) only adults are immunized, and (c) children and adults are immunized.

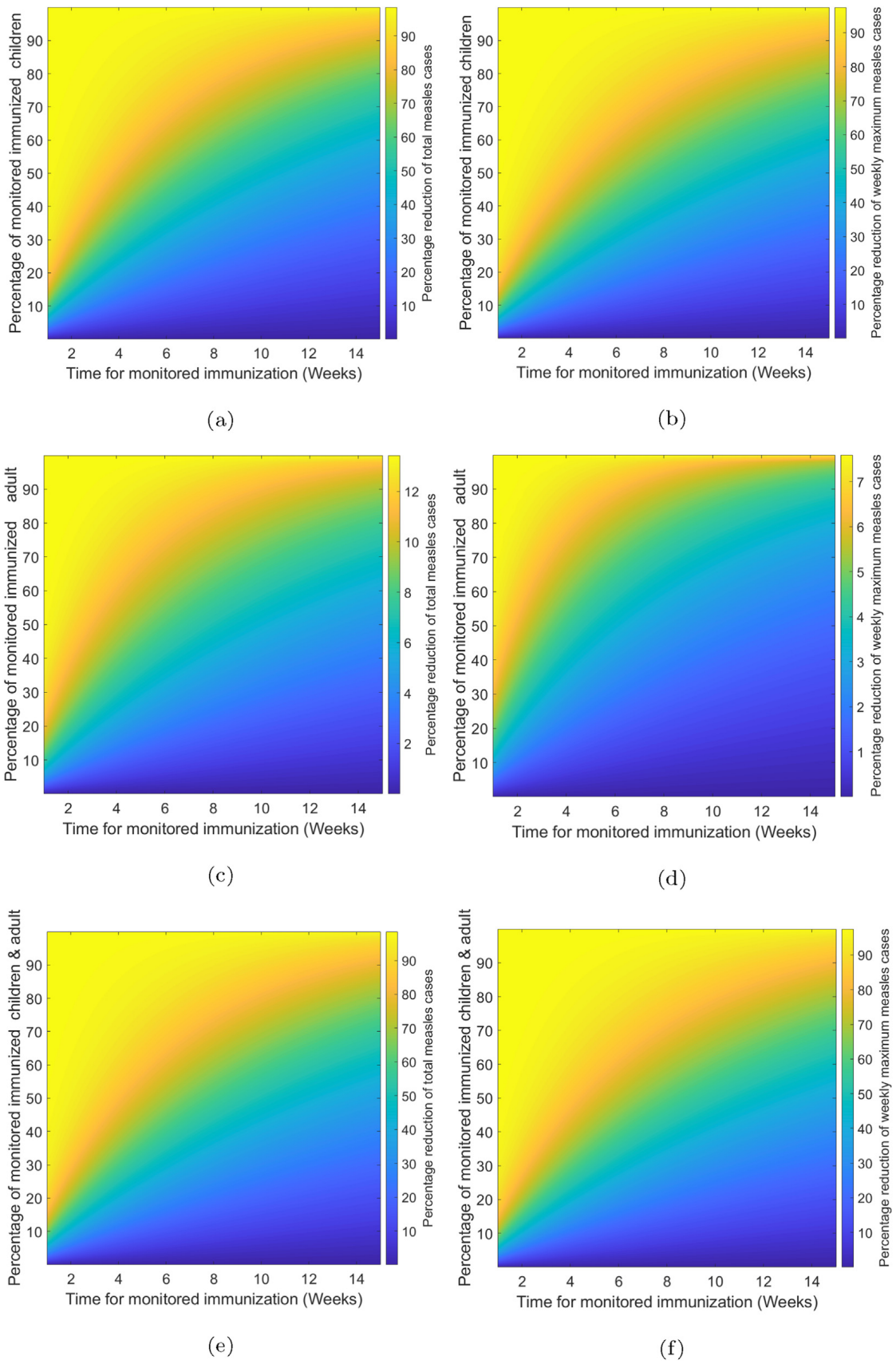

Fig. 9. Effects of monitored vaccination. Impact of the coverage of monitored children vaccination on the percentage reduction of (a) the total measles cases and (b) weekly maximum new cases of measles, adult vaccination on the percentage reduction of (c) the total measles cases and (d) weekly maximum new cases of measles, the children and adult vaccination on the percentage reduction of (e) the total measles cases and (f) weekly maximum new cases of measles.

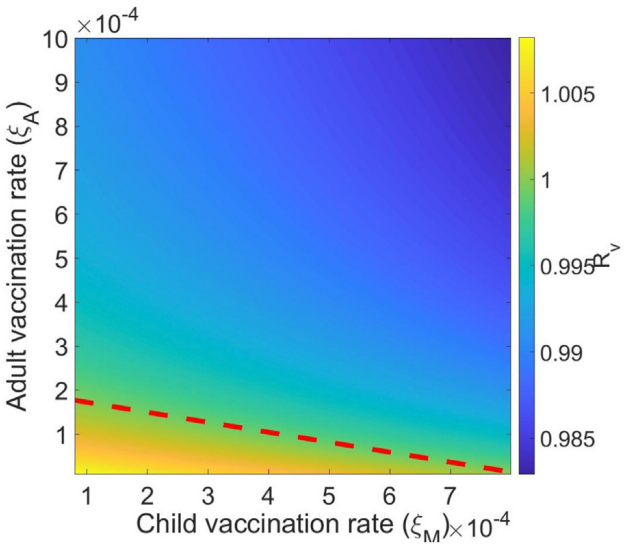

Fig. 10. Effects of vaccination on R_v. Value of R_v for combinations of children and adults vaccination rates (ξ_M-ξ_A parameter space). The dashed red line corresponds to $R_v = 1$.

prevalence is notably more pronounced in vaccination programs focused on children (Fig. 9a) than adults (Fig. 9c). However, it is worth noting that even though the adult vaccination may reduce the burden negligibly compared to childhood vaccination, it still plays a vital role in controlling the disease, especially for eradication, since adults may act as a potential reservoir source for persistent disease transmission.

4.5. Infections in adults: implications to disease eradication

As found above, vaccination focused on adults only has the negligible benefit of reducing the disease burden compared to vaccination focused on children. However, persistent infection in adults may pose an obstacle to measles eradication. Therefore, we further performed a deeper analysis to explore whether a realistic adult infection-related parameter range exists that may cause an obstacle to eradication. To examine this, we identified the region corresponding to the disease eradication ($R_v < 1$) and disease persistence ($R_v > 1$) in the ξ_M-ξ_A parameter space of children and adults vaccination rates (Fig. 10).

As illustrated in Fig. 10, with the parameter range $3 \leq \xi_M \leq 17(\times 10^{-5})$ and $0 \leq \xi_A \leq 10(\times 10^{-4})$, we observe that there exists a realistic parameter range (space below $R_v = 1$ curve in Fig. 10) for which $R_v > 1$. This indicates that unless the child vaccination rate is sufficiently large, the value of R_v may remain above one due to some persistent infection in adults. In this case, introducing adult vaccination on top of the child vaccination can reduce R_v below one. Therefore, in the situation when children-focused vaccination is not sufficiently large enough, which is likely the case in developing countries like Nepal, persistent infection in adults can be a major hurdle for disease eradication, and considering adult-focused vaccination along with children's vaccination becomes critical for global disease eradication.

5. Discussion

In recent years, measles outbreaks have occurred frequently in many places of the globe. The threat of measles is growing due to the expansion of immunity gaps, COVID-19's disruption of routine immunization, and the lack of planned global vaccination campaigns. The reduction of vaccination is also attributed to various factors, including societal and educational impacts and religious barriers. In Nepal, the decline in vaccination coverage corresponds to the patterns of measles epidemics. While a higher proportion of cases are observed in young infants and older children, a small number of cases have frequently been observed in Nepalese adults (WHO, 2023d), implying that the unvaccinated adults may serve as a virus reservoir to cause obstacles to WHO's eradication goal. The model developed in this study with both children and adult groups is essential to identify the ideal monitored vaccination strategy for both adults and children to ensure the global eradication of measles.

Using our model validated by the measles case data of different regions of Nepal from November 24, 2022, to March 10, 2023 (WHO-Nepal, 2023a), we estimated the measles-vaccinated reproduction number in Nepal to be $R_v = 11.677$. The value of R_v is much higher than one, indicating that significant efforts need to be put into the vaccination program in Nepal to meet WHO's global eradication goal. Most notably, our model predicts a critical adult vaccination level required in combination with a partially successful children's vaccination program to bring R_v less than one. Therefore, our study underscores the need for combined adult and children vaccination for measles eradication, in contrast to the often ignored adult group in vaccination programs.

We explored the effect of the contact network size on measles epidemics. We found that increasing contact networks ultimately increases the total and weekly measles cases in children and adults. Interestingly, the increase in measles burden is more pronounced due to the rise of contact networks among adults than children, mainly when the increased level is more than ten times the base case. This result further highlights the importance of adult vaccination, which lowers the adult susceptible population, thereby reducing the total infection and weekly infection.

We also examined the impact of vaccine coverage on disease trends (Fig. 8) and the disease burden (Fig. 9). Our model helps identify a reasonable level of child-adult vaccine coverage to ensure the decreasing trend of measles (i.e., $R_e < 1$). For example, 90% in three weeks or 30% in two weeks of vaccine coverage can bring R_e less than one in one day or six days, respectively. Similarly, our model allows us to properly evaluate the vaccination program for reducing the disease burden. For example, an 80% reduction in the total measles cases and an 80% reduction in the maximum weekly cases can be achieved by covering 90% adult and child population within two weeks of vaccination. Our results show that the vaccine focused entirely on children can reduce the disease burden more than that distributed among both children and adults, highlighting the significance of prioritizing childhood vaccine coverage as a primary strategy for reducing disease burden. However, as discussed above, adult vaccination should not be overlooked as it may have a critical role in disease eradication. Our result is consistent with the previous studies (Dipo & Dinda, 2019; Garba et al., 2017; Jaharuddin, 2020; Lessler et al., 2016; Pokharel et al., 2022).

We acknowledge some limitations of our study. The parameter estimations were based on the limited data of weekly incidence cases. The lack of granular data and information could have hindered the achievement of more accurate outcomes. Although we successfully derived the closed form of the distinct endemic equilibrium, we were unable to complete a thorough analysis of this equilibrium due to model complexities. For example, we couldn't achieve the stability condition of endemic equilibrium, while we only explored the stability of endemic equilibrium through numerical methods. We have ignored the potential effects of spatial heterogeneity on disease transmission and assumed a homogenous mixed population. Spatial heterogeneity may play a role in disease transmission, especially in the spread of measles in some specific districts of Nepal. Further study on the cost-effectiveness analysis based on the country's financial status would benefit the optimal policy design to achieve the measles eradication goal.

In summary, we developed a novel model of measles transmission in the context of Nepal, incorporating the two different age groups, children (15 and under) and adults (above 15). Our model demonstrates that the adult group is a potential reservoir of measles, causing obstacles to eradicating the disease. Our results suggest that implementing the adult vaccines along with the children's vaccine is critical for achieving WHO's global measles eradication goal. A well-planned adult-child combination of monitored vaccination programs may be necessary to facilitate the ambitious objective of eradicating measles from Nepal.

Declaration of competing interest

The authors declare that they have no known competing financial interests or personal relationships that could have appeared to influence the work reported in this paper.

Authors declare

No conflict of interest.

CRediT authorship contribution statement

Anjana Pokharel: Writing – original draft, Methodology, Investigation, Formal analysis. **Khagendra Adhikari:** Writing – original draft, Methodology, Investigation, Formal analysis. **Ramesh Gautam:** Writing – original draft, Methodology, Investigation, Formal analysis. **Kedar Nath Uprety:** Writing – review & editing, Supervision, Formal analysis. **Naveen K. Vaidya:** Writing – review & editing, Supervision, Formal analysis, Conceptualization.

Acknowledgments

This research is supported by the GRAID (Graduate Research Assistantships in Developing Countries) awards from the International Mathematical Union (IMU). AP acknowledges the University Grants Commission (UGC), Sanothimi Bhaktapur, Nepal, for the Small Research and Development and Innovation Grants-077/078 (SRDIG) award. KA acknowledges the Nepal Academy of Science and Technology (NAST) for Ph.D. Fellowship. RG acknowledges the University Grants Commission (UGC) Nepal for Ph.D. Fellowship 2021. The work of NKV was supported by NSF grants DMS-1951793 and DEB-2030479 from the National Science Foundation of USA and UGP award from San Diego State University.

Appendix A. Supplementary data

Supplementary data to this article can be found online at https://doi.org/10.1016/j.idm.2024.04.012.

References

Adhikari, K., Gautam, R., Pokharel, A., Dhimal, M., Uprety, K. N., & Vaidya, N. K. (2022). Insight into delta variant dominated second wave of covid-19 in Nepal. *Epidemics, 41*, Article 100642. https://doi.org/10.1016/j.epidem.2022.100642

Adhikari, K., Gautam, R., Pokharel, A., Uprety, K. N., & Vaidya, N. K. (2021). Transmission dynamics of covid-19 in Nepal: Mathematical model uncovering effective controls. *Journal of Theoretical Biology, 521*, Article 110680. https://doi.org/10.1016/j.jtbi.2021.110680

Castillo-Chávez, C., Zhilan, F., & Huang, W. (2002). On the computation of r0 and its role in global stability. *IMA Volumes in Mathematics and its Applications, 125*, 229–250. https://doi.org/10.1007/978-1-4757-3667-0_13

Dall, C. (2023). *Nepal hit by measles outbreak*. URL https://www.who.int/emergencies/disease-outbreak-news/item/2023-DON446.

Diekmann, O., & Heesterbeek, J. A. P. (2001). Mathematical epidemiology of infectious diseases: Model building, analysis and interpretation. *International Journal of Epidemiology, 30*(1), 186. https://doi.org/10.1093/ije/30.1.186, 186.

Diekmann, O., Heesterbeek, J. A. P., & Roberts, M. G. (1992). Seroepidemiology and evaluation of passive surveillance during 1988–1989 measles outbreak in Taiwan. *International Journal of Epidemiology, 21*(6), 1165–1174. https://doi.org/10.1098/rsif.2009.0386

Dipo, A., & Dinda, A. (2019). A deterministic model of measles with imperfect vaccination and quarantine intervention. *International Conference on Mathematics: Pure, Applied and Computation, 1218*. https://doi.org/10.1088/1742-6596/1218/1/012044, 012044–012054.

Edward, S., Kitengeso Raymond, E., Kiria Gabriel, T., Nestory, F., Mwema, G., Godfrey, P., et al. (2015). A mathematical model for control and elimination of the transmission dynamics of measles. *Applied and Computational Mathematics, 4*, 396–408. https://doi.org/10.11648/j.acm.20150406.12

Farman, M., Shehzad, A., Akgül, A., Baleanu, D., & Sen, M. D.l. (2023). Modelling and analysis of a measles epidemic model with the constant proportional caputo operator. *Symmetry, 15*(2). https://doi.org/10.3390/sym15020468

Garba, S. M., Safi, M. A., & Usaini, S. (2017). Mathematical model for assessing the impact of vaccination and treatment on measles transmission dynamics. *Mathematical Methods in the Applied Sciences, 40*(18). https://doi.org/10.1002/mma.4462

Gautam, R., Pokharel, A., Adhikari, K., Uprety, K. N., & Vaidya, N. K. (2022). Modeling malaria transmission in Nepal: Impact of imported cases through cross-border mobility. *Journal of Biological Dynamics, 16*(1), 528–564. https://doi.org/10.1080/17513758.2022.2096935

Haileyesus, T. A., & Asnakew, M. B. (2023). Modelling, analysis, and simulation of measles disease transmission dynamics. *Discrete Dynamics in Nature and Society, 2023*. https://doi.org/10.1155/2023/9353540

Ichimura, Y., Yamauchi, M., Yoshida, N., Miyano, S., Komada, K., Thandar, M., et al. (2022). *Effectiveness of immunization activities on measles and rubella immunity among individuals in east sepik, Papua New Guinea: A cross-sectional study, PMC- IJID 3*. https://doi.org/10.1016/j.ijregi.2022.03.001

Jaharuddin, B. T. (2020). Control policy mix in measles transmission dynamics using vaccination, therapy, and treatment. *International Journal of Mathematics and Mathematical Sciences, 2020*, 20. https://doi.org/10.1155/2020/1561569

Joshi, A. B. (2009). Measles deaths in Nepal: Estimating the national cases in fatality ratio. *Bulletin of the World Health Organization, 87*(6), 405–484. https://doi.org/10.2471/BLT.07.050427, 2009.

Khanal, et al. (2016). Progress toward measles elimination — Nepal, 2007–2014. *CDC Morbidity and Mortality Weekly Report (MMWR), 65*(8), 206–210. https://doi.org/10.15585/mmwr.mm6508a3externalicon

Kuddus, M., Mohiuddin, M., & Rahman, A. (2021). Mathematical analysis of a measles transmission dynamics model in Bangladesh with double dose vaccination. *Scientific Reports, 11*(1), Article 16571. https://doi.org/10.1038/s41598-021-95913-8

Kumar, S. S., Hartner, A.-M., Chandran, A., Gaythorpe, K. A. M., Li, X., et al. (2023). Evaluating effective measles vaccine coverage in the malaysian population accounting for between-dose correlation and vaccine efficacy. *BMC Public Health, 23*(2351). https://doi.org/10.1186/s12889-023-17082-9

Lessler, J., Metcalf, C., Cutts, F., & Grenfell, B. (2016). Impact on epidemic measles of vaccination campaigns triggered by disease outbreaks or serosurveys: A modeling study. *PLoS Medicine, 13*(10). https://doi.org/10.1371/journal.pmed.1002144

Lochlainn, L. N., de Gier, B., van der Maas, N., Strebel, P., Goodman, T., van Binnendijk, R., et al. (2019). Immunogenicity, effectiveness, and safety of measles vaccination in infants younger than 9 months: A systematic review and meta-analysis. *The Lancet Infectious Diseases, 11*. https://doi.org/10.1016/S1473-3099(19)30395-0, 1235–124.

Macrotrends, Nepal population 1950-2020. URL https://www.macrotrends.net/countries/NPL/nepal/population.

Meredith, G. D., Matt, F., Sebastien, A., Xi, L., Allison, P., Brian, L., et al. (2021). Progress toward regional measles elimination worldwide, 2000–2020. *Morbidity and Mortality Weekly Report, 70*(45).

Min-Shi, L., Chwan-Chuen, K., Jia-Yuh, J., Chuan-Liang, K., Chen, W. C., Mei-Shang, H., et al. (2009). The construction of next-generation matrices for compartmental epidemic models. *International Journal of Epidemiology*, (7), 1165–1174. https://doi.org/10.1098/rsif.2009.0386

Motulasky, H., & Arthur, C. (2003). *Fitting model to biological data using linear and non linear regression. A practical guide to curve fitting*. San Diego,CA: Graph Pad Software Inc. URL www.graphpad.com.

Mutua, J. M., Wang, F.-B., & Vaidya, N. K. (2015). Modeling malaria and typhoid fever co-infection dynamics. *Mathematical Biosciences, 264*, 128–144. https://doi.org/10.1016/j.mbs.2015.03.014

N. S. Office. (2021). *National population and housing census* (national report). URL https://censusnepal.cbs.gov.np/results.

Pantha, B., Giri, S., Joshi, H., & Vaidya, N. K. (2021). Modeling transmission dynamics of rabies in Nepal. *Infect. Dis. Model, 6*, 284–301. https://doi.org/10.1016/j.idm.2020.12.009

Peter, O. J., Fahrani, N. D., Fatmawati, W., & Chukwu, C. (2023). A fractional derivative modeling study for measles infection with double dose vaccination. *Healthcare Analytics, 4*, Article 100231. https://doi.org/10.1016/j.health.2023.100231

Peter, O. J., Ojo, M. M., Viriyapong, R., & Oguntolu, F. A. (2022). Mathematical model of measles transmission dynamics using real data from Nigeria. *Journal of Difference Equations and Applications, 28*(6), 753–770. https://doi.org/10.1080/10236198.2022.2079411

Peter, O. J., Qureshi, S., Ojo, M. M., Viriyapong, R., & Soomro, A. (2023). Mathematical dynamics of measles transmission with real data from Pakistan. *Model. Earth Syst. Environ, 9*, 1545–1558. https://doi.org/10.1007/s40808-022-01564-7

Pokharel, A., Adhikari, K., Gautam, R., Uprety, K. N., & Vaidya, N. K. (2022). Modeling transmission dynamics of measles in Nepal and its control with monitored vaccination program. *Mathematical Biosciences and Engineering, 19*(8). https://doi.org/10.3934/mbe.2022397

Poudel, A. (2019). *Low vaccine coverage rate, floating population leading to repeat measles outbreaks*. URL https://reliefweb.int/report/nepal/low-vaccine-coverage-rate-floating-population-leading-repeat-measles-outbreaks.

Roberts, T. M. M. (2000). Predicting and preventing measles epidemics in New Zealand. *Epidemiology and Infection, 124*, 279–287. https://doi.org/10.1017/S0950268899003556

Sekhar, B. A., Rai, P., Gupta, B. P., Pradhan, R., Lacoul, M., Shakya, S., et al. (2022). Nepal measles outbreak response immunization during covid-19: A risk-based intervention strategy. *Vaccine, 40*(20), 2884–2893.

MoHP, 2024. Government of Nepal, Ministry of Health and Population, National Immunization Programme. URL https://mohp.gov.np/program/national-immunisation-programme/en.

Simeone, M., Hogue, I. B., Ray, C. J., & Kirschner, D. E. (2008). A methodology for performing global uncertainty and sensitivity analysis in systems biology. *Journal of Theoretical Biology, 254*(1), 178–196. https://doi.org/10.1016/j.jtbi.2008.04.011

Song, X., Jiang, Y., & Wei, H. (2019). Analysis of a saturation incidence SVEIRS epidemic model with pulse and two time delay. *Applied Mathematics and Computation, 214*. https://doi.org/10.1016/j.amc.2009.04.005

Statista. (2023). *Share of children in total population in Nepal from 2013 to 2022*. URL https://www.statista.com/statistics/678090/nepal-children-as-a-percentage-of-the-population/.

Thakur, C. K., Gupta, N., Pokhrel, N., Adhikari, S., Dhimal, M., & Gyanwali, P. (2024). Stumbling blocks on the path to measles-free Nepal: Impact of the covid-19 pandemic. *Tropical Medicine and Health, 52*(10). https://doi.org/10.1186/s12889-023-17082-9

Supplimentary Materials

Modeling the impact of monitored adult-child vaccination on Measles control in Nepal

Anjana Pokharel[a], Khagendra Adhikari[b], Ramesh Gautam[c], Kedar Nath Uprety[d], Naveen K. Vaidya[e,f,g,*]

[a] *Padma Kanya Multiple Campus, Tribhuvan University, Kathmandu, Nepal*
[b] *Amrit Campus, Tribhuvan University, Kathmandu, Nepal*
[c] *Ratna Rajya Laxmi Campus, Tribhuvan University, Kathmandu, Nepal*
[d] *Central Department of Mathematics,Tribhuvan University, Kathmandu, Nepal*
[e] *Department of Mathematics and Statistics, San Diego State University, San Diego, CA, USA*
[f] *Computational Science Research Center, San Diego State University, San Diego, CA, USA*
[g] *Viral Information Institute, San Diego State University, San Diego, CA, USA*

Existence of Endemic Equilibrium.

We have vaccinated reproduction number

$$R_v = \frac{\delta\left(\beta_C S_C + \beta_A S_A + \beta_C U_C \epsilon + \beta_A U_A \epsilon\right)}{(\delta+\mu)(\gamma+d+\mu)}$$

$$R_v = \frac{\delta\Lambda\left(\beta_C \epsilon \xi_U\left(\eta_A+\mu\right)\left(\xi_A+\mu\right) + \beta_A \psi \epsilon \xi_U\left(\xi_A+\mu\right) + \beta_C Z\left(\eta_A+\mu\right)\left(\xi_A+\mu\right) + \beta_A \psi Z\left(\eta_A+\mu\right)\right)}{Z(\delta+\mu)\left(\eta_A+\mu\right)\left(\xi_A+\mu\right)\left(\gamma+d+\mu\right)\left(\mu+\xi_M+\xi_U+\psi\right)},$$

For

$$Z = \left(\mu+\eta_U+\psi\right).$$

---

*Fully documented templates are available in the elsarticle package on CTAN.

*Corresponding author
Email address: nvaidya@sdsu.edu (Naveen K. Vaidya)

Solving the system of eqution: The equations of the dynamical system:

$$\frac{dS_C}{dt} = \Lambda - (\mu + \xi_M + \xi_U + \psi)\, S_C - \beta_C\, (I_C + I_A)\, S_C, \tag{1}$$

$$\frac{dS_A}{dt} = \psi\ S_C - \beta_A\, (I_C + I_A)\, S_A - \mu\ S_A - \xi_A\ S_A, \tag{2}$$

$$\frac{dU_C^V}{dt} = \xi_U\ S_C - \epsilon\beta_C\, (I_C + I_A)\, U_C^V - (\mu + \eta_U + \psi)\, U_C^V, \tag{3}$$

$$\frac{dU_A^V}{dt} = \psi U_C^V - \eta_A U_A^V - \beta_A \epsilon\, (I_C + I_A)\, U_A^V U_A^V - \mu U_A^V, \tag{4}$$

$$\frac{dV_A}{dt} = \xi_A S_A - V_A\, (\mu + \eta_A)\,, \tag{5}$$

$$\frac{dM_C^V}{dt} = \xi_M S_C - (\mu + \eta_M)\, M_C^V, \tag{6}$$

$$\frac{dE_C}{dt} = \beta_C\, (I_C + I_A)\, S_C + \beta_C \epsilon\, (I_C + I_A)\, U_C^V - (\delta + \mu + \psi) E_C, \tag{7}$$

$$\frac{dE_A}{dt} = \beta_A\, (I_C + I_A)\, S_A + \beta_A \epsilon\, (I_C + I_A)\, U_A^V + \psi E_C - (\delta + \mu) E_A, \tag{8}$$

$$\frac{dI_C}{dt} = \delta E_C - (\gamma + d + \mu + \psi) I_C, \tag{9}$$

$$\frac{dI_A}{dt} = \delta E_A + \psi E_C - (\gamma + d + \mu) I_A, \tag{10}$$

$$\frac{dR_C}{dt} = \gamma I_C + \eta_M M_C^V - (\mu + \psi) R_C + \eta_U U_C^V, \tag{11}$$

$$\frac{dR_A}{dt} = \eta_A (U_A^V + V_A) + \gamma I_A - \mu R_A + \psi R_C. \tag{12}$$

we obtained the solution at the presence of disease is given

$$
\begin{aligned}
S_C^* &= \frac{\Lambda}{\beta_C I^* + \mu + \xi_M + \xi_U + \psi}, \\
S_A^* &= \frac{\Lambda\psi}{(\beta_A I^* + \mu + \xi_A)(\beta_C I^* + \mu + \xi_M + \xi_U + \psi)}, \\
(U_C^V)^* &= \frac{\Lambda\xi_U}{(\beta_C I^* + \mu + \xi_M + \xi_U + \psi)(\beta_C I^*\epsilon + Z)}, \\
(U_A^V)^* &= \frac{\Lambda\psi\xi_U}{(\eta_A + \beta_A I^*\epsilon + \mu)(\beta_C I^* + \mu + \xi_M + \xi_U + \psi)(\beta_C I^*\epsilon + Z)}, \\
V_A^* &= \frac{\Lambda\psi\xi_A}{(\eta_A + \mu)(\beta_A I^* + \mu + \xi_A)(\beta_C I^* + \mu + \xi_M + \xi_U + \psi)}, \\
(M_C^V)^* &= \frac{\Lambda\xi_M}{(\mu + \eta_M)(\beta_C I^* + \mu + \xi_M + \xi_U + \psi)}, \\
E_C^* &= \frac{\beta_C I^*\Lambda(\beta_C I^*\epsilon + \epsilon\ \xi_U + Z)}{(\delta + \mu + \psi)(\beta_C I^* + \mu + \xi_M + \xi_U + \psi)(\beta_C I^*\epsilon + Z)}, \\
E_A^* &= \frac{\Lambda\ I^*\ \psi\ N1}{D1}, \\
I_C^* &= \frac{\beta_C\delta I^*\Lambda(\beta_C I^*\epsilon + \epsilon\ \xi_U + Z)}{(\delta + \mu + \psi)(\gamma + d + \mu + \psi)(\beta_C I^* + \mu + \xi_M + \xi_U + \psi)(\beta_C I^*\epsilon + Z)}, \\
I_A^* &= \frac{\delta\lambda\Lambda\psi N2}{D2}, \\
R_C &= \frac{\Lambda N3}{D3}, \\
R_A &= \frac{\Lambda\psi N4}{D4}.
\end{aligned}
$$

Where expression for $N_1, N_2, N_3, N_4, D_1, D_2, D_3$, and D_4 are given as:

$$
\begin{aligned}
N1 &= \beta_C^2 I^*\epsilon(\xi_A + \beta_A I^* + \mu)(\eta_A + \beta_A I^*\epsilon + \mu) + \\
&\beta_A(\eta_A + \mu)(\delta+\mu+\psi)(\mu + \eta_U + \psi) + \beta_A(\delta+\mu+\psi)\epsilon\xi_U(\xi_A + \mu) + \beta_A I^*\epsilon(\mu + \eta_U + \xi_U + \psi) + \\
&\beta_C(\xi_A + \mu)(\eta_A + \beta_A I^*\epsilon + \mu)(\mu + \eta_U + \epsilon\xi_U + \psi) + \\
&\beta_C\beta_A I^*(\eta_A + \beta_A I^*\epsilon + \mu)(\epsilon(\delta + \mu + \psi) + (\eta_U + \epsilon\xi_U + \psi)), \\
D1 &= (\delta + \mu)(\delta + \mu + \psi)(\xi_A + \beta_A I^* + \mu) \\
&(\eta_A + \beta_A I^*\epsilon + \mu)(\beta_C I^* + \mu + \xi_M + \xi_U + \psi)(\beta_C I^*\epsilon + \mu + \eta_U + \psi) \\
N2 &= \beta_C^2 I^*\epsilon(\xi_A + \beta_A I^* + \mu)(\gamma + d + \delta + 2\mu + \psi)(\eta_A + \beta_A I^*\epsilon + \mu) \\
&+\beta_A(\delta + \mu + \psi)(\gamma + d + \mu + \psi)\ (\eta_A + \mu)(\mu + \eta_U + \psi) + \epsilon\xi_U(\xi_A + \mu) + \\
&\beta_A I^*\epsilon(\mu + \eta_U + \xi_U + \psi) + \beta_C(\eta_A + \beta_A I^*\epsilon + \mu)(\xi_A + \mu)(\gamma+d+\delta+2\mu+\psi)(\mu + \eta_U + \epsilon\xi_U + \psi) \\
&+\beta_C\beta_A I^*(\eta_A + \beta_A I^*\epsilon + \mu)(\gamma(\epsilon + 1)(\mu + \psi) + \delta\epsilon(\gamma + d) + d(\epsilon + 1)(\mu + \psi)) \\
&+\beta_C\beta_A I^*((\mu + \psi)((\epsilon + 1)(\delta + \psi) + \mu(\epsilon + 2)))(\eta_A + \beta_A I^*\epsilon + \mu)
\end{aligned}
$$

$$+\beta_C\left(\eta_A+\beta_A I^*\epsilon+\mu\right)\left(\beta_A I^*\eta_U(\gamma+d+\delta+2\mu+\psi)+\epsilon\xi_U(\gamma+d+\delta+2\mu+\psi)\right)$$

$$D2=(\delta+\mu)(\gamma+d+\mu)(\delta+\mu+\psi)(\gamma+d+\mu+\psi)$$

$$\left(\xi_A+\beta_A I^*+\mu\right)\left(\eta_A+\beta_A I^*\epsilon+\mu\right)\left(\beta_C I^*+\mu+\xi_M+\xi_U+\psi\right)\left(\beta_C I^*\epsilon+\mu+\eta_U+\psi\right),$$

$$N3=\beta_C^2\gamma\delta {I^*}^2\epsilon\left(\mu+\eta_M\right)+\left(\delta+\mu+\psi\right)(\gamma+d+\mu+\psi)$$

$$\left(\eta_M\left(\xi_M\left(\mu+\eta_U+\psi\right)+\eta_U\xi_U\right)+\mu\eta_U\xi_U\right)$$

$$+(\delta+\mu+\psi)(\gamma+d+\mu+\psi)\left(\eta_M\left(\xi_M\left(\mu+\eta_U+\psi\right)+\eta_U\xi_U\right)+\mu\eta_U\xi_U\right)+$$

$$\beta_C I^*\eta_M\left(\epsilon\xi_M(\delta+\mu+\psi)(\gamma+d+\mu+\psi)+\gamma\delta\eta_U+\gamma\delta\left(\mu+\epsilon\xi_U+\psi\right)\right),$$

$$D3=(\delta+\mu)(\gamma+d+\mu)(\delta+\mu+\psi)(\gamma+d+\mu+\psi)$$

$$\left(\xi_A+\beta_A I^*+\mu\right)\left(\eta_A+\beta_A I^*\epsilon+\mu\right)\left(\beta_C I^*+\mu+\xi_M+\xi_U+\psi\right)\left(\beta_C I^*\epsilon+\mu+\eta_U+\psi\right),$$

$$N4=\beta_C^2\gamma\delta {I^*}^2\epsilon((\delta+2\mu+\psi)(\gamma+d+\mu+\psi)+\mu(\delta+\psi))\left(\eta_A+\beta_A I^*\epsilon+\mu\right)+$$

$$\left(\mu+\eta_M\right)\left(\xi_A+\beta_A I^*+\mu\right)+\beta_C\gamma\delta I^*\left(\xi_A+\mu\right)((\delta+2\mu+\psi)(\gamma+d+\mu+\psi)+\mu(\delta+$$

$$\psi))\left(\eta_A+\beta_A I^*\epsilon+\mu\right)\left(\eta_M\eta_U+\epsilon\xi_M+\mu\left(\mu+\eta_U+\epsilon\xi_U+\psi\right)+\left(\mu+\epsilon\xi_U+\psi\right)\right)+\beta_A\beta_C\gamma\delta {I^*}^2\mu(\mu+$$

$$\psi)\left(\eta_A+\beta_A I^*\epsilon+\mu\right)((\gamma+d+\mu+\psi)(\delta\epsilon+\delta+2\mu+\psi+\mu\epsilon+\psi\epsilon)+\mu(\delta+\mu))+$$

$$\eta_U((\delta+2\mu+\psi)(\gamma+d+\mu+\psi)+\mu(\delta+\psi))+\beta_A\beta_C {I^*}^2((\delta+2\mu+\psi)(\gamma+d+\mu+$$

$$\psi)+\mu(\delta+\psi))\left(\eta_A+\beta_A I^*\epsilon+\mu\right)\left(\gamma\delta\eta_M\eta_U+\epsilon\xi_U\right)+$$

$$\beta_A\beta_C\gamma\delta I^*I^*(\mu+\psi)\eta_M\left(\eta_A+\beta_A I^*\epsilon+\mu\right)((\gamma+d+\mu+\psi)(\delta\epsilon+\delta+2\mu+\psi+$$

$$\mu\epsilon+\psi\epsilon)+\mu(\delta+\mu))+\beta_A\beta_C\gamma\delta I^*I^*\epsilon\eta_M\xi_U((\delta+2\mu+\psi)(\gamma+d+\mu+\psi)+\mu(\delta+$$

$$\psi))\left(\eta_A+\beta_A I^*\epsilon+\mu\right)+\left(\delta+\mu\right)\left(\xi_A+\mu\right)(\gamma+d+\mu)(\delta+\mu+\psi)(\gamma+d+\mu+$$

$$\psi)\left(\eta_M\left(\xi_M\left(\eta_A+\mu\right)\left(\mu+\eta_U+\psi\right)+\xi_U\left(\eta_A\left(\mu+\eta_U+\psi\right)+\mu\eta_U\right)\right)+\mu\xi_U\left(\eta_A\left(\mu+\eta_U+\psi\right)+\mu\eta_U\right)\right)$$

$$+\beta_A^2 {I^*}^2\mu\epsilon(\delta+\mu+\psi)(\gamma+d+\mu+\psi)\left(\eta_U\left(\gamma\delta(\mu+\psi)+(\delta+\mu)\xi_U(\gamma+d+\mu)\right)+\gamma\delta(\mu+\psi)\left(\mu+\xi_U+\psi\right)\right)$$

$$+\beta_A^2 {I^*}^2\epsilon\eta_M\eta_U(\delta+\mu+\psi)(\gamma+d+\mu+\psi)\left(\gamma\delta(\mu+\psi)+(\delta+\mu)(\gamma+d+\mu)\left(\xi_M+\xi_U\right)\right)+$$

$$\beta_A^2 {I^*}^2\epsilon(\mu+\psi)\eta_M(\delta+\mu+\psi)(\gamma+d+\mu+\psi)\left((\delta+\mu)\xi_M(\gamma+d+\mu)+\gamma\delta\left(\mu+\xi_U+\psi\right)\right)$$

$$\beta_A\beta_A I^*I^*\eta_A\eta_M(\delta+\mu+\psi)(\gamma+d+\mu+\psi)\left(\mu+\eta_U+\psi\right)$$

$$(\gamma\delta(\mu+\psi)+(\delta+\mu)\xi_M(\gamma+d+\mu)+(\delta+\mu)\xi_U(\gamma+d+\mu))+$$

$$\beta_A I^*\mu(\delta+\mu+\psi)(\gamma+d+\mu+\psi)$$

$$\beta_A I^*\eta_M(\delta+\mu+\psi)(\gamma+d+\mu+\psi)$$

$$\eta_U\left((\delta+\mu)(\gamma+d+\mu)\left(\xi_M+\xi_U\right)\left(\epsilon\xi_A+\mu+\mu\epsilon\right)+\gamma\delta\mu(\mu+\psi)\right)+\beta_A I^*(\delta+\mu)(\mu+$$

$$\psi)\eta_M\xi_M(\gamma+d+\mu)(\delta+\mu+\psi)\left(\epsilon\xi_A+\mu+\mu\epsilon\right)\left(\gamma+d+\mu+\psi\right)$$

$$+\beta_A\gamma\delta I^*\eta_M(\delta+\mu+\psi)(\gamma+d+\mu+\psi)\left(\epsilon\xi_U\left(\xi_A+\mu\right)+\mu(\mu+\psi)\right),$$

$$D4=\mu(\delta+\mu)(\mu+\psi)(\gamma+d+\mu)(\delta+\mu+\psi)\left(\mu+\eta_M\right)(\gamma+d+\mu+\psi)$$

$$\left(\xi_A+\beta_A I^*+\mu\right)\left(\eta_A+\beta_A I^*\epsilon+\mu\right)\left(\beta_C I^*+\mu+\xi_M+\xi_U+\psi\right)\left(\beta_C I^*\epsilon+\mu+\eta_U+\psi\right).$$

Since $I^* = I_C + I_A$, we obtained polynomial equation of degree 5 in I^*:

$$A_4(I^*)^5 + A_3(I^*)^4 + A_2(I^*)^3 + A_1(I^*)^2 + A_0 I^* = 0.$$

gives one of the zeros of the equation $(I^* = 0)$ provided that DFE of the system.

And $A_0,\ A_1,\ A_2,\ A_3,\ A_4$ are given as

$A_0 = (\delta+\mu)(\eta_A+\mu)(\xi_A+\mu)(\gamma+d+\mu)(\mu+\eta_U+\psi)(\mu+\xi_M+\xi_U+\psi)$
$-\beta_C\delta\Lambda(\eta_A+\mu)(\xi_A+\mu)(\mu+\eta_U+\epsilon\xi_U+\psi)$
$-\beta_A\delta\Lambda\psi\left(\eta_A(\mu+\eta_U+\psi)+\epsilon\xi_A\xi_U+\mu^2+\mu\psi+\mu\eta_U+\mu\epsilon\xi_U\right),$
$A_0 = (1-R_v)(\delta+\mu)(\eta_A+\mu)(\xi_A+\mu)(\gamma+d+\mu)(\mu+\eta_U+\psi)(\mu+\xi_M+\xi_U+\psi)$

$A_1 = -\beta_C^2\delta\Lambda\epsilon(\eta_A+\mu)(\xi_A+\mu)+$
$\beta_A((\delta+\mu)(\gamma+d+\mu)(\mu+\eta_U+\psi)(\eta_A+\epsilon\xi_A+\mu+\mu\epsilon)(\mu+\xi_M+\xi_U+\psi)-\beta_A\delta\Lambda\psi\epsilon(\mu+\eta_U+\xi_U+\psi))$
$+\beta_C(\delta+\mu)(\eta_A+\mu)(\xi_A+\mu)(\gamma+d+\mu)(\mu+\epsilon\xi_M+\eta_U+\epsilon\xi_U+\psi+\mu\epsilon+\psi\epsilon)$
$+\beta_A\beta_C\delta\Lambda\left(\mu\epsilon\xi_A+\psi\epsilon\xi_A+\mu^2+\mu\psi+\mu^2\epsilon+2\mu\psi\epsilon\right)+$
$\beta_A\beta_C\delta\Lambda\eta_U\left(\epsilon^2\xi_A\xi_U+\eta_A(\mu+\eta_U+\epsilon\xi_U+\psi+\psi\epsilon)+(\epsilon\xi_A+\mu+\mu\epsilon)+\mu\epsilon^2\xi_U+\mu\epsilon\xi_U\right),$

$A_2 = \beta_C^2\epsilon((\delta+\mu)(\eta_A+\mu)(\xi_A+\mu)(\gamma+d+\mu)-\beta_A\delta\Lambda(\eta_A+\epsilon\xi_A+\mu+\mu\epsilon))$
$+\beta_A^2\epsilon(\delta+\mu)(\gamma+d+\mu)(\mu+\eta_U+\psi)(\mu+\xi_M+\xi_U+\psi)-\beta_C\beta_A\beta_A\delta\Lambda\epsilon(\mu+\eta_U+\epsilon\xi_U+\psi+\psi\epsilon)$
$+\beta_C\beta_A(\delta+\mu)(\gamma+d+\mu)(\eta_A+\epsilon\xi_A+\mu+\mu\epsilon)(\mu+\epsilon\xi_M+\eta_U+\epsilon\xi_U+\psi+\mu\epsilon+\psi\epsilon)$

$A_3 = \beta_C\beta_A\beta_C\epsilon((\delta+\mu)(\gamma+d+\mu)(\eta_A+\epsilon\xi_A+\mu+\mu\epsilon)-\beta_A\delta\Lambda\epsilon)+\beta_C\beta_A\beta_A\epsilon(\delta+$
$\mu)(\gamma+d+\mu)(\mu+\epsilon\xi_M+\eta_U+\epsilon\xi_U+\psi+\mu\epsilon+\psi\epsilon),$

$A_4 = \beta_C^2\beta_A^2\epsilon^2(\delta+\mu)(\gamma+d+\mu).$

Clearly $A_4 > 0$ and $A_0 < 0$ for $R_v > 1$ implies that existence of at least one positive I^* provided that existence of at least one endemic point.